Random close packing (RCP) of equal spheres: structure and implications for use as a model porous medium

Thesis

RANDOM CLOSE PACKING (RCP) OF EQUAL SPHERES: STRUCTURE AND IMPLICATIONS FOR USE AS A MODEL POROUS MEDIUM

A thesis presented for the degree of

Doctor of Philosophy

By

David W Mellor

(B.Sc. (Hons) University of Manchester)

(M.Sc. University of Liverpool)

Department of Earth Sciences

The Open University

Walton Hall

Milton Keynes

July 1989

Volume I

EX12

HIGHER DEGREES OFFICE

LIBRARY AUTHORISATION FORM

STUDENT: D. W. MELLOR SERIAL NO: M7023555

DEGREE: PhD

TITLE OF THESIS: " RANDOM CLOSE PACKING (RCP) OF EQUAL SPHERES : STRUCTURE AND IMPLICATIONS FOR USE AS A MODEL POROUS MEDIUM "

I confirm that I am willing that my thesis be made available to readers and maybe photocopied, subject to the discretion of the Librarian.

SIGNED:  DATE: 6th MAY 1989

ABSTRACT

The structure of the Finney Random Close Packing (RCP) of equal spheres has been analysed, together with the influence which such structure exerts over the capillary pressure characteristics of geometrically similar sphere packings.

The analysis is centred on the simplicial, or Delaunay cell, which is an irregular tetrahedron with apices defined by four immediate neighbour sphere-centres. In terms of using RCP as a model porous medium, an individual simplicial cell is equivalent to an individual pore. A number of measured pore-size distribution parameters are presented for the Finney packing, from which it is shown from first principles that drainage-imbibition hysteresis is not an intrinsic property of the individual pore.

The nature and degree of randomness which characterises the Finney packing is evaluated on two levels. First, by classifying edgelengths as either short or long, seven mutually exclusive cell classes are defined. Using the binomial theorem it is shown that cells (pores) are not random on the level of the individual cell. There are less of the extreme cells (with 6 long edges, or with 6 short edges) and more of the bland cells (with 3 short and 3 long edges) in the Finney packing than predicted on the basis of simple random expectations. Second, the distribution of cell classes within the packing is shown to be essentially homogeneously random. Evidence for extremely slight cell class clustering is found.

The drainage and imbibition processes within the packing are simulated using pore-level algorithms. The algorithms utilise both the Haines' insphere approximation and the MS-P approximation for critical drainage meniscus curvature, and the cell cavity insphere radius approximation for critical imbibition meniscus curvature. Good agreement with experimental data is obtained, and the results confirm that drainage-imbibition hysteresis is a direct consequence of the connectivity between cells (pores), and is not an intrinsic property of the individual pore. Finally, the drainage and imbibition algorithms are adapted to emulate percolation theory models. The results prove that the classical bond problem of percolation theory does not adequately describe the drainage process for RCP, and that the classical site problem does not adequately describe the imbibition process for RCP.

CONTENTS

LIST OF FIGURES

VOLUME I

CHAPTER 1

Page

Page

Page

CHAPTER 4

LIST OF TABLES

VOLUME I

CHAPTER 2

CHAPTER 3

Page

CHAPTER 4

CHAPTER 5

Acknowledgements

This research was funded by BP. It seems to me to be fairly meaningless to express gratitude towards an organisation as vast as BP. Instead I wish to thank Mike Collett for approving my original request, and David Gair for helping to talk him into it. I would also like to thank those people at the BP Research Centre, Sunbury who have shown some interest in my work, and who have offered helpful suggestions. These people include (not in any particular order), Mervyn Grist, Nick Quirke, Jeremy Walton, Peter King, Steve Begg, David Buller, Rick Carter and Steve Bryant. Geoff Bullen performed the particle size analysis reported in Chapter 7, and Gill ter Kuile performed the mercury injection measurements of samples of Brigham Bank sandstone kindly provided by Richard Steele of BP Exploration. This thesis was skilfully deciphered and typed by Billa Davis.

Outside BP, I would like to express my thanks to Professor Geof Brown for his guidance and support. I would also like to thank Professor J L Finney for agreeing to allow me access to the sphere centre co-ordinates of his packing, without which this work could not have been completed. I extend my thanks to Adrain Wright who provided the simplicial cell sub-division of Professor J L Finney's sphere packing. I want to extend my gratitude towards my external supervisor, Geoff Mason, who provided me with not just a high level of intellectual and moral support but also his friendship. Finally, and most importantly, I wish to thank my wife Sue for bearing all this nonsense with rare good humour, and my children for suggesting that the letters Ph.D must stand for "please help Daddy!".

CHAPTER 1: INTRODUCTION TO RANDOM CLOSE PACKING (RCP)

1.1 Context of the present work

The work presented in this thesis combines two main strands - the structure of random close packing (RCP) of equal spheres, and the influence exerted by this structure over the capillary properties of RCP regarded as a model porous medium. There are extensive literatures directly relevant to both strands. The structure of RCP, for example, is an important subject in its own right in the theoretical physics of the solid state (see for example Finney 1981, 1982, Ziman 1982 and Zallen 1983), and the now classical literature pertaining to the earlier Bernal model of the liquid state (Bernal 1959, 1960(i), 1960(ii), 1962, 1965, 1967 and Finney 1968). Although certain geometrical aspects of real RCP structure are well known, the actual definition of RCP structure as a whole is still not well posed mathematically (Ziman 1982), and hitherto, no real RCP model has been analysed at a level of detail appropriate to understanding internal capillary processes. The problem of interest here is the displacement of one fluid within the interstitial spaces of the RCP structure by another, immiscible fluid.

When two immiscible fluids are in contact within the pore space of a porous medium, a discontinuity in pressure exists between the two fluids. This pressure discontinuity is called the capillary pressure, and its magnitude depends upon the curvature of the interface, or meniscus, which separates the two fluids. By

convention, one fluid is deemed to wet the surface of the porous medium, whilst the other fluid does not. The pore-volume fraction occupied by an individual fluid phase is known as the saturation of that phase. Thus for a two phase system, the sum of the phase saturations must equal unity. A reduction in wetting phase saturation, corresponding to an increase in non-wetting phase saturation, is described as a drainage process. The converse situation, wherein the wetting phase saturation increases at the expense of the non-wetting phase is termed imbibition. In order to maintain a constant value of the two phase saturations, it is necessary to sustain a constant capillary pressure, such that the fluid pressure of the non-wetting phase is greater than that of the wetting phase. Progressively de-saturating an individual porous medium from 100% wetting phase saturation results in the drainage capillary-pressure curve for that medium, also shown in figure 1.1. It is generally not possible to achieve total desaturation, and a residual wetting phase saturation remains in the sample. Progressively increasing the wetting phase saturation from the residual saturation results in the imbibition capillary - pressure curve for the medium, also shown in figure 1.1. The difference between the drainage and imbibition curves is known as capillary pressure hysteresis.

In general terms, the capillarity problem can be reduced to a consideration of changes in fluid saturations as a function of changing the pressure differential across the fluid-fluid interface. Increasing the curvature of the convex meniscus of a non-wetting, invading (i.e. displacing) phase, for example, results in a net increase in invading phase saturation provided the increase in pressure is sufficient to permit the increased meniscus curvature to

Figure 1.1 Typical capillary pressure curve

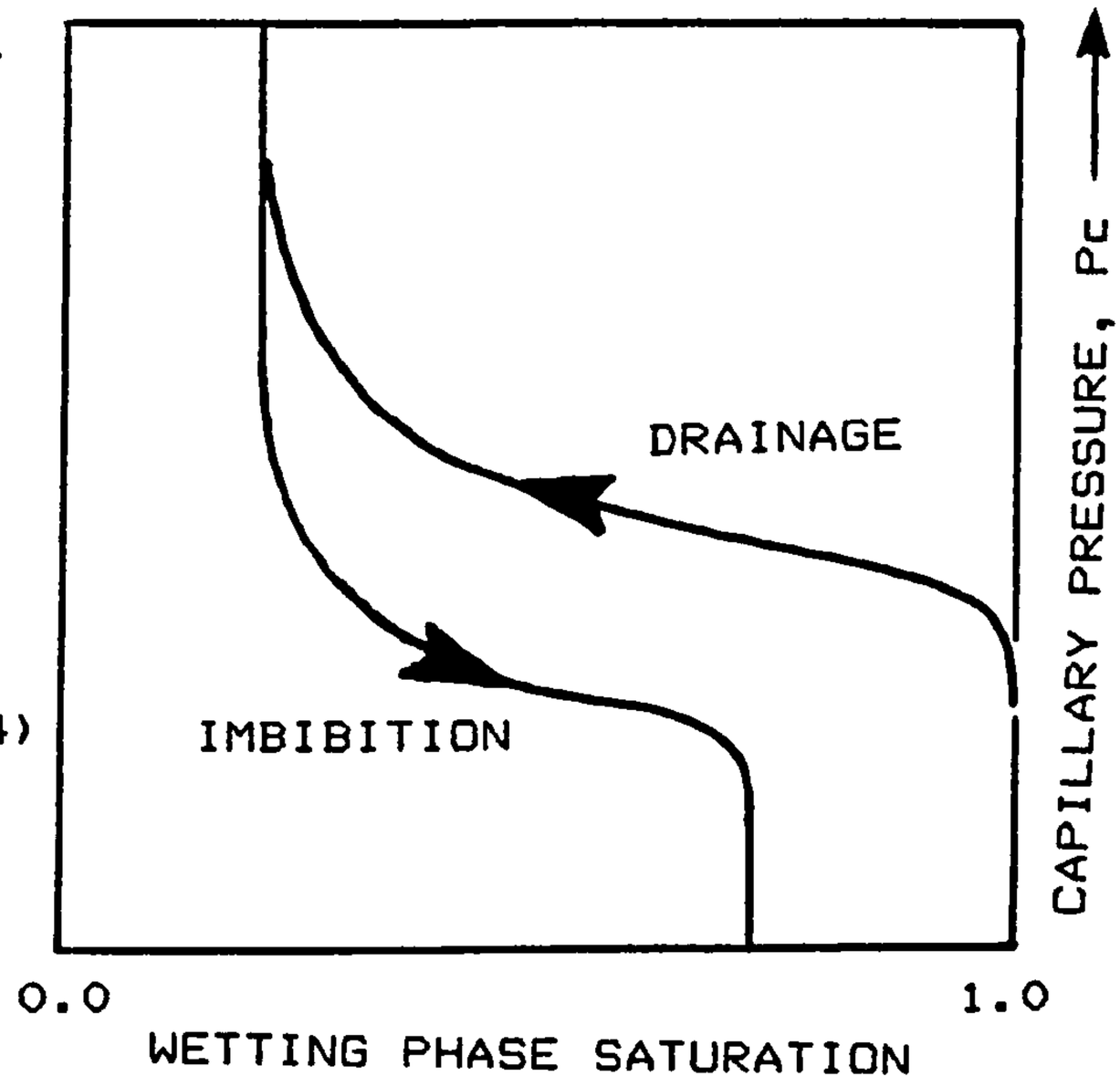

(after Melrose & Brandner, 1974)

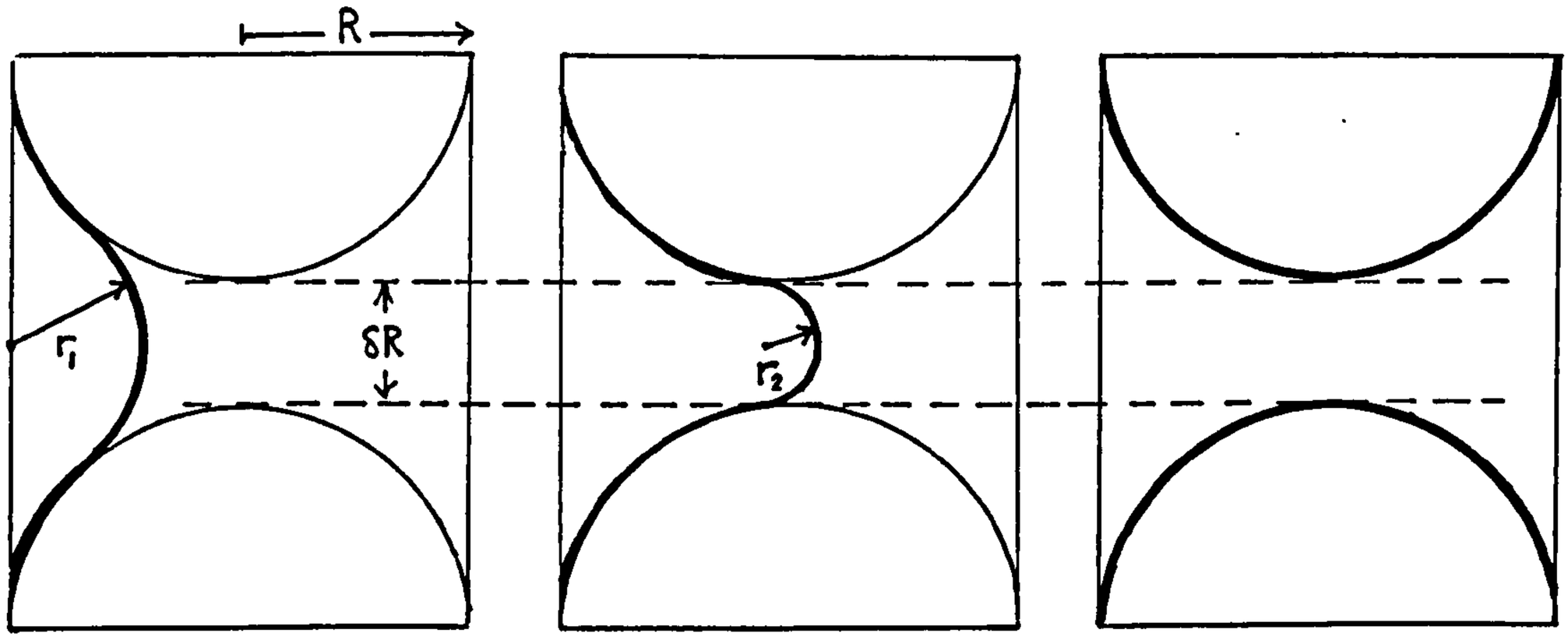

(a)

$P_c = 2\gamma / r_1$

$S_n < S_w$

(b)

$P_c = 2\gamma / r_2$

$S_n \leq S_w$

critical condition

for entry: $2r_2 = \delta R$

(c)

$P_c > 2\gamma / r_2$

$S_n = 1.0$

$S_w = 0.0$

Figure 1.2 Idealised 2-dimensional element of RCP pore space illustrating the control of structure (δR) on capillary pressure (P_c).

S_n = Saturation of non-wetting phase

S_w = Saturation of wetting phase

γ = Interfacial tension

pass through the pore opening, as shown in figure 1.2. Given the complete description of pore volume elements and pore opening elements for a porous medium it is, in theory, possible to derive the capillary pressure curve for that material. This approach is well known in principle (Scheidegger 1957, Dullien 1979), however the limiting factor in any practical application is generally held to be that the structure, geometry and topology of the pore space of most disordered porous materials are so chaotic that a precise physical description, based on observation, is beyond reach (see for example review of porous media properties in Pathak 1981, Heiba 1985, Sharma 1985, Jerauld 1985 and Ghabaee 1986). The purpose of the present work is to undertake just such a physical description for a specific random close packing of equal spheres, which embodies sufficient disorder to be representative of the general problem, whilst remaining a tractable proposition.

1.2 Sphere Packings

The study of sphere packings in general, and random close packing (RCP) in particular, is truly interdisciplinary. Studies involving packings of spherical particles span hundreds of years and many fields, from plant physiology (Hales 1727) to the design of novel nuclear reactors (Susskind et al 1970, Thadani and Peebles 1966). There are unifying themes running through all these works, however, which are those of three-dimensional space filling and irregularity.

The purpose of this section of the introduction is to review the

main fields where sphere packings are of interest (section 1.2.1) and subsequently to outline the development of interpretations of the structure of random close packing (RCP) of equal spheres.

1.2.1 The interdisciplinary nature of sphere packings

1.2.1.1 Some definitions

Some note regarding terminology is important here, because the term random close packing (RCP) is specifically taken to mean the local energy minimum configuration in space of an assembly of perfect, monodisperse spheres. Such a description of random close packing only emerged during the 1960's following the work of Bernal (see Bernal and Mason 1960 for example), Finney (1968) and Scott (1960, 1962). One of the most characteristic and constant attributes of RCP is that volume fraction of the packing which is occupied by the solid phase (i.e. the spheres). This volume fraction is termed the packing density, and for RCP it is generally held to be consistent with a value of 0.636 ± 0.001 (Gotoh and Finney, 1974). Random Close Packing is very reproducible in terms of many of its overall physical properties. Such uniformity is, of course, attained in the statistical sense, since no two discrete packings can have component spheres with identical spatial co-ordinates. Just as no two physical RCP structures can be precisely identical, computer visualisation of RCP do not all converge on the same structure, since there exists no simple algorithm for computing sphere packing structure without producing long-range order (Ziman, 1982).

Forms of sphere packings which do not represent RCP include all

regular packings in which some form of identifiable lattice or exact periodicity is a characteristic property. Such regular packings are well reviewed by Graton and Fraser (1935), Allen (1982, 1985), Haughey and Beveridge (1969), Hrubiseck (1941) and Mason (1968). Other forms of packing embodying disorder, but not conforming to maximum packing density are also well known. Such packings are generally known as loose, and have been shown to be characterised by packing densities of around 0.60 to 0.61 (Haughey and Beveridge 1969, Scott 1960). Variations on the theme of random, but relatively low density arrays of spheres include very loose random packings which may be encountered in fluidised beds typical of certain chemical engineering processes (Ergun and Orning, 1949), and poured random packings in which spheres are poured directly into a container (Haughey and Beveridge, 1969).

1.2.1.2 Hydrology and Soil Science

The earliest systematic use to which sphere packings have been put is attributable to hydrologists and soil scientists, as models for examining fluid flow and capillary properties of soils. Schlicter (1899) introduced the expression "ideal soil" to describe the use of regular sphere packings to represent particulate soil systems. Since its introduction, the term ideal soil has taken on a wider meaning and has been applied to any packing of equal sized spheres (Green and Ampt 1912, Waldron et al 1961, Smith 1933, Morrow and Graves 1969). The mathematics and physics of capillary processes within a variety of sphere configurations were developed extensively during the 1920's and 1930's, despite the absence of a detailed understanding of the overall structure of real, disordered packings

(Keen 1924, Haines 1925, 1927, Fisher 1926, Hackett and Strettan 1928, Wilsdon 1924, Smith 1933, Smith et al 1930, 1931).

1.2.1.3 Geology: Physical Sedimentology

Packing of detrital particles in a rock produces sedimentary structures of considerable importance. The primary deposition of particles and their primary packing impacts directly on the subsequent porosity, permeability and capillary properties of the final rock. Not surprisingly, therefore, sphere packings have been occasionally used as analogues for sedimentary deposition (e.g. Pettijohn 1957). Dealing with the geometry of several ideal and near ideal assemblages of spheres, Graton and Fraser (1935) completed an extensive analysis of the interstitial void spaces arising from a range of packings. Although not central to their arguments, they also identified the concept of "throat-planes", which are effective constricting regions of the pore space. Graton and Fraser concluded that their Case 6 configuration (a rhombohedral unit arrangement) is the most common form of packing, occurring as colonies within other configurations. Figure 1.3 shows the six unit cells considered by Graton and Fraser, and the associated unit voids are shown in figure 1.4. Fraser (1935) completed the Graton and Fraser (1935) treatise on the application of sphere packing studies to natural sediments. Allen (1985) makes reference to the significance of sphere packings as an analogue of sedimentary structure, and presents a very comprehensive review in his earlier work (Allen 1982). His review presents interesting summary diagrams showing the relationship between packing density (which Allen refers to as concentration) and co-ordination number, which is the mean

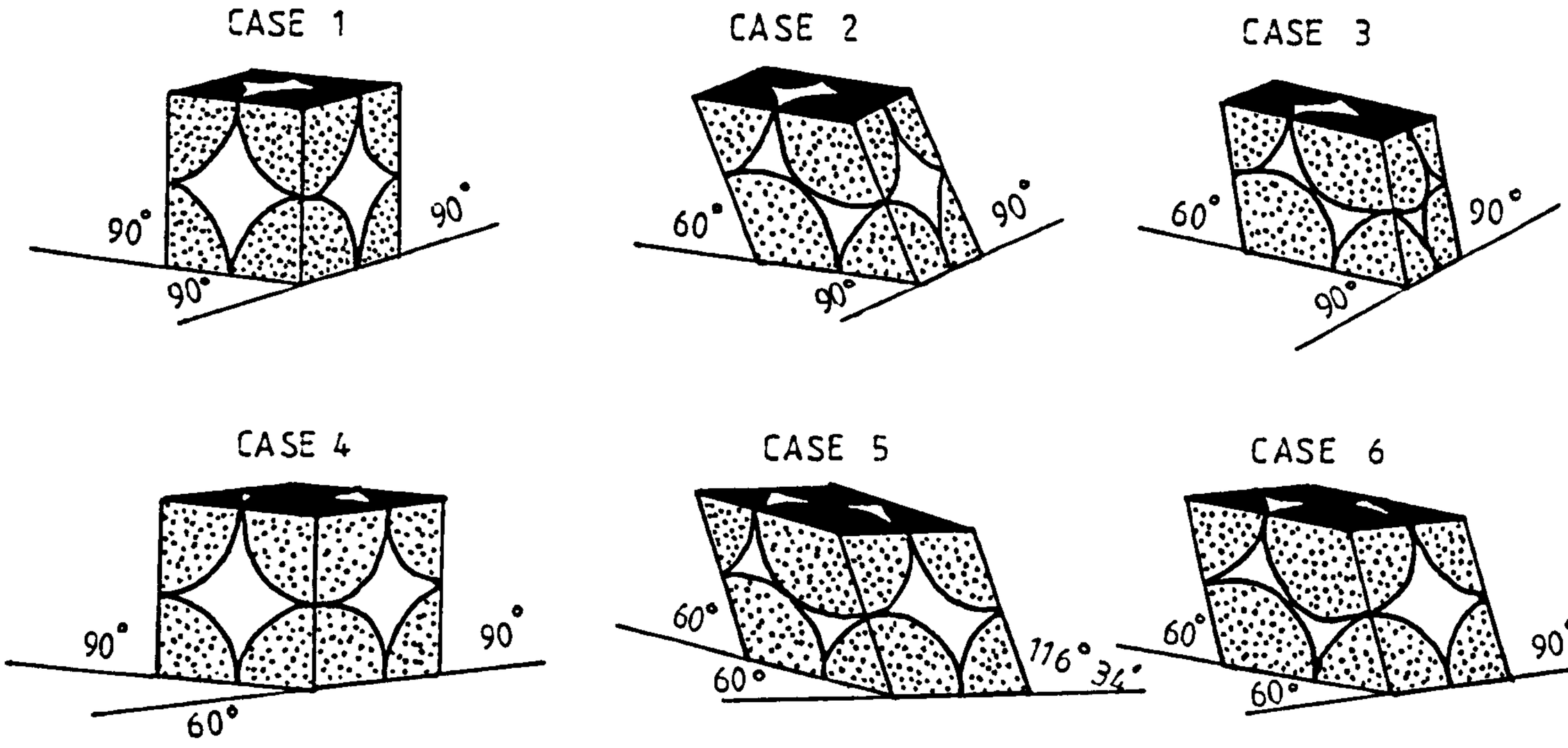

Figure 1.3 Unit cells of the six sphere packing cases studied by Graton and Fraser (1935). The angles shown are cell face angles.

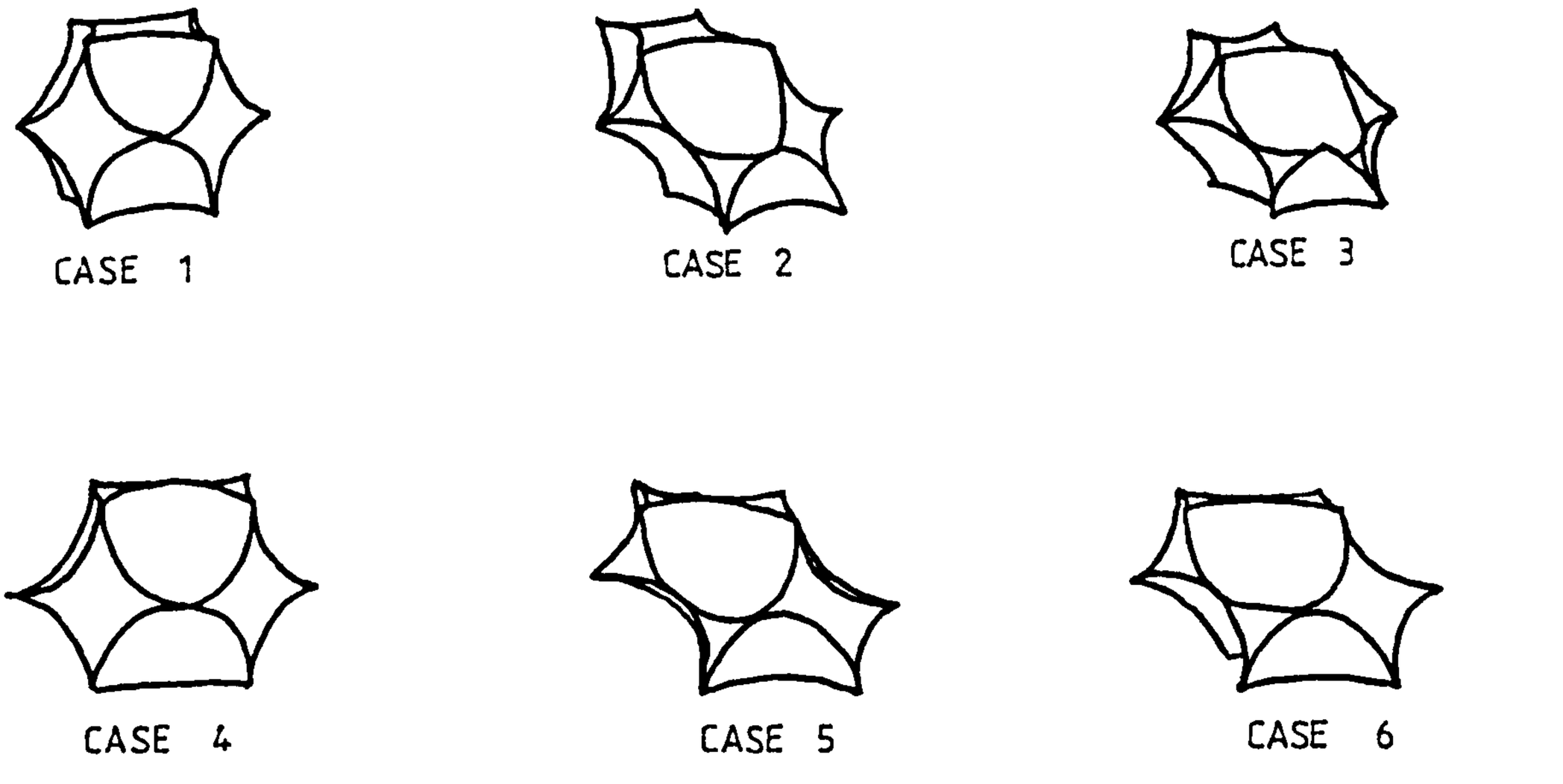

Figure 1.4 Unit voids of the six cases presented in figure 1.2 (after Graton and Fraser, 1935).

number of particle contacts per particle. These summary diagrams are reproduced in figures 1.5 and 1.6. It is not possible, however, to make any significant quantitative inferences regarding the capillary properties of any of the packing systems considered in Allen's work.

The nature of the packing between grains in real sedimentary rocks plays a signficant part in controlling the storage and permeation of fluids within the pore space. Chemical processes including the introduction of, and removal of, material within the pore space are consequently influenced by packing. Fatt (1958), however, has pointed out that microscopic examination of thin sections from consolidated sandstones shows that the grains are generally not in point contact as they are in sphere packs. In order to investigate this aspect Fatt experimented with compressible (rubber) spheres, measuring the porosities, electrical resistance of interstitial brines and permeabilities as functions of degree of compaction. Fatt's work was an early precurser to the grain consolidation model of Roberts and Schwartz (1985) and Schwartz and Kimminau (1987) discussed in section 1.2.1.4. The problems of physical sedimentology for which sphere packings are useful analogues are essentially those of the single phase interstitial fluid, in contrast to the two phase interstitial fluids (i.e. air and water) problem encountered in hydrology and agriculture.

1.2.1.4 Petroleum and Reservoir Engineering

Two phase and three phase interstitial fluid distributions are of considerable interest to petroleum and reservoir engineers. Combinations of phases can include oil, water and gas, and there is

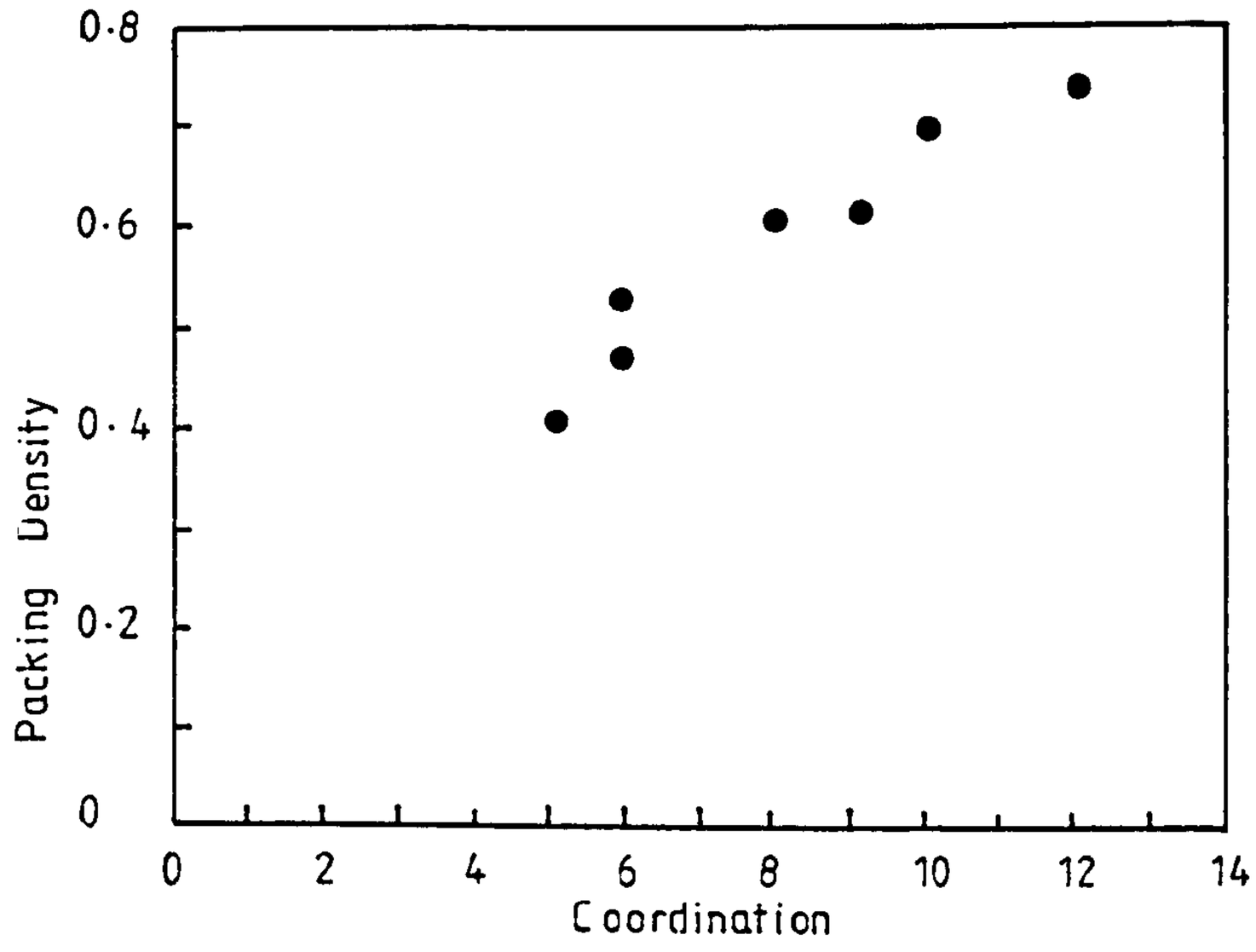

Figure 1.5 Packing density as a function of coordination in some simple sphere packings (after Allen 1982).

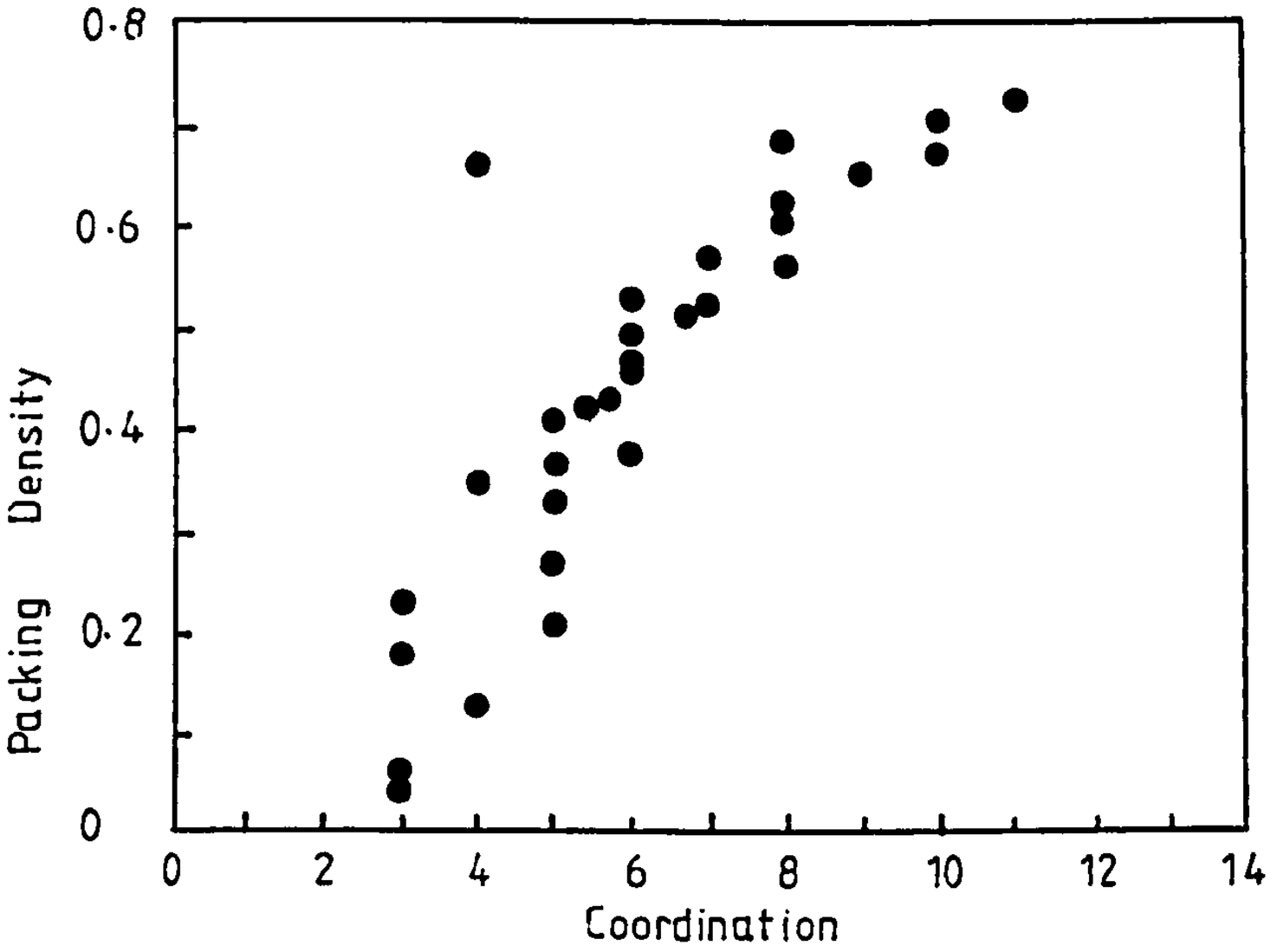

Figure 1.6 Packing density as a function of coordination in some non-simple sphere packings (after Allen 1982).

an extensive literature on this broad subject. Within that literature are numerous references to sphere packings. Morrow (1970), for example, makes reference to sphere packings in his review of basic principles relevant to the retention of connate water in hydrocarbon reservoirs, as do Melrose and Brandner (1974) in their review of the role of capillary forces in determining oil recovery efficiency during waterflooding of reservoirs.

During production of oil from porous reservoir rocks, significant residual quantities of oil remain entrapped and unproduced. Some proportion of this residual oil may exist as snapped-off ganglia and blobs of oil, surrounded by water, within the pore space. Egbogah et al. (1981) used a cubic packing of steel spheres in order to investigate experimentally the movement of residual blobs, or ganglia, of oil. In their study on residual oil saturation, Chatzis et al. (1982) used bimodal sizes of glass sphere in random packings.Two pack structures were used: in one structure clusters of small spheres surrounded by larger spheres were investigated, whilst the other structure consisted of clusters of large spheres surrounded by smaller spheres. Residual oil saturation was shown to be independent of absolute pore size (and therefore permeability) but was influenced by packing structure. The work by Egbogah et al. (1981) and Chatzis et al. (1982) may be regarded as an improvement and logical extension of the earlier work of Chatenever and Calhoun (1951), who used thin packings of spheres sandwiched between glass plates in order to visualise two phase displacement mechanisms.

Ng et al. (1978) presented a theory for the mobilisation of a blob in the pore space of a random packing of equal spheres. However,

because Ng et al. used average meniscus curvatures they were able to predict only average conditions for blob movement. Mason (1983) was able to use a model of the pore space of a random packing of equal spheres (Mason 1971) to estimate the specific theoretical probabilities of a particular oil blob advancing in single step jumps within the pore space. This theory was subsequently evaluated experimentally, using random sphere packs, by Yadav and Mason (1983) who found good agreement between theory and experiment. Mason and Yadav (1983) used the movement of a liquid blob within a packing of spheres to test the hypothesis that the capillary meniscus radius of a pore, when filling, is the same as the largest meniscus radius of the same pore when emptying. They found agreement between experiment and theory, confirming the hypothesis and lending considerable weight to the argument that multiple interconnections between the pores are largely responsible for capillary pressure hysteresis in RCP-like structures. Using the approximation for RCP radial distribution function proposed by Mason (1971), Mellor (1987) also demonstrated that the largest of the four tetrahedral pore throats is virtually identical to the tetrahedral pore cavity insphere radius for the same pore. This forces the result that an individual pore will drain and fill at the same pressure. An individual pore within RCP structure, therefore, cannot exhibit capillary pressure hysteresis, which must be considered to arise from interconnectivity between pores in the packing, as proposed earlier by Mason (1982). Mason and Morrow (1984) defined a procedure for calculating meniscus curvatures for the complex spatial configurations encountered in random sphere packings. Knowledge of the curvature of such menisci is central to any pore-level analysis of capillary-controlled processes within RCP

structures.

Within the field of petroleum engineering, there is frequent need for a rapid and low cost assessment of the range of sizes of pores which characterise a particular sample of reservoir rock. Although optical and electron microscopy methods are occasionally used to measure or visualise pore space (Soeder and Randolph 1984, Ruzyla 1984, Lin and Hamasaki 1983, Morgan and Gordon 1969, Wardlaw and Casson 1978), the most commonly used technique is that of mercury porosimetry. The basic method of mercury porosimetry is well known and will not be reviewed here (see Dullien 1979 and Scheidegger 1957 for comprehensive reviews) save to state that the so-called "pore size distribution" of mercury injection is in fact not the frequency distribution of pore sizes which the name implies. For reservoir rocks it is essentially impossible to use mercury injection to derive unique relationships regarding the distribution of pore throats, pore bodies and interconnectivities between these elements. RCP structures, however, have been used frequently as a reference material in mercury injection research programmes, primarily because RCP is a somewhat less chaotic system than reservoir rocks, for which independent meaningful estimates of pore dimensions are very difficult to achieve (Iczkowski 1967, Frevel and Kressley 1963, Bell et al 1981, Smith and Stermer 1985, Smith and Schentrup 1987, Smith and Stermer 1987 and Smith et al 1987).

Another area of interest within the field of reservoir engineering, in which sphere packs have been used, is the general problem of electrical conduction within porous media. This is of interest in terms of the static distribution of interstitial fluid phases which

can be deduced from direct electrical measurements, and forms the basis of several downhole (electric) logging techniques. Roberts and Schwartz (1985) introduced the idea of the grain consolidation model as a way of understanding the basic phenomenon of electrical conduction within granular materials. The model begins with a disordered, monodisperse sphere pack and proceeds by uniformly growing the spheres to progressively choke off the pore space, simulating compaction and diagenesis. This model is developed further by Schwartz and Kimminau (1987), and is a special case of the void percolation problem for spheres posed by Elam et al, (1984). Using simple models based on regular sphere packings, Yuan (1981) argued that the formation resistivity factor and Archie's lithological exponent are both sensitive to pore co-ordinaton, a packing controlled phenomenon. Arulanaden and Mehan (1977) extended work begun by Willie and Gregory (1953) using packings of spheres and other objects to show that particle shape, pore geometry and packing all have a significant influence on the formation resistivity factor. Sen et al (1981) conducted experiments on fused glass beads to evaluate a theoretical self-similar model of sedimentary rocks relevant to determining the dielectric constant of water saturated media. Perez-Rosales (1981) used packings and suspensions of spheres, amongst other shaped granules, in order to investigate experimentally the relationship between resistivity and formation factor.

Petroleum engineering is essentially a pragmatic discipline which deals with multiphase fluids in porous media. Very often the problems encountered are either extremely ill-posed or intractable at the level of the individual pore. Sphere packings have been

consistently useful in elucidating some of the key physical processes central to the industry.

1.2.1.5 Chemical Engineering

Chemical engineers are mainly concerned with sphere packings within the context of the design and performance analysis of packed beds. Unless it is sufficient simply to estimate gross average properties, the chemical engineer needs some detailed understanding of hydrostatic, rheological, hydrodynamic and mass/energy transport coefficients for his particular system. In addition, information on acoustic, optical or electrical properties may be required. It is axiomatic that none of these properties can be predicted a priori unless an understanding of the bed structure is available. With this in mind, Haughey and Beveridge (1969) reviewed some 239 papers directly relevant to the structural properties of packed beds for chemical engineering processes. Within this review the concepts of disorder, packing densities and distributions of void space emerge as important, although the effects of polydispersity, sedimentation, pouring and departures from spherical shape are also significant for many engineering applications. The variation of local voidage is of particular interest in defining transport coefficients, and has been studied by Haughey and Beveridge (1966), Thadani and Peebles (1966), Lees (1969) and Franzen (1979). The problems associated with forming homogeneous and reproducible packings are addressed in the monograph of Gray (1968) and by Van Brakel and Heertzes (1974). Variations in flow properties of packings adjacent to confining walls have been examined by Cohen and Metzner (1981). Chemical engineering research continues to address the problem of sphere pack

structure (e.g. Le Goff et al 1985) which is regarded as extremely complex, and for which no complete description has yet been given (Dodds 1980).

1.2.1.6 Solid State Physics

The history and development of solid state physics has, for the most part, been consistent with the physics of the crystalline state. Within the last few years, the study of amorphous, non-crystalline materials has emerged as a large field in its own right, and useful reviews of the juxtaposition of studies of amorphous, disordered systems and the old, crystalline solid state physics are found in Ziman (1982) and Zallen (1983). The significance of RCP structure to solid state physics is that the Bernal model of liquid structure (e.g. Bernal 1959) represents the simplest possible structural model of the liquid state upon which thermodynamic calculations may be made. This feature of conceptual simplicity often forms the basis of the main objection to the Bernal model which is that the RCP system has a hard sphere potential by definition; this is unrepresentative of real liquids which are characterised by soft potentials (Pang et al, 1973, for example). Nevertheless, the notion of RCP structure as an analogue for the liquid state is still seen as the key to any quantitative or qualitative understanding of the physics of liquids (Ziman 1982, Rowlinson 1970). Because the Bernal model is equivalent to a liquid at its densest possible configuration (i.e. a disordered solid) it has become widely used as a model of the solid state appropriate to certain amorphous metallic glasses. Thus the largest and most detailed physical model of random close packing of equal spheres ever built is that of Bernal's

student, Finney (1968), which was originally conceived as a liquid structure model. Since that time, however, Finney's RCP model has been extensively used in understanding amorphous solid materials (Ichikawa 1975, Cargill 1975, Finney 1977, Finney 1981, Cargill 1981 (i), Cargill 1981 (ii), and Finney et al 1982). Despite the same sort of objection to the hard sphere potential which applies to the liquid structure analogue (see for example Koskenmaki 1976), RCP is currently viewed as the most satisfactory general model for the structure of amorphous metals (Zallen 1983).

1.2.2 Interpretation of RCP structure

Before reviewing briefly the development of interpretations of RCP structure, some definitions of relevant terminology are given.

1.2.2.1 Packing density

Packing density is defined as the fractional solids volume:

$$\rho = \frac{v}{v + v_o}$$

where v = the volume of sphere solid, and v_o = the volume of interstitial space. The average packing density is now widely recognised as one of the characteristic features of RCP structure.

Whilst the definition of packing density is simple, measurement of packing density is far from simple. The main difficulty encountered

in measuring packing density lies in dealing with the container wall. In order to avoid introducing regular layers of spheres building up against the container wall, the surface of the container must be made irregular. This may be achieved by a variety of methods, including mechanically dimpling rigid containers, and using deformable bladders held in tension around the pack. Although the introduction of regular layers of spheres is eliminated by these procedures, the wall of the container becomes, in effect, an integral part of the packing itself. Measured densities of such packings have been shown to be dependent upon the size of the container. The most successful method of removing this size dependency is the so-called extrapolation to infinite volume method, devised by Scott and Kilgour (1969). The basis of this method is to make several discrete sphere packings in a number of dimpled cylinders of various radii. The resulting straight line graph of measured packing density against reciprocal cylinder radius is then extrapolated to zero reciprocal radius. The packing density at this value corresponds to that density which would be obtained with a container of infinitely large radius.

Although a wide variety of methods and materials have been used in the past to determine average packing density for sphere packings (Hildebrand and Scott 1962, Rutgers 1962, Westman and Hughill 1930, Smith et al 1929, McGeary 1961, Ayers and Soppet 1965, Susskind and Becker 1966), there is only a small number of density determinations of direct relevance. In two separate experiments, Scott (1960, 1962) achieved estimates of 0.637 for RCP packing density. Bernal and Finney (1967) derived an average figure of 0.6342 for 407 Voronoi polyhedra constructed from co-ordinates from Scott's (1962)

experiment, and succeeded in showing that the polyhedra represented quite a wide distribution of densities within the packing. The figure of 0.6342 obtained by Bernal and Finney agreed moderately well with the figure of 0.64 obtained by Bernal and Mason in their earlier estimate (1960). The two most definitive experimentally derived estimates of average RCP packing density are those of Scott and Kilgour (1969) and Finney (1968). Scott and Kilgour used the extrapolation to infinite volume method to derive an estimate of 0.6366 ± 0.0005, based on a series of measurements of RCP structures with up to 80000 spheres in an individual pack. Finney (1968) obtained a value of 0.6366 ± 0.0004 for his packing, although his later work suggests that a little less precision may be appropriate. Gotoh and Finney (1974), for example, agree that the experimental evidence supports a value of 0.636 ± 0.001, and a statistical-theoretical argument is presented which provides arguably the best theoretically based estimate of packing density as 0.6357. A curious feature of experimentally derived packing densities is that, within experimental error, they converge on 2/pi.

The packing density of RCP is extremely useful, as it provides an "instant" check on the integrity of the pack. Values of packing density less than 0.636 ± 0.001 are indicative of loose, or poured packings.

1.2.2.2 Co-ordination number

This is defined as the number of other spheres in direct contact with a given, reference, sphere. For an individual sphere, this is not generally held to be particularly useful (Mason 1968), and it is

more customary to quote the average co-ordination number of the packing, or to present the co-ordination number frequency distribution function for the packing.

The term is occasionally broadened to include all spheres within a certain distance, as for example in the case of Bernal's structural neighbours (Bernal 1965) which increases the co-ordination distance out from 1.0 sphere diameters to 1.05 sphere diameters. Bernal also proposed structural co-ordination distances of 1.5 and 2.0 sphere diameters, but these alternative definitions have largely fallen into disuse.

1.2.2.3 Radial distribution function

The definition of radial distribution function is the probability of finding a sphere within a certain distance of the centre of a reference sphere. Radial distribution functions are therefore probability distribution functions. In practical terms it is only possible to measure the frequency with which a sphere is found within a certain distance of the reference sphere. Experimentally determined radial distribution functions are therefore frequency distributions, presented as histograms. Theoretical radial distributions, in contrast, are often presented as continuous curves.

Experimentally derived radial distribution functions are conventionally normalised by dividing the observed frequency in each interval by $4\pi r^2$. It is common practice to calculate an average radial distribution function for sphere packings. This is achieved

by averaging the observed frequencies within each interval for several reference spheres in the packing.

The terms Pair Correlation Function and Pair Distribution function are occasionally used instead of radial distribution function, particularly in statistical mechanics. The terms pair correlation function and pair distribution function have identical meaning, and are equivalent to the radial distribution function for all practical purposes.

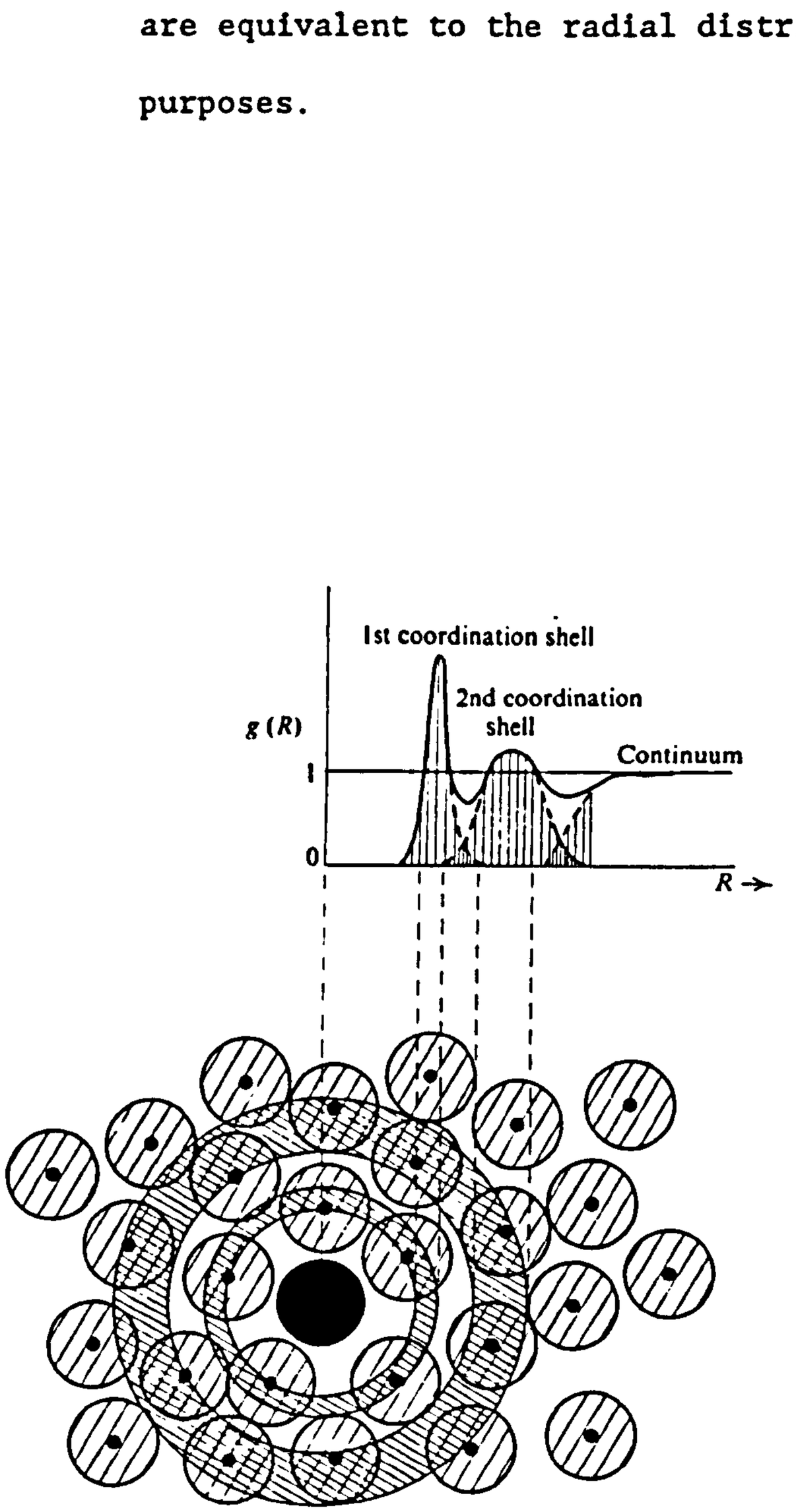

Figure 1.7

Neighbour distributions of the radial distribution function for an idealised two dimensional case.

(after Ziman, 1982)

The physical signficance of the radial distribution function is that it can be measured for random close packings of equal spheres, and can also be calculated for simple liquids from neutron and X-ray diffraction data. Early studies on the physics of liquid structure and the solid state made much use of the radial distribution function. Since the mid 1970's the radial distribution function has been used largely for validating computer simulations of RCP, and for teaching the basic physics of amorphous solids at the undergraduate level. Figure 1.7 shows an idealised theoretical radial distribution function for a two dimensional array of discs.

1.2.2.4 Geometric neighbours and Voronoi polyhedra

There is, for any point in an array, a region containing all space which is nearer to that point than to any other point. In three dimensional arrays these regions are polyhedra, and are called Voronoi polyhedra or Dirichlet zones after the mathematicians who formalised them. The significance of these polyhedra is that they pack together to fill space completely, and can be uniquely defined for any random sphere packing for which co-ordinates are known. Any point around a central point which contributes a face to a Voronoi polyhedron is, by definition, identified as a geometric neighbour. The number of faces of a Voronoi polyhedron is therefore identical to the number of geometric neighbours for the sphere at the centre of that polyhedron. In two dimensions, the Voronoi cell is a polygon, and the principle of Voronoi division in two dimensions is illustrated in figure 1.8 (two Voronoi cells are shown shaded in that figure). The properties of Voronoi cells are central to the present work, and are discussed in much more detail in Chapter 2.

Figure 1.8

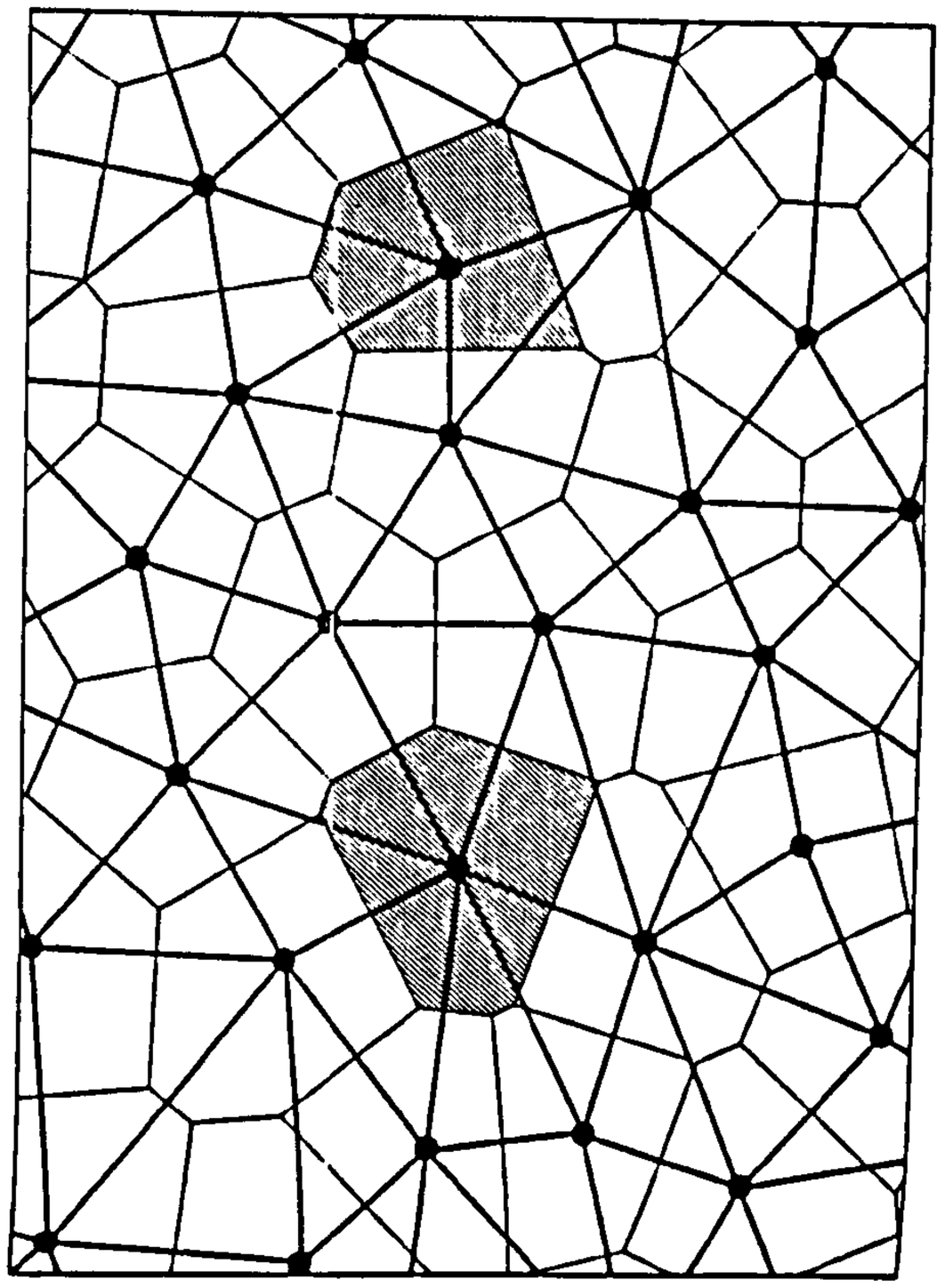

Voronoi division of space in 2 dimensions. Heavy dots denote random (sphere) centres.

1.2.2.5 Angular Distribution Function

This function may be defined by considering a reference sphere and two adjacent spheres. One of the adjacent spheres defines a pole to the reference sphere, and the other adjacent sphere defines a plane containing the pole. The angular positions of the remaining spheres in the same co-ordination shell are then calculated relative to these polar co-ordinates, and the process is subsequently repeated for all other triple sets of reference and adjacent pairs to yield average values. The distribution is attributable to Scott (1964) and, although undeniably a valid description of RCP space, it is not commonly used.

1.2.3 Physical Realisations of RCP Structure

1.2.3.1 Early attempts

Hales' (1727) is probably the first account of the kind of space filling problem addressed here. He was interested in the swelling properties of peas, which he constrained in an iron pot with a heavy lid. Roughly describing the resulting compressed peas as "pretty regular dodecahedrons", he provides the basic clue to the structure of randomly packed spheres. Many years later, Bernal (1962) repeated Hales' experiment using chalk-dust covered plasticene spheres, and found a predominance of polyhedra with five edged

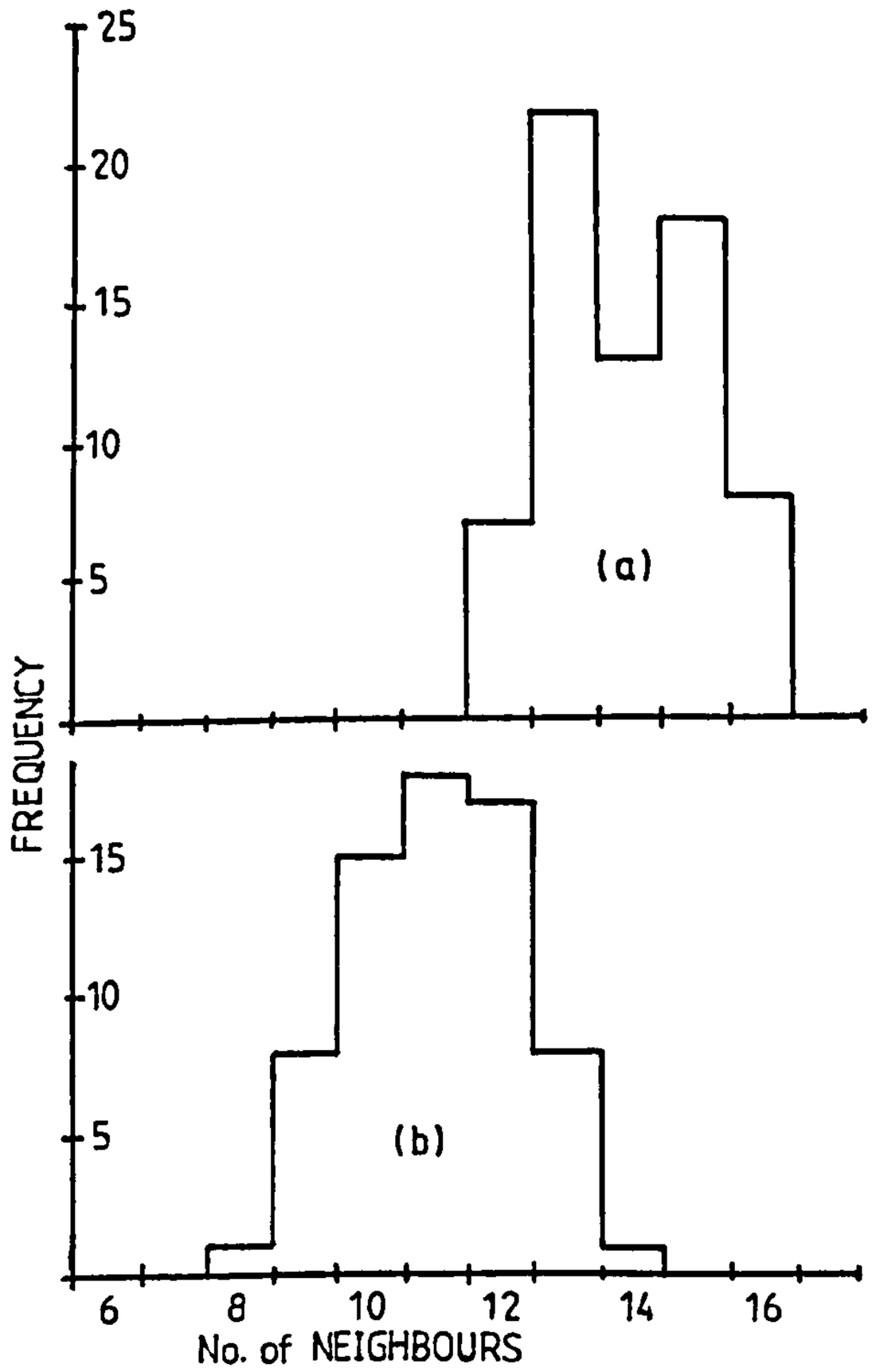

Figure 1.9

Histograms of (a) geometrical and (b) physical neighbours derived from plasticene spheres.

(after Bernal, 1959)

faces. More importantly, the number of pentagonal faces varied over a wide range as shown in figure 1.9, confirming that there is not a simple polyhedron "unit cell" in random packings. This is consistent with the findings of Marvin (1939) and Matzke (1950) who had also repeated Hales' experiment using lead shot, finding a predominance of fourteen sided polyhedra, frequently with pentagonal faces. The distribution of co-ordination (i.e. the variation in numbers of neighbours) was recognised by Bernal (1959, 1965) as a property of the packing. The problem of estimating co-ordination within a packing without first compressing it has been addressed by Smith et al. (1929). They packed lead shot into a container which was subsequently filled with acetic acid and then drained. Liquid bridges of acetic acid formed at contacts, which attacked the lead forming the base acetate as white marks on the lead shot surfaces. Packings at several different densities were achieved, and dismantled for contact counting, though none of these packings conforms exactly with RCP structure. The results of Smith et al are presented in figure 1.10. Bernal solved the problem of finding immediate co-ordination number distributions by pouring black japan paint into a packing of steel ball bearings contained in a balloon (Bernal and Mason, 1960). The balls had come straight from the manufacturer, and had a light coating of grease so that the paint ran off, except where liquid bridges formed at the contacts and near-contacts. After the paint had dried, the pack was stripped of several hundred outer balls, and dissected for contact counting. The results are shown in figure 1.11.

Figure 1.10

Coordination numbers for packings of lead shot (after Smith et al 1929)

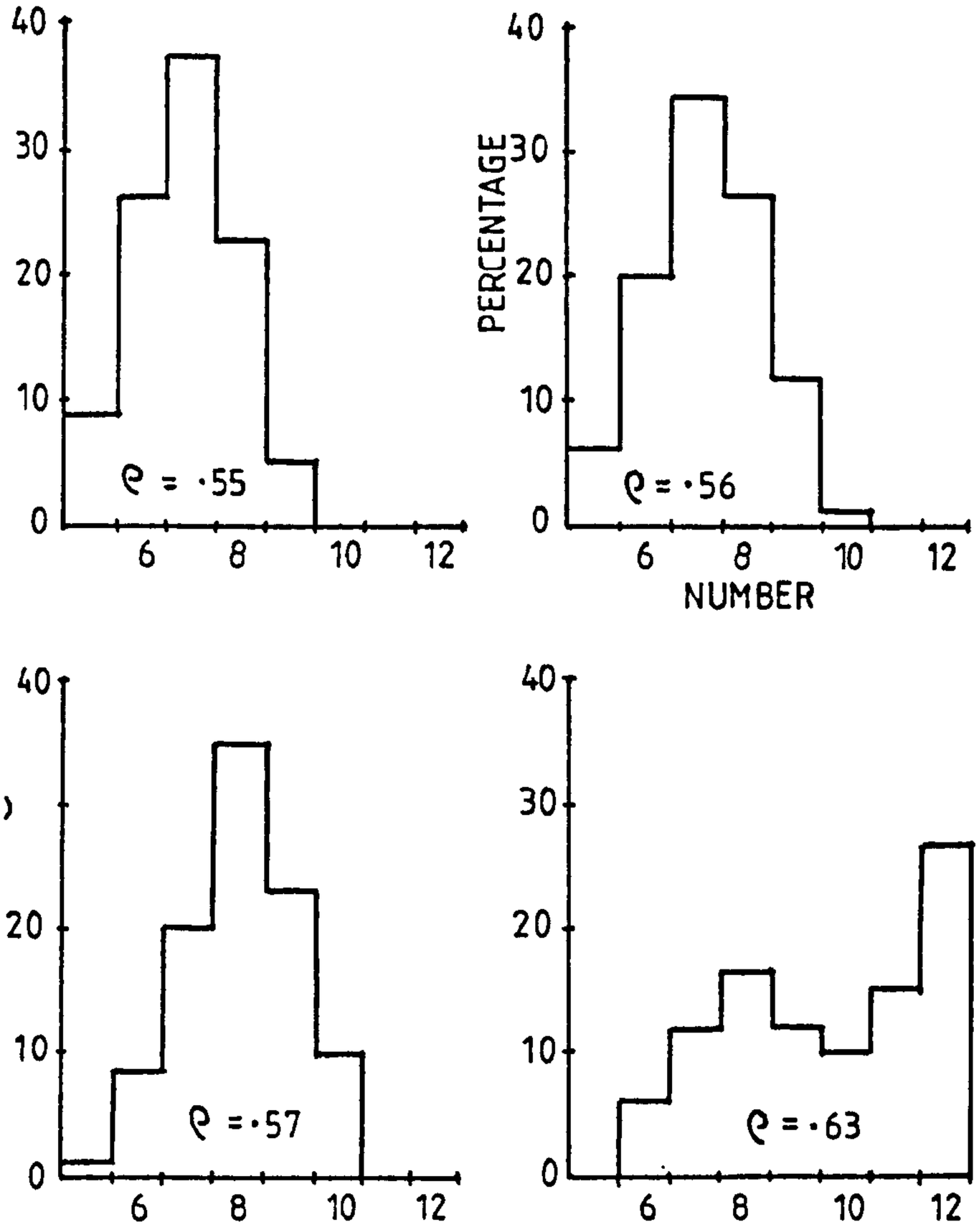

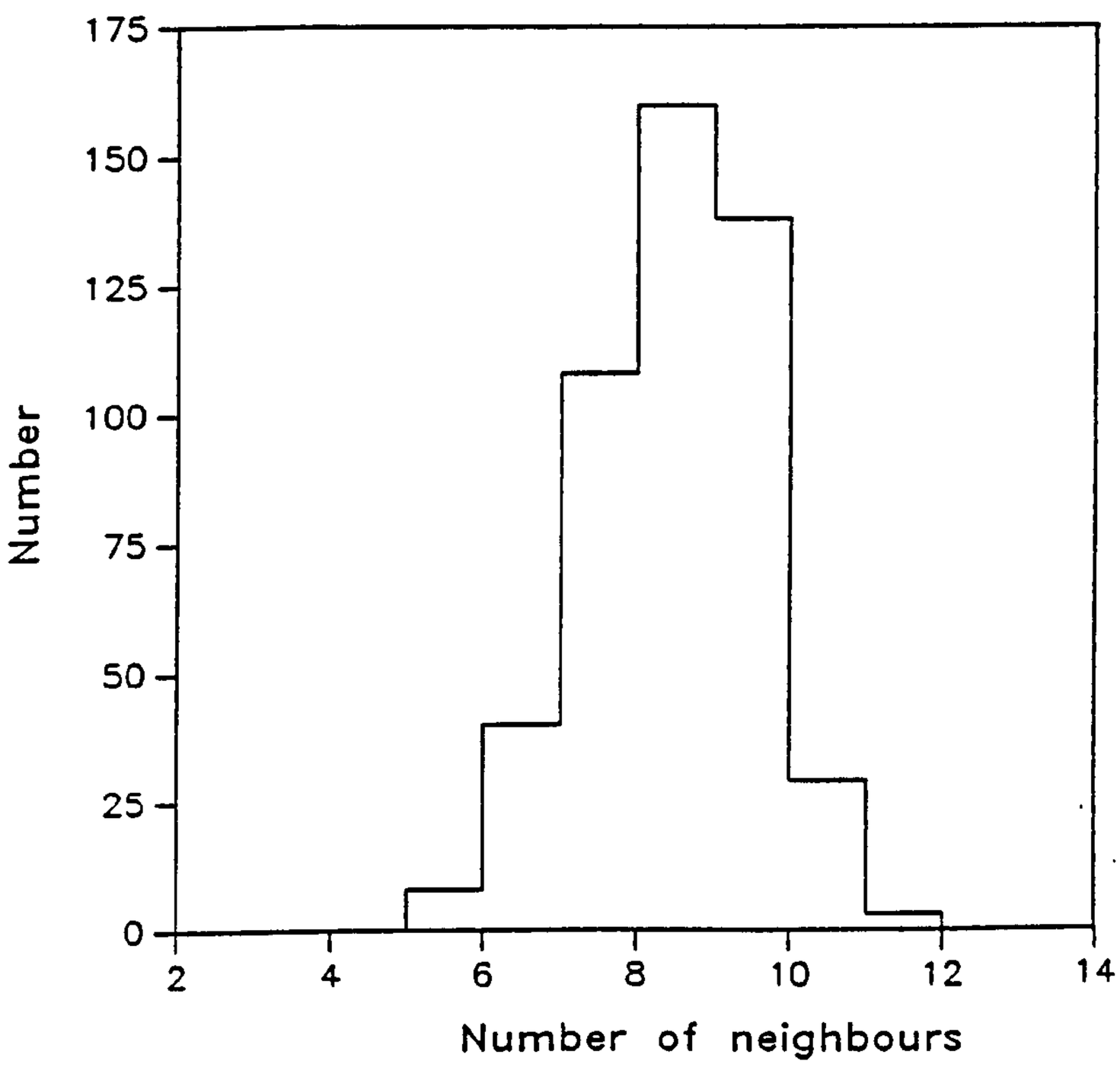

Figure 1.11

Histogram of contact numbers (coordination) from paint-coated ball bearings

(after Bernal and Mason, 1960)

1.2.3.2 Bernal's and Scott's models

Shortly following the paint and ball bearing experiment, Bernal began the task of randomly close packing 1000 steel balls, with the intention of dissecting the packing piece-by-piece to determine all the individual sphere co-ordinates. Unknown to Bernal, Scott was working on the identical task, and had forwarded to Bernal an advance copy of his publication (Scott 1962) at about the same time as Bernal's own work was ready for publication. At this point Scott and Bernal exchanged information and Bernal continued his analysis largely on the results of Scott's Model (Bernal 1965). Scott's was therefore the first detailed analysis of RCP structure, albeit by a very small margin. Scott determined the radial distribution function for his packing for intervals of $^1/_5$ of a sphere diameter. His radial distribution function is reproduced in figure 1.12, and the Voronoi edge and face statistics for Scott's packing are shown in figure 1.13.

The similarities between distribution functions for the Scott model and the Bernal model are very marked, as shown in figure 1.14 which compares both models with the structure of a simple liquid (argon) based on neutron diffraction data. Mason (1968) derived an elegant method for compensating for the boundary limitations of finite packings, enabling the resolution of the radial distribution function for the Scott packing (with one or two co-ordinate corrections by Bernal) to be enhanced, as shown in figure 1.15. The distribution of cumulative near neighbours within a radial distance of between 1.0 and 1.5 sphere diameters was also derived from the Scott model by Mason (1968), and is shown in figure 1.16.

Figure 1.12

Scott's radial distribution function

(after Scott, 1962)

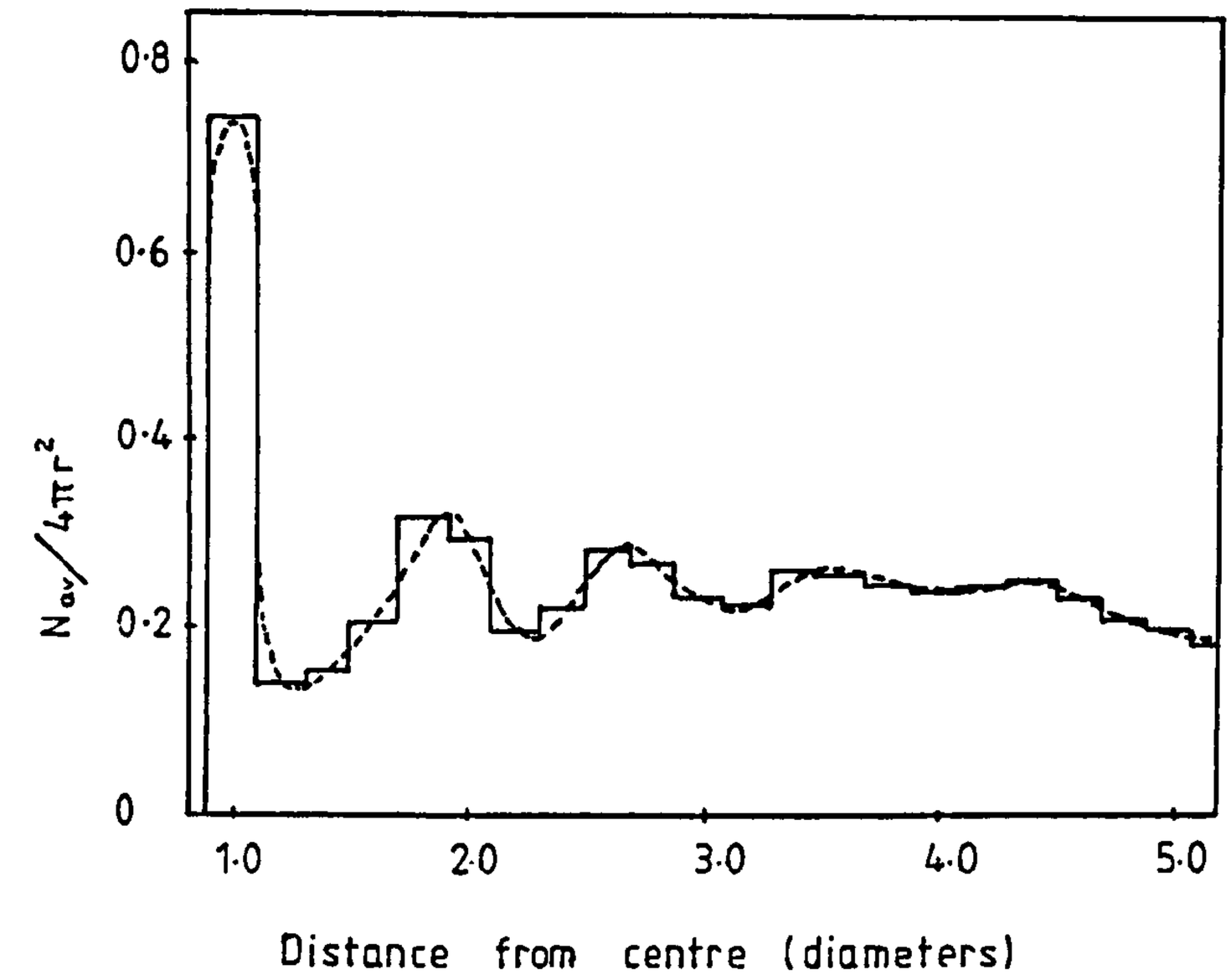

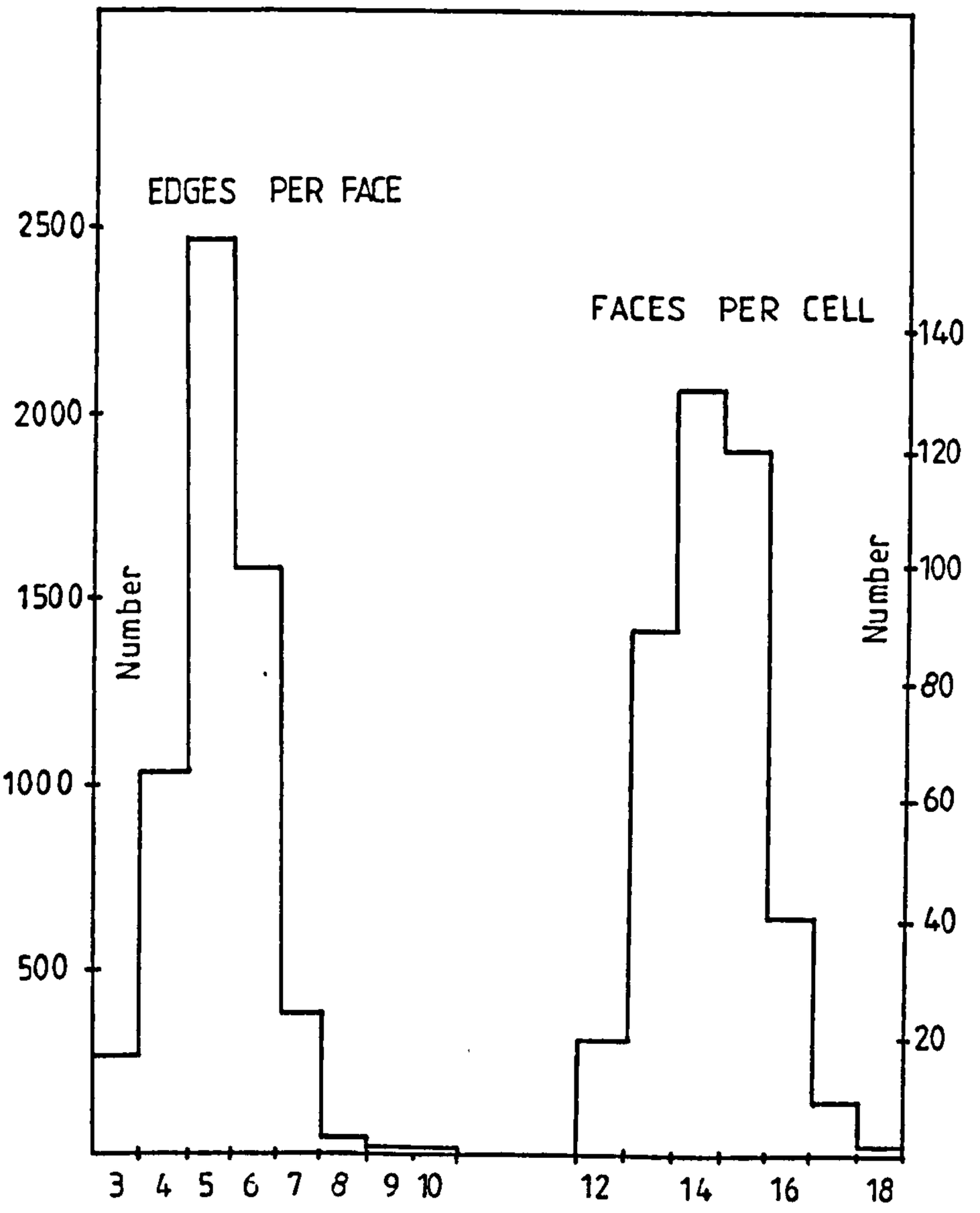

Figure 1.13

Voronoi polyhedra face and edge statistics for the Scott model

(after Finney, 1968)

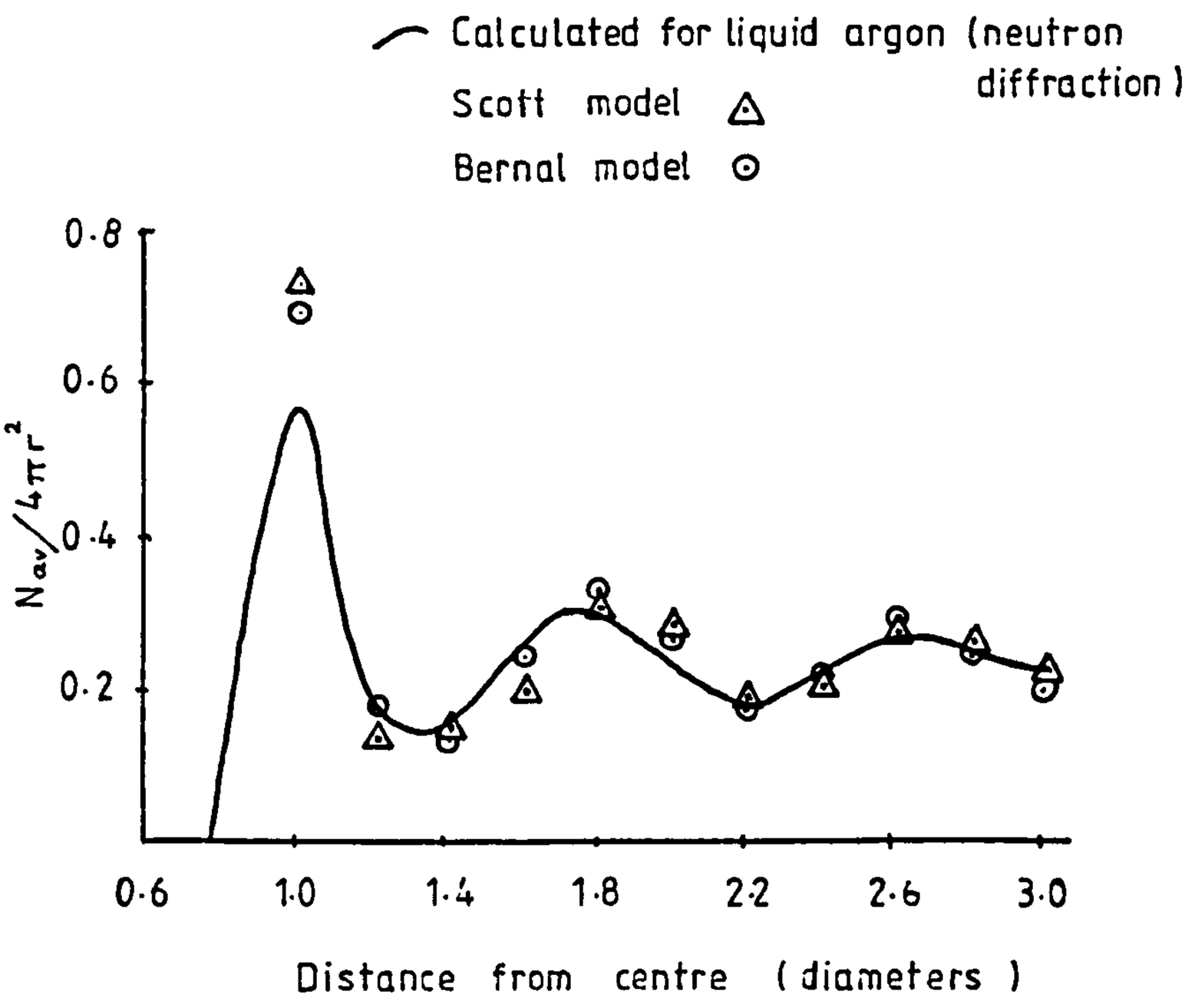

Figure 1.14

Radial distribution function for Bernal and Scott models

(after Bernal 1965)

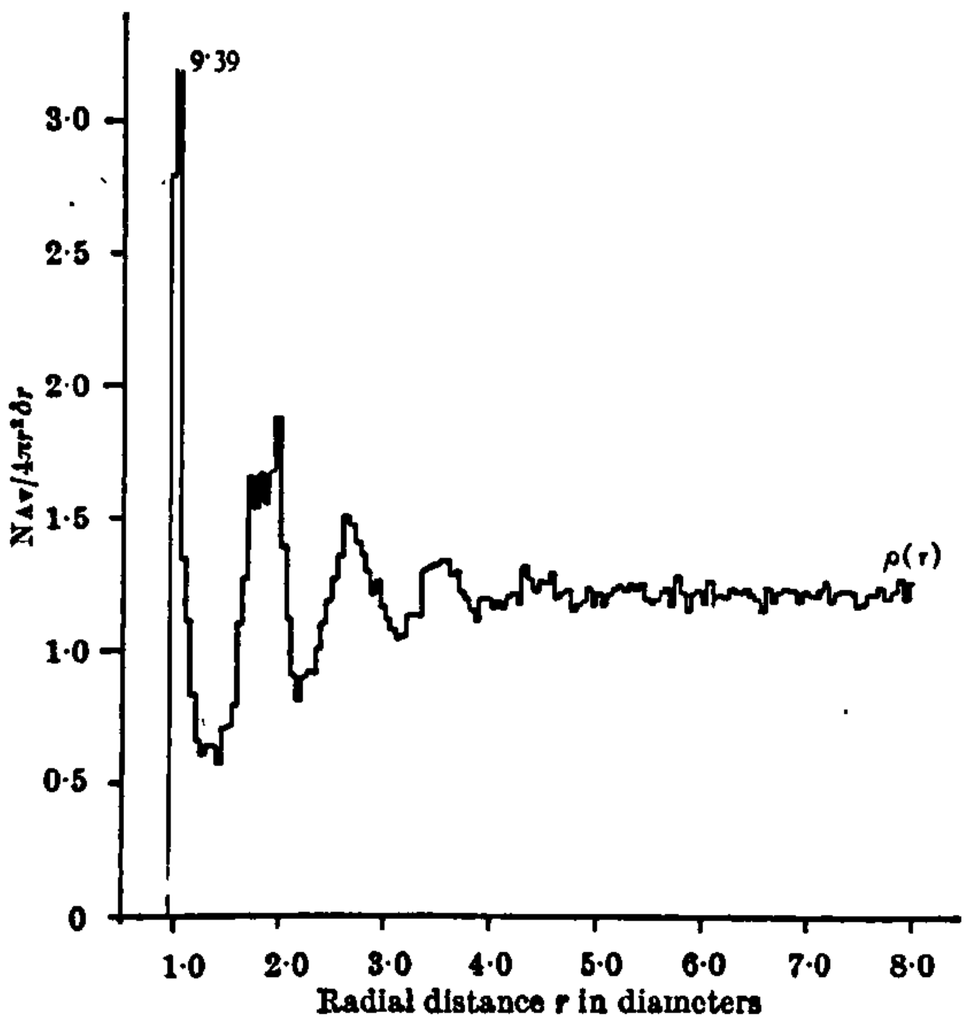

Figure 1.15

Radial distribution function for Scott model - enhanced using Mason's correction

(after Mason, 1968)

Figure 1.16

Cumulative near neighbour distribution function for Scott's model

(after Mason, 1968)

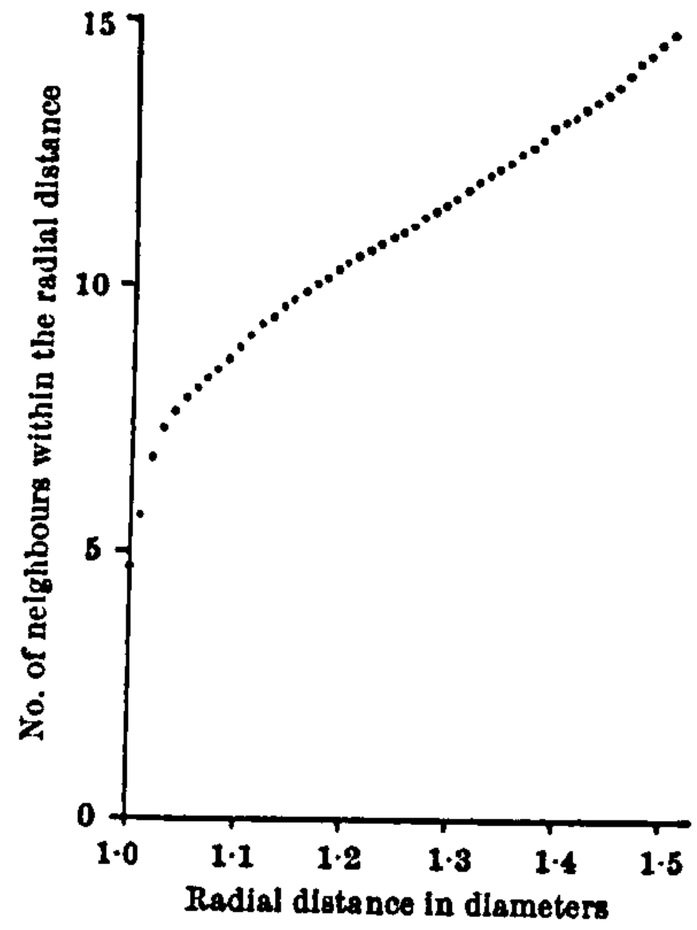

1.2.3.3 Finney's model

The limitations of the size of the packing and the measuring accuracy of Scott's model were 1006 spheres and approximately ± 1% in co-ordinate position respectively. This error in co-ordinate position corresponds to about ± 1.4% error in the distance between sphere centres (Finney, 1968). In order to improve on both these limitations, Finney (1968) constructed a large packing of about 17000 spheres, with an estimated precision of around ± 0.6% in the distance between sphere centres for the central 8000 spheres. After setting the packing in wax, and stripping back approximately 9000 of the outer spheres Finney measured the co-ordinates of the remaining 7934 spheres. The radial distribution function for the Finney packing is shown in figure 1.17 and comparisons between the Scott packing and the Finney packing for Voronoi polyhedral faces and edges are shown in figure 1.18 and 1.19 respectively.

Although larger RCP structures had been built both before Finney's (e.g. Susskind and Becker, 1966) and after (Scott and Kilgour, 1969), no co-ordinate measurements were performed. Finney's packing thus remains as the largest, and most accurately measured RCP structure for which sphere centre co-ordinates exist. The task of constructing and measuring this packing took Finney several months. It seems unlikely that a larger physical model will ever be constructed and analysed.

1.2.4 Computer realisations of RCP structure

Computer programs which simulate packings of spheres find application in a wide variety of areas. However, there is one feature of interest common to virtually all computer models of sphere packings, namely that of validation. When a program has been developed and de-bugged, some standard or reference is helpful in checking that the code is satisfactory. Despite the substantial

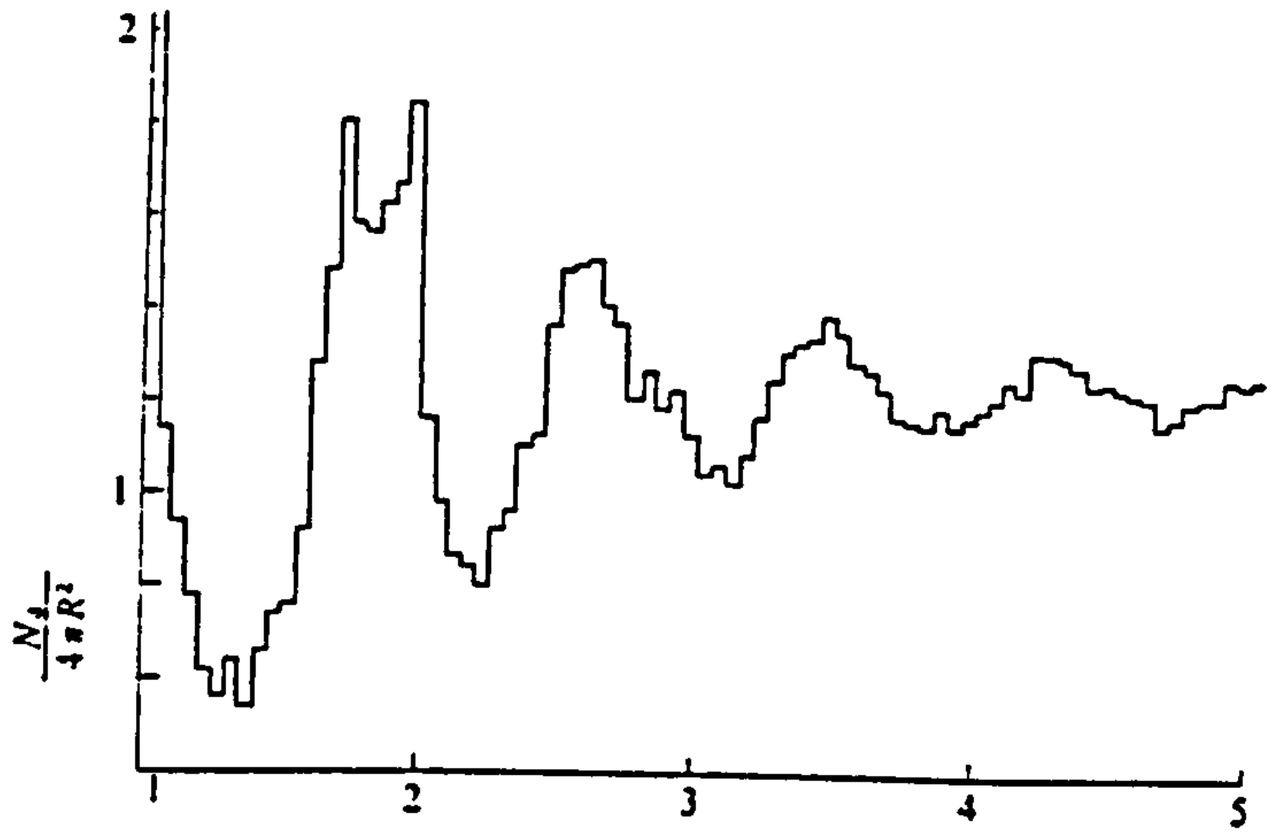

Figure 1.17

Radial distribution function for the Finney model.

(after Finney, 1968)

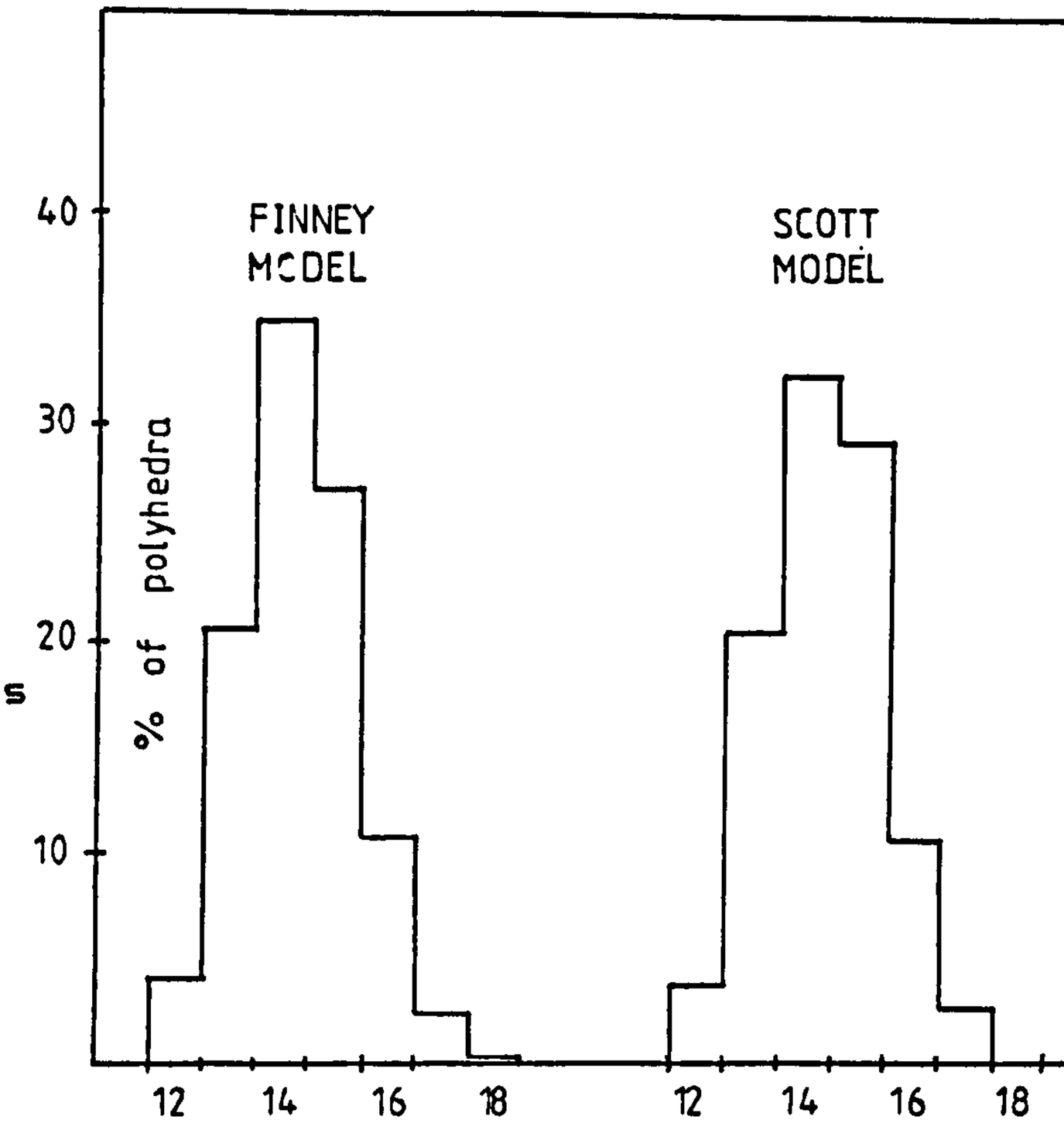

Figure 1.18

Distribution of Voronoi polyhedron faces per cell for Scott and Finney models

(after Finney, 1968)

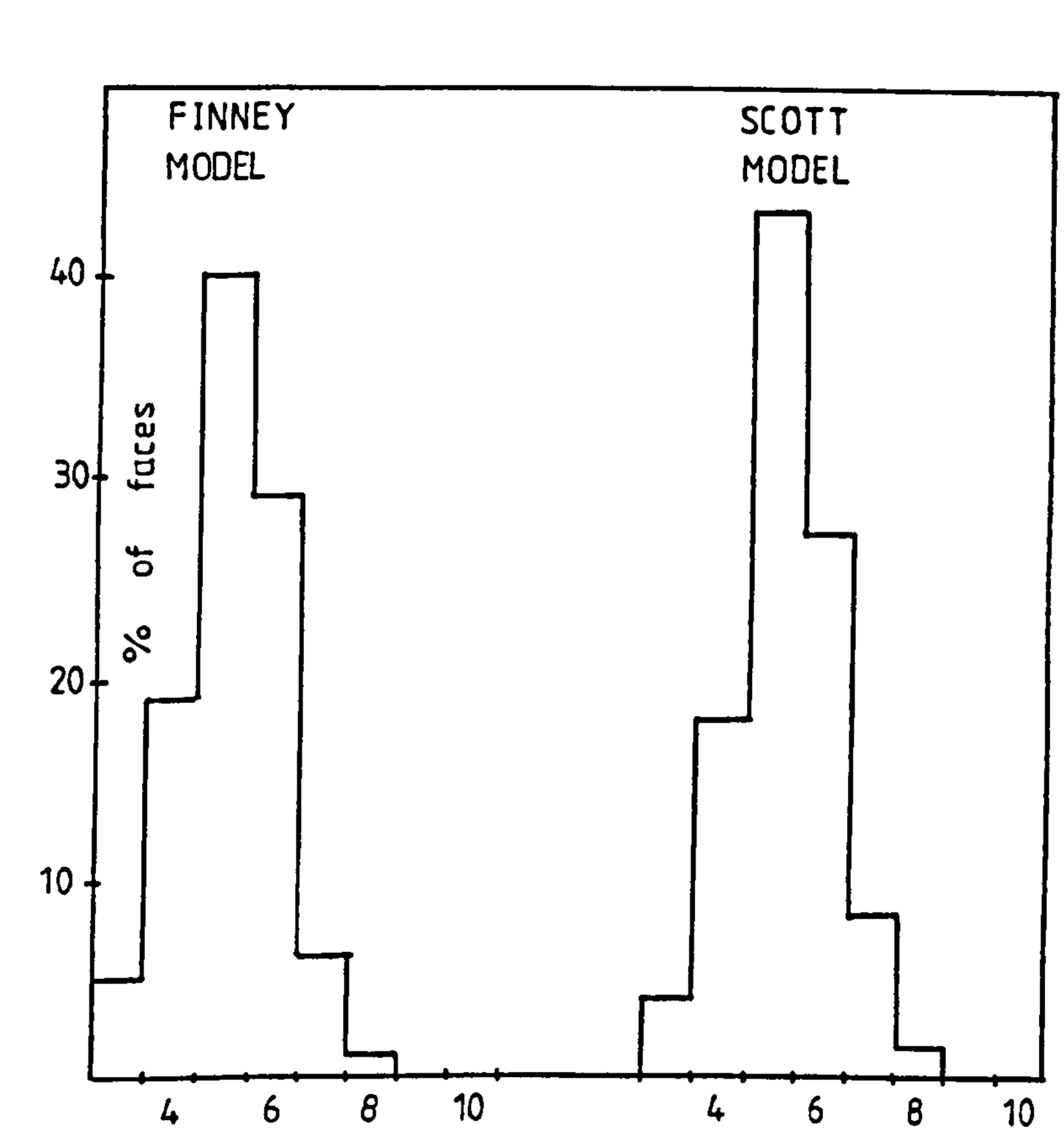

Figure 1.19

Distribution of Voronoi polyhedron edges per face for Scott and Finney models

(after Finney, 1968)

improvements in computer hardware and program development over the past twenty years, the basis for this point of comparison with the "right answer" remains broadly constant. Invariably some property of the Finney model (or occasionally the Scott model) is used. Typically, the property selected is either the radial distribution function, or the packing density. Frequently it is both.

Early computational models produced packs with consistently low values of packing density. Tory et al (1968) produced a pack with an average density of 0.59 using a simulation of sedimentation of spheres from a dilute slurry. This value is more consistent with loose random packing than RCP, as is the value of 0.609 arrived at computationally by Levine and Chernick (1965). Bennett (1972) developed a method of computing aggregates of several thousand spheres by depositing successive spheres, one at a time, onto a small seed cluster. Each deposited sphere contacted three already present in the seed cluster, and was not permitted to be subsequently moved. The resulting aggregate is completely determined by two factors - the seed cluster and the criterion used to select the deposition site. Bennett used two different criteria, one global to the aggregate, and one satisfying only local conditions on the aggregate surface. Using the global criterion, Bennett obtained packing densities of between 0.62 and 0.63, whilst the local criterion yielded values of around 0.60. All packing densities obtained by Bennett were somewhat lower than the Finney model average value of 0.6366, although an improvement over earlier attempts had been achieved. In addition to deriving estimates of average packing density, Bennett also produced radial distribution functions (pair correlation functions) for comparison with the

Finney model, as shown in Figure 1.20.

Visscher and Bolsterli (1972) developed a Monte Carlo approach to random sphere packing, by simulating the dropping of spheres into a container. Their method produces packings formed under a unidirectional (gravitational) force. This is a critical point, since RCP requires a radial force in order to produce an isotropic packing. Not surprisingly, therefore, Visscher and Bolsterli's estimates for packing density are between 0.58 and 0.60, fractionally lower than experimentally determined values of loose random packing.

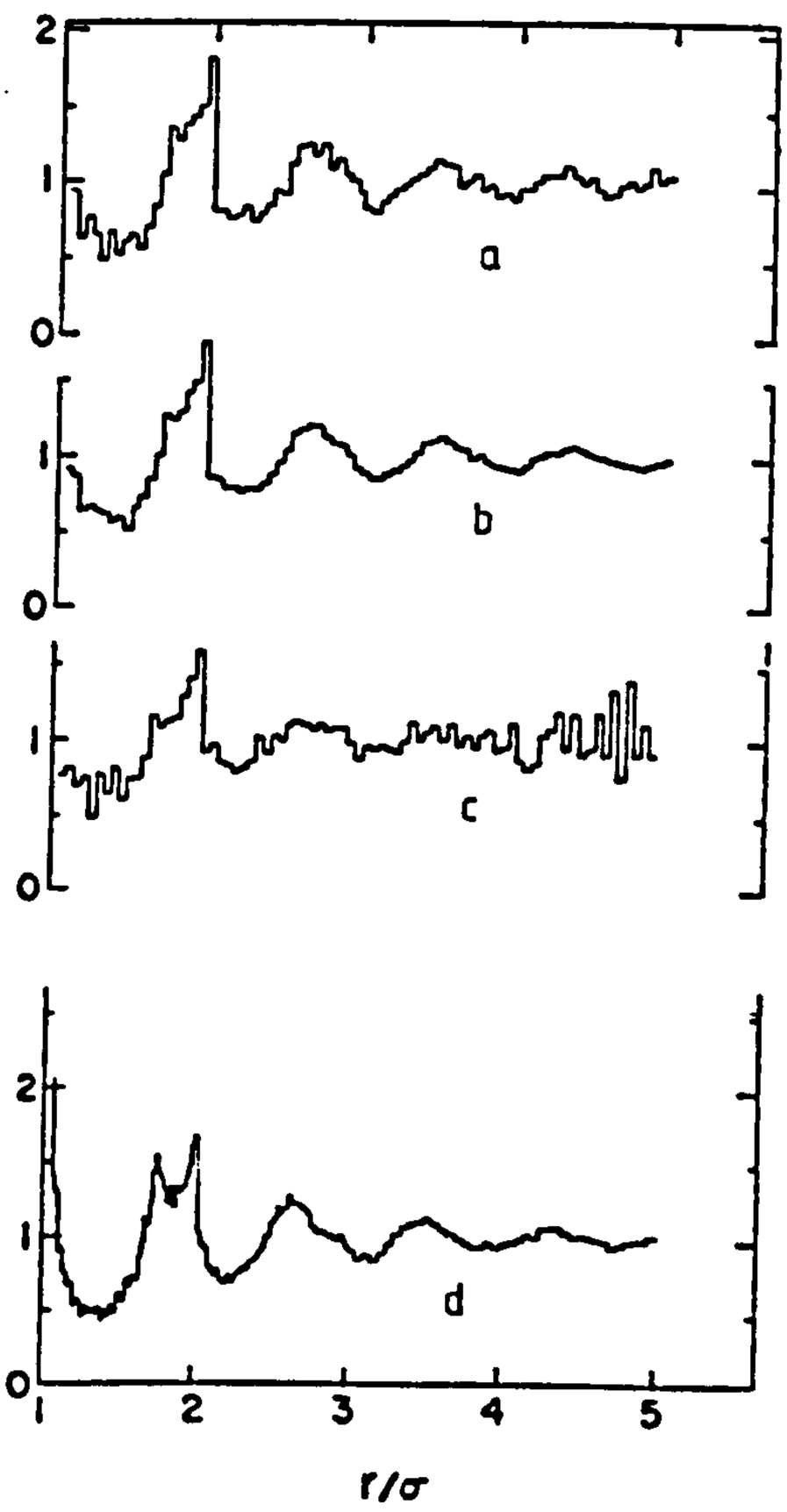

Figure 1.20

Pair correlation functions for Bennett's hard sphere packing.

a) Simulation of 1600 spheres: global criterion.

b) Simulation of 3999 spheres: global criterion.

c) Simulation of 1500 spheres: local criterion.

d) Finney model, radial distribution function.

Adams and Matheson (1972) described a serial aggregation method, adding spheres to touch three other spheres, conforming to the rule that the next sphere added must be on the site nearest to the cluster origin. This is analogous to the global criterion of Bennett (1972). The best packing density achieved by the Adams and Matheson model is 0.628, which is moderately close to the experimentally determined value of 0.6366 (Finney, 1968, Scott and Kilgour, 1969), though still outside the accepted value of 0.636 ± 0.001 (Gotoh and Finney, 1974). Adams and Matheson derived the radial distribution function for their model, comparing it directly with that of the Scott model, both models having first been corrected for finite sample size using Mason's (1968) correction, as shown in figure 1.21.

Figure 1.21

Pair distribution functions:

a) Adams & Matheson, 3900 spheres.

b) Scott model, 800 spheres.

(both models adjusted for finite size using Mason's correction)

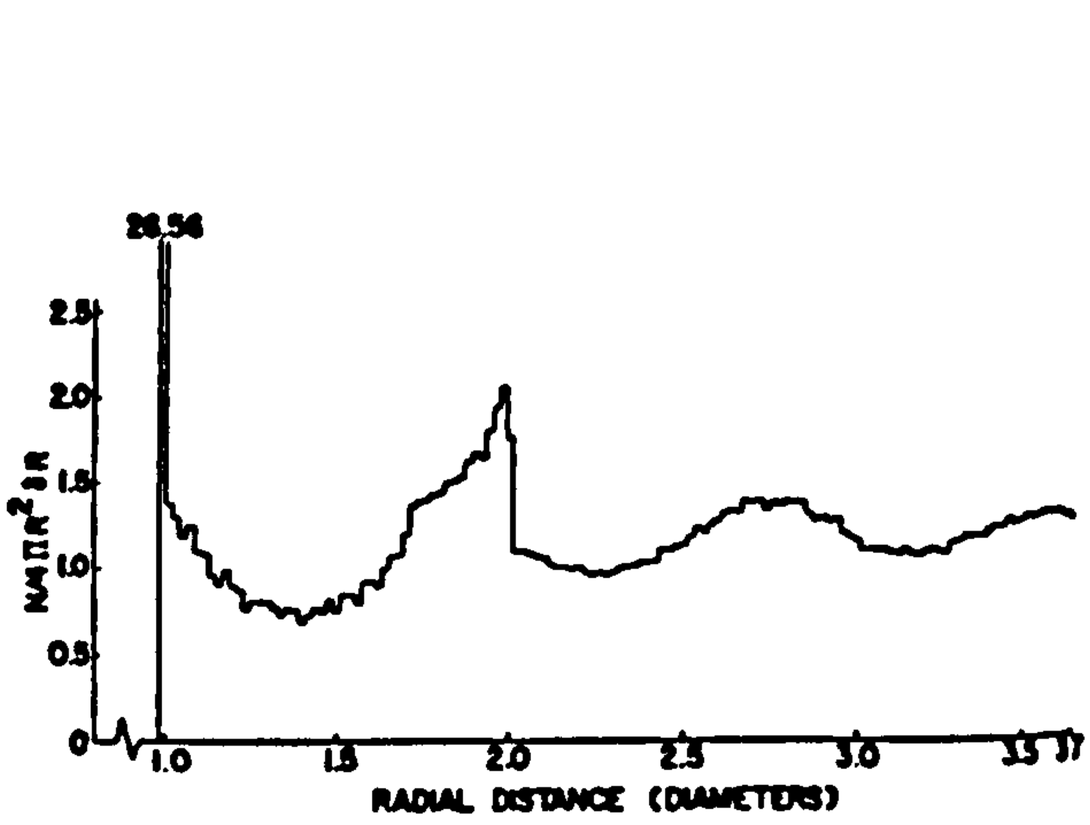

Tory et al. (1973) developed the concept of very slow settling of rigid spheres from a dilute slurry, to form a packed bed. Their simulation prohibits bumping, or bouncing of spheres into more stable locations, and consequently produces the rather low packing density of 0.58. Tory et al. also compared their radial distribution function with that of the Scott model, although they are careful to point out that their implicit uni-directional anisotropy effectively smooths out features in the distribution.

Matheson (1974) reported a method, similar to that of Bennett (1972) and Adams and Matheson (1972), using serially deposited spheres on a cluster. Obtaining an average packing density of 0.606, Matheson also produced comparisons between the radial distribution function for his model, and those for both the Finney and the Scott model as shown in figures 1.22 and 1.23 respectively.

Although Matheson is clearly reproducing the essential features of loose random packing, he makes the strong suggestion that RCP models characterised by packing densities of 0.6366 are not true random packings at all. Rather, Matheson proposes, RCP is a structure consisting largely of small ordered groups of spheres. In support of this somewhat desperate claim, Matheson points out that up to the date of his own work (1974), no algorithm had been found which could simulate observed RCP packing densities, despite intensive efforts by a considerable number of workers. This suggestion has subsequently been shown to be without foundation, though at that time, simulation of RCP structure must have seemed like an almost intractable problem.

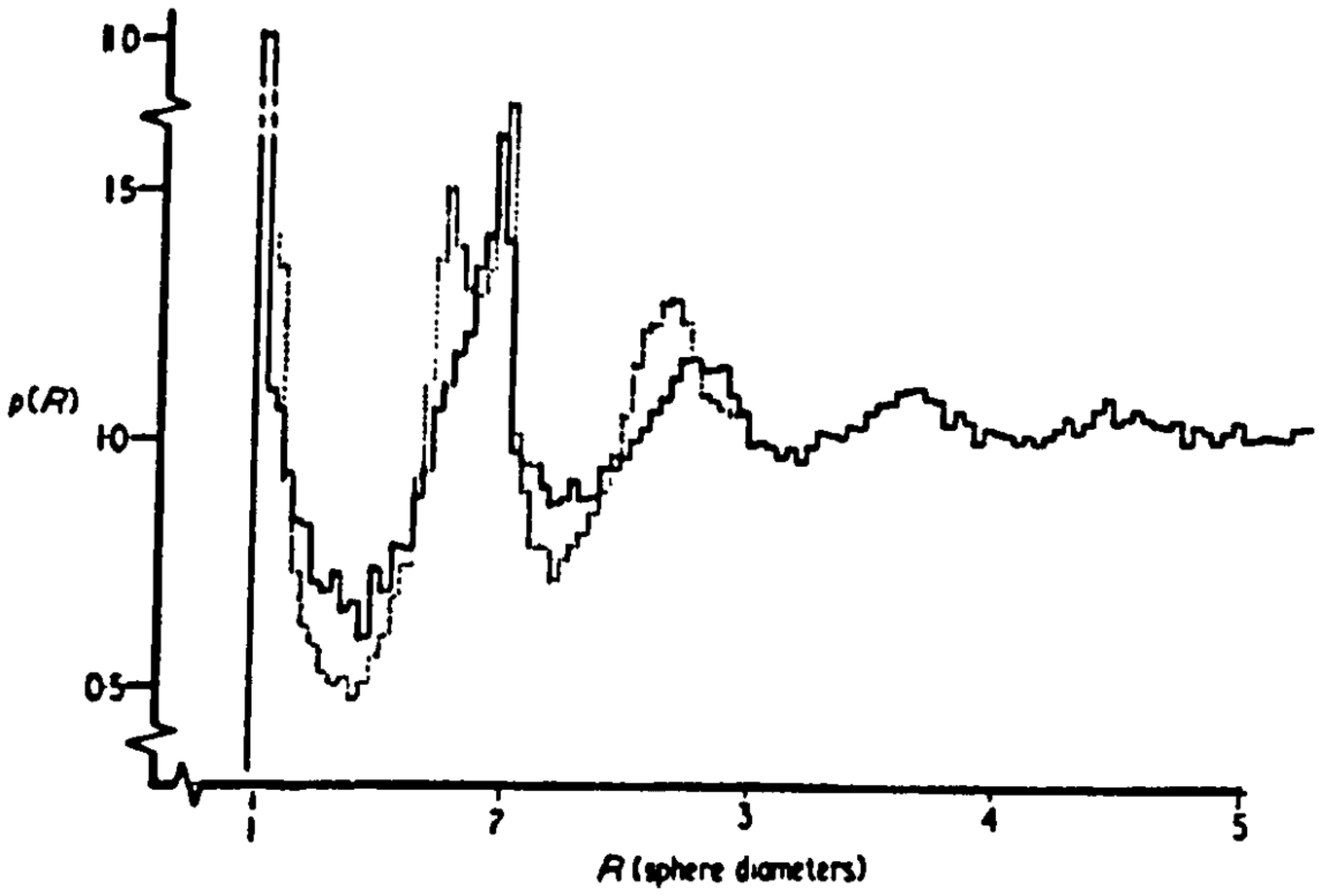

Figure 1.22

Comparison of the Matheson radial distribution function with that of the Finney model (shown dotted)

(both models adjusted for finite size using Mason's correction)

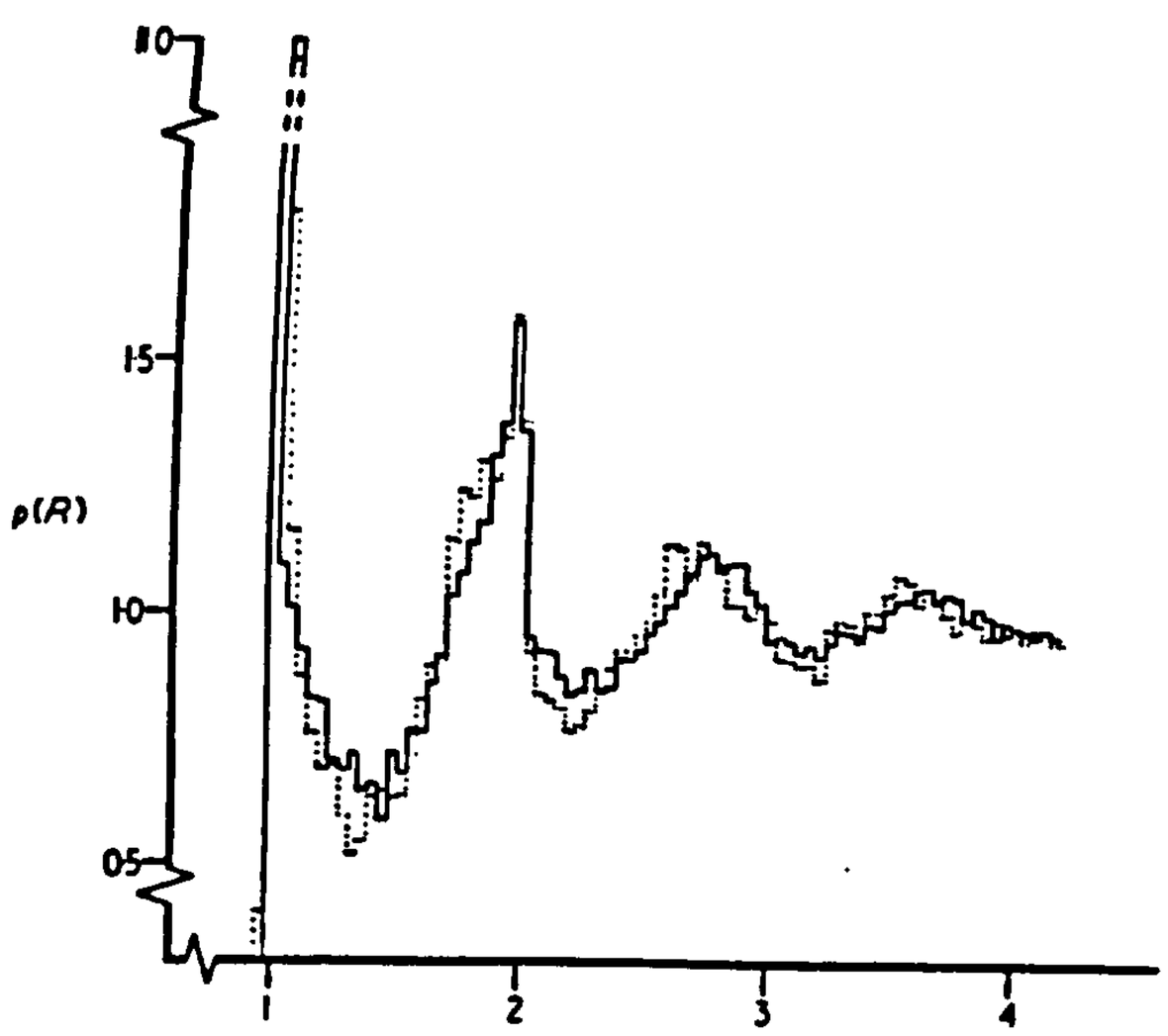

Figure 1.23

Comparison of the Matheson radial distribution function with that of the Scott loose packed model (shown dotted)

(both models adjusted for finite size using Mason's correction)

Rahman et al (1976) used a molecular dynamics simulation of 500 spheres characterised by a Lennard-Jones (soft) potential. They obtained a packing density of 0.64, and a radial distribution function similar to that of the Finney model, although the soft potential used smoothed out otherwise sharp features.

Kincaid and Weiss (1977) presented a numerical list for the radial distribution functions for a system of 864 hard spheres. Their Monte Carlo calculations assumed as a starting point a close-packed face-centred cubic lattice (packing density = 0.74048). Although they give the radial distribution functions for four densities of interest between 0.73 and 0.52, Kincaid and Weiss's work represents one of the first published simulations in which no reference to any physical (i.e. experimentally measured) model is made.

Powell (1980) extended the Matheson-Tory et al technique for monodisperse spheres to polydispersity for any given particle size distribution, although he gives no detailed comparison between his results for a monodisperse pack, and any physical model.

Jodrey and Tory (1981) developed a method of simulating the vibration and radial force characteristic of an experimental RCP structure. Their algorithm produced an ultimate packing density of 0.6366 (the "right" answer), and a radial distribution function which compares spectacularly well with that of the Finney model, as shown in figure 1.24.

Clarke and Wiley (1987) produced a new algorithm designed to simulate binary mixtures of spheres. For a monodisperse packing, they achieved excellent agreement with the computational results of

Jodrey and Tory, and with the experimental Finney model. Clark and Wiley obtained (monodisperse) packing densities ranging between 0.637 and 0.645 depending on sample size and duration of the computation. They took the unusual step of calculating the Voronoi cell statistics for their computational model. These statistics are shown in figures 1.25 to 1.27, from which it is clear that there is excellent agreement with the Voronoi cell statistics obtained by Finney (1968).

Figure 1.24

Radial distribution function for the Jodrey and Tory model.

(after Jodrey and Tory, 1981)

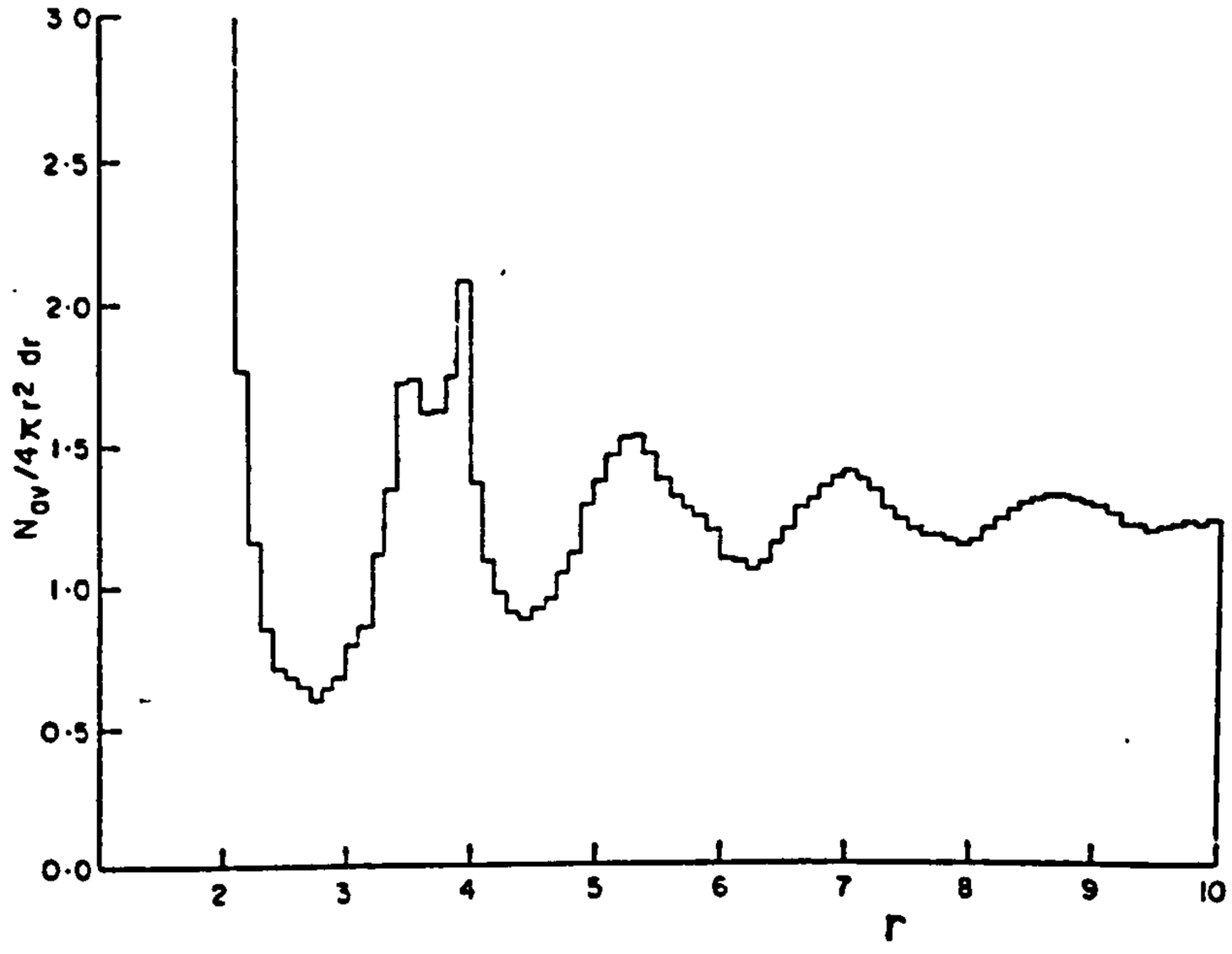

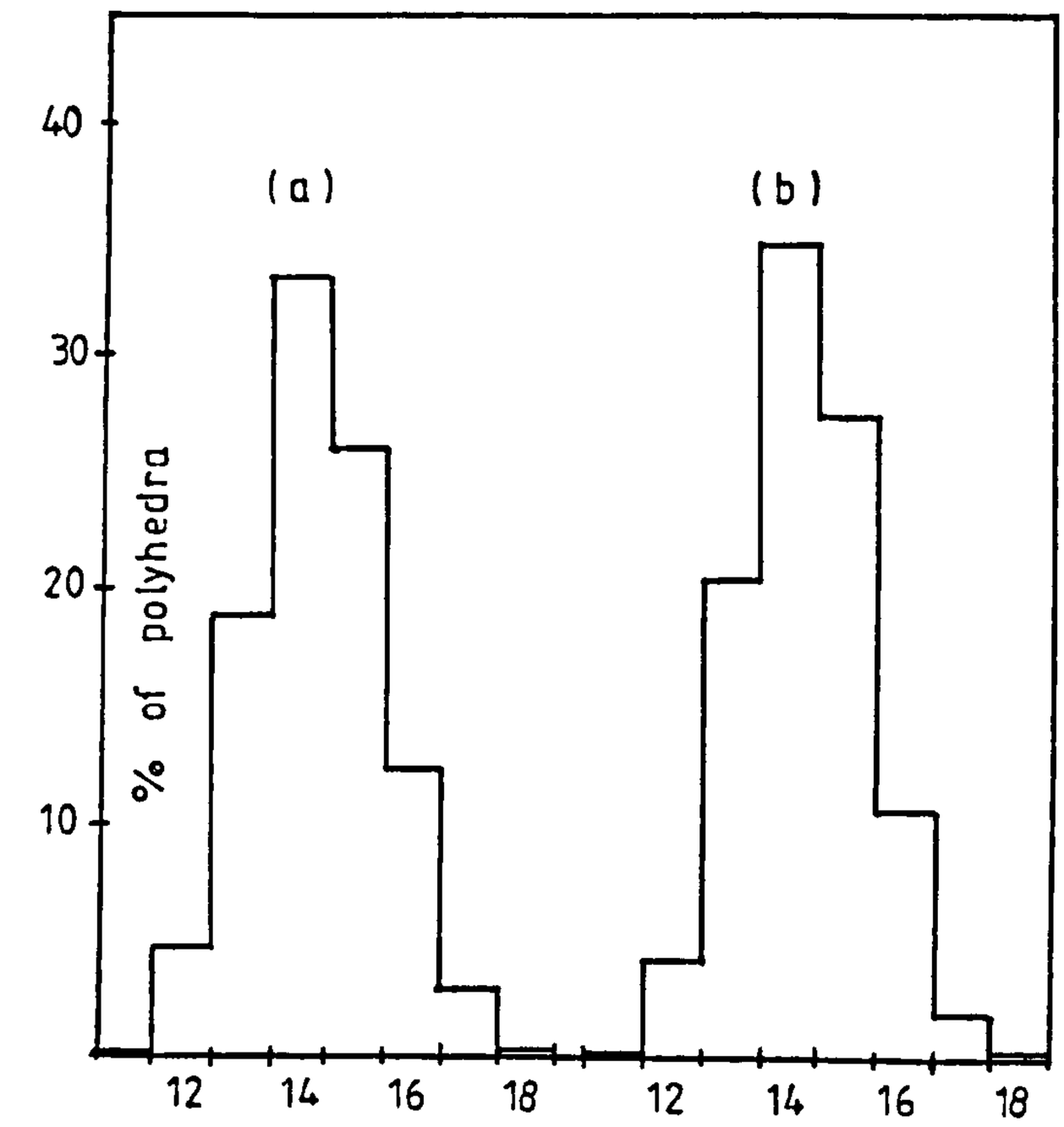

Figure 1.25

Voronoi cell statistics: Distribution of cells with F faces for:-

(a) Clark and Wiley, and

(b) Finney models.

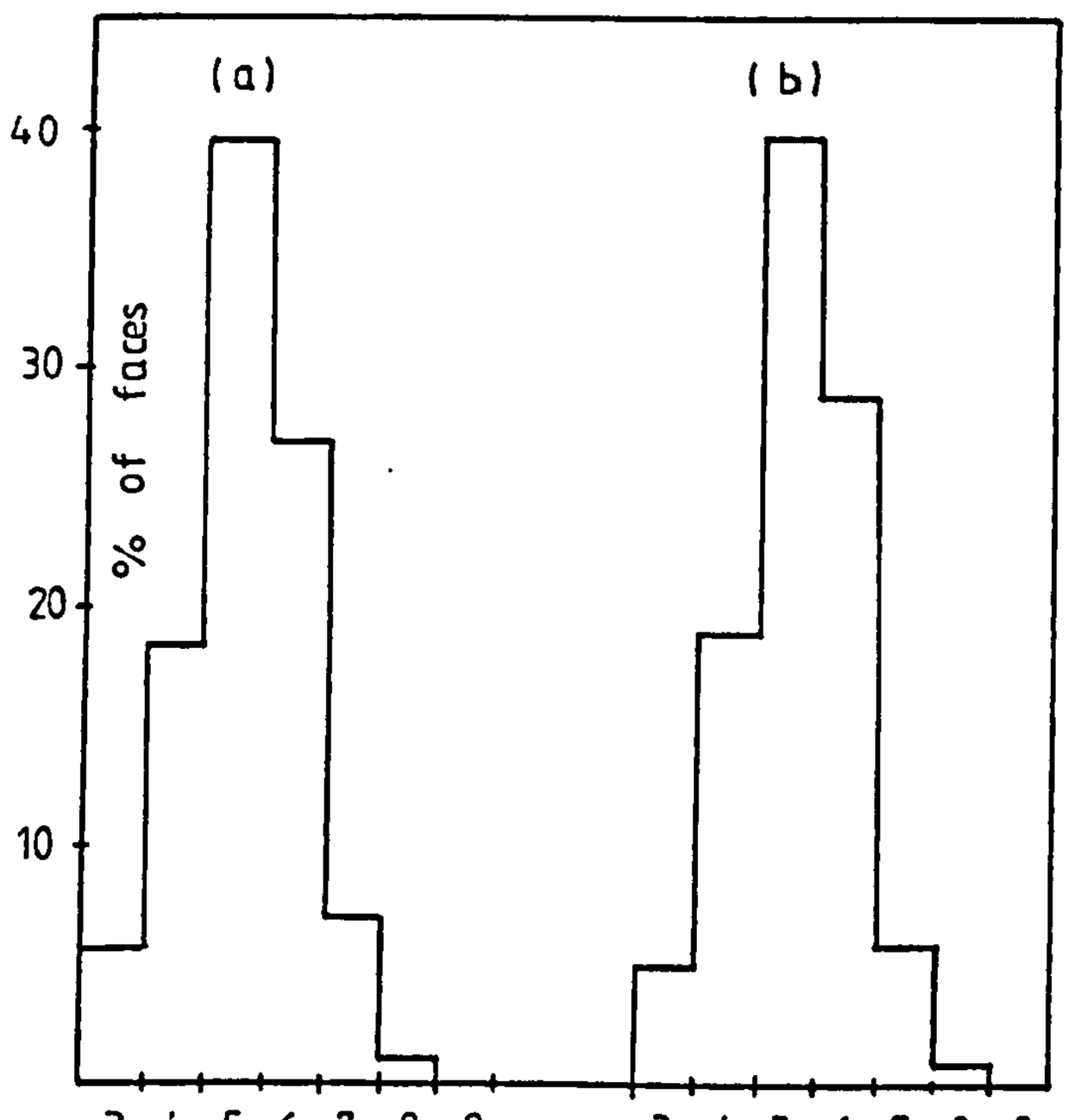

Figure 1.26

Voronoi cell statistics: Distribution of faces with N edges for:-

(a) Clark and Wiley, and

(b) Finney models.

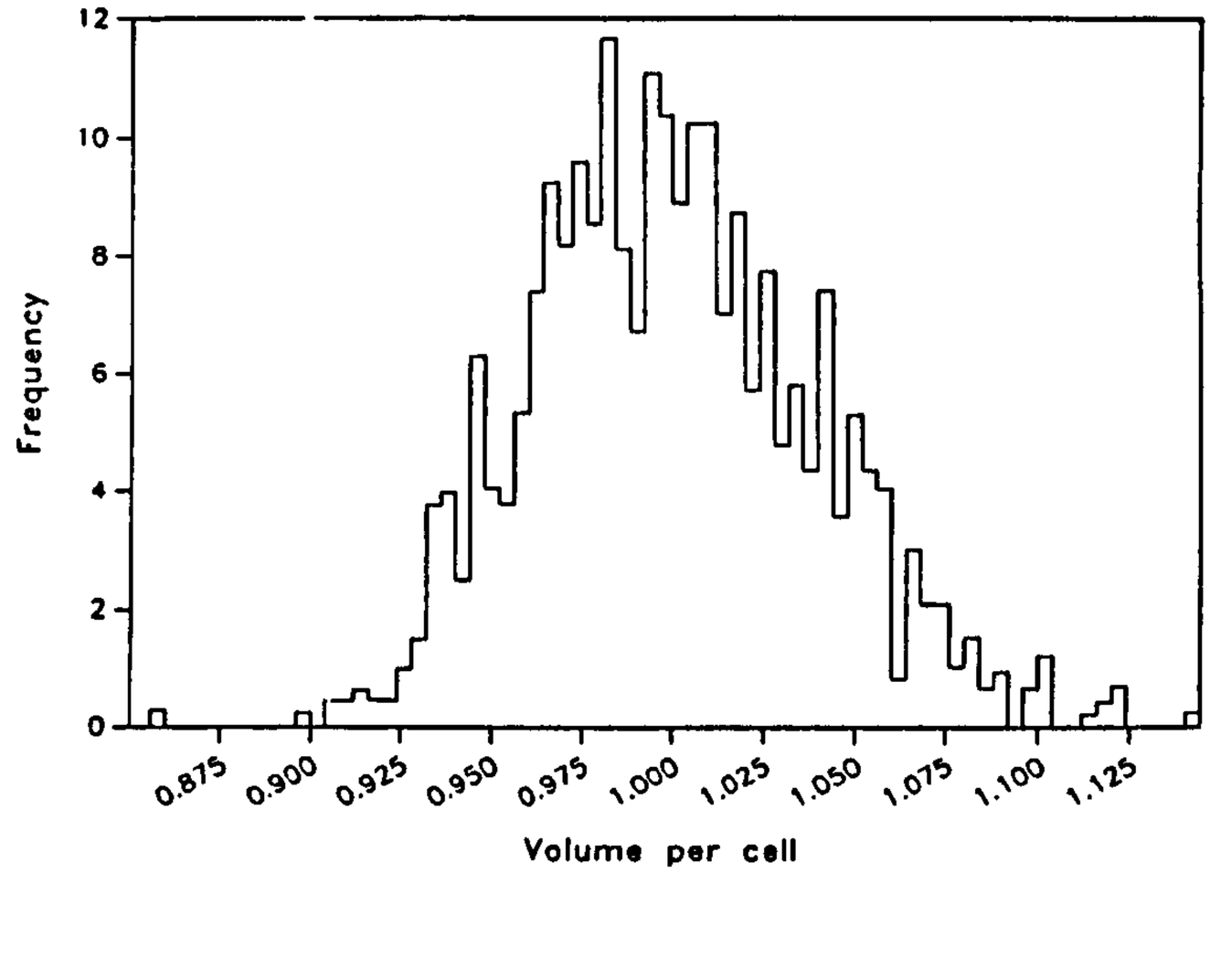

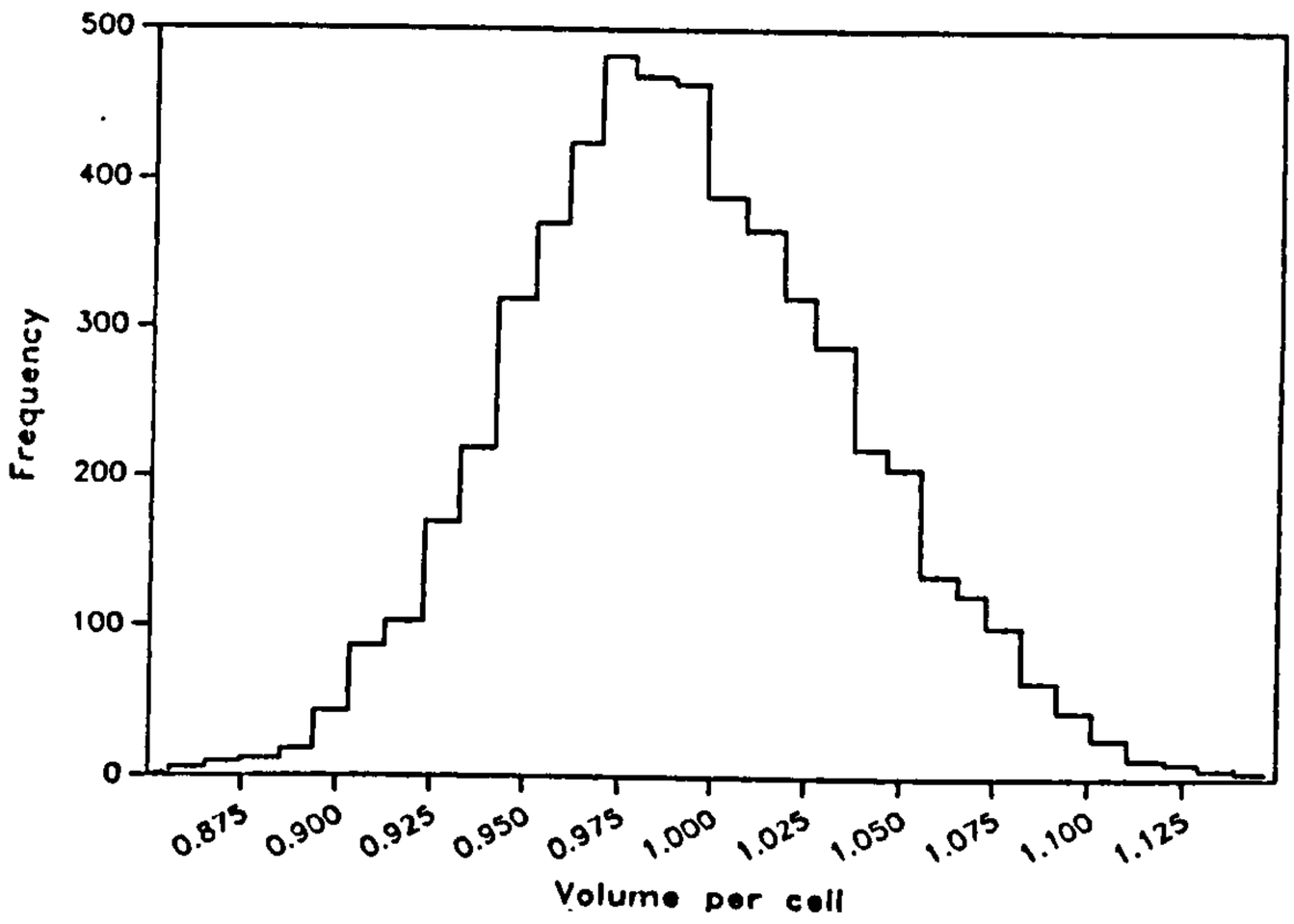

Figure 1.27

Voronoi cell statistics.

Cell volumes for:

(a) Clark and Wiley model.

(b) Finney model.

The approach adopted by Clark and Wiley towards validating their algorithm is particularly interesting, since theirs is the first attempt to use distributions of Voronoi cell properties. One of the conclusions of the next chapter in this thesis is that both the radial distribution function and the Voronoi cell are volume averaging measures of RCP structure. For physical processes dominated by the voids in the packing, and the network of

interconnections between voids, the level of detail available from the Voronoi cell is severely limited. The arguments developed in the next chapter are directly relevant to the general problem of validating computer simulations of RCP, and form the basis of structural description of RCP at a more fundamental, and less volume averaging, level than that afforded by Voronoi statistics.

1.3 Objectives, approach and synopsis

The objectives of the present work are (i) to analyse the structure of random close packing (RCP) of equal spheres, and (ii) to determine the extent to which this structure influences the distributions of two immiscible fluids within the void space of the packing, under capillary forces. An additional objective is to investigate the extent to which the structure of RCP is random, and to formulate guidelines for pore-level modelling of RCP and RCP-like materials.

To achieve these objectives, the procedures conventionally used to discretise RCP space are reviewed, and compared with the requirements of a pore-level model in Chapter 2. The main conclusion of Chapter 2 is that the conventional Voronoi cell sub-division is essentially volume averaging in respect of the important void regions between spheres, and is therefore of extremely limited value in developing a microscopic structure description appropriate to any physical properties of RCP which are likely to be dominated by the void regions of the packing. Chapter 2 is therefore

essential to the subsequent chapters of the thesis, since the other important conclusion to emerge from it is that the simplicial cell not only meets all the requirements of a pore level model, but also represents a much more fundamental description of RCP structure than has hitherto been attempted. Chapter 3 contains a comprehensive simplicial cell analysis of the Finney model. Chapter 4 is dedicated to the thorny problem of establishing the degree to which RCP structure is random at the simplicial cell level. Chapter 5 extends some of the concepts raised in Chapter 4, and considers the degree to which the network connecting the simplicial cells is random. In Chapter 6, the capillary properties of the Finney model are investigated by simulating the drainage and imbibition processes within the packing. Finally, in Chapter 7, an aeolian sandstone is injected with mercury, and the resultant capillary pressure curve and pore size distributions are compared with those of the simulated RCP capillary pressure curve.

Previous studies on the structure of random close packings of equal spheres have concentrated on the nature of the Voronoi cell, and have almost entirely neglected the nature of the simplicial (or Delaunay) cell. Additionally, previous studies on porous media have, in general, systematically failed to develop rigorous analytical descriptions of the entire porespace of any individual chaotic porous medium. Indeed such a comprehensive description is commonly accepted as impractical, if not actually impossible. However, by good fortune, the simplicial graph of a random close packing of equal spheres provides, by itself, a complete and perfect description of the entire porespace of the packing. This fact appears to have gone largely unnoticed in the literature and therefore unexploited until the present work was undertaken. One

consequence of this situation is that the present work probably represents the largest and most detailed description of a real, disordered porous material attempted to date.

Trigonometry and geometry used in the present work are reproduced in Appendix A to this thesis. The relevant analytical subroutines are presented in Appendix B. These subroutines are written in BASIC (DEC compiled BASIC), and many are suitable for simple adaptation to desk top or personal computers. Some of the programs developed, however, may require relatively large data files, and several hours of CPU time, since optimisation of the code for run-time efficiency was not an objective of the present work.

CHAPTER 2: RCP SPACE DISCRETISATION

2.1 General Considerations: Voronoi Tessellation

The problem addressed here is that of dividing up the space of RCP structure such that fundamental spatial properties from two, or more, sphere packings may be directly compared. The essence of the problem lies in the need to compare properties of one structure with the properties of another. The dividing-up process is therefore a means to an end, and is not an end in itself.

Although we are concerned here with the concept of dividing-up something, it is perhaps more instructive to begin by considering the concept of putting-together something. The ancient Romans had a passion for tiling floors and walls to form mosaics. The latin word for the small tiling pieces which they used is tessera, and the fully assembled mosaic is known as a tessellation. A simple definition of the art of tessellation might be that it is a process by which a plane surface is covered by polygonal shapes which fit together, and which do not overlap. This definition need not be restricted to two dimensions, in theory, space of any dimension may be tessellated. However, in order to proceed further with the geometry of tessellations, two features which exist in Roman mosaics must be excluded. Gaps (termed "frustrations") between tessera are not permitted, and concave tessera are not permitted. Figure 2.1 shows examples of both concave and convex tessera in two dimensions.

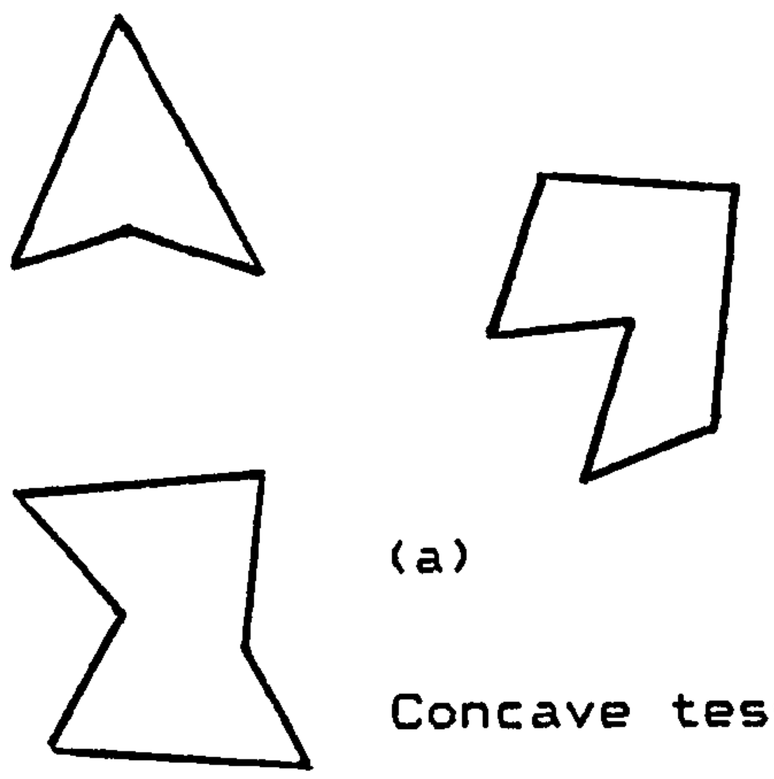

Figure 2.1 : Forbidden tessera forms (a)
and permitted tessera forms (b).

It is now possible to consider a formal definition of a tessellation. Thus a tessellation comprises an aggregate of convex, N-dimensional polytopes (tessera) which perfectly fill N-dimensional space (after Winterfeld, 1981). It is relatively straightforward to apply this definition to identical, regular polygons in two dimensions. Thus if the problem of tessellating a plane with a set of perfect and identical polygons is considered, there are only three solutions possible (Coxeter, 1963). These are the triangular, the square and the hexagonal tessellation, shown in figures 2.2 to 2.4 respectively.

If the problem of tessellating three dimensional space with a set of perfectly regular and identical polyhedra is considered, there are at least two possible solutions. These are the cubic and the tetrakaidecahedral tessellations.

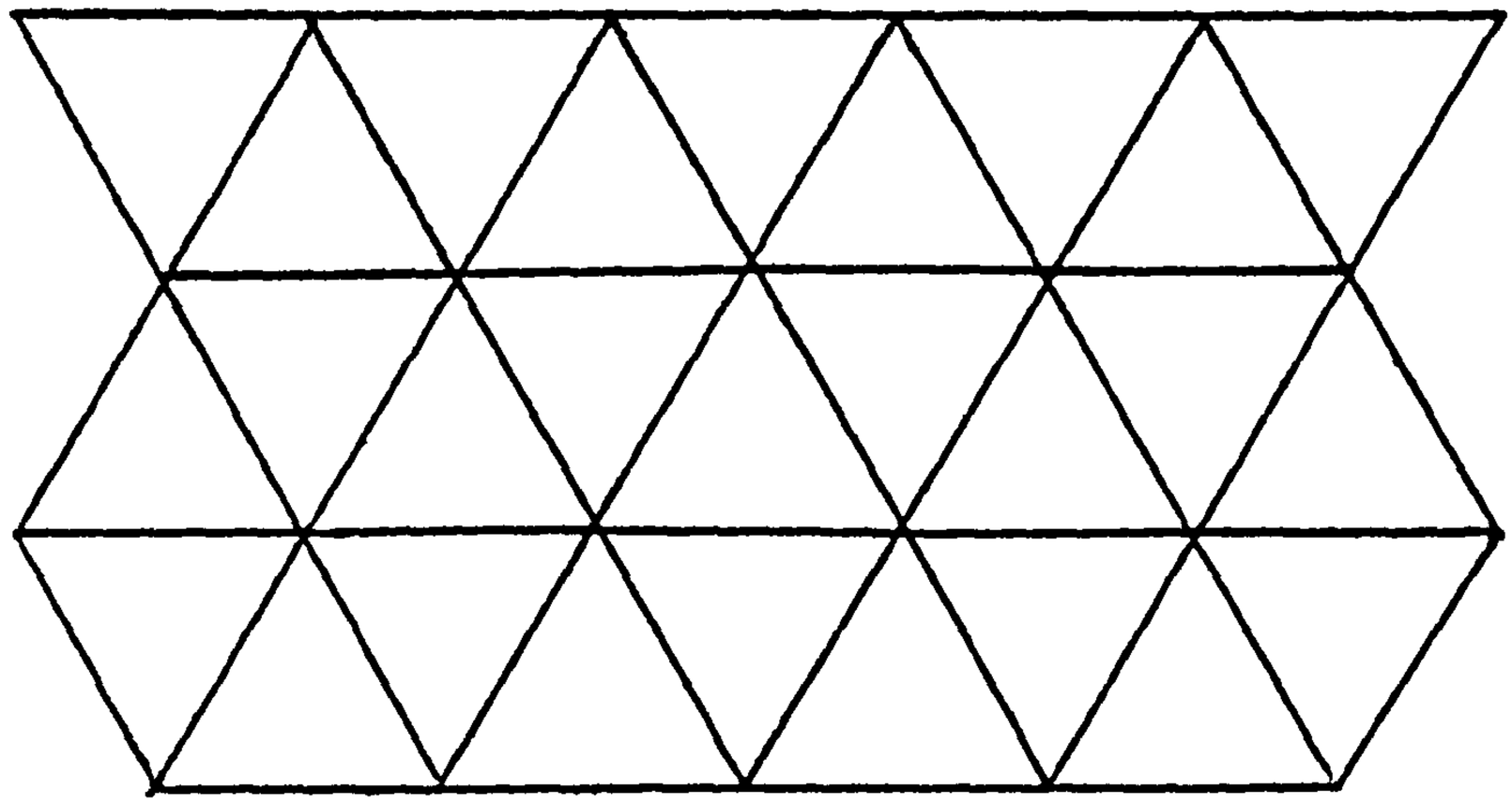

Figure 2.2 : The triangular plane tessellation

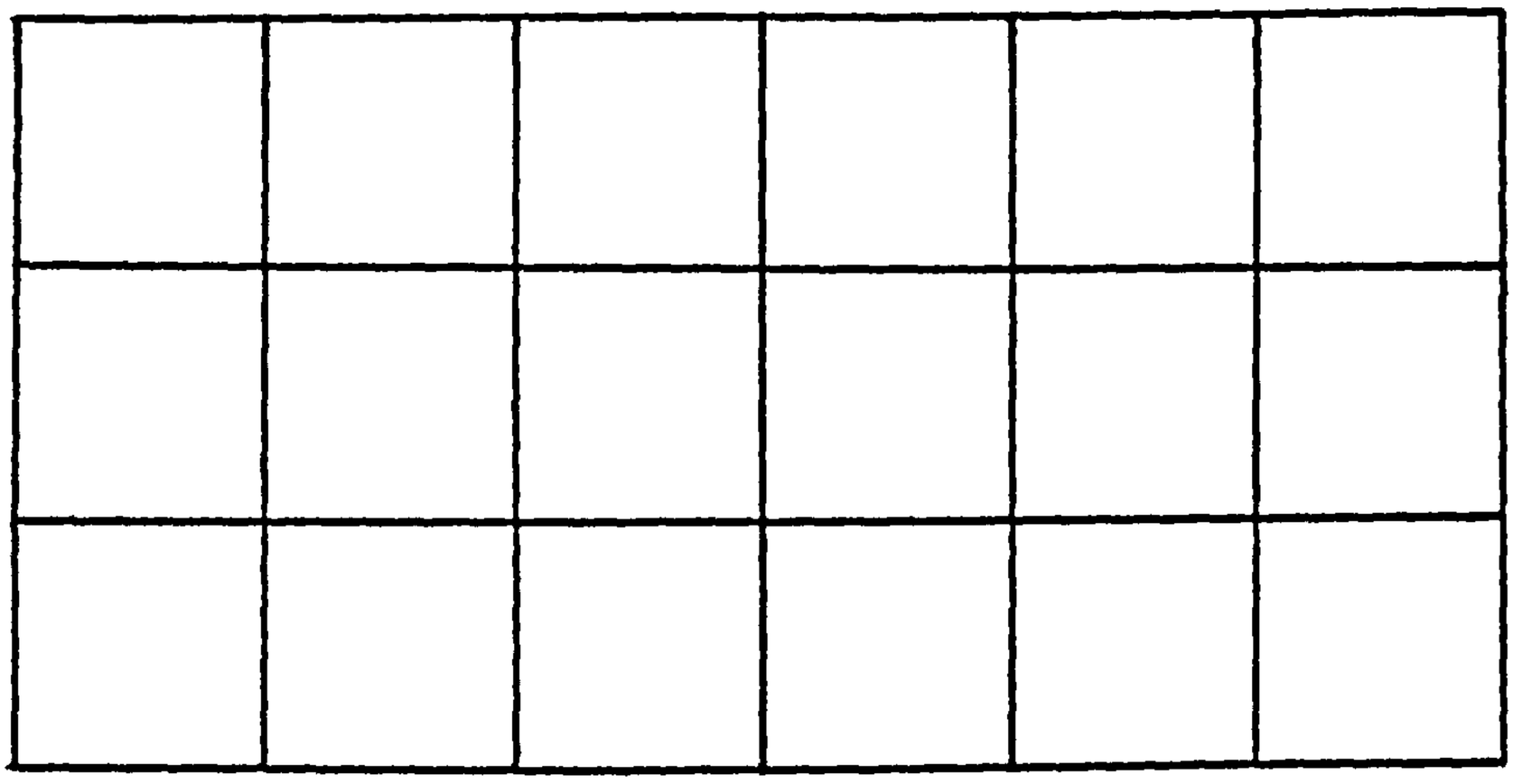

Figure 2.3 : The square plane tessellation

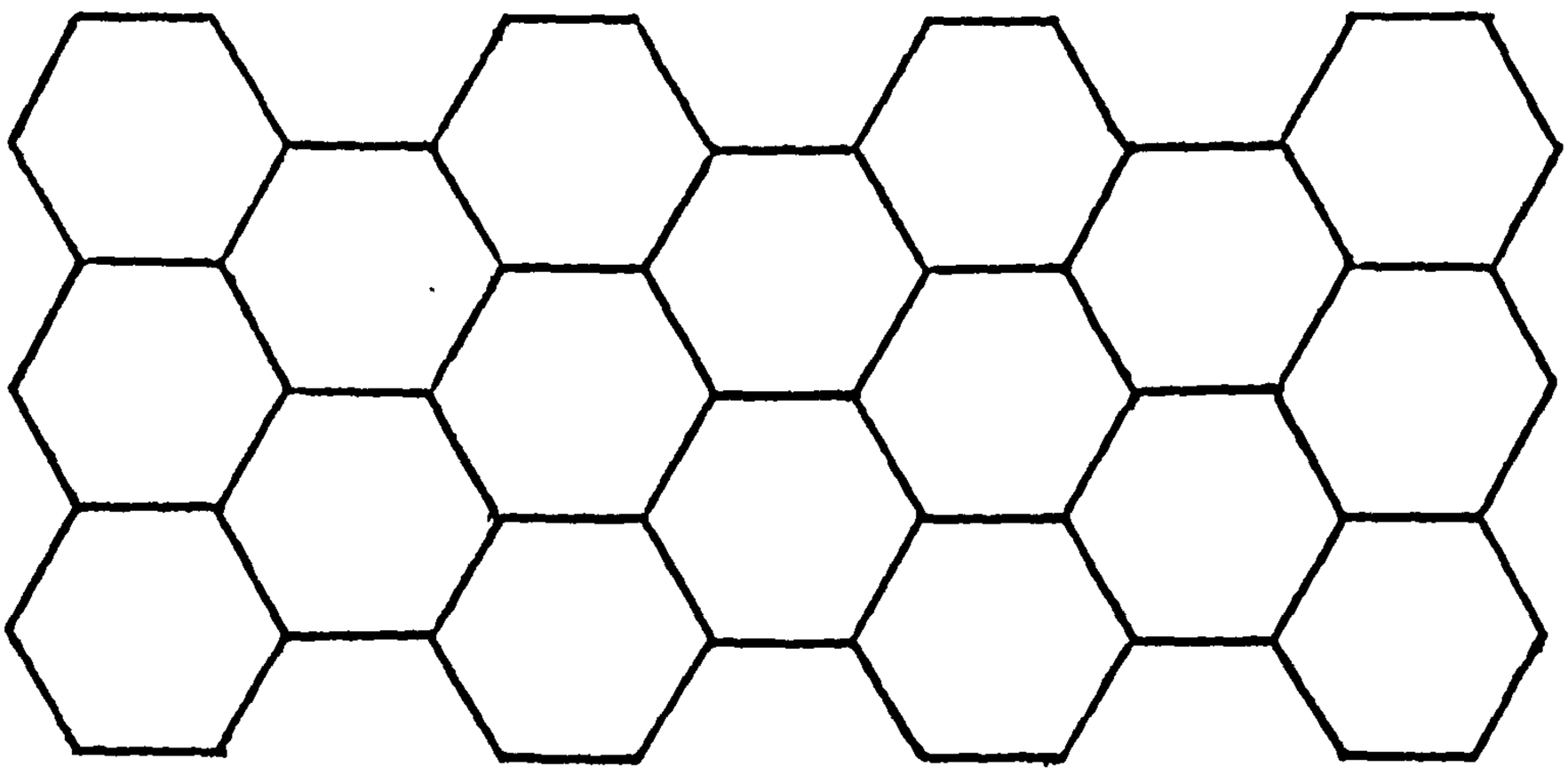

Figure 2.4 : The hexagonal plane tessellation

The cubic tessellation may be visualised as a perfect stack of children's building blocks (cubes). The tetrakaidecahedral tessellation is somewhat more difficult to visualise. The tetrakaidecahedron was first described by Kelvin (1887), and is a fourteen faced polyhedron which may be formed by truncating the six vertices of an octahedron to produce eight hexagonal faces and six square faces as shown in figure 2.5.

Figure 2.5

The tetrakaidecahedron

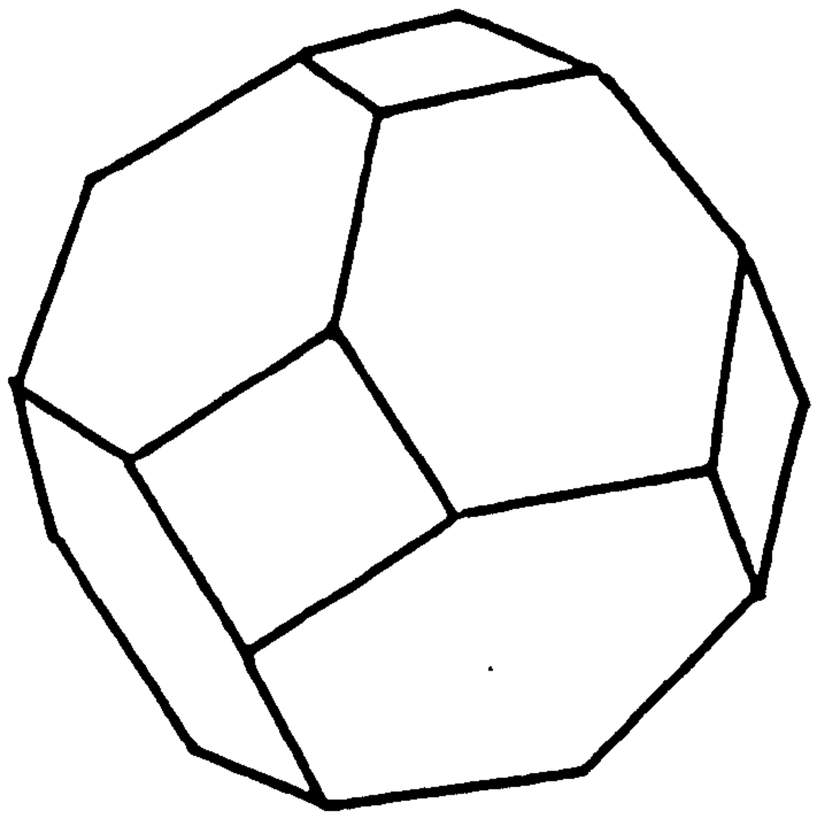

At first, the concept of tessellating three dimensional space with the tetrahaidecahedron might seem a somewhat bizarre and artificial exercise. This form of tessellation is, however, extremely common in nature, occurring as the fundamental repeat cell (also known as the Wigner-Seitz cell) in all body-centred cubic (BCC) lattices. All crystalline materials with their component atoms in a BCC lattice may therefore be considered to be "constructed", or tessellated, by sticking the basic tetrakaidecahedron tessera together ad infinitum. Figure 2.6 shows the BCC lattice, together with the Wigner-Seitz

cell (a tetrakaidecahedron) for the same lattice.

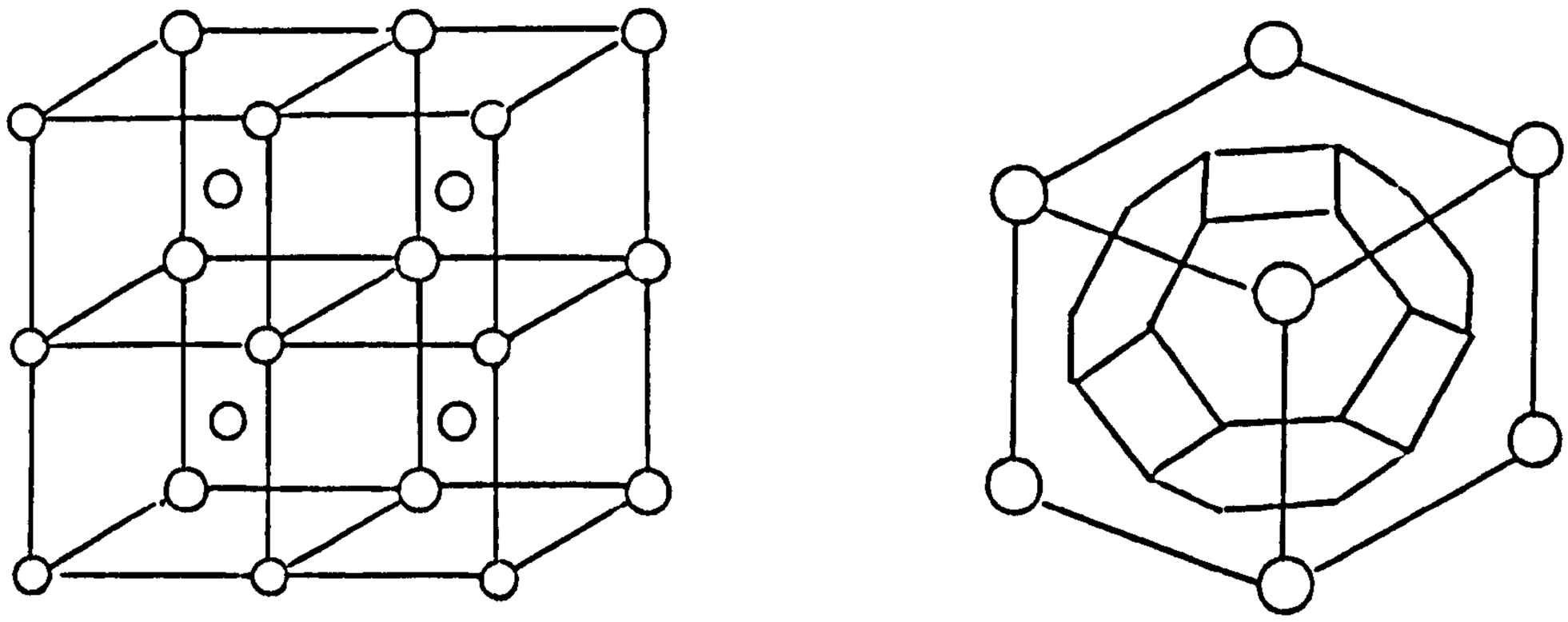

Body centred cubic lattice

Wigner-Seitz cell for the BCC lattice

Figure 2.6 : Tessellation of the Body Centred Cubic (BCC) lattice

Clearly the notion of building up an atomic lattice using tessera is entirely artificial. However, it is possible to use the concept of tessellation to subdivide the space occupied by the component atoms of the lattice into a number of simple, regular repeat cells. In general, crystalline materials may be subdivided into basic repeating geometric building blocks, or tessera. Some complex crystals may require several different kinds of tessera, but the subdivision of space is still (conceptually) relatively simple.

The concept of subdividing a random array of atoms, or points, in space is, in principle, no more difficult than the concept of

subdividing a regular lattice of atoms, or points, in space. Careful examination of figure 2.6 will show that the tetrakaidecahedron repeat cell must contain, at its centre, the body-centred atom from which this particular cubic lattice derives its name. The eight hexagonal faces of the tetrakaidecahedron repeat cell all occur such that the eight imaginary lines connecting the body-centred atom to its nearest neighbour atoms all pass through the centre of the hexagon. Furthermore, these imaginary lines are normal to the hexagonal faces which perfectly bisect the imaginary lines. Figure 2.7 shows one of these imaginary lines bisected by one of the hexagonal faces of the tetrakaidecahedron.

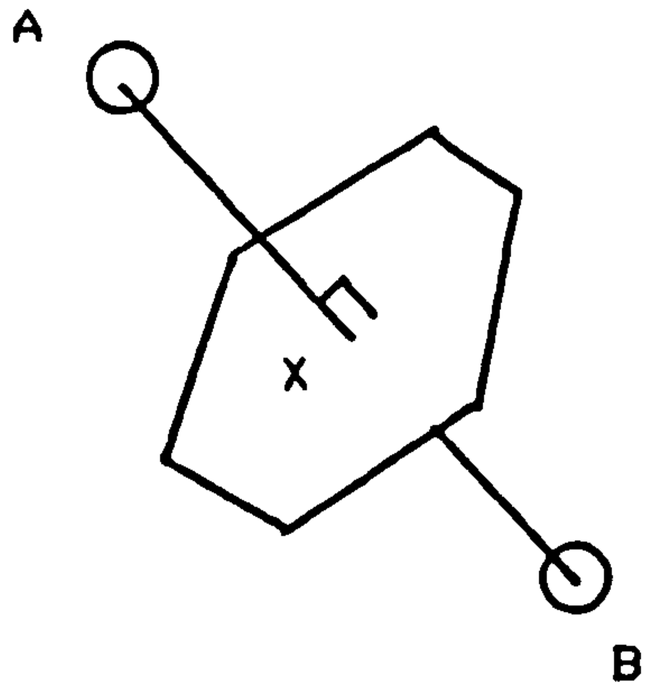

Figure 2.7 : Hexagonal face of the tetrakaidecahedral Wigner-Seitz cell of the BCC lattice

The six square faces of the tetrakaidecahedral repeat cell occur such that the six imaginary lines connecting the body-centred atom to adjacent body centred atoms all pass through the centre of the square. These imaginary lines are also normal to the square faces, and are perfectly bisected by the square faces, as shown in figure 2.8:

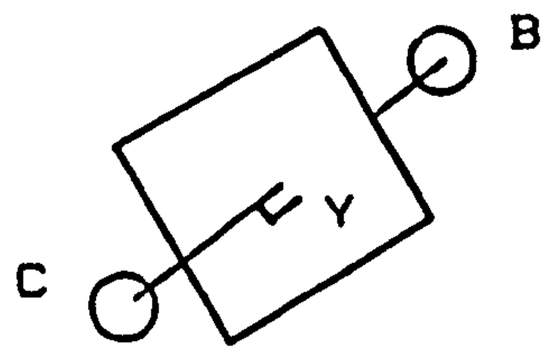

B = Body centred atom inside the tetrakaidecahedron

C = Adjacent body centred atom

Length BY = YC

Figure 2.8 : Square face of the tetrakaidecahedral Wigner-Seitz cell of the BCC lattice

The tetrakaidecahedral surface must therefore enclose all imaginary points in space which are nearer to its own body-centred atom than to any other atom in the lattice. All imaginary points on the outside of the tetrakaidecahedral surface are nearer to some other atom in the lattice then they are to the atom at the centre of that

tetrakaidecahedron. Any polytope which encloses all imaginary points in space closer to its own central reference point than to central reference points of other, adjacent polytopes is known as a Voronoi cell, after the mathematician who formalised this definition (Voronoi, 1908). The tetrakaidecahedral repeat cell of the BCC lattice is therefore also a legitimate Voronoi cell.

The concept of the Voronoi cell is somewhat clumsy when applied to a perfect, regular and repeating lattice. It will, however, always correctly identify the repeat cell, or cells, of the crystalline lattice without requiring any assumptions regarding symmetry. The concept of the Voronoi cell is immensely powerful when it comes to subdividing a chaotic, or disordered array of points (or atoms) in space, and finds application in a wide variety of two and three dimensional space filling problems (e.g. Winterfeld, 1981; Lambert and Weaire, 1983; Hanson, 1983; Weaire and Rivier, 1984 and Weaire et al, 1986).

The reference point at the centre of the Voronoi cell in the preceding example of the BCC lattice is an atom. In dividing up other arrays of points, the reference points of the Voronoi cells may be the measured co-ordinates of the centre of the spheres of a random packing. Alternatively, the reference points may be the co-ordinates of random points in space, generated arbitrarily by some convenient algorithm. In the latter case, the reference points are usually referred to as Poisson points. The construction of Voronoi cells from the co-ordinates of a set of Poisson points may proceed by several different methods. Computer algorithms for subdividing

two and three dimensional arrays of points are available (see for example Winterfeld, 1981). Whichever method for subdivision is adopted, certain formal rules must be obeyed. These rules have been adapted for N-dimensional space by Winterfeld (1981) from Green and Sibson (1977), and are as follows:

Consider the set of Poisson points $P_1(r_1)$, $P_2(r_2)\ldots$ $P_z(r_z)$. The interior space of the Voronoi cell of point P_i is the set of points closer to P_i than to P_j:-

$$|\underset{\sim}{r}-\underset{\sim}{r}_i| < |\underset{\sim}{r}-\underset{\sim}{r}_j| \quad i \neq j \qquad -2.1-$$

In two dimensions, an edge of a Voronoi cell is equidistant from two Poisson points P_i and P_k. In three dimensions the face of a Voronoi cell is equidistant from two Poisson points, P_i and P_k:-

$$|\underset{\sim}{r}-\underset{\sim}{r}_i| = |\underset{\sim}{r}-\underset{\sim}{r}_k| < |\underset{\sim}{r}-\underset{\sim}{r}_l| \quad l \neq i,k \qquad -2.2-$$

In two dimensions an edge of a Voronoi cell lies on the perpendicular bisector of the line connecting P_i to P_k, and vertices of the Voronoi cell are equidistant from three Poisson points, P_i, P_k and P_l. In three dimensions a face of a Voronoi cell lies on the plane perpendicular bisector of the line connecting P_i to P_k, and an edge of such a Voronoi cell is equidistant from three Poisson points, P_i, P_k and P_l:-

$$|\underset{\sim}{r}-\underset{\sim}{r}_i| = |\underset{\sim}{r}-\underset{\sim}{r}_k| = |\underset{\sim}{r}-\underset{\sim}{r}_l| < |\underset{\sim}{r}-\underset{\sim}{r}_m| \quad m \neq i,k,l \qquad -2.3-$$

In three dimensions, the vertices of a Voronoi cell are equidistant from four Poisson points, P_i, P_k and P_l and P_m:-

$$|\underset{\sim}{r}-\underset{\sim}{r}_i| = |\underset{\sim}{r}-\underset{\sim}{r}_k| = |\underset{\sim}{r}-\underset{\sim}{r}_l| = |\underset{\sim}{r}-\underset{\sim}{r}_m| < |\underset{\sim}{r}-\underset{\sim}{r}_n| \quad n \neq i,k,l,m \qquad -2.4-$$

Finney (1968) conformed to these rules in dividing the sphere centres of his spheres packing into Voronoi cells. The method he used was to perpendicularly bisect the vectors between sphere centre co-ordinates, producing a large number of intersecting planes. It is therefore possible to select a number of these intersecting planes to form a range polyhedral candidates for the Voronoi cell about any individual sphere centre. The correct choice is simply the smallest polyhedron which can be formed about the reference point (sphere centre), whilst ensuring that no further planes can cut the chosen set.

Winterfeld (1981) favours the expanding disc process for two dimensional problems. In this process, all the Poisson points are simultaneously considered to expand into circular discs at a constant, and equal, rate. No disc is permitted to impinge upon, or overlap, another. Consequently when two discs meet they must deform, producing a straight line common boundary. The discs thus ultimately evolve into polygons which are identical to the Voronoi cells for the Poisson points. This process is illustrated in figure 2.9.

The three dimensional Voronoi tessellation of Poisson points is a logical extension of the expanding disc process. Hence the array of points is simply allowed to expand into spheres which evolve into polyhedra. Each of these polyhedra is the Voronoi cell for the original reference (Poisson) point.

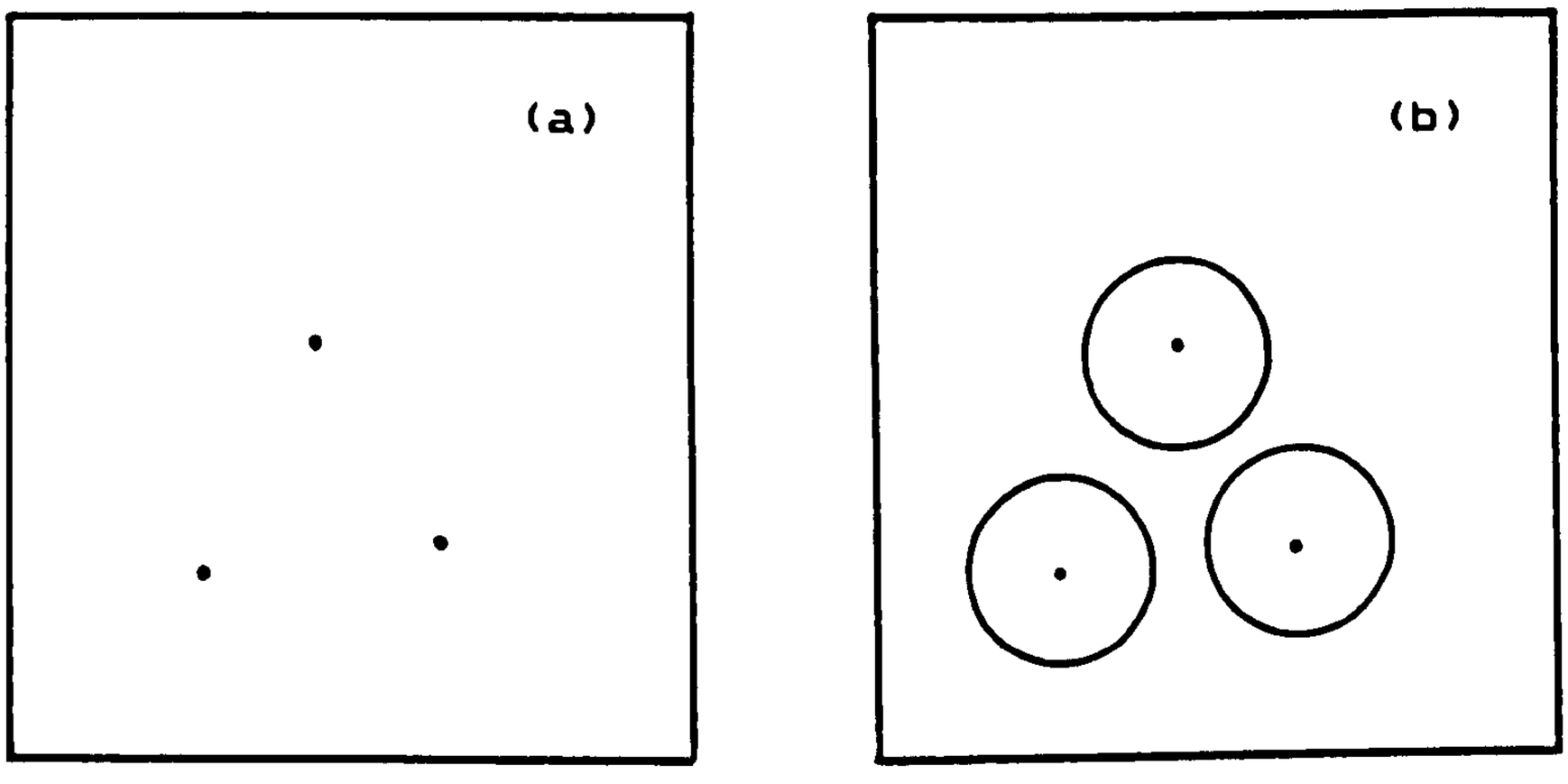

Figure 2.9 : Expanding disc process. Poisson points (a) expand into discs (b). No disc is permitted to impinge on another (c) resulting in space filling polygons (d)

(after Winterfeld, 1981)

2.2 General Considerations: Simplicial Tessellation

For any given N-dimensional array of Poisson points there is a unique Voronoi tessellation. The Voronoi tessellation, in turn has a unique topological property - that of duality. The topological dual, or inverse, of the Voronoi tessellation is known variously as the simplicial graph, the simplicial tessellation or the Delaunay tessellation. The term simplicial tessellation will be used throughout the present work. The adjective "simplicial" means simplest, or most fundamental. The simplicial cell has the absolute minimum number of faces or edges appropriate to the dimension of the parent array of Poisson points. Thus for two dimensional problems the simplicial cell is always a triangle. In three dimensional problems the simplicial cell is always a tetrahedron. Any Voronoi tessellation can be transformed into its simplicial counterpart without loss of information. Conversely, any simplicial tessellation can be transformed into its equivalent Voronoi tessellation without loss of information. The precise nature of this topological duality is easily appreciated from figure 2.10.

The Voronoi cell has proved to be an extremely useful unit of space in studies of the structure of the liquid state (e.g. Finney 1968). However, the approach adopted in this chapter is to explore the suitability of the simplicial cell as a unit of space appropriate to understanding the behaviour of fluids within the porespace of a sphere packing. The main aim of this section of chapter two, therefore, is to introduce the concept of the simplicial tessellation.

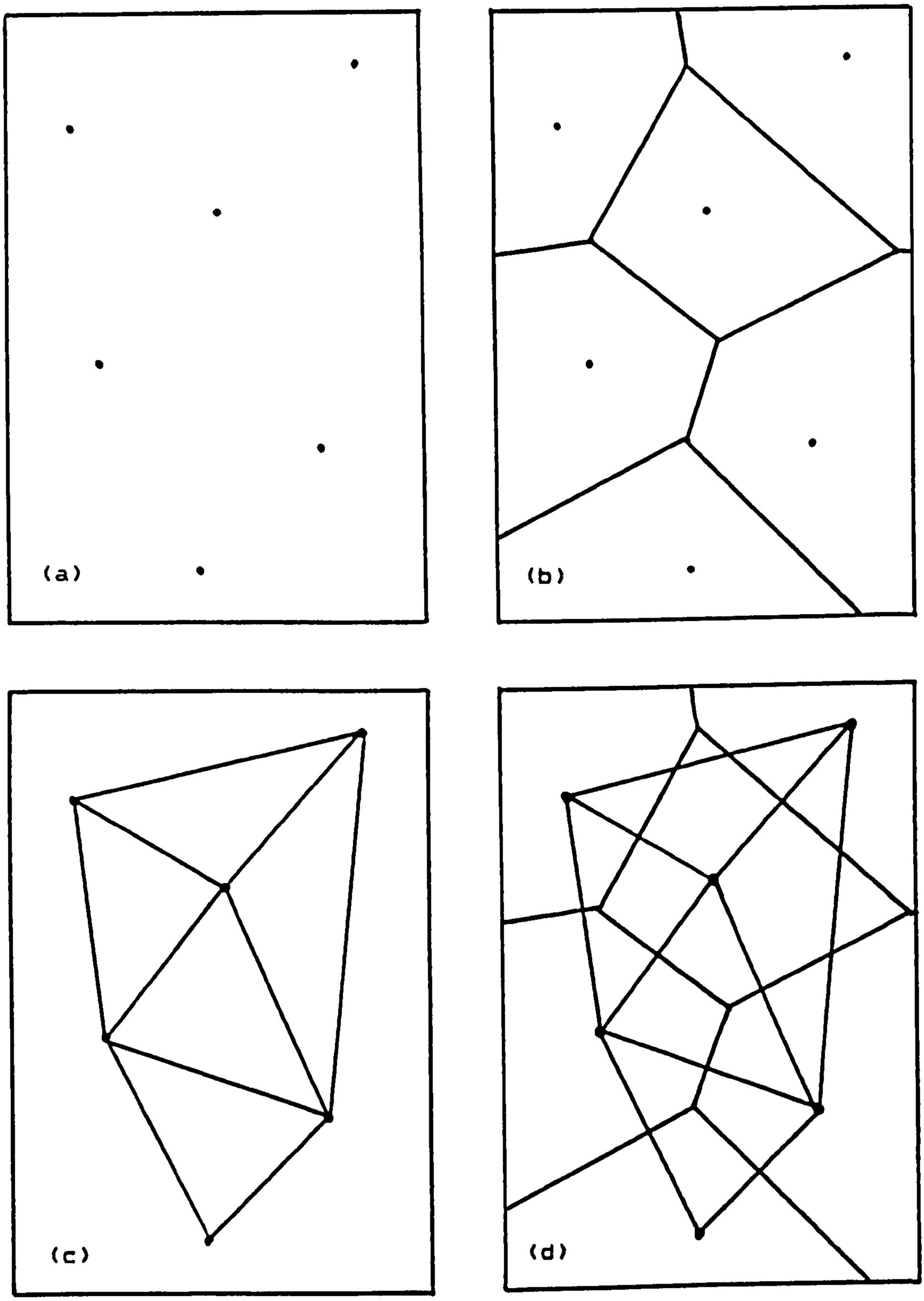

Figure 2.10 : Poisson points (a) discretised into Voronoi tessellation (b) and simplicial tessellation (c). Voronoi and simplicial tessellations superimposed (d).

2.3 Mathematical theories of Voronoi statistics

There exists no universal mathematical theory for the spatial relationships between Voronoi cells in three dimensions. Distributions of cell forms are therefore purely observational. Despite the absence of such a universal theorem, Coxeter (1958) obtained a value of 13.56 for the average number of faces for Voronoi polyhedra, based on a theoretical examination of four and five dimensional polytopes. Coxeter was not completely satisfied with his own derivation, however, and gave an equally valid derivation of 13.398 (Coxeter, 1958). Using Coxeter's estimate of 13.56, Bernal (1965) used Euler's equation (see Coxeter 1960 for example) for three dimensional polytopes to derive an estimate for the average number of edges per face as 5.115:

$$V-E+F = 2 \qquad \text{-2.5-}$$

Since there are 3 edges at each vertex,

$$3V = 2E \qquad \text{-2.6-}$$

So $$3F-E = 6 \qquad \text{-2.7-}$$

Average number of edges per face is 2E/F,

and $$2E/F = 6(F-2)/F \qquad \text{-2.8-}$$

i.e. $$2E/F = 5.115 \text{ (for } F = 13.56) \qquad \text{-2.9-}$$

Where V = number of vertices, F = number of faces and E = number of edges.

Meijering (1958) analysed a set of random co-ordinates and derived an estimate for the average numbers of faces, edges and vertices

per cell. In an earlier study, Johnson and Mehl (1939) had derived estimates for these parameters via a different theoretical route. More recently, Hanson (1983) reports a Voronoi analysis of random points and random spheres. The results of Coxeter's, Bernal's, Meijering's, Johnson and Mehl's and Hanson's theoretical estimates of mean Voronoi statistics for random arrays are summarised and compared with the strictly observational data for the Finney (1968) and the Scott (1962) RCP models in table 2.1. From this table, it is apparent that, although theoretical models can roughly predict the mean Voronoi statistics for RCP space, none to date has achieved satisfactory convergence with the observed statistics.

Table 2.1 : Comparison of Voronoi cell statistics based on theory, and on observation.

Study	Type	Mean Faces	Mean Edges	Mean Vertices
Coxeter	T	13.56	-	-
Bernal	T	-	5.115	-
Meijering	T	15.54	5.226	27.07
Johnson and Mehl	T	>13.28	-	22.56
Hanson (points)	T	15.63 ± 0.06	5.23 ± 0.01	27.18 ± 0.12
Hanson (spheres)	T	14.96 ± 0.07	5.20 ± 0.01	25.92 ± 0.13
Finney	O	14.251 ± 0.015	5.158 ± 0.003	-
Scott	O	14.28 ± 0.05	5.160 ± 0.013	-

T = Theoretical work
O = Observational data

2.4 Relationship between Voronoi and simplicial cells

2.4.1 Two dimensional space

The topological relationship between Voronoi and simplicial cells is shown in figure 2.11 for a small, two dimensional random array. In two dimensions, the simplicial polygon is always a triangle. Whilst the Voronoi polygon can have a range of forms (from three to eight or more sides), the average number of sides in a large array is exactly six. Both the simplicial cells and the Voronoi cells pack perfectly to fill two dimensional space. The Voronoi polygon can be regarded as unique to an individual point, whereas the simplicial cell is common to three points. The duality (inverse relationship) between Voronoi and simplicial networks, or graphs, is evident from figure 2.11 since the simplicial cell sides a-b to a-h are also the perpendicular bisectors a-b to a-h which define the sides of the Voronoi polygon.

The ensemble of seven simplicial cells in figure 2.11a forms the seven sided polygon, bcdefgh. This polygon has no formal name, and so for the purposes of distinguishing it from other polygons, will be referred to here as the ensemble polygon. Clearly, the ensemble polygon has the same number of sides as the Voronoi polygon which it "contains". The significance of the ensemble polygon is that if the need arises to examine properties of simplicial cells associated with particular types of Voronoi cells, then individual ensemble polygons in the array have to be identified, and their component simplicial cells examined, or counted. In this event,

Figure 2.11 (a)

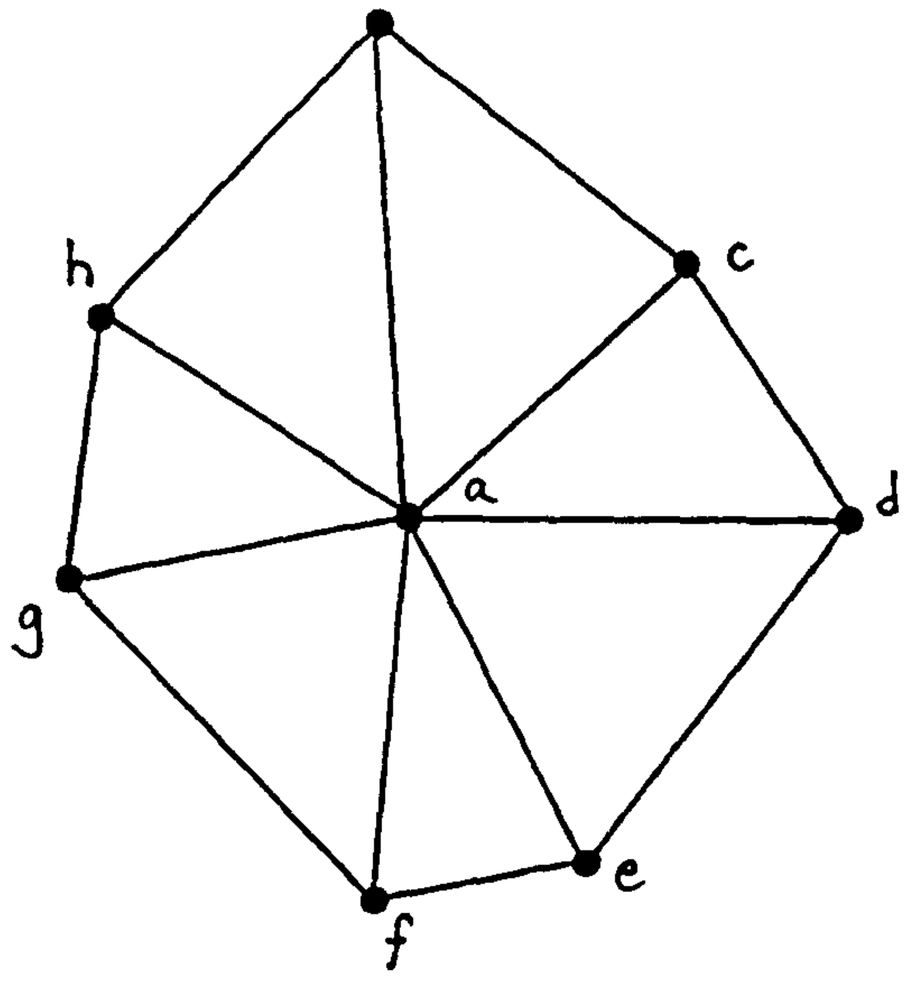

Simplicial graph for random array of points a-h on a plane.

Triangles abc, acd, ade, aef afg, agh & ahb are simplicial cells.

Polygon bcdefgh is the ensemble polygon.

Figure 2.11 (b)

Voronoi graph for random array of points a-h on a plane.

Polygon around point 'a' is the Voronoi, or Dirichlet zone.

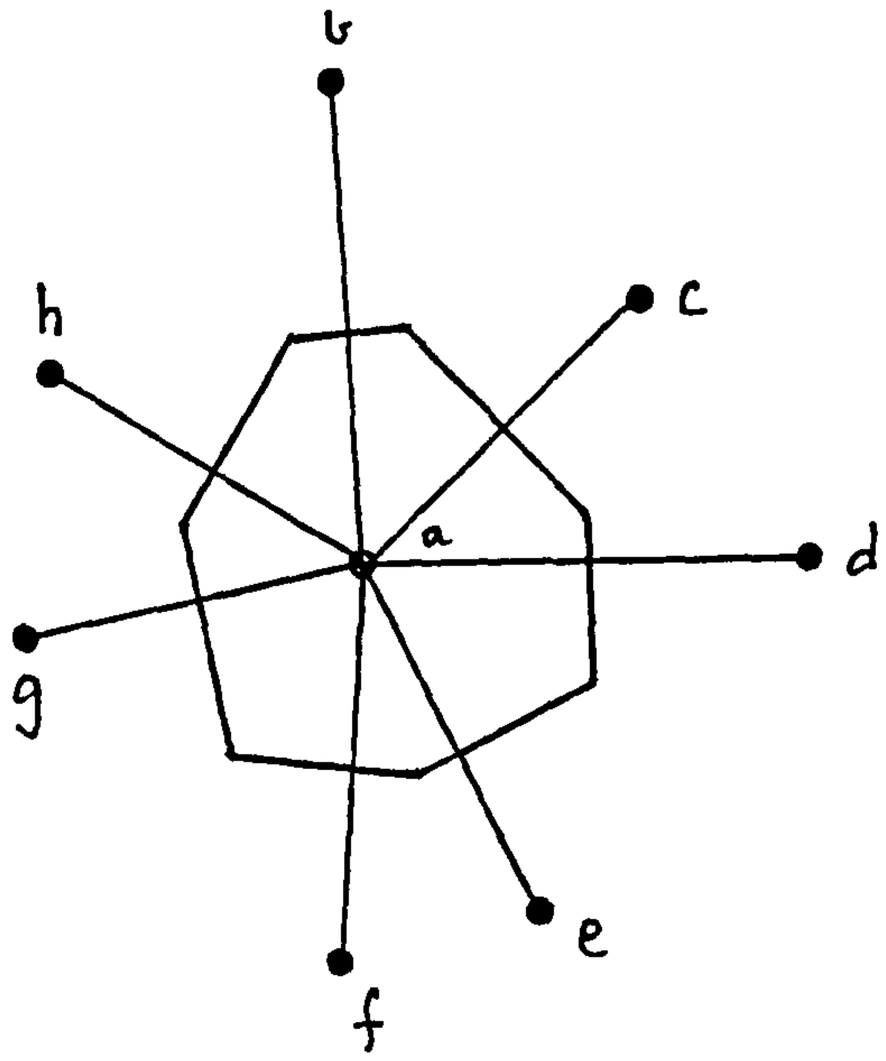

each simplicial cell must be counted three times, as it is common to three ensemble polygons. If no distinction regarding Voronoi cell type is made, then each simplicial cell is only counted once.

Given either the Voronoi polygon, or the ensemble polygon, it is a trivial matter to transform from one to the other, since both represent precisely the same information in different geometrical form. However, it is clearly not possible to transform from one simplicial polygon to anything else, since that structure represents only a fraction (on average a sixth, in two dimensions) of the information represented by either the Voronoi cell or the ensemble polygon. The simplicial cell is therefore a much more fundamental unit than the Voronoi cell. This is clearly shown in table 2.2, which lists the key topological parameters for simplicial and Voronoi cells.

Table 2.2 : Comparison of topological attributes for Voronoi and simplicial cells in 2-dimensions

Topological parameter	Simpicial cell (triangle)	Voronoi cell ('n'-gon)
Number of edges per cell	invariant 3	variable 3 to 9
Coordination from cell to cell	invariant 3	variable 3 to 9

2.4.2 Three dimensional space

In three dimensions, the simplicial cell is always a tetrahedron. The Voronoi polyhedron, however, is unconstrained by theory, and is observed to generally have between eleven and eighteen faces (Finney, 1968). Both the simplicial and the Voronoi polyhedra pack together perfectly to fill space.

In three dimensions, an individual Voronoi polyhedron is unique to an individual point in the array, whilst the simplicial cell is common to four points in the array. The Voronoi cell "exists" entirely within the space formed by the ensemble of simplicial cells which have the same reference point at the centre of the ensemble as the Voronoi polyhedron. This ensemble of simplicial cells does not have a formal name, and is referred to in the present work as the ensemble polyhedron. As in the two dimensional case, the significance of the ensemble polyhedron is that in order to examine properties of all simplicial cells associated with particular types of Voronoi cells, the individual ensemble polyhedra in the array have to be identified, and their component simplicial cells examined, or counted. In so doing, each simplicial cell must be counted four times, since it is common to four ensemble polyhedra. If no distinction regarding Voronoi cell type is made, then each simplicial cell need be counted only once.

As with the two dimensional case, in three dimensions the Voronoi polyhedron represents precisely the same spatial information as the ensemble polyhedron. It is a trivial step, conceptually, to transform from one to the other. The simplicial cell cannot be

transformed into anything else, as it represents a fraction of the information required to define either the Voronoi or the ensemble polyhedron. The numerical value of that fraction, based on observation, may be calculated using Euler's formula given by equation 2.5. For the ensemble polyhedron (this does not apply to the Voronoi polyhedron), each external face is also the face of a component simplicial cell, and is therefore a triangle. Each edge of an ensemble polyhedron face is shared with one other face, and so the relationship between faces and edges for the ensemble polyhedron is:

$$3F=2E \qquad -2.10-$$

substitution for E in 2.5 gives,

$$2V-F=4 \qquad -2.11-$$

$$\text{or,}\quad 2N-T=4 \qquad -2.12-$$

where N= the number of geometric neighbours to the central reference point (sphere), and T= the number of component tetrahedra (simplicial cells).

Equation 2.12 represents a formal and original proof that the ensemble polyhedron cannot exist with an odd number of component simplicial cells. From Finney's (1968) observations, the closed interval of values for geometric neighbours for RCP is $11 \leq N \leq 18$. This forces the result that there can only be eight classes of ensemble polyhedra, consisting of 18, 20, 22, 24, 26, 28, 30 and 32 component simplicial cells. Since a Voronoi cell contains space

also defined by fractions of not less than 18, and up to 32 simplicial cells, it is clear that the Voronoi cell may be regarded as a volume-averaging unit, and not a fundamental structural unit, of RCP space. This is not true for the simplicial cell, which is the most fundamental spatial unit possible. In principle, therefore, an analysis of the simplicial cell statistics for a packing provides the most cardinal description for RCP structure.

There are profound differences in the topological properties for simplicial and Voronoi cells, as summarised in table 2.3. In essence, these differences amount to the simplicial cell having perfect regularity, and simplicity, of form. The signficance of this simplicity appears to have been largely overlooked in the literature, and the conventional description of RCP is through the use of Voronoi statistics. Although some early suggestions were made to the effect that simplicial cell statistics might offer advantages over Voronoi statistics (Collins, 1967; Mason, 1967), no such analysis of RCP structure has been attempted prior to the present work.

Bernal and Finney (1967) and Finney (1968) developed the idea of Voronoi cell "shapes" in terms of an array representing frequencies of occurrences of n_i of "shape" types A_i. Finney further developed the concept of a "shape" type neighbour matrix, showing the frequency of occurrence of n_{ij} of "shape" type A_j:

	A_1	A_2	A_i ....
A_1	n_{11}	n_{21}	n_{i1} ...
A_2	n_{12}	n_{22}	n_{i2} ...
.	.	.	.
.	.	.	.
.	.	.	.
A_j	n_{1j}	n_{2j}	n_{ij} ...
.	.	.	.
.	.	.	.

- a further extension adds a third dimension to the matrix, indicating the type of face B_k which is shared by A_i and A_j. Convenient "shape" types are the number of faces on the Voronoi cell with n edges. For example, Finney proposed that a cell may have n(3) trigonal, n(4) quadragonal, n(5) pentagonal faces and so forth. Its "shape" type would therefore be:

n(3)n(4)n(5)n(6)n(7).....

This is, in principle, a powerful topological tool in analysing RCP structure. When he analysed his packing, however, out of a total of 5500 Voronoi cells, Finney found 478 different "shape" types (excluding sub-types), demonstrating the difficulty of using the concept as a model description by which RCP can be visualised. Finney (1968) concluded that the formulation of the shape-type matrix does not appear to be useful in the light of such topological complexity, and up to the present time, the approach has been abandoned.

For the simplicial cell, Finney's proposed array collapses to a linear array of one element for A_i, a two dimensional array of one element for A_{ij}, and a three dimensional array of one element for A_{ijk} when applied to simplicial cells. All simplicial cells are topologically identical, and can only share with triangular faces. This result has several particularly useful aspects, including the description of the network which links simplicial cells to form RCP structure, and the relative ease with which the degree of randomness in RCP structure can be quantified.

Table 2.3 : Comparison of topological attributes for Voronoi and simplicial cells in 3-dimensions

Topological parameter	Simplicial cell (tetrahedron)	Voronoi cell ('n'-hedron)
Number of edges per face	invariant 3	variable 3 to 8
Number of faces per cell	invariant 4	variable 11 to 18
Number of edges per cell	invariant 6	variable
Coordination from cell to cell	invariant 4	variable 11 to 18

2.5 Pore level considerations

In adopting any RCP structure as a model porous medium, it is essential to define the requirements of a pore level model and to satisfy these requirements from the structural description of RCP space. These requirements comprise a meaningful definition of an individual pore, together with a definition of the way in which an individual pore is connected to other pores in the medium.

2.5.1 Pore shape aspects: general

In order to visualise pore shape aspects, some two or three dimensional conceptual model is required. In pore-level studies of porous media, the most frequently encountered two dimensional schematic pore is that shown in figure 2.12. Shape component 'A' in figure 2.12 is variously referred to as the pore, pore body, bulge or cavity. Shape component 'B' is termed the (pore) throat, neck, window, foramina or constriction. Further shape aspects have been suggested by de Boer (1958), who produced fifteen shape groups, and discussed the influence which these groups might have over capillary properties. Variations of some of de Boer's schemes, shown in figure 2.13, are sufficiently fundamental in conceptual terms to occur independently in many subsequent theoretical studies of pore structure (eg Wardlaw 1982; Mahers and Dawe, 1985; Olbricht and Leal, 1983; Koplik and Lasseter, 1982 and Lin and Slattery, 1981). It is clear that in the two dimensional models, only one dimension (ie a discontinuous curve) is needed to define boundaries between solid phases and void space. Real porous

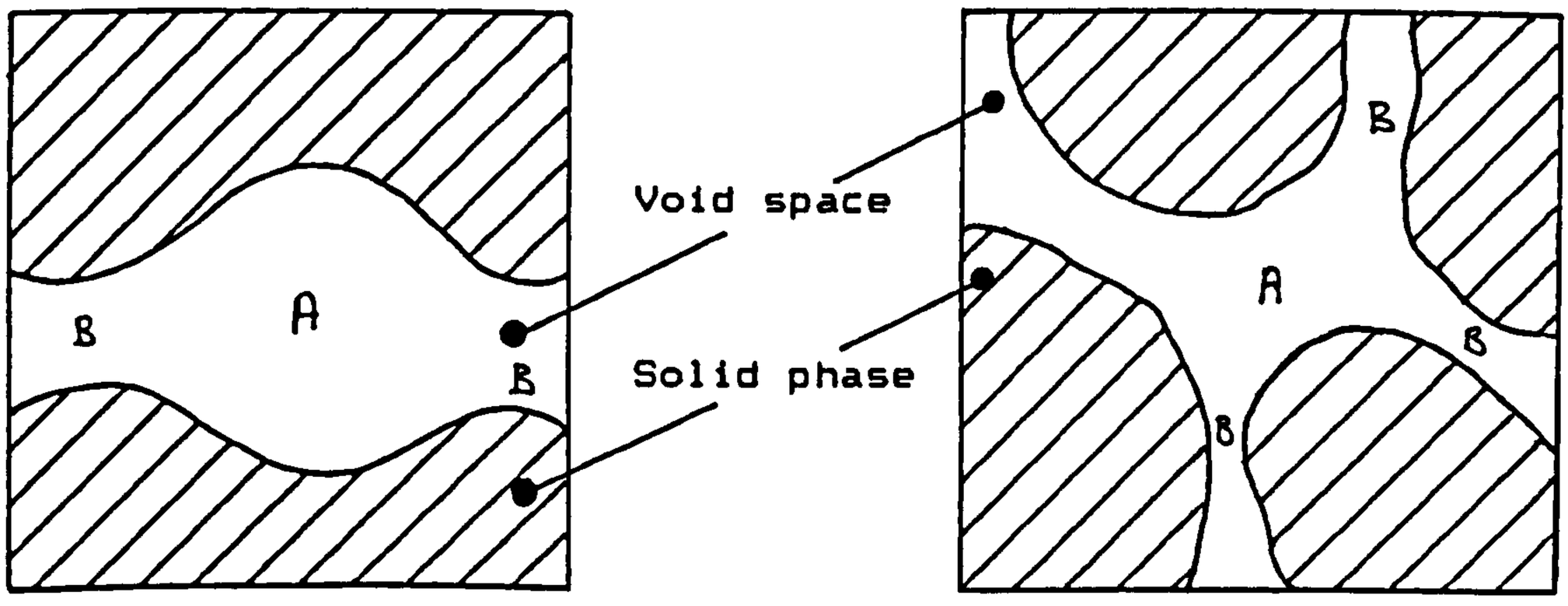

Figure 2.12 : Schematic, two dimensional idealised pores showing common shape attributes 'A' and 'B'.

media are not adequately described by this scheme. Thus a pore body element in a real material is linked, or interconnected, to other pore body elements by throats. The simplest three dimensional representations which can be made are variations of those shown in figure 2.14.

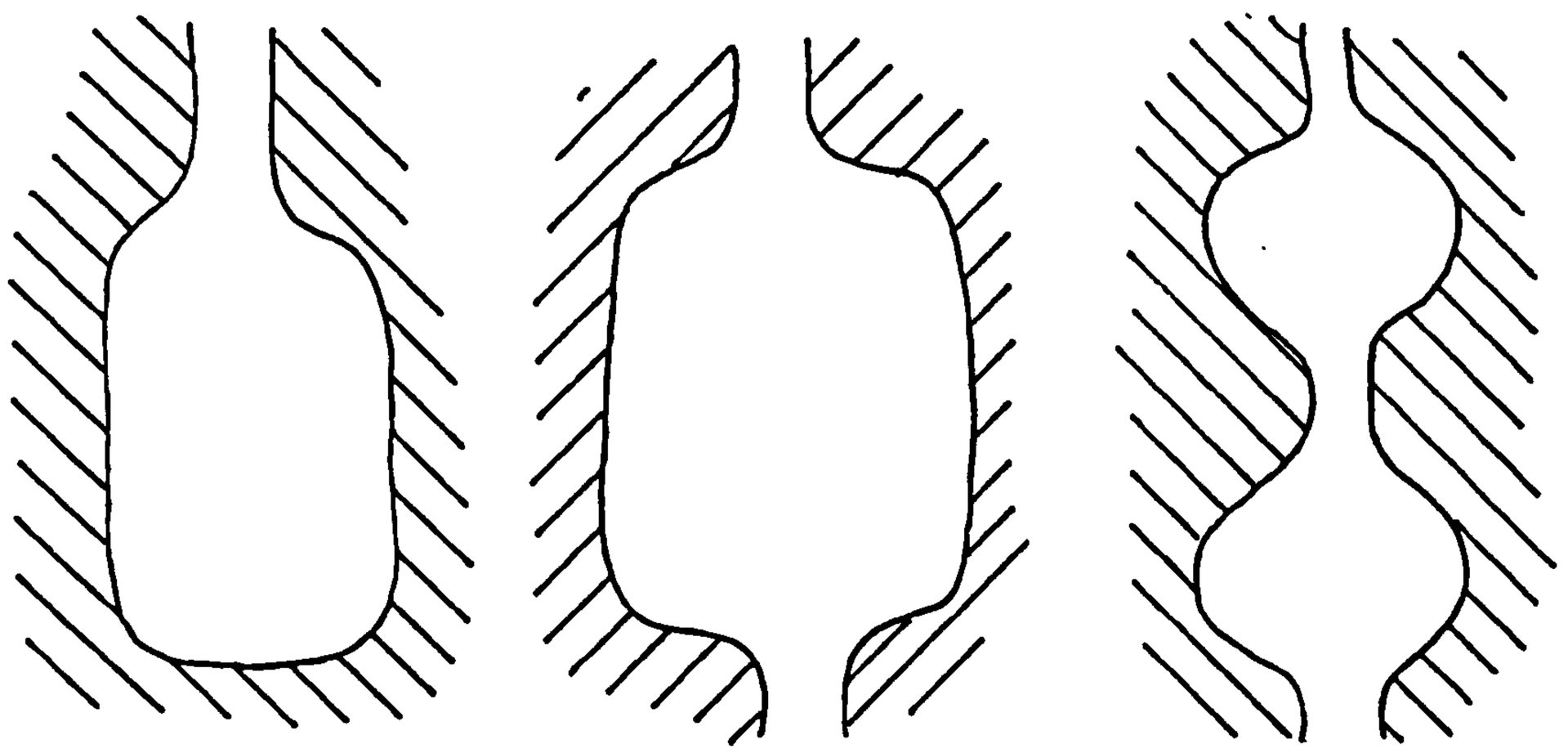

Shape-group IV
Ink-bottle form
(wide necked)

Shape-group VII
Open both ends
with wide parts
and narrow necks

shape-group XV
Tubular with wide
parts of various
widths

Figure 2.13 Shape-groups of capillaries (pores), after de Boer, (1958).

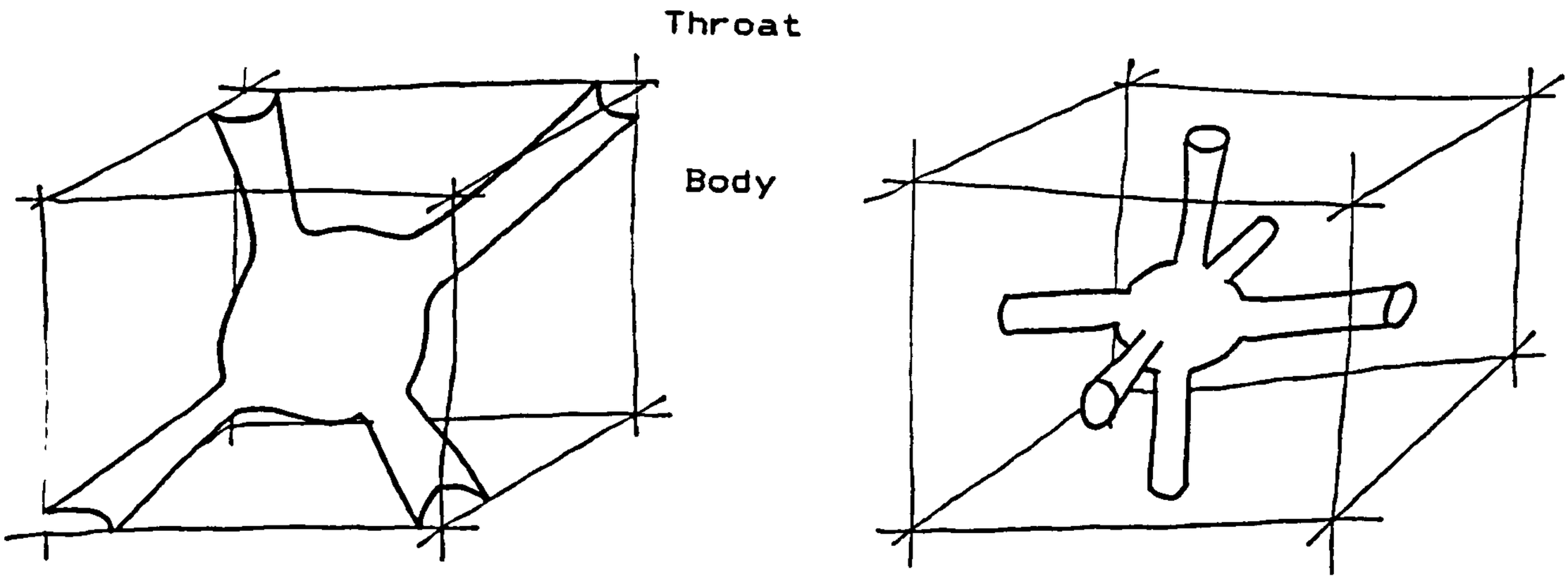

Figure 2.14 : Schematic, three dimensional view of idealised single pores with fourfold coordination (a) and sixfold coordination (b).

The co-ordination number (Z) is used to describe the number of throats entering (or leaving) the pore body. Many disordered materials will not necessarily have an integer co-ordination number for the whole system. In this event, Dulien (1979) suggests the use of the average co-ordination number, $(\bar{Z})$:

$$\bar{Z} = \sum_{r=1}^{R} Z_r f_r \qquad -2.13-$$

and $$Z_r = \tfrac{1}{2}(\Sigma m)_r + 1 \qquad -2.14-$$

Where $(\Sigma m)_r$ is the number of pores connected to a pore of type r, and f_r is the relative frequency of such pores. Yuan (1981)

explores empirically the relationship between ($\bar{Z}$) and porosity, finding that, for granular systems, as ($\bar{Z}$) increases the porosity increases:

$$\Phi = 49.5-(115.1/\bar{Z}) \qquad -2.15-$$

Equation 2.15 serves only to illustrate the functional form of the relationship between porosity and (Z), which is a complex (and generally unknown) function for many disordered particulate systems.

Although the average co-ordination number may be an important aspect of describing pore geometry, the shape aspects of the throats in relation to those of each pore body may be critically important. This has been identified by Wardlaw (1976, 1982) as a pore body to pore throat size ratio problem, and its effect on a single, constant (Z) two dimensional model is evident from figure 2.15.

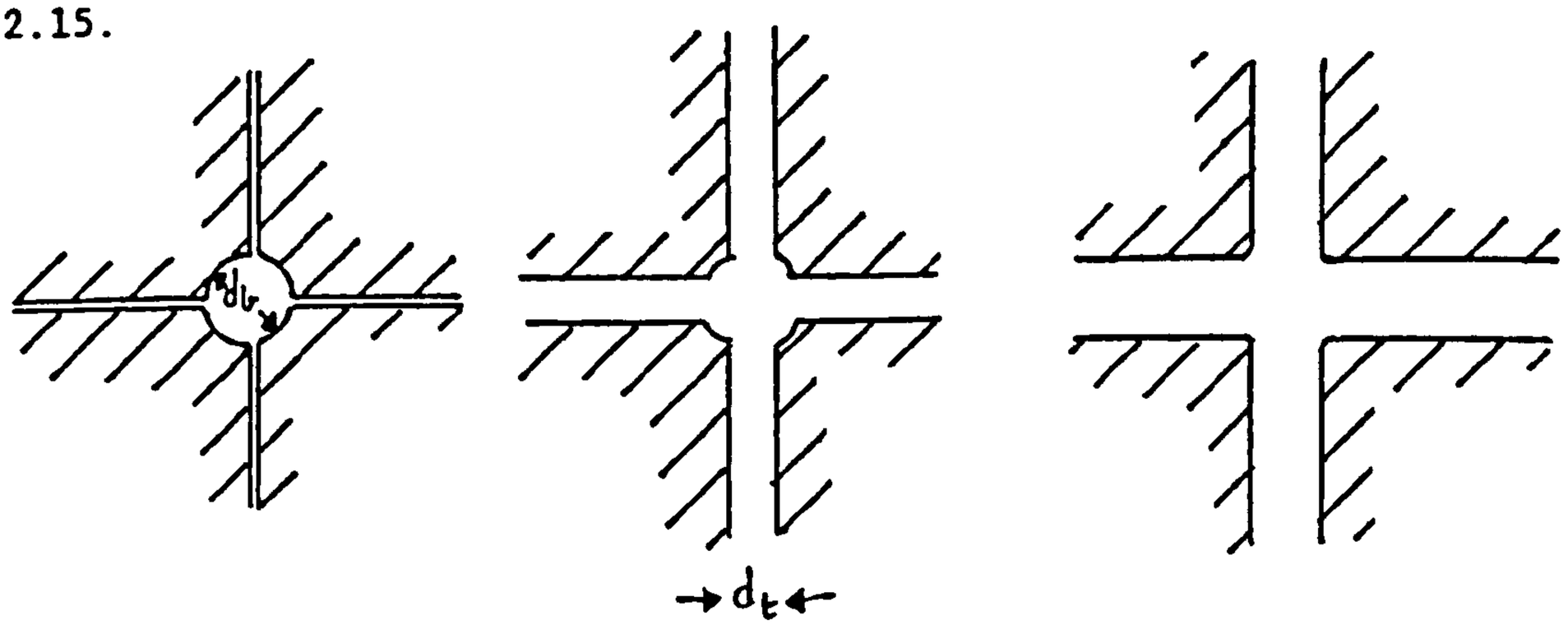

(a) Z=4 $\frac{d_b}{d_t}$ =10

(b) Z=4 $\frac{d_b}{d_t}$ =2

(c) Z=4 $\frac{d_b}{d_t}$ =1

Figure 2.15 : Pore-throat ratios and coordination numbers of simple pore models (after Wardlaw, 1976, 1982).

A satisfactory pore level model appropriate to RCP structure must embody the critical concepts of pore-body and pore-throat dimensions and co-ordination. It is equally important to define the network which connects pores. A fixed (Z) pore implies a regular network, though this is not necessarily the case for disordered systems. Table 2.4 summarises the possible relationships between co-ordination number (Z) and network.

Coordination (Z)	Network structure	Examples
FIXED	REGULAR	Simple simulations
FIXED	VARIABLE	RCP
VARIABLE	VARIABLE	Rocks

Table 2.4 : Range of permissible combinations of pore coordination and network form.

2.5.2 Pore shape aspects: RCP simplicial cell specific

The three dimensional simplicial cell for RCP structure is a tetrahedron, and as shown in figure 2.16 embodies the shape aspects of a pore level model as suggested by Mason (1967, 1971, 1972, 1981, 1983) and Mason and Morrow (1984).

Mason (1971) has shown theoretically that the four simplicial cell faces must be effective constricting elements, equivalent to pore throats, and that the internal void space of the simplicial cell is equivalent to the pore body. Thus the capillary properties of the simplicial cell may be approximated in terms of the meniscus curvatures most likely to fill and empty the cell. Mason (1971) uses the Haines (1927) insphere radius approximation to define the curvature of the sphere (meniscus) that would just pass through the

Figure 2.16

Three dimensional view
of a simplicial cell
for RCP structure.

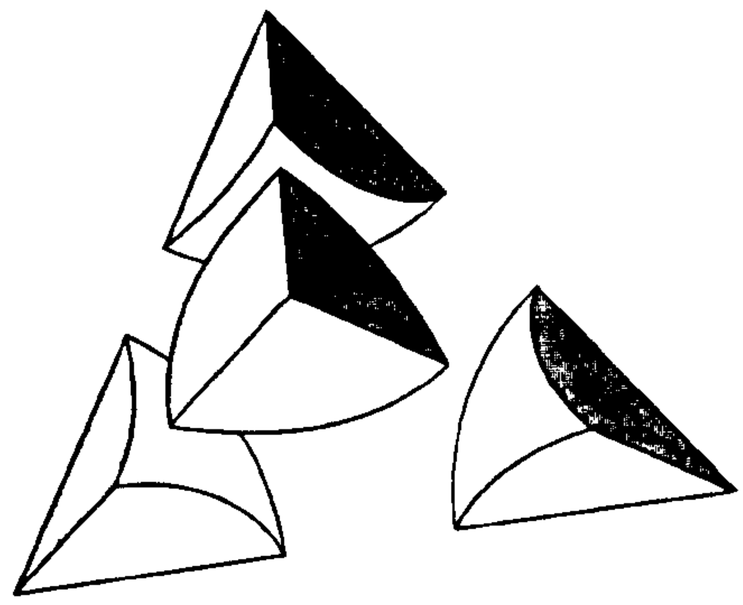

hole in the simplicial cell face as representing the drainage pressure for that face. The approximate imbibition pressure for the simplicial cell has been defined by Mason (1971) as the meniscus curvature equivalent to the sphere which can just fit inside the cell, simultaneously contacting all four apex sphere surfaces. These two forms of in-sphere are illustrated in figure 2.17, which shows the face inspheres relevant to cell drainage, and figure 2.18, which shows the cavity insphere relevant to cell imbibition.

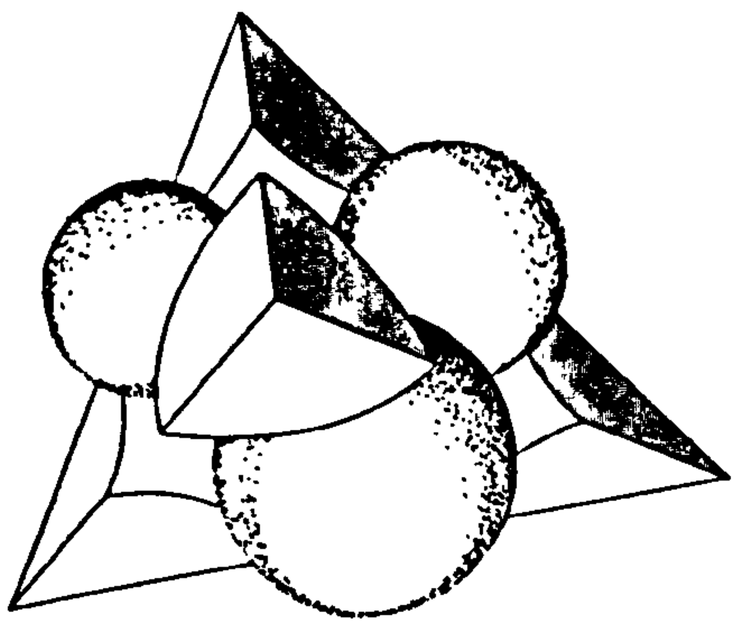

Figure 2.17

The simplicial cell and three of the four face inspheres.

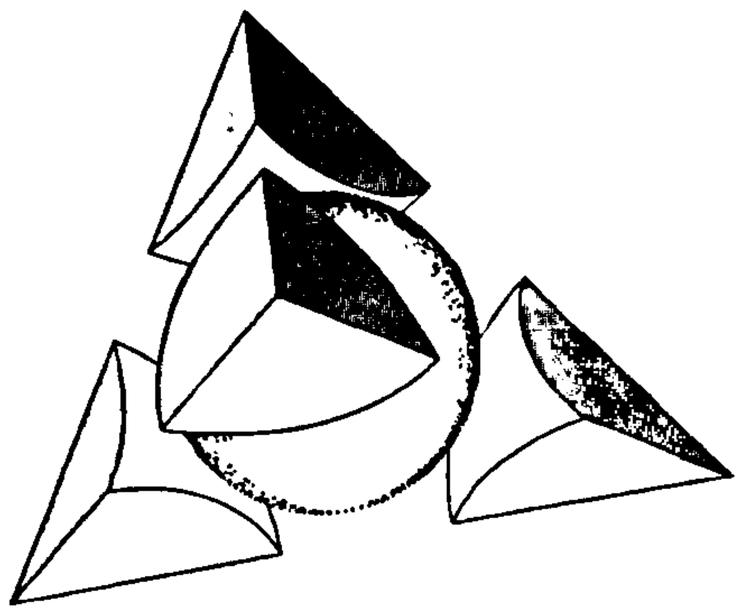

Figure 2.18

The simplicial cell and the cavity insphere.

2.6 RCP pore network

Having defined the individual simplicial cell as a pore, one of the objectives of the present work is to investigate the capillary properties of all such pores in a real packing of spheres. This step requires a complete description of the network which connects all pores in the system, in order to compute saturation changes in individual cells as a function of both neighbouring cell saturations and capillary pressure. Using the convention that the entire void region in an individual simplicial cell is represented by a site, and that the entry/exit condition into or out of the cell is represented by a bond, then that individual cell may be represented as a discrete portion of the network, as shown in figure 2.19.

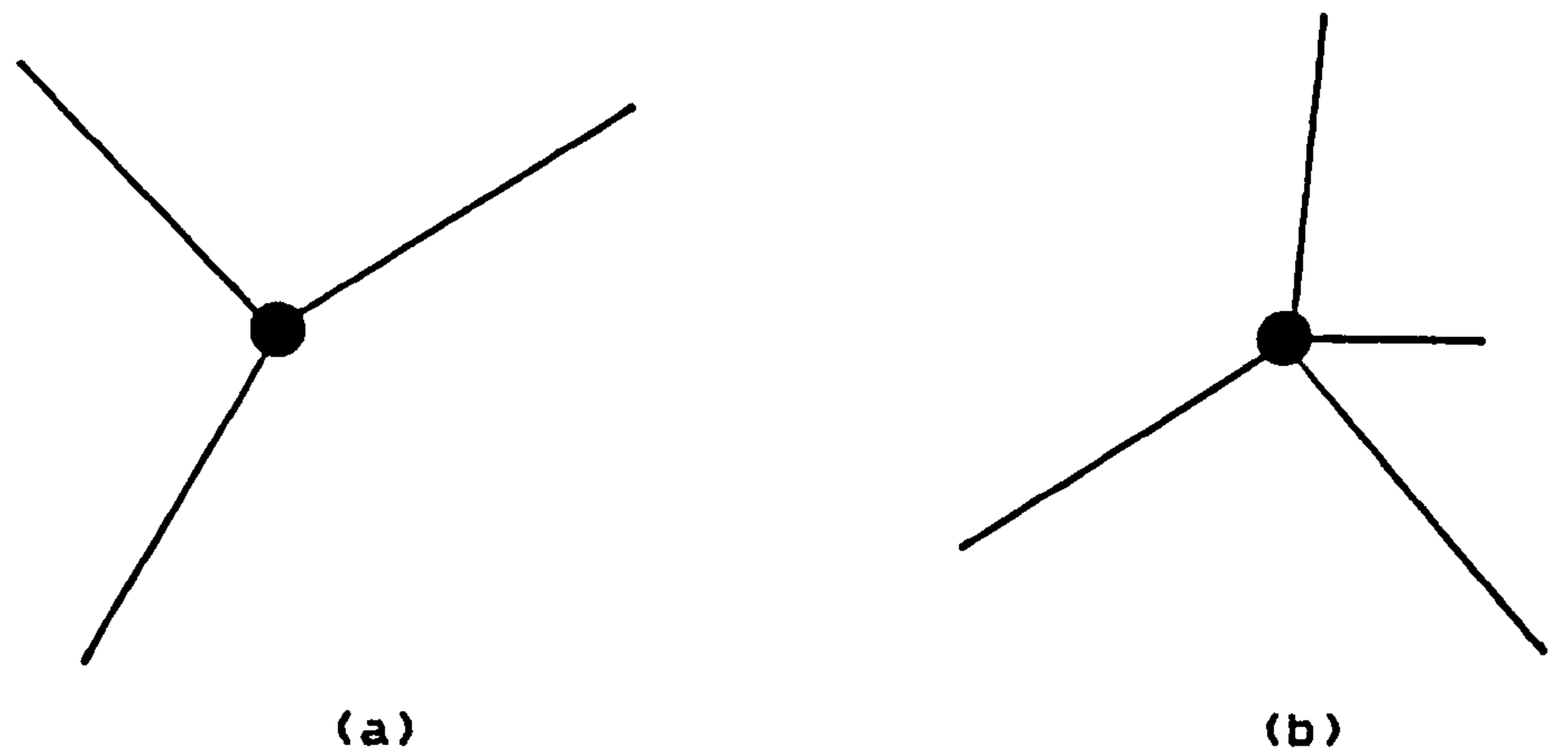

Figure 2.19 : Bond-site representation of an individual simplicial cell in (a) two dimensions and (b) three dimensions.

For capillary pressure-saturation relationships, one appropriate set of dimensions and magnitudes of the sites is void area (for a 2-D cell) and void volume (for a 3-D cell). For the bonds, face incircle radius (for a 2-D cell) and face insphere radius (for a 3-D cell) may be appropriate. In the complete network, each site is connected via Z bonds to Z immediately accessible sites. For a simplicial cell in two dimensions, Z is exactly equal to three, whilst in three dimensions, Z equals four. The form, or structure, of the network is identical to the Voronoi graph. In a real packing of discs or spheres, therefore, once the simplicial cells have been identified, the network connecting all the simplicial cells (in the form of the Voronoi graph) is automatically available. This relationship between simplicial cells and their connecting network is now examined in more detail for a hypothetical, two dimensional case.

Imagine twelve loosely packed circles on a plane, as shown in figure 2.20. The simplicial tessellation defining all thirteen simplicial cells dictated by the pack is shown in figure 2.21. Close examination of figure 2.21 shows that there are three entire ensemble polygons - a five cell ensemble centred on circle 11, a six cell ensemble centred on circle 12 and a seven cell ensemble centred on circle 10. Figure 2.22 shows the corresponding Voronoi graph, defining three entire Voronoi cells centred on circles 10, 11 and 12. The Voronoi cell centred on circle 10 has seven edges, but only just. A slight relative shift in the centre co-ordinates for circles 1 and 3 would result in circle 2 falling outside the current tessellation, eliminating one edge from the Voronoi cell. Whilst this clearly has a marked effect on the frequency

Figure 2.20

Twelve loosely packed circles on a plane.

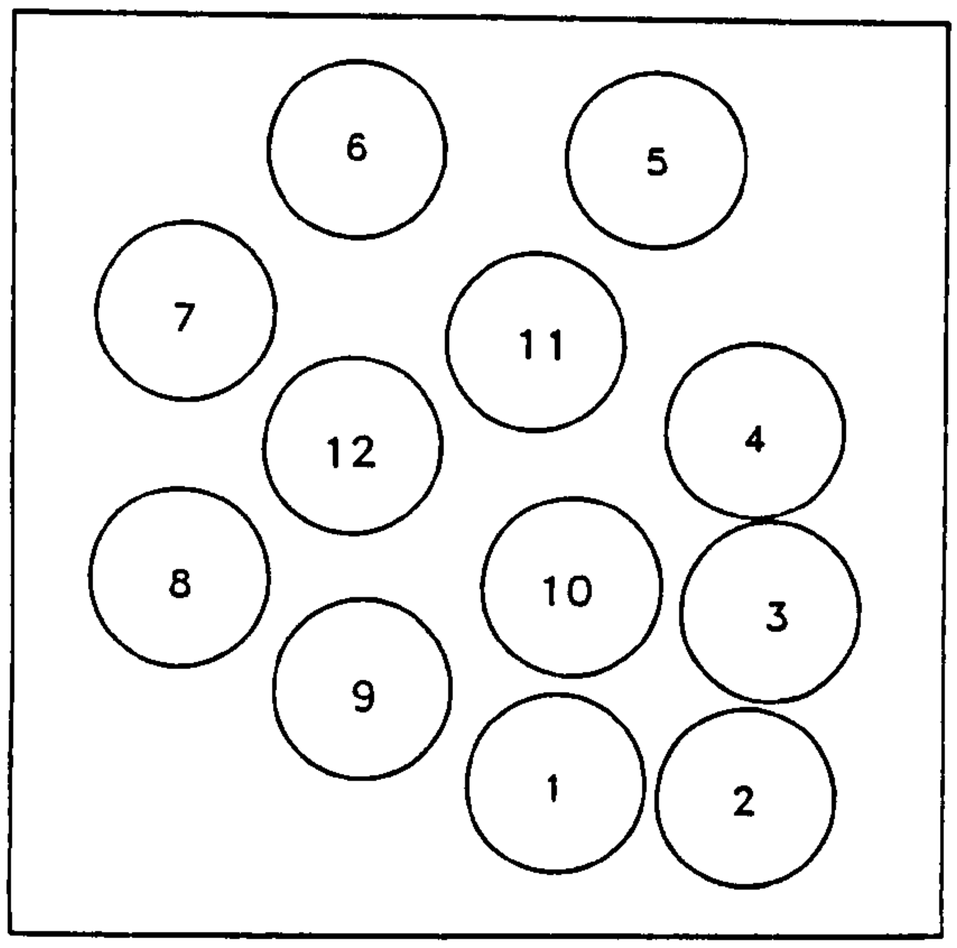

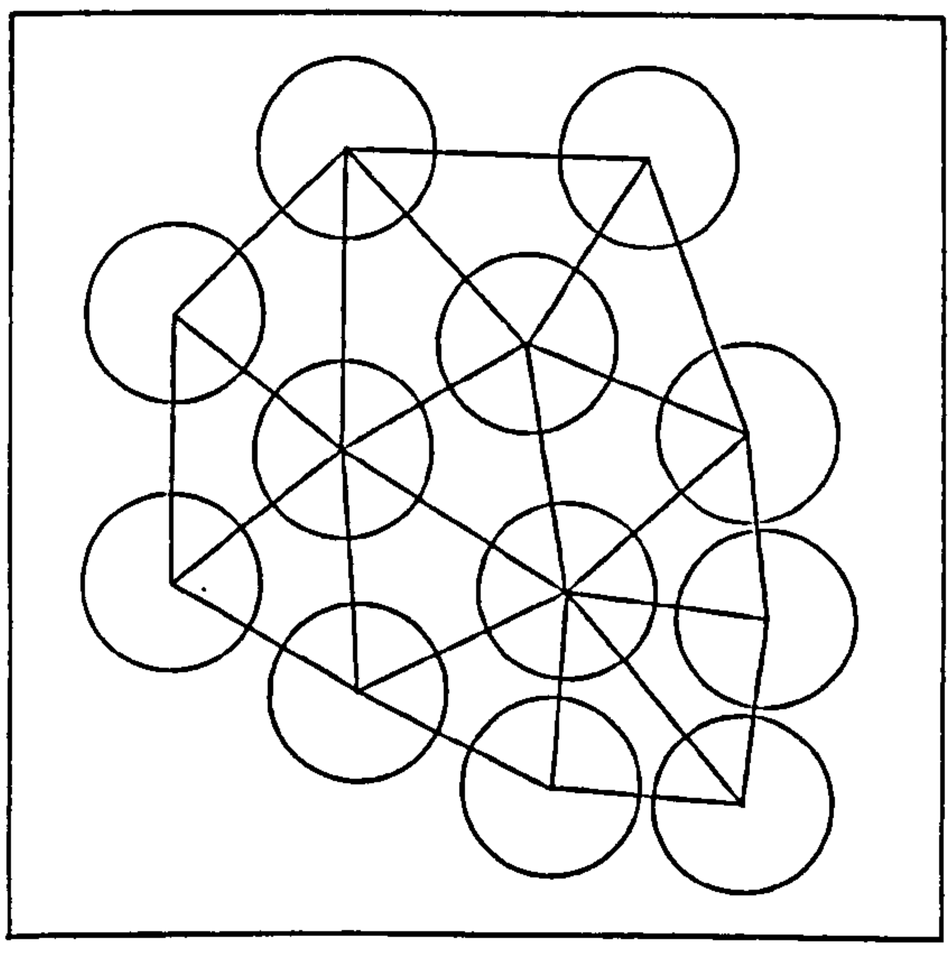

Figure 2.21 : Simplicial graph, simplicial cells and ensemble polygons for the twelve circles.

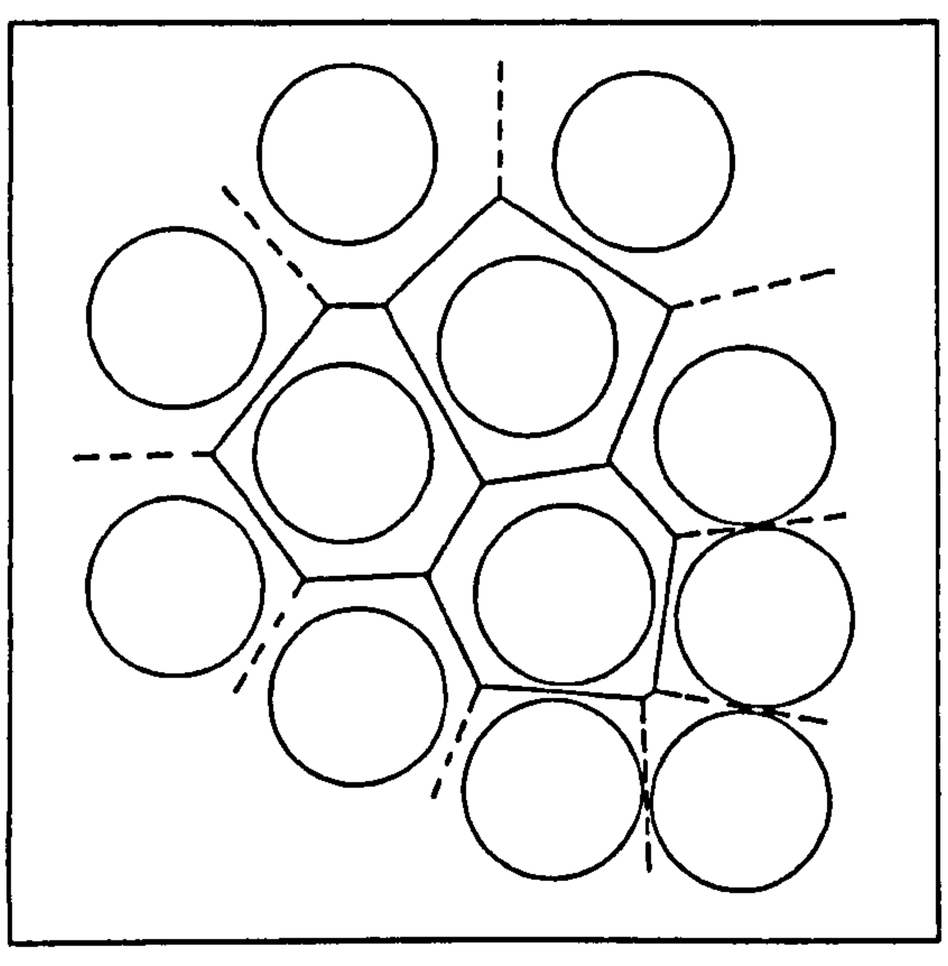

Figure 2.22 : Voronoi graph, and Voronoi cells for the twelve circles.

distribution of Voronoi cell types (i.e. changing from 5, 6 and 7 edges to 5, 6 and 6 edges), there is no frequency distribution change to the basic simplicial cell types. It is intuitively reasonable to expect that such a small change in relative positions for circles 1 and 3 would have a minimal impact on the capillary properties of the pack. The following calculations show this expectation to be correct.

Figure 2.23 shows the site identities adopted for the network connecting all thirteen simplicial cells. Figure 2.24 shows the corresponding bond identities adopted for the network. It should be noted that the network connecting all cells in figures 2.23 and 2.24 is identical to the Voronoi graph shown in figure 2.22, and

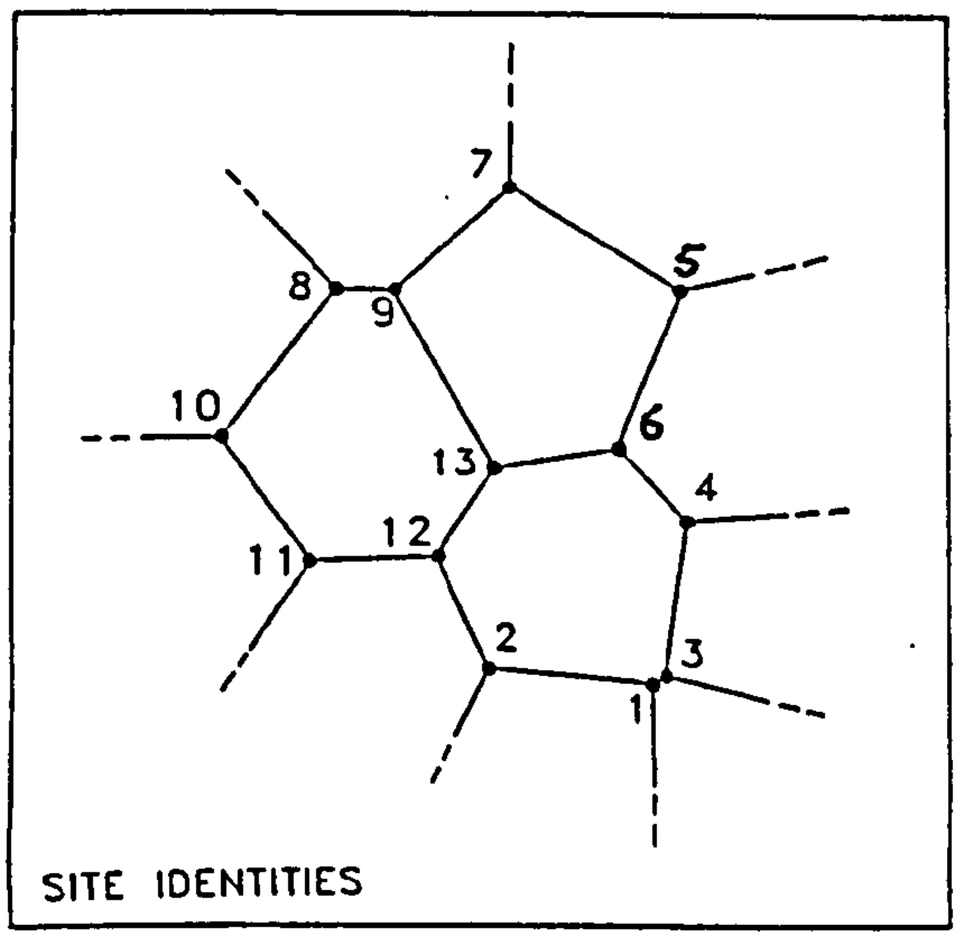

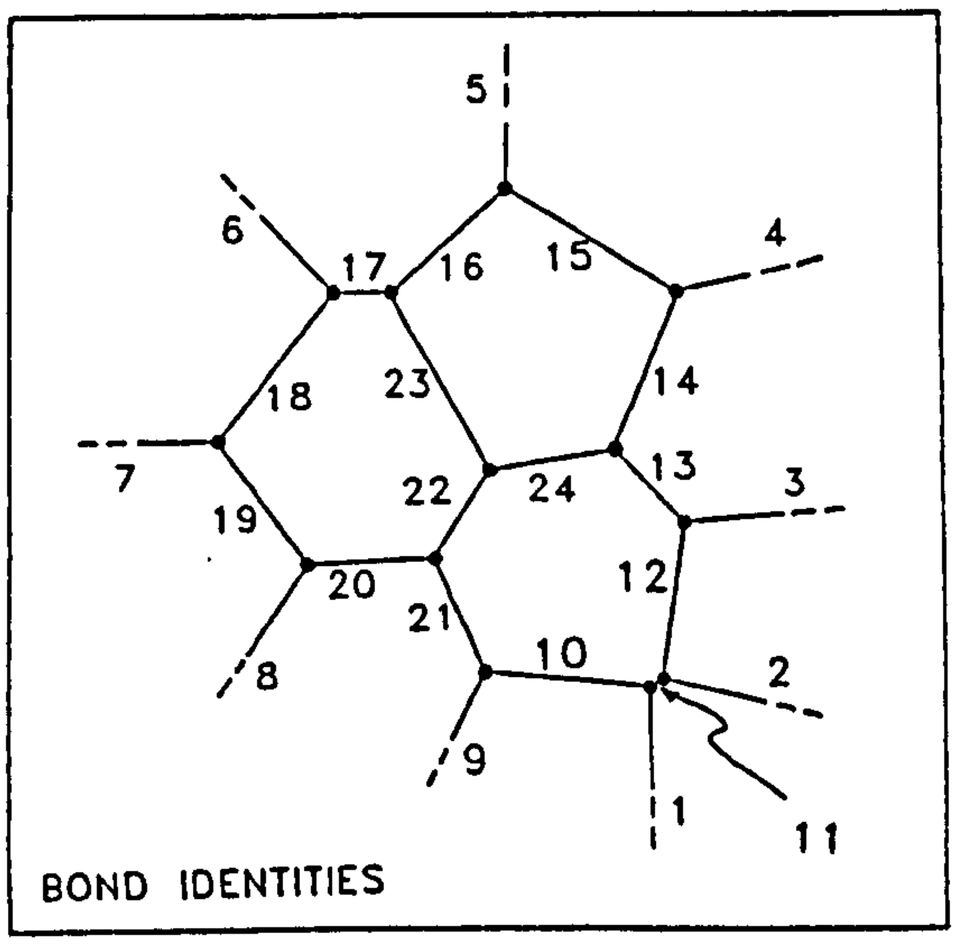

Figure 2.23 : Site identities for the network which connects the simplicial cells

Figure 2.24 : Bond identities for the network which connects the simplicial cells

that the sites correspond with the Voronoi cell vertices, and the bonds with the Voronoi cell edges. The capillary pressure curve for the twelve loosely packed circles is readily calculated by making the assumption that the critical two-dimensional meniscus curvature which describes the invading, non-wetting phase (simulating mercury injection) is simply:

curvature = 2/r

where r is the dimensionless radius (i.e. radius in circle-diameters) of the incircle which just fits in between two circles defining one edge of the simplicial cell. The dimensionless magnitude of the bonds shown in figure 2.24, therefore, is equal to the linear distance between the circle centres minus one (in circle-diameters). These bond magnitudes, and the relationship between bond numbers and circle numbers is shown in table 2.5.

The dimensionless magnitude of the sites is conveniently defined as the void (pore) area. The pore area is the two dimensional analogue of pore volume in three dimensions. The pore area is used to calculate the two dimensional saturation changes resulting from invasion of the packing by a non-wetting fluid. Since the sum of the face angles of each simplicial cell is always 180 degrees, this is calculated using elementary trigonometry as follows:

Void space (area) - $[s(s-a)(s-b)(s-c)]^{\frac{1}{2}}-pi/8$ -2.16-

where a, b, c are the lengths of the simplicial cell sides in circle-diameters, and $s=\frac{1}{2}(a+b+c)$. The dimensionless site

Table 2.5 : Dimensionless bond magnitudes, and relationships between bond and circle identities.

Circle Numbers	Bond Number	Bond Magnitude (circle diameters)
1-2	1	0.0625
2-3	2	0.0469
3-4	3	0.0313
4-5	4	0.6406
5-6	5	0.6875
6-7	6	0.3281
7-8	7	0.5000
8-9	8	0.2031
1-9	9	0.2188
1-10	10	0.0938
2-10	11	0.5313
3-10	12	0.1250
4-10	13	0.3438
4-11	14	0.3438
5-11	15	0.2344
6-11	16	0.4844
6-12	17	0.6875
7-12	18	0.2188
8-12	19	0.2344
9-12	20	0.3750
9-10	21	0.3125
10-12	22	0.4688
11-12	23	0.1875
10-11	24	0.3906

magnitudes, and the relationship between site and circle numbers is shown in table 2.6.

The capillary properties of the loose, two dimensional packing are described by finding the critical meniscus curvatures (critical bond values) which will permit a non-wetting, invading fluid phase to increase its own saturation in the thirteen simplicial cells from initially zero to unity. For the small numbers of bonds and sites involved here, this process can be carried out by inspection, and the results are listed in table 2.7 and presented graphically in figure 2.25.

Table 2.6 : Dimensionless site magnitudes, and relationships between site and circle identities.

Circle Numbers	Site Number	Site Magnitude (Pore area, dia^2)
1,2,10	1	0.188
1,9,10	2	0.229
2,3,10	3	0.205
3,4,10	4	0.192
4,5,11	5	0.399
4,10,11	6	0.412
5,6,11	7	0.494
6,7,12	8	0.419
6,11,12	9	0.474
7,8,12	10	0.328
8,9,12	11	0.299
9,10,12	12	0.443
10,11,12	13	0.392

Table 2.7 : Capillary properties of the 12 circle loose pack.

Invasion Step	Critical Bond Value	Critical Meniscus Radius (r)	Critical Meniscus Curvature (2/r)	Sites Filled	Pore Area Filled
1	0.6875	0.3438	5.82	7	0.1104
2	0.6406	0.3203	6.24	5,7	0.2000
3	0.5000	0.2500	8.0	5,7,10	0.2728
4	0.4844	0.2422	8.26	5,7,8, 9,10	0.4725
5	0.3438	0.1719	11.63	4,5,6, 7,8,9, 10,11,12, 13	0.8609
6	0.3125	0.1563	12.8	2,4,5,6, 7,8,9,10, 11,12,13	0.9121
7	0.1250	0.0625	32.0	1,2,3,4, 5,6,7,8, 9,10,11, 12,13	1.000

The last two simplicial cells to be filled are (sites) 1 and 3, which are filled simultaneously via bond 12. As discussed earlier, moving circles 1 and 3 slightly would significantly alter the Voronoi and simplicial graphs, replacing sites 1 and 3 by two new sites. The net change in pore area, and the net change in critical bond dimensions caused by such a shift, however, is negligible. The overall effect on capillary properties of such a small spatial perturbation is therefore also negligible, and the capillary properties of the pack are seen not to be sensitive to the number

Figure 2.25

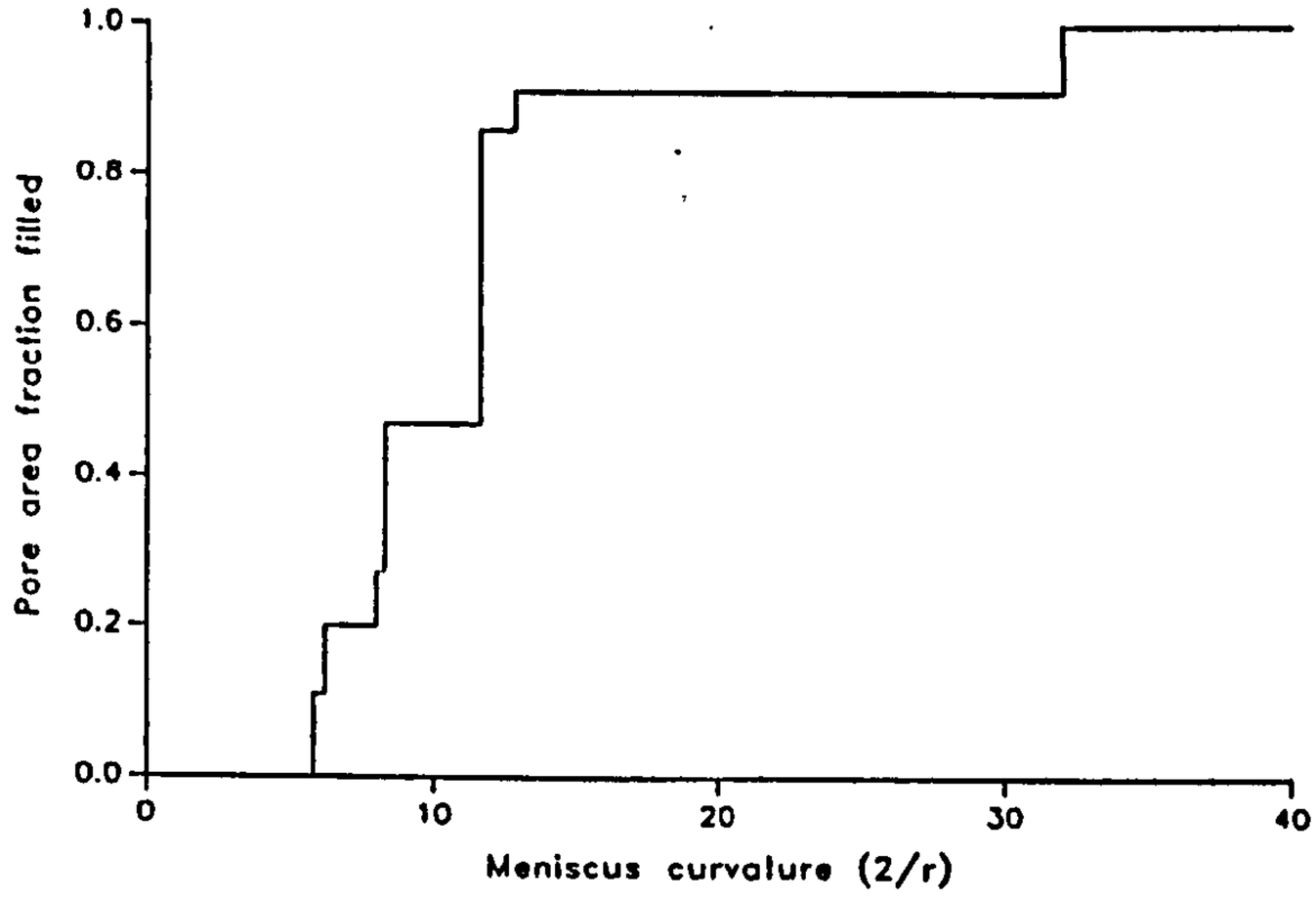

Capillary pressure curve (invading, non-wetting phase) for the loose circle packing shown in figure 2.20

of edges in the component (2 dimensional) Voronoi cells. Although not demonstrated here, the same argument must apply equally well to three dimensions. In other words, minor shifts in sphere positions result in only minor changes in capillary properties, despite the fact that an individual Voronoi cell which is affected experiences a quantum change in the number of its faces.

2.7 Summary of RCP space discretisation

The novel concept of ensemble polyhedra has been used to show that the Voronoi polyhedron is a comparatively large, volume averaging irregular unit of RCP space. The simplicial cell, on the other hand, is a completely fundamental structural unit of RCP space, with constant topological properties. These two aspects of the simplicial cell constitute an intrinsically more useful measure of RCP structure than the Voronoi cell. A novel proof based on Euler's formula is presented which shows that a Voronoi cell cannot exist with an odd number of component simplicial cells in the equivalent ensemble polyhedron. This proof is of practical value in validating any subdivision of RCP space, as an odd number of component cells in a fully closed ensemble polyhedron (i.e. one not partially complete at the pack outer surface) is direct evidence of a subdivision error. The range of the number of "fragments" of simplicial cells which a Voronoi polyhedron "contains" is $18 \leq N \leq 32$.

With reference to the use of RCP structure as a model porous medium, the Voronoi cell is shown to be perfectly useless as a pore-level descriptor of space relevant to capillary processes within the pack. The simplicial cell, however, has been shown to fully embody all the essential geometrical and topological properties required of an individual pore, including pore body and pore throat attributes, as well as constant co-ordination (Mason, 1971). The network fully linking all simplicial cells (pores) in the pack is the Voronoi graph. Any analysis which yields the

identity of all simplicial cells automatically also provides the identity of the network connecting those cells, as well as the identity of all the ensemble polyhedra. The co-ordination (z) of the network connecting all simplicial cells is constant. In two dimensional networks the co-ordination number is always three, whilst in three dimensional networks the co-ordination number is always four.

CHAPTER 3: SIMPLICIAL CELL ANALYSIS OF THE FINNEY MODEL

The Finney model is the largest and most accurate of all real sphere packings. The purpose of this Chapter, then, is to derive simplicial cell frequency distributions for the Finney packing. Such distributions shed considerable light on the structure of the Finney packing, particularly from the porous medium perspective.

3.1 Size and shape of the RCP structure

The method of construction of the packing is described by Finney (1968). In order to restrict the analysis to regions least likely to be affected by the outer boundary of the packing, only the central 2000 Voronoi polyhedra were used. In order to reconstruct the Voronoi cells for these 2000 central spheres, the co-ordinates of an additional 1367 spheres surrounding the central 2000 are required to define the ensemble polyhedra needed in the construction process, totalling 3367 spheres in all. Figures 3.1 and 3.2 show isometric and sectional views of the packing.

The subdivision of this set of 3367 sphere centre co-ordinates into its component simplicial cells was not undertaken by me. Some years prior to the present work, Wright (1986) had already completed the subdivision for other purposes, as part of his work on the physics of amorphous solids. Accordingly, the sphere centre co-ordinates, together with the 14870 simplicial cell identities obtained by Wright (1986) were transferred to the BP Research Centre on magnetic tape from the Reading University Computer Department.

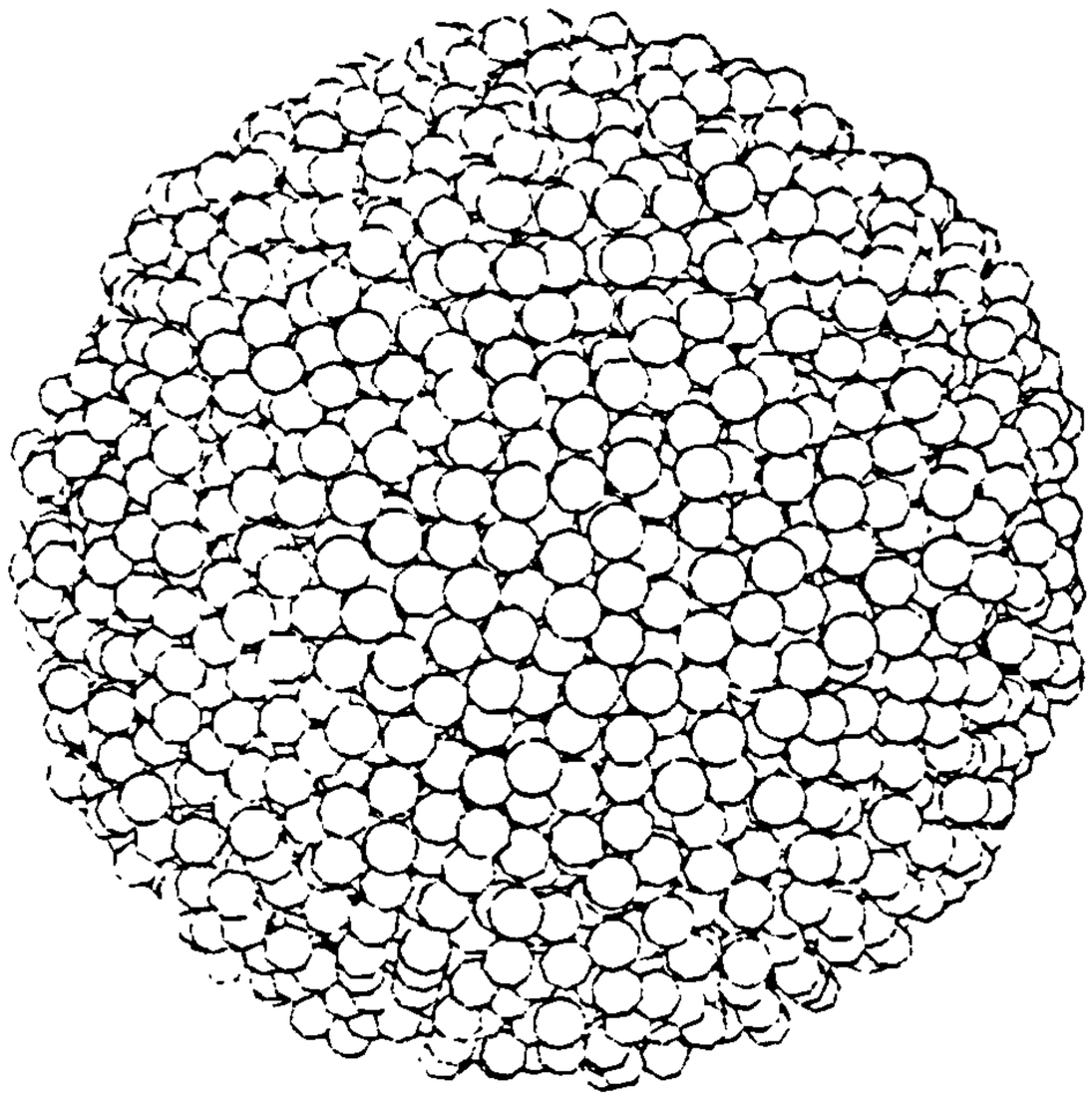

Figure 3.1

Central portion of the Finney model (looking down the Z axis)

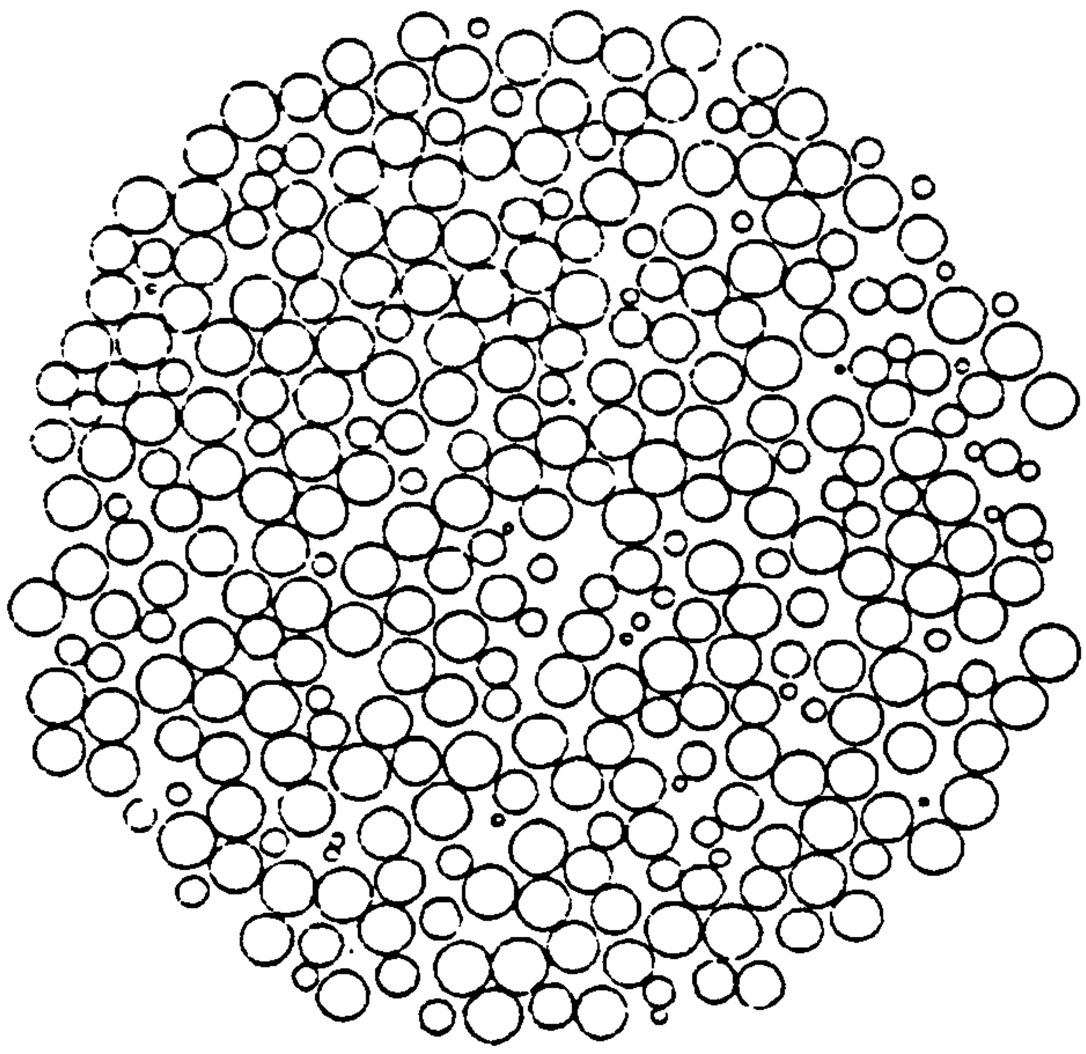

Figure 3.2

Section through the Finney model in the X-Y plane at Z=0

Although the analysis of the 14870 simplicial cells of the Finney model is central to this, and to subsequent chapters of this thesis, the actual subdivision process itself is not. This is for three reasons:

(i) Suitable subdivision routines are available in the open literature (e.g. Winterfeld, 1981). The development of another subdivision routine is therefore unnecessary, and would not necessarily constitute useful, original work.

(ii) The specific subdivision of the Finney packing itself is not original work, having been performed originally by Finney (1968) in order to determine the identity of the spheres defining the component Voronoi cells of the packing.

(iii) Writing a subdivision routine is time consuming, and would involve extremely heavy CPU usage.

What is important is to establish that the subdivision performed by Wright is correct. The verification procedures developed in this chapter, and in chapter five, are important and represent original work which will be useful to other workers attempting a simplicial cell subdivision. The procedure used by Wright does produce a very small proportion of errors in the subdivision process. These errors appear to be associated with machine precision, and are not errors of logic. It seems to be a possibility that <u>any</u> subdivision routine may be subject to similar sorts of machine precision error, increasing the requirement for stringent validation procedures.

It is worth recording here a brief outline of the subdivision process used by Wright (1986), since the process differs very

considerably from Winterfeld's (1981) expanding sphere process. Wright's (1986) procedure comprises essentially five stages. These stages are:-

(i) Decide on the maximum simplicial cell edgelength. Test the decision by gradually increasing the maximum cell edgelength value on a trial section of the packing until no change in the subdivision is observed. The maximum value selected in practice was 1.65 sphere diameters.

(ii) Take each sphere in turn as the reference sphere, i, and find the identity of all neighbouring spheres within the maximum simplicial edgelength distance (i.e. 1.65 sphere diameters).

(iii) For all neighbours to sphere i, re-calculate their co-ordinates relative to i, and produce a table which lists neighbour identities, distances to i, and new co-ordinates of neighbours (co-ordinates of sphere i are now 0, 0, 0).

(iv) Choose two spheres j and k. Check that j is a neighbour of k. Take sphere l so that l is a neighbour of i, j and k. The four spheres i, j, k and l form a possible simplicial cell. Now calculate the co-ordinates of the equidistant point, p, from spheres i, j, k and l.

(v) Suppose that i, j, k and l are all true geometric neighbours forming a true simplicial cell. The equidistant point, p, is then a supposed vertex of the Voronoi polyhedron.

Now, examine every other neighbour to i, and call each of these h in turn. Take the perpendicular distance of the supposed vertex to the plane which is a perpendicular bisector plane of the line joining i to h. The sign of that distance determines which side of the perpendicular bisector plane the supposed vertex is on. If the supposed vertex is on the same side as the reference sphere, i, it is a true vertex. Otherwise, the supposed vertex is not a true vertex. This stage completes the procedure used by Wright (1986).

The final stage, (v), may be prone to a small but finite chance of machine error, since the decision to accept or reject a point as a true vertex hinges on the precision with which two numbers (distances) can be compared in order to derive the sign of the distance.

3.2 Analytical Procedure

It is clearly an important step in the analysis to verify that the simplicial cell division of the model is consistent with Finney's (1968) detailed analysis of Voronoi cells. However, in order to begin this verification, a basic analytical procedure must be defined and adhered to throughout. The first, and most essential, part of this procedure is to define a consistent reference tetrahedron geometry. This is shown in figure 3.3, and the convention is used throughout the present work. The sequence of edgelengths is critical to analytical accuracy since, although the four sphere centre co-ordinates alone uniquely define the tetrahedron, an unsequenced list of six edgelength values does not.

Figure 3.3 : STANDARD TETRAHEDRON GEOMETRY USED IN THE PRESENT WORK

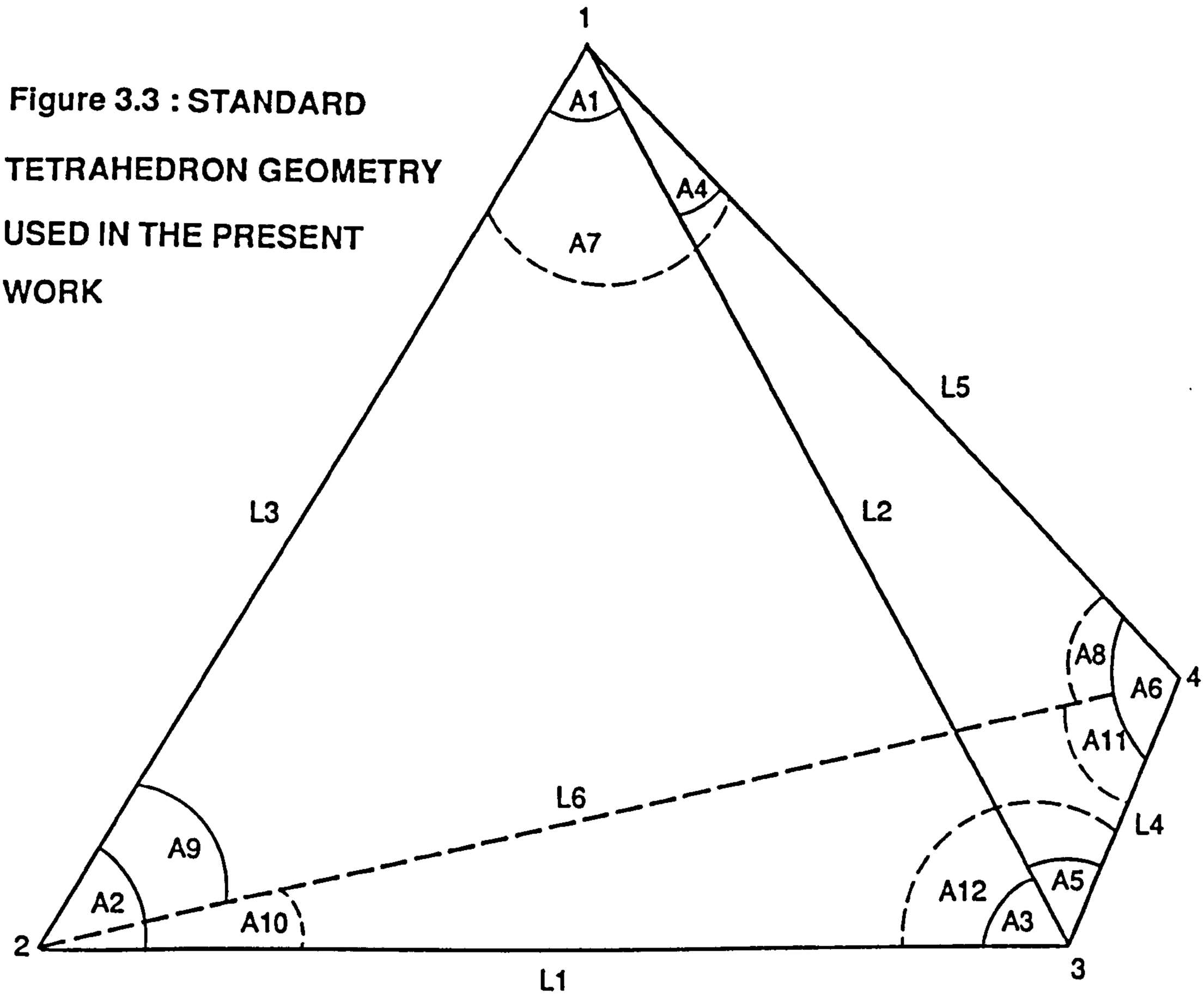

A pre-set sequence of edgelengths in relation to the sphere centre co-ordinates is required to define uniquely the tetrahedron by using edgelength values only.

The relationship between angles, faces, edges and apices for the standard geometry adopted in the present work is summarised in table 3.1.

All relevant properties of the simplicial cell may be derived from the array L_i which contains the six edgelength values in the preset

TABLE 3.1 : Geometrical relationships of the standard tetrahedron.

	Face angles	Edges	Apices
Face 1	A1,A2,A3	L1,L2,L3	1,2,3
Face 2	A4,A5,A6	L2,L4,L5	1,3,4
Face 3	A7,A8,A9	L3,L5,L6	1,2,4
Face 4	A10,A11,A12	L1,L4,L6	2,3,4

sequence shown in table 3.1. The values of L_i for the 14870 tetrahedra used are obtained from the apex sphere centre co-ordinates. For two such apex sphere centres at P and Q:

Point P at (X_p,Y_p,Z_p)

Point Q at (X_q,Y_q,Z_q)

Distance PQ = $((X_q-X_p)^2+(Y_q-Y_p)^2+(Z_q-Z_p)^2)^{\frac{1}{2}}$

The array L_i is conveniently held in the two dimensional array (matrix) [F] in which the first of the seven columns is the simplicial cell number, or identity, The array [F] is therefore (14870,7) in size, and is held in the data file FINEDGE.DAT, written by program LENGTHS (see Appendix B). The dimensions of edgelengths are conventionally hard sphere diameter, not radius (Mason, 1971). This convention is adhered to for [F].

3.3 Verification of RCP space discretisation

3.3.1 Packing density

As packing density is one of the characteristic attributes of RCP structure, the calculated average simplicial cell packing density must conform with the average value obtained by Finney (1968).

The average packing density for the 14870 simplicial cells was calculated by finding the cumulative total tetrahedron volume (V_t) and the cumulative solid (i.e. sphere segment) volume (V_s) as shown in Appendix A. The average simplicial cell packing density is the quantity V_s/V_t. The result so obtained for the 14870 simplicial cells is a value of average cell packing density of 0.6380. This compares with Finney's result of 0.6366 ± 0.0004 for the Voronoi cells of entire packing. The reason that the two estimates do not match closely is that there are fluctuations in density in the Finney pack, as shown in table 3.2. It is evident from this table that the average Voronoi cell packing density obtained by Finney (1968) for the first 2000 spheres is higher than the average density for the whole pack. The figure of 0.6382 obtained by Finney for the first 2000 Voronoi cells agrees well with the figure of 0.6380 obtained here for the first 14870 simplicial cells surrounding the first 2000 spheres. There cannot be identical correspondence between the component simplicial cells and the Voronoi cells, since the former protrude through the space defined by the latter, contacting the outer surface of the 1367 additional spheres of the ensemble polyhedra needed to define the central 2000 Voronoi cells. Despite this inexact geometric correspondence, the agreement (within 0.03% of the expected value) between packing density obtained by

this work and Finney's work suggests that the subdivision performed by Wright (1986) and used in this work is correct in general.

TABLE 3.2 : Packing density variations in the Finney model, as measured by Finney (1968).

Centres	Average density
Central 327	0.6399
1-2000	0.6382
2001-4050	0.6368
4051-6340	0.6353
6341-7934	0.6365

3.3.2 Simplicial and Voronoi cell relationships

The formal proof derived in section 2.3.2 shows:

$$2N-T = 4 \qquad \text{-2.8-}$$

where T = the number of component tetrahedra in the individual ensemble polygon which is required in order to define uniquely the Voronoi cell, and N = the number of geometric neighbours (= the number of faces on the Voronoi cell, = the total number of spheres in the construction minus one). Counting the numbers of simplicial cells which share a sphere at the centre of a Voronoi cell,

therefore, constitutes another form of verification test for the subdivision. In order to pass this verification test, all correctly subdivided Voronoi cells must be associated with an even number of component simplicial cells in the equivalent ensemble polyhedron. Analysis programs written to undertake this test (VORONOI and VORONHIST in Appendix B) reveal an error associated with the subdivision of space surrounding sphere number 2000, for which the Voronoi cell was found to be associated with 27 simplicial cells. This single error was rectified by assigning the "rogue" simplicial cell to the 26 class of ensemble polyhedra. The error is not considered to be particularly significant, as it represents only one error in 14870 cell divisions detected by this test. This error assumes a slightly greater significance when the network connecting all cells is considered. This error is discussed in more detail in Chapter five.

3.3.3 Voronoi cell statistics

The distribution of the eight classes of Voronoi cells found by the present work is shown in table 3.3, and in figure 3.4, in which it is compared with the distribution of cells for the central 5500 spheres of the original Finney pack. The correspondence is excellent.

As a final check on the subdivision of space, the average number of Voronoi polyhedron faces is calculated.

Since the number of Voronoi cell faces is identical with the number of ensemble polyhedron vertices, and also with the number of nearest

neighbour spheres, the expression for average number of faces for all Voronoi cells for the central 2000 spheres is:

$$\bar{F} = \sum_{j=1}^{2000} N_i f_i \; / \; \sum_{j=1}^{2000} f_i \qquad \text{-3.1-}$$

Evaluating equation 3.1 from the data in table 3.3 yields a value for the average number of faces for the central 2000 Voronoi cells of 14.252. This compares with a figure of 14.251 ± 0.015 obtained by Finney for the central 5500 Voronoi cells. This is the final verification test, and all four together (packing density, even frequencies of component simplicial cells, Voronoi cell statistics and average number of faces per cell) confirm that, despite the one identified error, the 14870 simplicial cells used in the present

TABLE 3.3 : Relationship between Voronoi cells and simplicial cells for central 2000 spheres of the Finney model (this work).

Number of component simplicial cells in ensemble polyhedron	Frequency	Number of nearest neighbours
(T_i)	(f_i)	(N_i)
17		
18	4	11
19		
20	86	12
21		
22	418	13
23		
24	683	14
25		
26	566	15
27	(1)*	
28	195	16
29		
30	39	17
31		
32	8	18

* Rogue cell

work represent an accurate, and valid description of the Finney RCP model. The identified error is not considered to be significant for the work reported in Chapter 3.

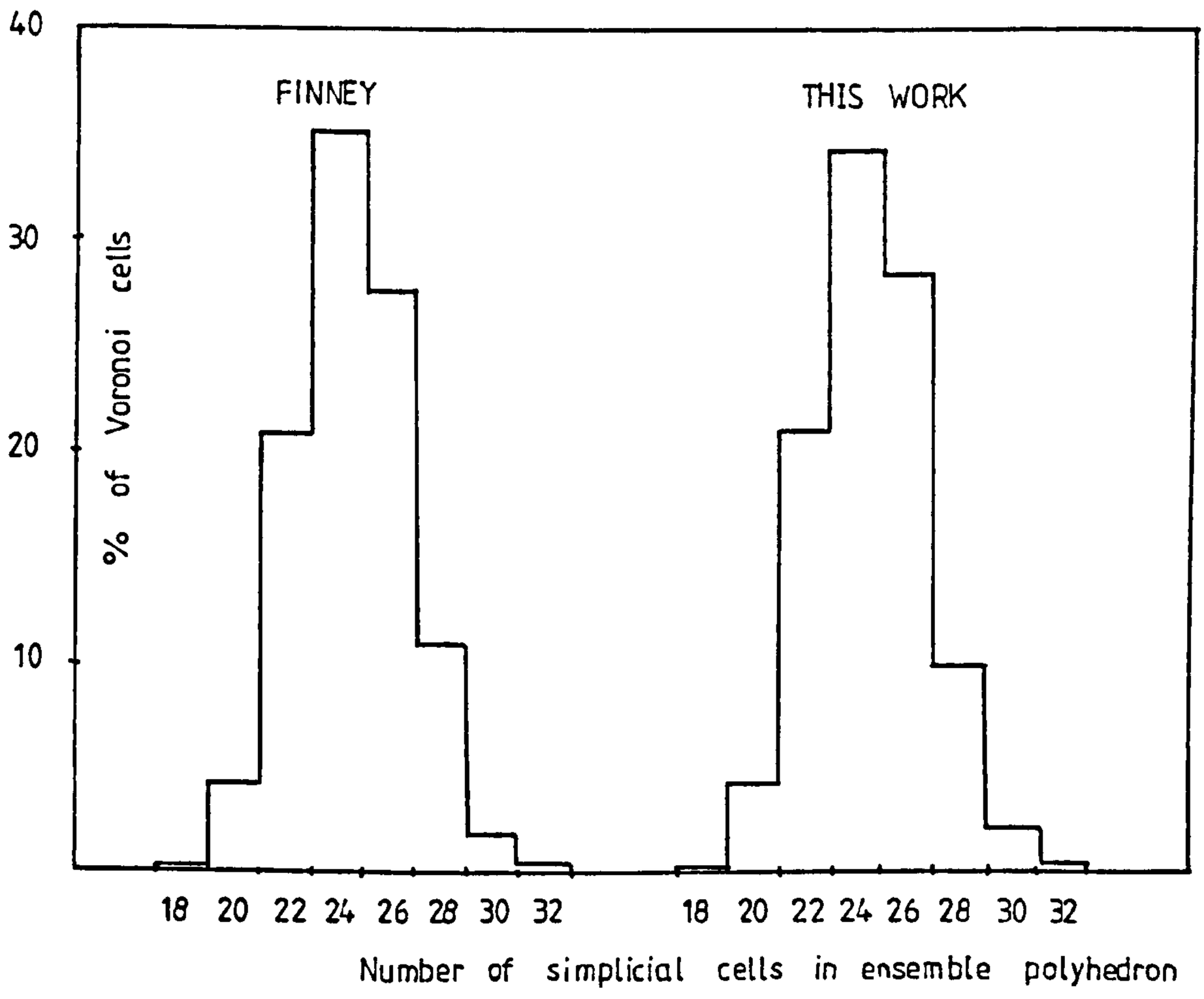

Figure 3.4 : Comparison of Voronoi statistics (faces per cell) for this work (central 2000 spheres) and Finney's analysis (central 5500 spheres) for the Finney (1968) model.

3.4 Experimental error and precision

The main emphasis of the work presented in this chapter is to derive frequency distributions for the Finney model, based on simplicial cell structure, which characterise RCP space. As all of these distributions are derived from the pre-sequenced edgelength file FINEDGE.DAT, it is important to derive an estimate of the precision with which an edgelength measurement is known. There are two main reasons for this importance, perhaps the most obvious of which is that it allows some overall statistical view of errors to be estimated for any particular cell property. Somewhat less apparent, but equally important, is the need to be able to estimate the confidence with which a sphere to sphere contact can be distinguished from a near contact. This aspect assumes particular significance in the next chapter.

The basis of the method devised is to produce the histogram of edgelength frequency for that fraction of the 89220 cell edges which fall into the interval 0.992 to 1.013 sphere diameters (i.e. contacts and near-contacts). This histogram is shown in figure 3.5, and is hereafter referred to as the observed (numerical) series, S.

Inspection of figure 3.5 shows that there is a likelihood of a normal distribution of errors associated with the determination of simplicial cell edgelengths. A reasonable expectation of Finney's measured RCP sample is that, in the absence of all errors from all sources, there should be no edgelength smaller than one sphere diameter. The spheres used by Finney were ¼ inch steel ball

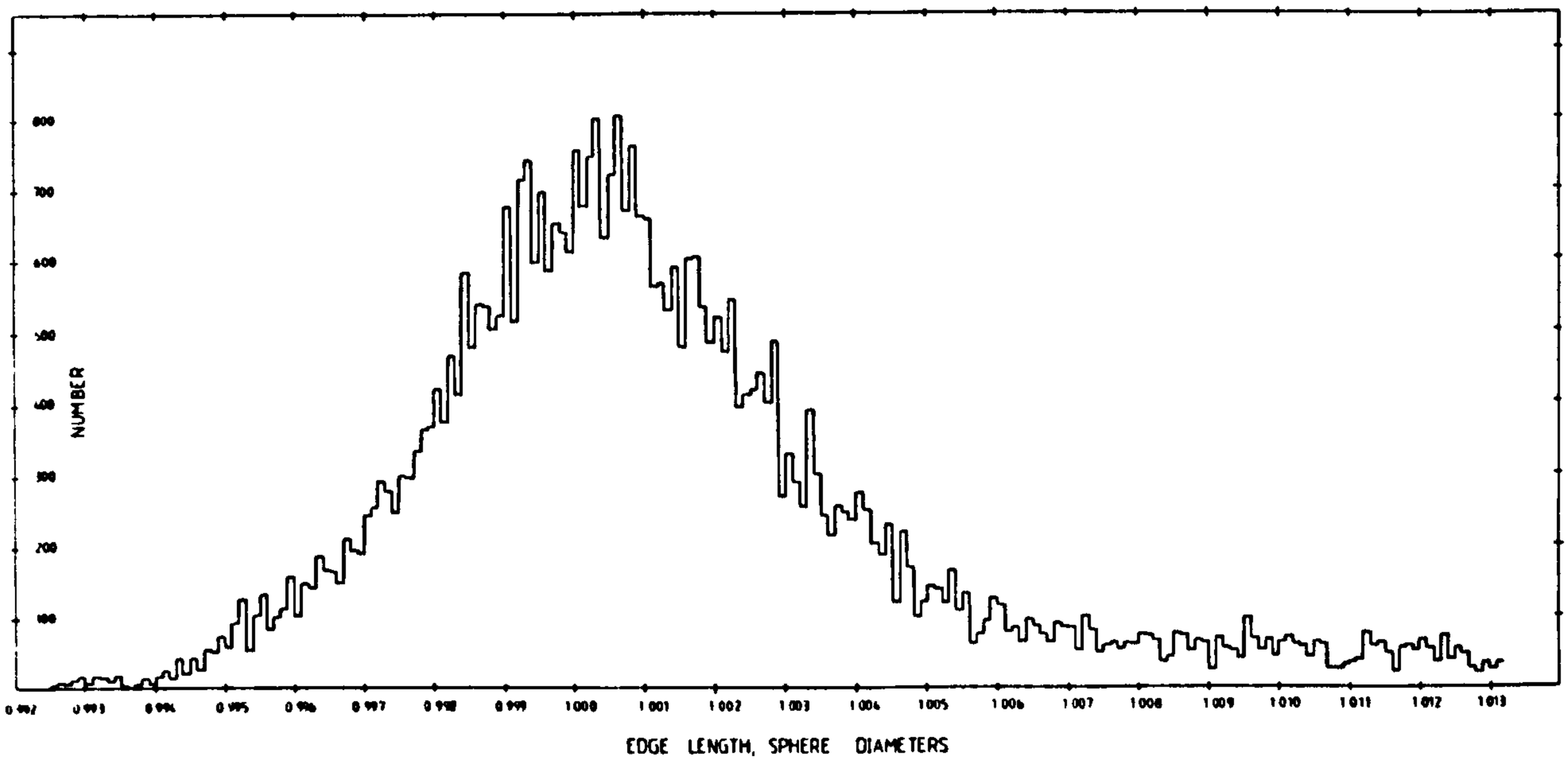

Figure 3.5 : Histogram of edgelength frequency for all edgelengths occuring in the interval 0.992 to 1.013 sphere diameters (for 14870 simplicial cells, 89220 edges).

bearings, manufactured to a claimed tolerance of ± 0.25×10^{-6} sphere diameters. Thus the smallest edgelength expected from Finney's pack is 0.9999975 diameters, neglecting measurement errors. Clearly, from inspection of figure 3.5, this total absence of experimental error is not realistic. In order to derive an estimate of the real experimental error, two assumptions are made here:

Assumption A: The experimental error is normally distributed and well characterised by a Gaussian function.

Assumption B: **It is reasonable to have an approximate expectation of what a large, perfectly error-free sample of simplicial cell edgelengths might look like.**

Assumption 'A' allows a second series, G, (for Gaussian) to be invoked, whilst assumption 'B' permits the third series, E, (for Expectation) to be fabricated. The assumed relationship between all three series is that the convolution of the two hypothetical series G and E should resemble the observed series, S:

$$\text{i.e. } S = G*E \qquad \text{-3.2-}$$

where the star symbol represents the convolution:

$$S_i = E_i G_o + \sum_{j=1}^{m} E_{(i+j)} G_j + \sum_{j=1}^{m} E_{(i-j)} G_j \qquad \text{-3.3-}$$

where G_0 is the central (i.e. maximum) value of the series G which is (2xj)+1 elements in length.

The series E may be resolved into two components. In a perfect, error-free sample, there is expected to be an infinitesimally thin delta function or "spike" in the element in E carrying the unit sphere diameter edgelength, corresponding to the frequency of hard contacts. The series E contains null values for all elements less than the unit sphere diameter, and positive values for all elements greater than the spike position. These elements, excluding the spike element, are referred to here as the boxcar component of E.

Thus:

$$E = E_S + E_B \qquad \text{-3.4-}$$

where E_S is the spike expectation series, and E_B is the boxcar expectation series.

Since the series G describes a normally distributed error, it must apply equally well to the measurement of both contacts(i.e. E_S) and near-contacts (i.e. E_B) alike:

$$\text{i.e. } S = G*E_S + G*E_B \qquad \text{-3.5-}$$

Expression 3.5 cannot be solved analytically to give a unique solution for G, since there are three unknowns (G, E_S and E_B). However, it is possible to estimate iteratively all three unknowns, and measure the best fit between ($G*E_S + G*E_B$) and S. This process is described under the following separate headings:

3.4.1 Estimation of E_B

3.4.2 Estimation of G

3.4.3 Best fit of ($G*E_S + G*E_B$) with S

3.4.4 Results

3.4.1 Estimation of E_B

Since we have only limited prior knowledge about E_B, there is no unique way of estimating E_B. The method adopted here is to use the observed series S as the starting point. Visual inspection of

figure 3.5 shows that there is a considerable amount of noise in the series S - values do not increase or decrease smoothly from one element position to the next. This noise may be brought under some degree of control by smoothing. Visual inspection of figure 3.5 shows the standard deviation to be greater than 0.001 (by definition, 68.27% of a normal distribution is to be found within ± 1 standard deviation). Using a nine point moving average filter, therefore, provides a new series, S′, which is smoothed, but which has had no real structure removed from it by the smoothing process, since the width of the filter is (at 0.0009 diameters) less than a conservative estimate of the standard deviation for the distribution desribed by S. The data for S′ is contained in data file VSMOOTHEDGE.DAT, and is written by program VSMOOTH (presented in Appendix 'B') which uses the operator:

$$S'_i = (S_i+S_{i+1}+S_{i-1}+S_{i+2}+S_{i-2}+S_{i+3}+S_{i-3}+S_{i+4}+S_{i-4})/9 \qquad \text{-3.6-}$$

The series S is shown in figure 3.6 and superimposed on the series S in figure 3.7. An initial estimate of E_B is made by symmetrically subtracting out elements on the left hand side of the spike position (element 201) from those elements on the right hand side of the spike position in series S′:

$$E_{B1} = S'_{(201+1)} - S'_{(201-1)} \qquad \text{-3.7-}$$

This procedure is completed by program FOLD (presented in Appendix 'B') which writes the output to VMODEL1.DAT, and the resultant trend is presumed to reflect the real, underlying trend of E_B. Consistent with this presumed trend, five "eyeball" estimates of E_B

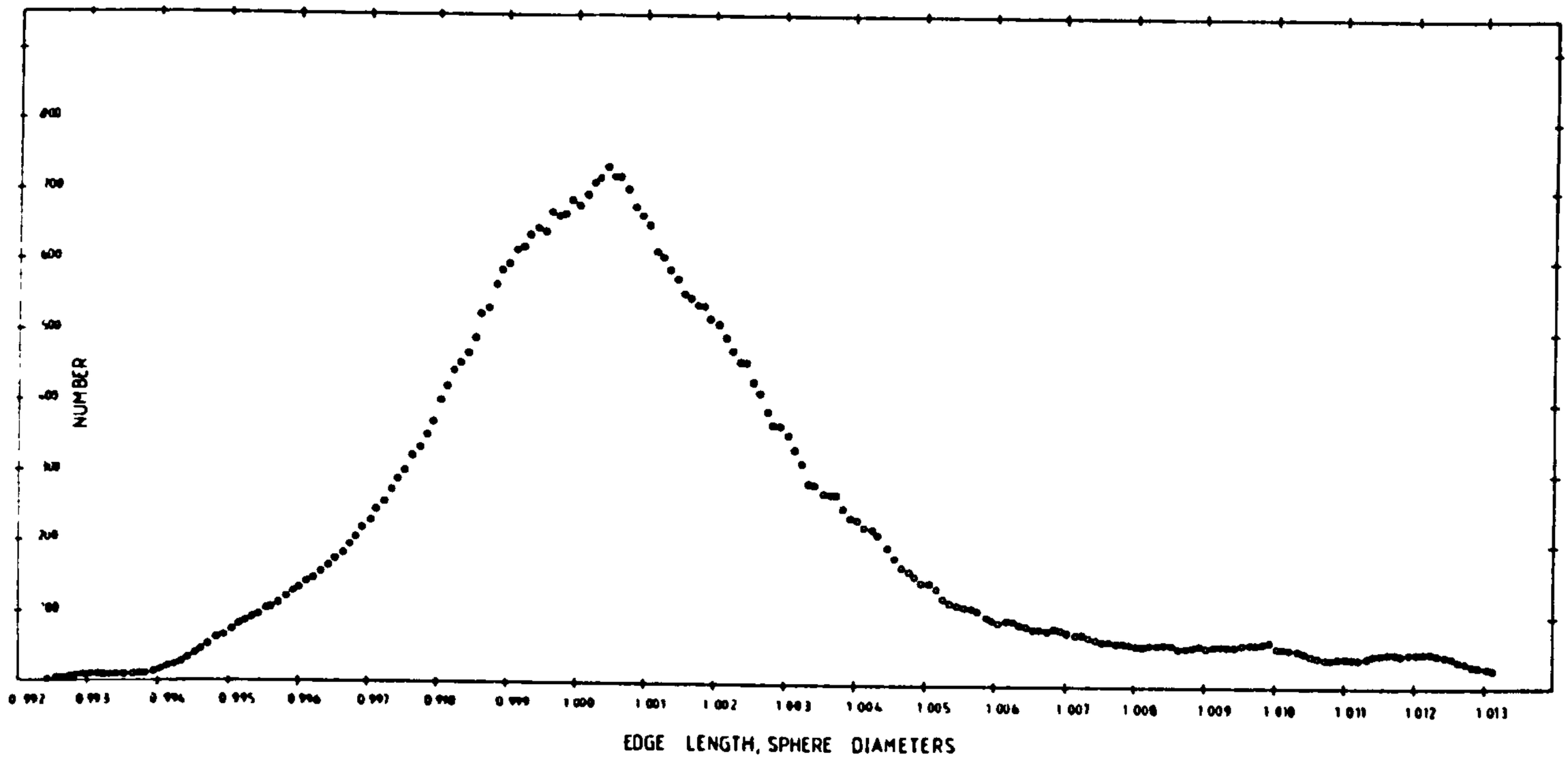

Figure 3.6 : Smoothed edgelength frequency histogram - the series S′.

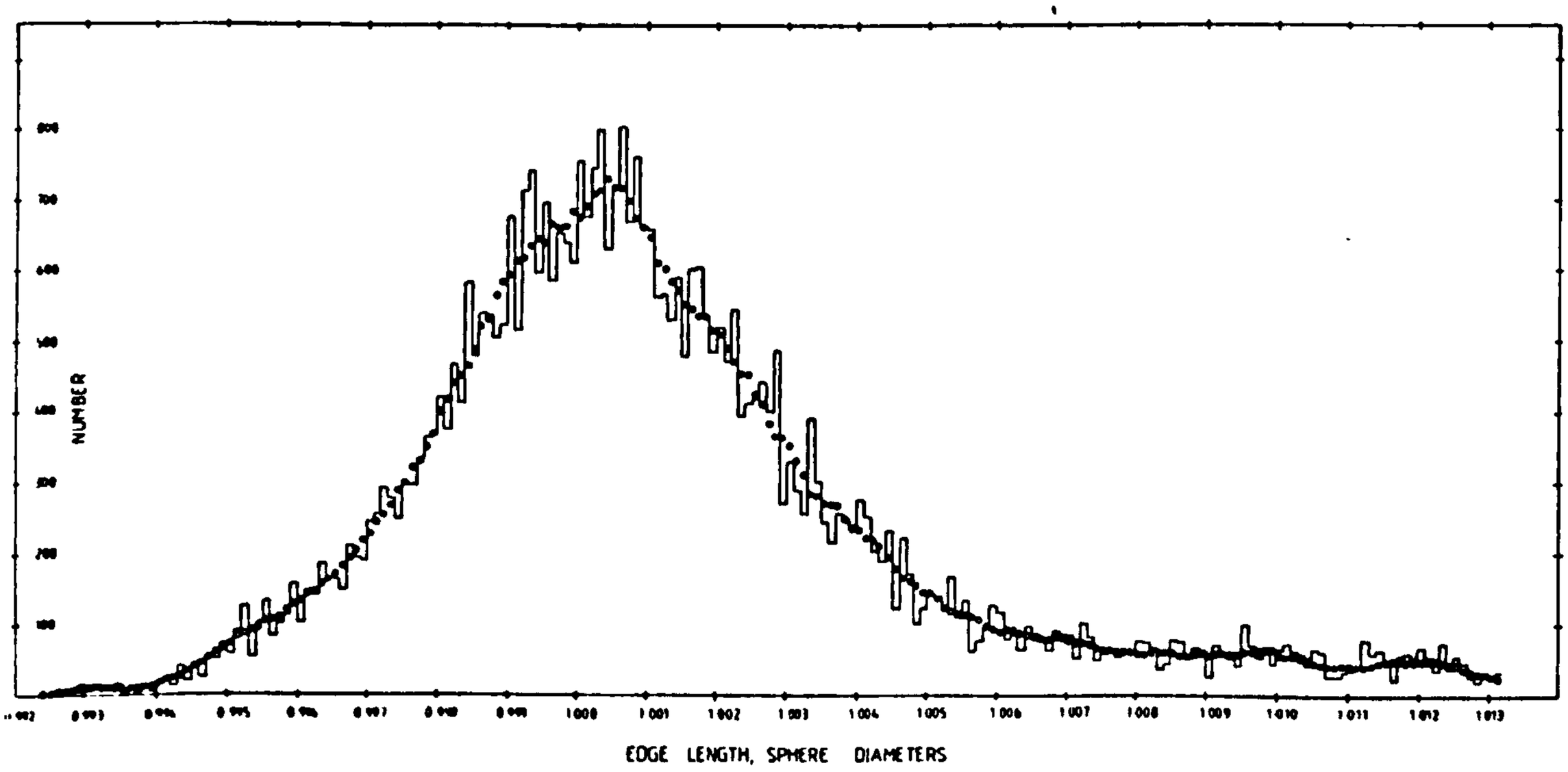

Figure 3.7 : Series S with the series S′ superimposed.

were drawn. These estimates, or models, are termed EB0, EB1, EB2, EB3 and EB4 and are held in data files EB0.DAT to EB4.DAT. These models are shown in figure 3.8, together with four variants of model EB3 termed EB3-1, EB3-2, EB3-3 and EB3-4. This gives a total of nine models, or estimates, of the boxcar expectation series E_B. The next step is to discover which of these nine arbitrary models best fits the observed series S, as part of the overall procedure to estimate the (assumed) normally distributed error, G.

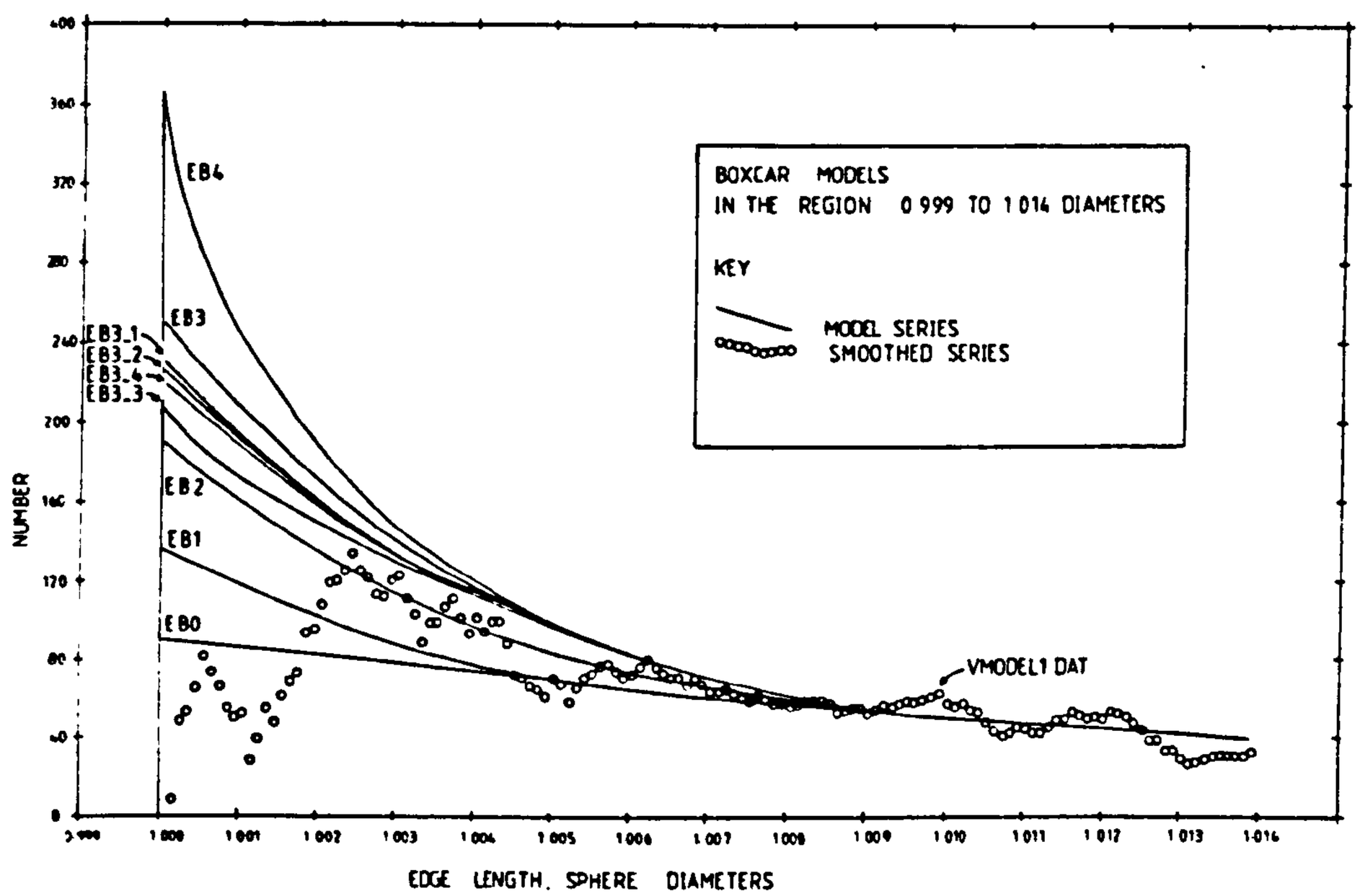

Figure 3.8 : Boxcar models of E_B in the region 0.999 to 1.014 sphere diameters.

3.4.2 Estimation of G

The series G is readily calculated from the expression:

$$G_i = \exp(-0.5(\chi_i-\mu_o)^2/\sigma^2) \qquad \text{-3.8-}$$

where G_i is the ith value of the series G, χ_i is the ith edgelength position, μ_o is the central edgelength position and σ is the standard deviation.

It is essential to normalise G in this application:

$$G_i = G_i/\sum_{j=i}^{n} G_i \qquad \text{-3.9-}$$

A value of 199 elements is used in the iterative calculations of the series G. Thus the central value, G_o occurs at element 100.

3.4.3 Best fit of ($G*E_S + G*E_B$) with S

The definition of best fit between the modelled and the observed series is achieved here by minimising the absolute difference in area under the curves described by the two series. This is achieved by subroutine DIFF which is called by the main iterative program, VORWARD. The iterative procedure used in program VORWARD begins with the user selecting one of the (nine) available boxcar models. The user then specifies an estimate (a guess initially) of the amplitude of the spike in E_S, and an estimate of the minimum value of sigma. The user then specifies an increment value for spike amplitude, and an increment value for sigma. The program then

computes ($G*E_S + G*E_B$) and calculates the absolute difference in area between ($G*E_S + G*E_B$) and S. This absolute difference in area is output as the diagnostic parameter, delta. The program continues by incrementing first sigma and then spike amplitude and calculates a value for delta at each step. This results in a 5 x 5 matrix of delta values for various (selected) combinations of sigma and spike amplitude. By manual inspection of the matrix, and by re-running the program several times for different input values, the user is able to focus in on the best fit combination of spike amplitude and sigma for that particular boxcar model. This iterative process is summarised in figure 3.9.

3.4.4 Results

Program VORWARD was run using boxcar models EB0, EB1, EB2, EB3 and EB4 a total of twenty two times, amounting to some 550 iterative estimates for G. The overall minimum value of delta for all five boxcar models was associated with EB3, and so the variants of EB3 (EB3-1, EB3-2, EB3-3 and EB3-4) were used in a further 11 runs of VORWARD, amounting to an additional 275 iterative estimates for G. In satisfying expression 3.5, therefore, the best parameters available from the analysis presented here are:

SIGMA = 0.002168

SPIKE AMPLITUDE = 32340 ± 10

BEST MODEL OF E_B = EB3-2

Of all boxcar models tested in this way, the worst fit with S was with model EB0. Model EB1 was somewhat more successful, and EB2 was

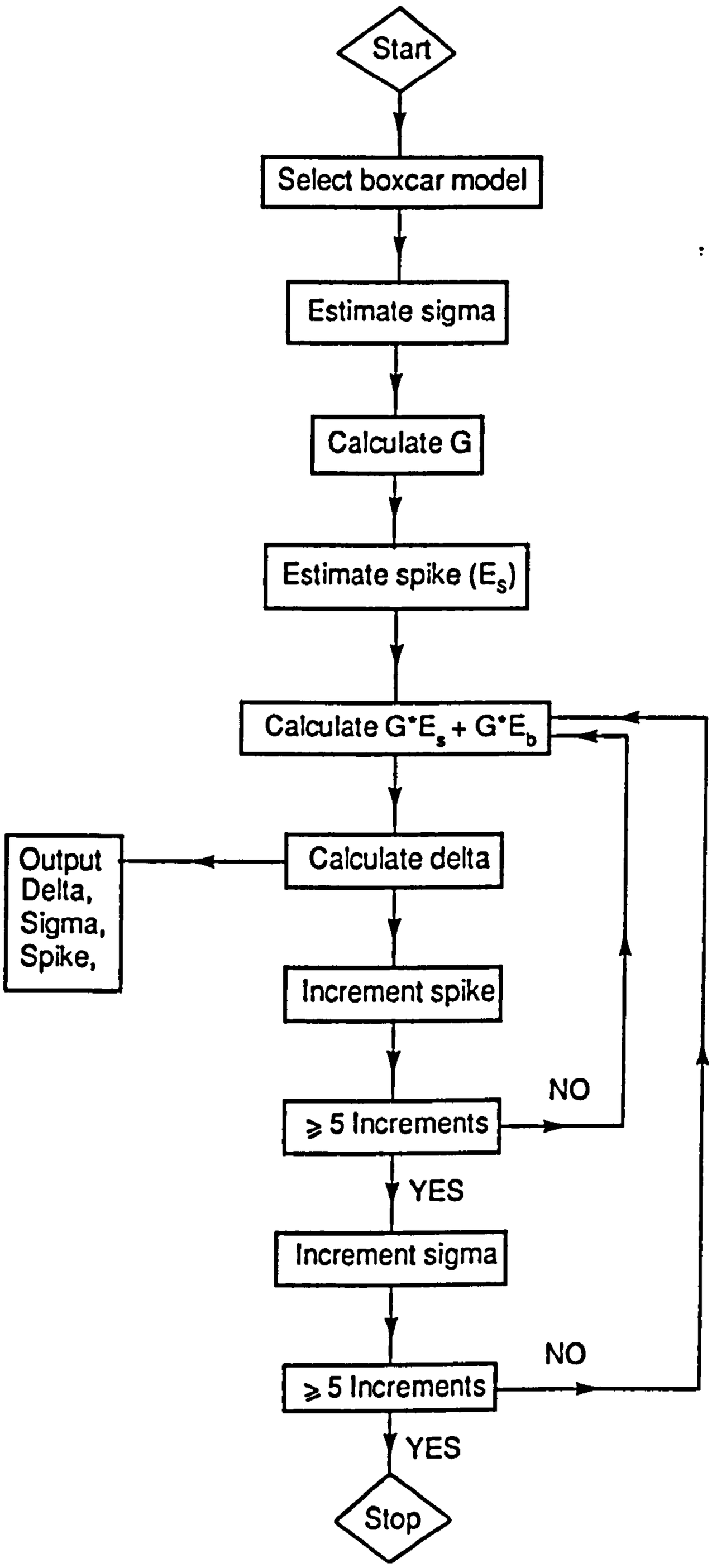

Figure 3.9 : FLOW DIAGRAM FOR PROGRAM VORWARD

better still. EB3, and its variants were the best of the group, and EB4 proved to be marginally worse than EB2. Figure 3.10 summarises these findings, showing the graph of delta versus spike amplitude for all nine models and figure 3.11 shows the graph of delta versus sigma for all nine models.

Figure 3.12 shows the series ($G*E_S + G*E_B$) obtained using the best fit EB3-2 values, superimposed on the series S. Qualitatively, the fit between these two series is seen to be excellent. Figure 3.13 shows the series $G*E_S$ superimposed on the series S. From this graph it is clear the effect that the boxcar region (not represented by $G*E_S$ alone) must have on the series S. A perfectly symmetrical

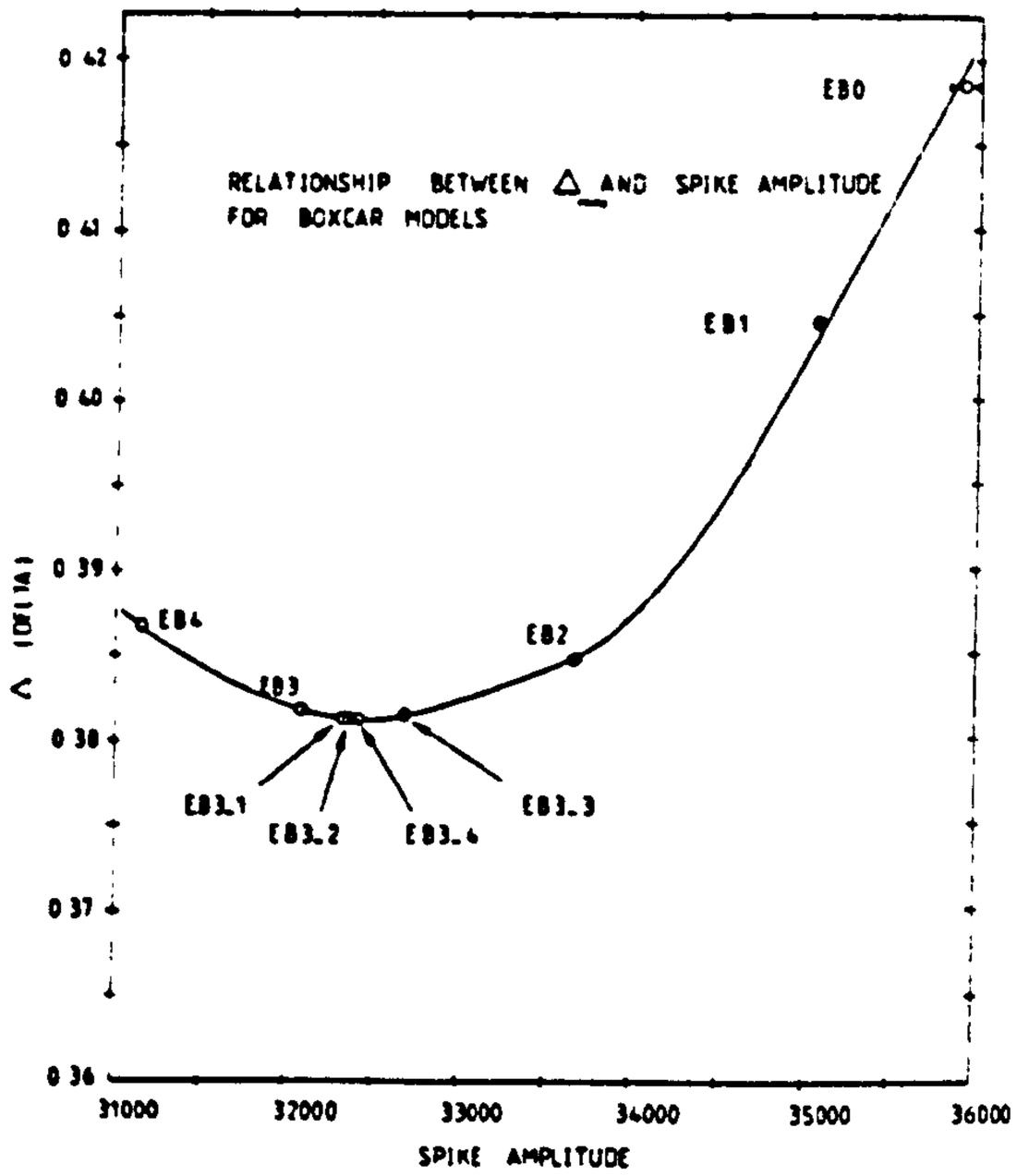

Figure 3.10 : Relationship between parameters delta and spike amplitude for boxcar models.

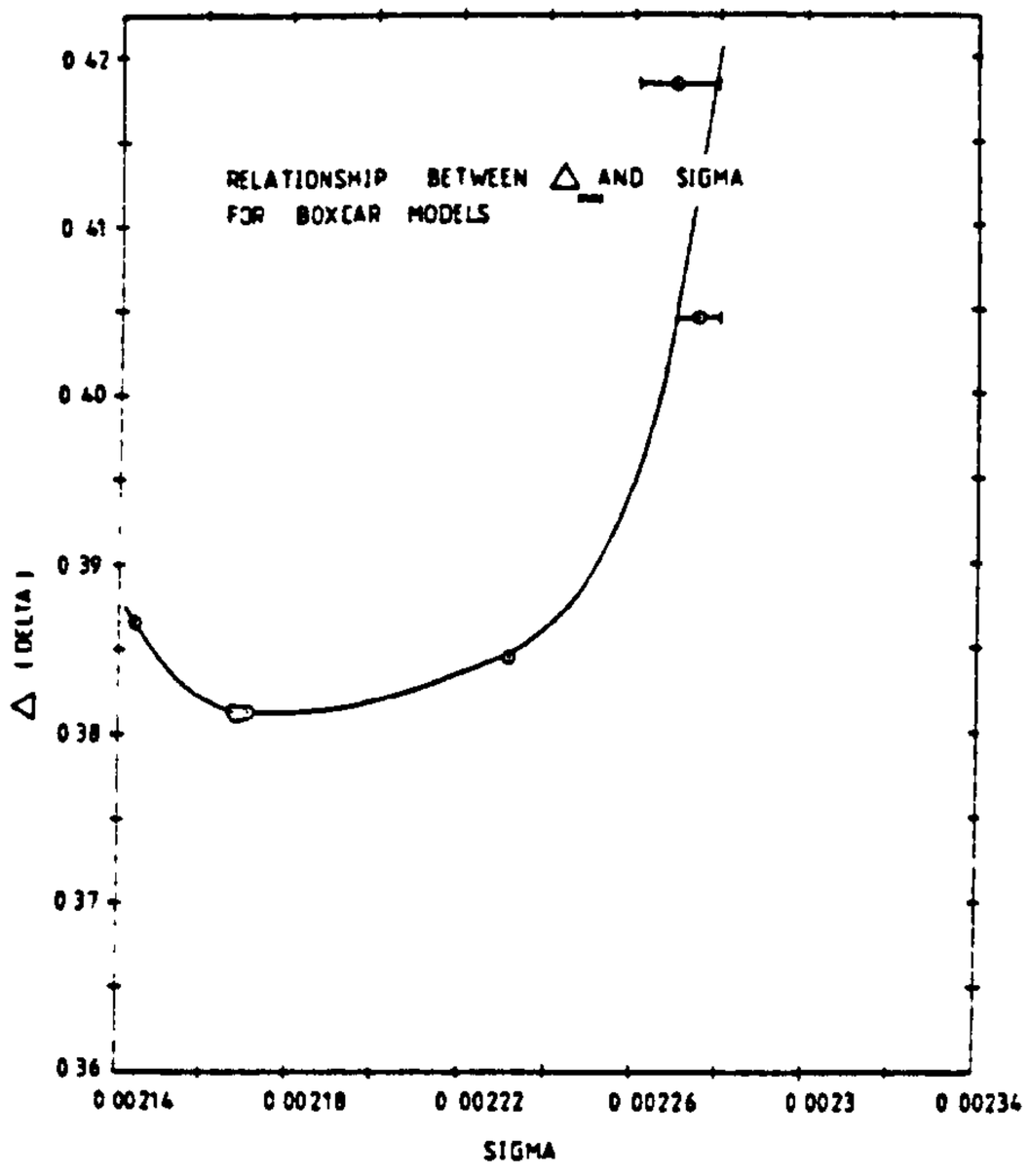

Figure 3.11 : Relationship between parameters delta and sigma for boxcar models.

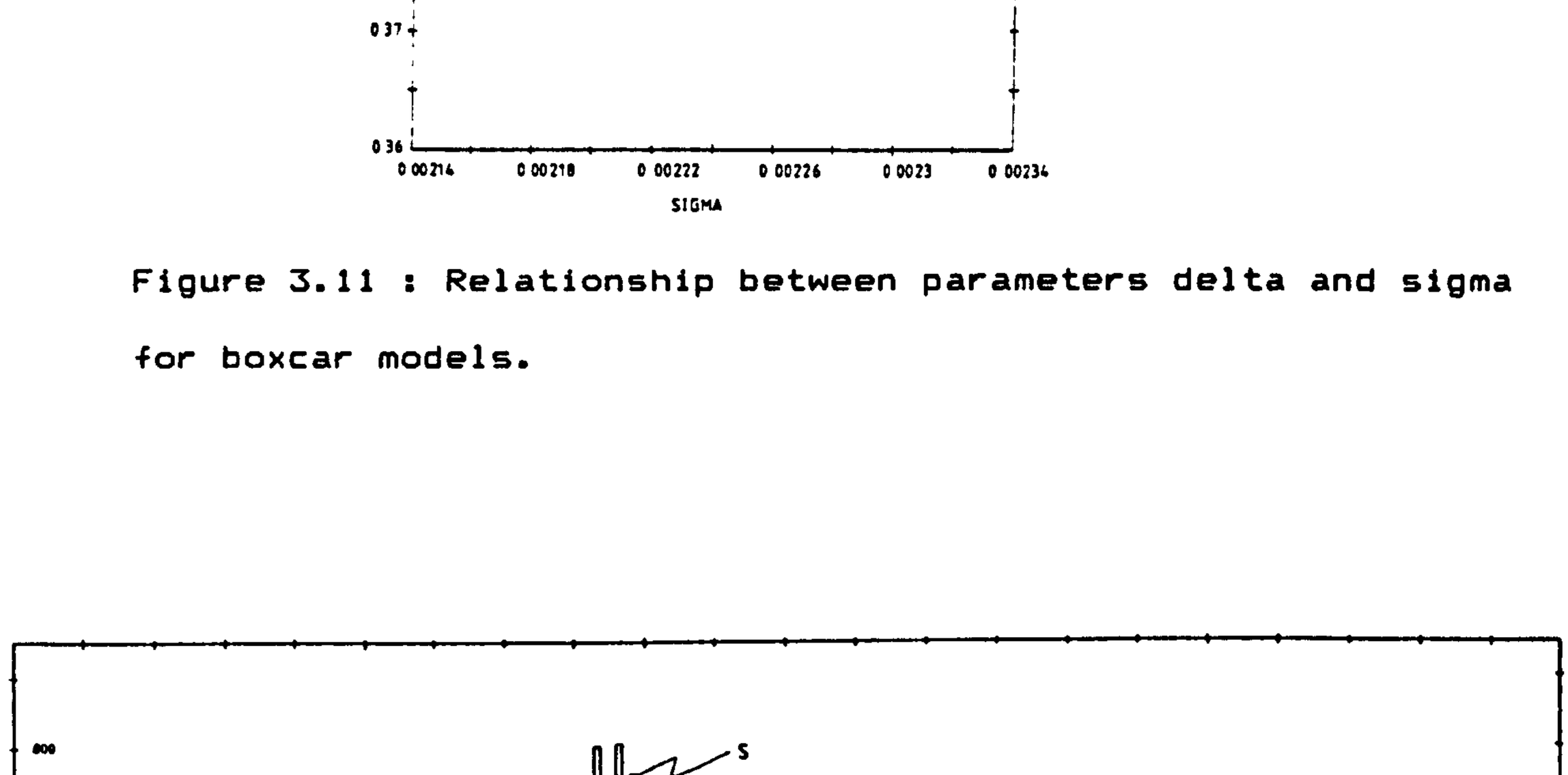

Figure 3.12 : Convolution series ($G*E_b + G*E_m$) and the observed series S.

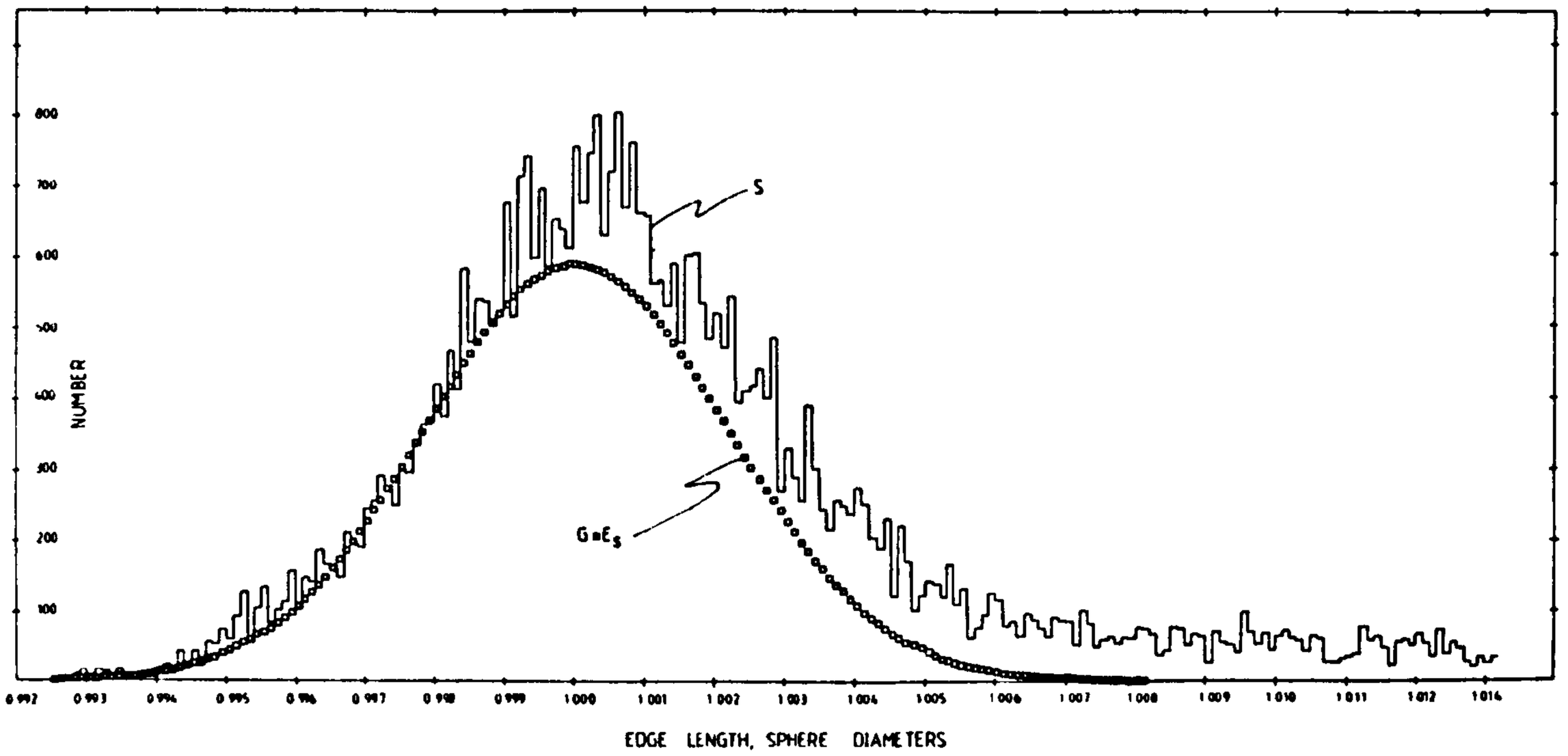

Figure 3.13 : Convolution series G*E_S and observed series S

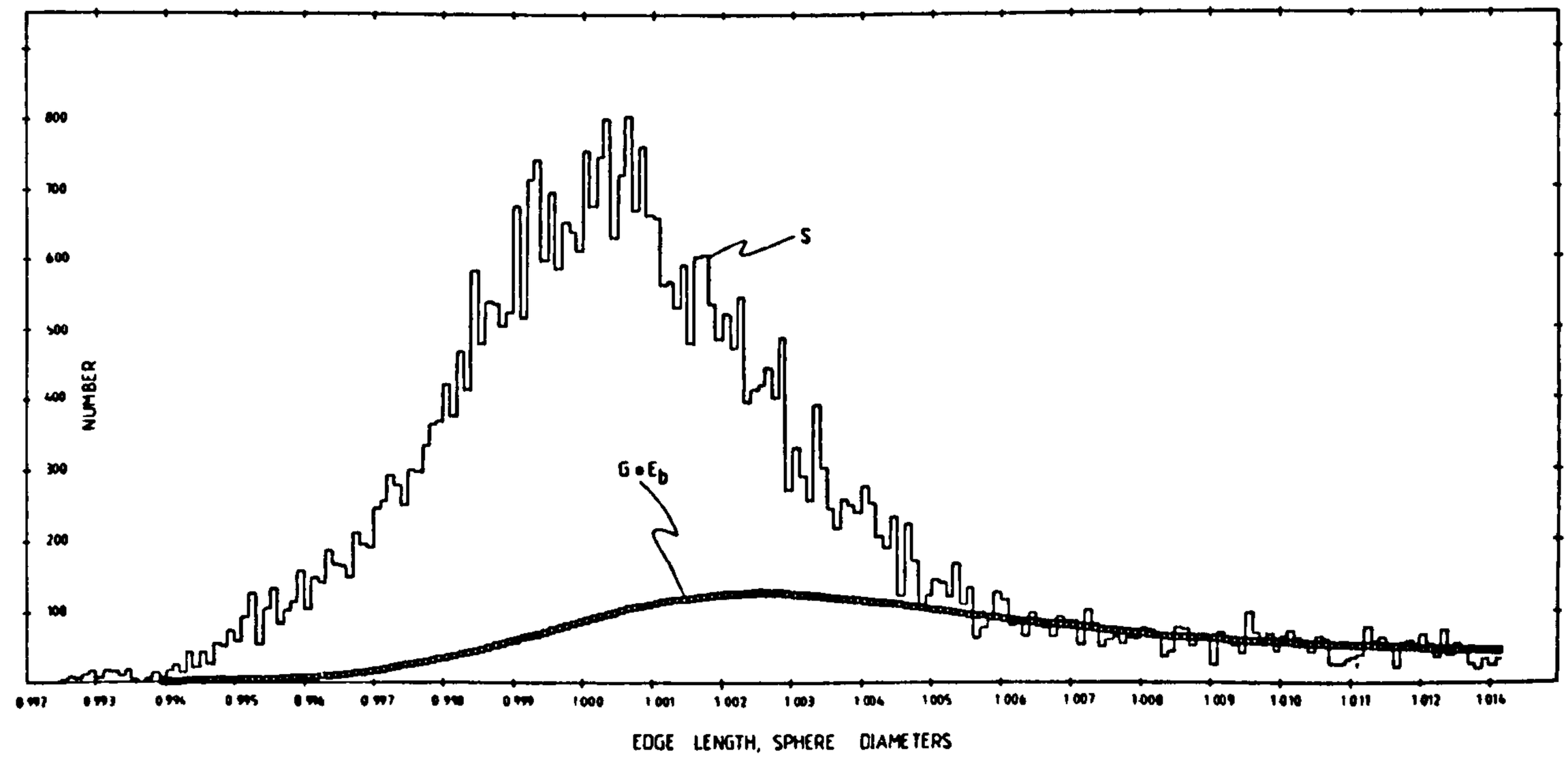

Figure 3.14 : Convolution series G*E_B and observed series S

gaussian function alone centres exactly on the spike interval (the edgelength interval containing edgelengths = 1.00000) but cannot adequately match both the left hand (low edgelength values) and the right hand values of the series S. Figure 3.14 shows the series $G*E_B$ which, when added to $G*E_S$ forms the non-symmetrical, but gaussian controlled series which matches S so well in figure 3.12.

In order to evaluate the significance of a standard deviation of 0.002168 (σ of equation 3.8) one thousand tetrahedra were randomly generated from a normal distribution of edgelengths with a mean of 1.0 sphere diameters, and a standard deviation of 0.002168. These regular tetrahedra were analysed using subroutines presented in appendix 'B' to this thesis, and found to have a mean packing density of 0.779675 ± 0.002064 (one standard deviation), or ± 0.265% of the mean value. The mean total tetrahedron volume was 0.94276 ± 0.0025 sphere radii cubed (one standard deviation) or ± 0.265% of the mean value. For comparison, the packing density of a perfect, regular tetrahedral cell is 0.779635, and the total volume of a tetrahedron defined by such a simplicial cell is 0.942809 sphere radii cubed. This volumetric error of ± 0.265% at one standard deviation is considered to be so small that, for all practical purposes in the rest of this chapter it can be neglected.

One curious feature of the smoothed series S' is that the maximum value of this series does not occur at an edgelength value of precisely 1.000 sphere diameters. Rather, as is evident from figure 3.6, it occurs at a value of 1.0004 sphere diameters. The reasons for this are not understood, but it is possible to speculate that it is due to the absolute diameter of the steel ball bearings used by

Finney being slightly less than 0.25 of an inch. Although, as stated earlier, the manufacturer's claimed tolerance was 0.25×10^{-6} sphere diameters, this tolerance may only apply to matched sets of ball bearings. One particular matched set may well conform to tolerance, but have a significantly different average ball diameter to that of another matched set of the same nominal diameter (Mason, 1988). If this speculation were true, then it may be the case that the ball bearings used by Finney were slightly smaller (by about $0.0004 \times 0.25" = 0.0001"$) than the ¼ inch value assumed by Finney. The likelihood of this speculation cannot be assessed.

3.5 RCP Simplicial Cell Frequency Distributions

There are four objectives to this section, and these are:

(i) to present those simplicial cell frequency distributions which characterise the Finney model,

(ii) to provide frequency distributions relevant to the characterisation of RCP space from the perspective of capillarity. This aspect is important, as the present work represents the most detailed analysis of any real, disordered porous medium attempted to date.

(iii) to provide frequency distributions specific to the characterisation of RCP space from the perspective of single phase permeability.

(iv) to interpret frequency distributions generated from all three preceding items in order to improve the understanding of capillary and permeability processes within RCP structure.

The first of these four objectives is important because, although Voronoi statistics for the Finney model have become widely accepted as characteristics of RCP structure, no definitive simplicial cell statistics have been derived for any real RCP model prior to the present work. The roles of the second and third objectives are self-evident in attempting to undertake the fourth objective.

All of the simplicial cell properties presented in this section are derived on the basis that each simplicial cell is a discrete tetrahedral unit, entirely separate from any neighbours with which it may share edges or faces. The trigonometry used to derive the cell properties is presented in appendix "A", and the relevant analytical subroutines are listed in appendix "B" to this thesis.

The full set of simplicial cell properties which are derived for the Finney model in the present work is summarised for reference in table 3.4. Table 3.5 provides a reference list of the simplicial cell properties of the perfectly regular unit tetrahedral cell. This last table is useful for interpreting some of the frequency distributions which follow.

3.5.1 Edgelength Frequency

The edgelength frequency distribution for all 89220 edges (14870

TABLE 3.4: SUMMARY OF FREQUENCY DISTRIBUTIONS PRESENTED IN SECTION 3.5

FREQUENCY DISTRIBUTION	PRIMARY RELEVANCE	FIGURE NUMBER
Edgelength	RCP characterisation	3.15, 3.16
Cell mean edglength	RCP characterisation	3.17
Face angle	RCP characterisation	3.18
Apex solid angle	RCP characterisation	3.19
Cell solid angle	RCP characterisation	3.20, 3.21
Cell total volume	RCP characterisation	3.22
Cell solid volume	RCP characterisation	3.23
Cell pore volume	RCP characterisation	3.24
Cell packing density	RCP characterisation	3.25
Cell porosity	Capillary pressure	3.26
Cavity insphere radius	Capillary pressure	3.27
All face insphere radii	Capillary pressure	3.28
Largest face insphere	Capillary pressure	3.29
2nd largest face insphere	Capillary pressure	3.30
3rd largest face insphere	Capillary pressure	3.31
Smallest face insphere	Capillary pressure	3.32
Equivalent chamber radius	Permeability	3.33
Radii of constriction	Permeability	3.34
Largest radii of const.	Permeability	3.35
2nd largest " " "	Permeability	3.36
3rd largest " " "	Permeability	3.37
Smallest radius of const.	Permeability	3.38
All hydraulic radii	Permeability	3.39
Largest hydraulic radius	Permeability	3.40
2nd largest " "	Permeability	3.41
3rd largest " "	Permeability	3.42
Smallest " "	Permeability	3.43

TABLE 3.5: CELL PARAMETERS FOR UNIT REGULAR TETRAHEDRON

Cell mean edgelength, sphere radii	2
Face angle, degrees	60
Individual solid angle, radian	.551286
Total solid angle, radian	2.20514
Total tetrahedron volume, sphere radii cubed	.942809
Solid tetrahedron volume, sphere radii cubed	.735047
Tetrahedron pore volume, sphere radii cubed	.207762
Tetrahedron porosity	.220365
Tetrahedron packing density	.779635
Cavity insphere radius, sphere radii	.224745
Individual face insphere radius, sphere radii	.154701
Equivalent pore chamber radius, sphere radii	.367417
Individual face area, sphere radii squared	1.73205
Constriction face area, sphere radii squared	.161254
Areal porosity of constriction	.931003E-01
Equiv. radius of constriction, sphere radii	.226559
Individual hydraulic radius, sphere radii	.513289E-01

cells) is shown in figure 3.15. Details of the edgelength frequency distribution for edgelengths greater than 1.1 sphere diameters can be seen in figure 3.16, showing that the frequency of edgelengths greater than $\sqrt{2}$ falls off rapidly.

3.5.2 Cell Mean Edgelength Frequency

The cell mean edgelength is the average value of the six edges which form the simplicial cell. This parameter is particularly significant in terms of the structure of random close packing, and the frequency distribution is shown in figure 3.17.

3.5.3 Face Angle Frequency

The face angle frequency distribution for all 178440 discrete face angles is shown in figure 3.18. The distribution shows the relatively high frequency of face angles close to 60 degrees. The observed maximum frequency is in the interval 59.0 to 59.999 degrees, and not in the interval 60.0 to 60.999 degrees.

3.5.4 Apex Solid Angle Frequency

The frequency distribution for the 59480 individual cell apex solid angles is rather wide, and is shown in figure 3.19. Most apex solid angles are between about 0.3 and 0.7 radian in magnitude. There is, however, a small number of apex solid angles close to zero, and several in excess of 1.0 radian.

3.5.5 Total Solid Angle Frequency

The cell solid angle is the sum of the four individual apex solid angles. The frequency distribution for the 14870 cell solid angles is shown in figure 3.20. Most cells have a total solid angle of around 2.1 to 2.25 radian, a much tighter distribution than that of the individual solid angles of figure 3.19. There is a sharp upper limit to the total solid angle, and the frequency distribution falls away rapidly above 2.30 radian, with no occurrences above 2.5 radian. The lower end of the distribution falls away less rapidly, however, as shown in figure 3.21, from which it is evident that a significant number of cells have a full solid angle of less than 1.5 radian. Several cells have a full solid angle of less than 0.25 radian. As will be discussed in more detail in chapter 4, this tendency to form cells with small total solid angles constitutes a trend towards cell-flattening, and is a hitherto undiscovered characteristic feature of RCP structure.

3.5.6 Cell Total Volume Frequency

The frequency distribution of the total volume of the 14870 cells is given in Figure 3.22. The average total cell volume is 1.072 sphere radii cubed, and the standard deviation of the distribution is 0.161. The average RCP simplicial cell total volume therefore is only 13% greater than the total volume of the unit regular cell (0.9428 sphere radii cubed). Some cells greater than 1.8 sphere radii cubed are observed, though none are larger than 2.0 sphere radii cubed.

3.5.7 Cell Solid Volume Frequency

The solid volume (i.e. sphere segment volume) frequency distribution, (figure 3.23) is of the same form as the cell solid angle frequency distribution.

3.5.8 Cell Pore Volume Frequency

The distribution of pore volumes is shown in figure 3.24, in which it can be seen that most cells have a pore volume in the range 0.25 to 0.5 sphere radii cubed. A very small fraction of cells have pore volumes close to zero, whilst a significant fraction have pore volumes greater than 0.8 sphere radii cubed. The cells with small pore volumes are relatively "flat" tetrahedra.

3.5.9 Cell Packing Density Frequency

The distribution of cell packing densities is shown in Figure 3.25. No cell has a packing density higher than 0.779635, which is that of the unit regular tetrahedron. No cell has a packing density less than 0.3, most cells falling in the range 0.6 to 0.7.

3.5.10 Cell Porosity Frequency

Figure 3.26 shows the distribution of all cell porosities. This distribution is essentially a "mirror image" of Figure 3.25, since porosity is (1 - packing density). It is interesting to note that, of all the material properties of RCP systems, porosity is usually regarded as the most predictable and constant. Figure 3.26 shows that this overall packing consistency is achieved with considerable cell to cell variation, from just over 0.2 to around 0.65.

3.5.11 Cavity Insphere Radius Frequency

The cavity insphere radius is an approximate measure of the imbibition meniscus radius for the individual cell, as proposed by Mason (1971). The frequency distribution for the 14870 cavity insphere radii is shown in Figure 3.27, from which it is evident that no cell can have a cavity insphere radius of less than 0.224745 sphere radii (that of the unit regular tetrahedron). The observed frequency of cavity inspheres in the range 0.22 to 0.23 sphere radii is less than 0.005 of the total, confirming that the unit regular tetrahedron is almost completely absent from RCP structure. This is an important result and is discussed in more detail in Chapter 4. The relevance of the cavity insphere radius to imbibition is discussed in detail in Chapter 6.

3.5.12 All Face Insphere Radius Frequency

This distribution for all 59480 face inspheres is shown in Figure 3.28. The face insphere radius provides an approximate estimate of the drainage pressure for that particular face as suggested by Mason (1971), and this is discussed in considerable detail in Chapter 6. For example, in mercury injection into sphere packings, the mercury enters the pore space defined by the simplicial cell once the mercury/mercury vapour meniscus curvature is approximately equal to that of the largest accessible face insphere.

No cell can have a face insphere radius less than 0.1547 sphere radii (i.e. that of the unit regular tetrahedron). From Figure 3.28 it is apparent that the approximately regular unit face (i.e. three edgelengths of 1.000 sphere diameters forming an equilateral

triangle) is extremely frequent, with face insphere radii in the interval 0.15 to 0.2 having a frequency of around 0.25. However, from the preceding discussion on the cavity insphere radius frequency distribution, it is clear that there is a very low probability that any individual cell is a unit regular tetrahedron. The dominance of small face insphere radii in Figure 3.28, therefore, is not due to a significant presence of the unit regular tetrahedron. This point becomes more obvious when the four face inspheres for an individual cell are ordered (ranked) according to size, and counted separately in four discrete distributions as described in section 3.5.13 to 3.5.16 following.

3.5.13 Largest Face Insphere Frequency

Figure 3.29 shows the distribution of the largest of the four individual cell face insphere radii for the 14870 cells. There are two important features of this distribution. Firstly, as discussed above, there is a very low frequency of the unit regular face, and therefore of the unit regular tetrahedron. Secondly, the overall form of the distribution is extremely close to that of the cavity insphere radius distribution shown in Figure 3.27. The implication of this finding is that an individual cell can drain and imbibe at the same, or very similar, pressures. Individual cells therefore exhibit little or no capillary pressure hysteresis. This very important finding is discussed in more detail in section 3.5.19 following, and again in Chapter 6.

3.5.14 2nd Largest Face Insphere Radius Frequency

Figure 3.30 shows the distribution of the 2nd largest face insphere

radius. The form of this distribution is very similar to that of the largest face insphere radius shown in Figure 3.29. The significance of this is that the scope for capillary pressure hysteresis in the pack itself is surprisingly low, since half the cell entry/exit points are of roughly the same size as each other and roughly the same size as the cavity insphere.

3.5.15 3rd Largest Face Insphere Radius Frequency

This distribution is presented in Figure 3.31, and is quite different from the distributions of the two largest face insphere radii. Together with the distribution for the smallest face insphere radius, this distribution accounts for the prominent "spike" at low radii in figure 3.28.

3.5.16 Smallest Face Insphere Radius Frequency

Figure 3.32 shows the frequency distribution for the smallest face insphere radius per cell.. As with the third largest face insphere radius frequency distribution, Figure 3.32 is dominated by faces formed by three spheres in contact.

3.5.17 Equivalent Radius of Pore Chamber Frequency

The pore volume of a cell can be quantified uniquely in terms of an equivalent radius, for the purpose of defining a characteristic pore-length as proposed by Chan and Ng (1988). The parameter is defined for convenience, and does not reflect any real geometrical property of the pore body. It does, however, constitute a sort of

pore size distribution (PSD) parameter, and the distribution of equivalent pore chamber radii for the Finney model is shown in Figure 3.33 for the sake of completeness. The distribution for the Chan and Ng (1988) model is also shown in Figure 3.33 (as a dashed line) for comparison with the Finney model. It is evident that the Finney distribution is appreciably "tighter" than that of the Chan and Ng model. This difference between the two models is attributable primarily to the polydispersity inherent in the Chan and Ng (1988) model, and will not be discussed further here.

3.5.18 Equivalent Radii of Constriction and Hydraulic Radii

Figures 3.34 to 3.43 show distributions specific to the consideration of fluid flow within the void space of RCP structure. The essential feature of fluid flow through individual cells is that streamlines must alternately converge, to pass through face constrictions, and diverge within the (cell) pore bodies. One of the most important aspects of this process is, therefore, the nature of the constricting region. The cell face constricting area may be accounted for by either of two conventional methods. Perhaps the most common concept appropriate to this problem is that of hydraulic radius (see, for example, Scheidegger 1957 or Dullien 1979) which is defined as the ratio of flow cross-sectional area to wetted perimeter. Alternatively, the notion of equivalent radius of constriction as proposed by Chan and Ng (1988) may be used. There exists a simple, hitherto undiscovered relationship between these two parameters which is specific to a simplicial cell analysis of monodisperse sphere packings. Thus the wetted perimeter of a simplicial cell face is constant and equal to pi sphere radii:

Cell face wetted perimeter = pi sphere radii

Cell constriction area = A sphere radii^2

Hydraulic Radius, r_h = (A/pi) -3.10-

Equiv. Rad. of constriction, r_c = $(A/pi)^{0.5}$ -3.11-

<u>hence $r_c = r_h^{0.5}$</u> -3.12-

The full distribution of all 59480 equivalent radii of constriction is shown in figure 3.34. This distribution is bimodal, with a primary peak at 0.22 to 0.24 sphere radii. The latter peak is predominantly due to the occurrence of regular, equilateral faces formed by three spheres in contact. As table 3.5 shows, no face can have an equivalent radius of constriction less than 0.226559 sphere radii, unless the component edgelengths are less than 1.0 sphere diameters. The small, but signficant, estimated error of ± 0.002168 sphere diameters (one standard deviation) derived in section 3.4 of this chapter is sufficient to account for the small frequency of faces evident from figure 3.34 which have equivalent radii of constriction in the range 0.21 to 0.22 sphere radii.

As with the analysis of the face insphere radii, the four equivalent radii of constriction of each individual cell can be subdivided, or ranked, according to size. Thus figures 3.35 to 3.38 show the frequency distributions for the largest, second largest, third largest and smallest equivalent radii of constriction respectively. As might be expected, the frequency distribution for the largest equivalent radius of constriction (figure 3.35) is monomodal. The frequency distribution for the second largest equivalent radius (figure 3.36) is very "tight" indeed, with a prominent modal value

in the interval 0.36 to 0.37 sphere radii. The third largest equivalent radius distribution (figure 3.37) is still monomodal at 0.36 to 0.37 sphere radii, but shows considerable widening towards lower values. The frequency distribution for the smallest equivalent radius of constriction (figure 3.38) is dominated by faces at, and close to, equilateral triangular contact.

Since the equivalent radius of constriction for simplicial cells of a monodisperse sphere packing is identical to the square root of the hydraulic radius (equations 3.10 to 3.12), there exists a simple relationship of form between the frequency distributions for these two parameters. The five relevant frequency distributions for hydraulic radii are presented in figures 3.39 to 3.43.

This completes the set of individual simplicial cell parameter distributions considered in the present work. The implications for use of the Finney packing as a model porous medium arising from some of these distributions, and from joint frequency distributions are considered in the next section. Although certain conclusions regarding the capillary properties of the Finney packing are drawn in the following section, more rigorous conclusions are derived in Chapter 6.

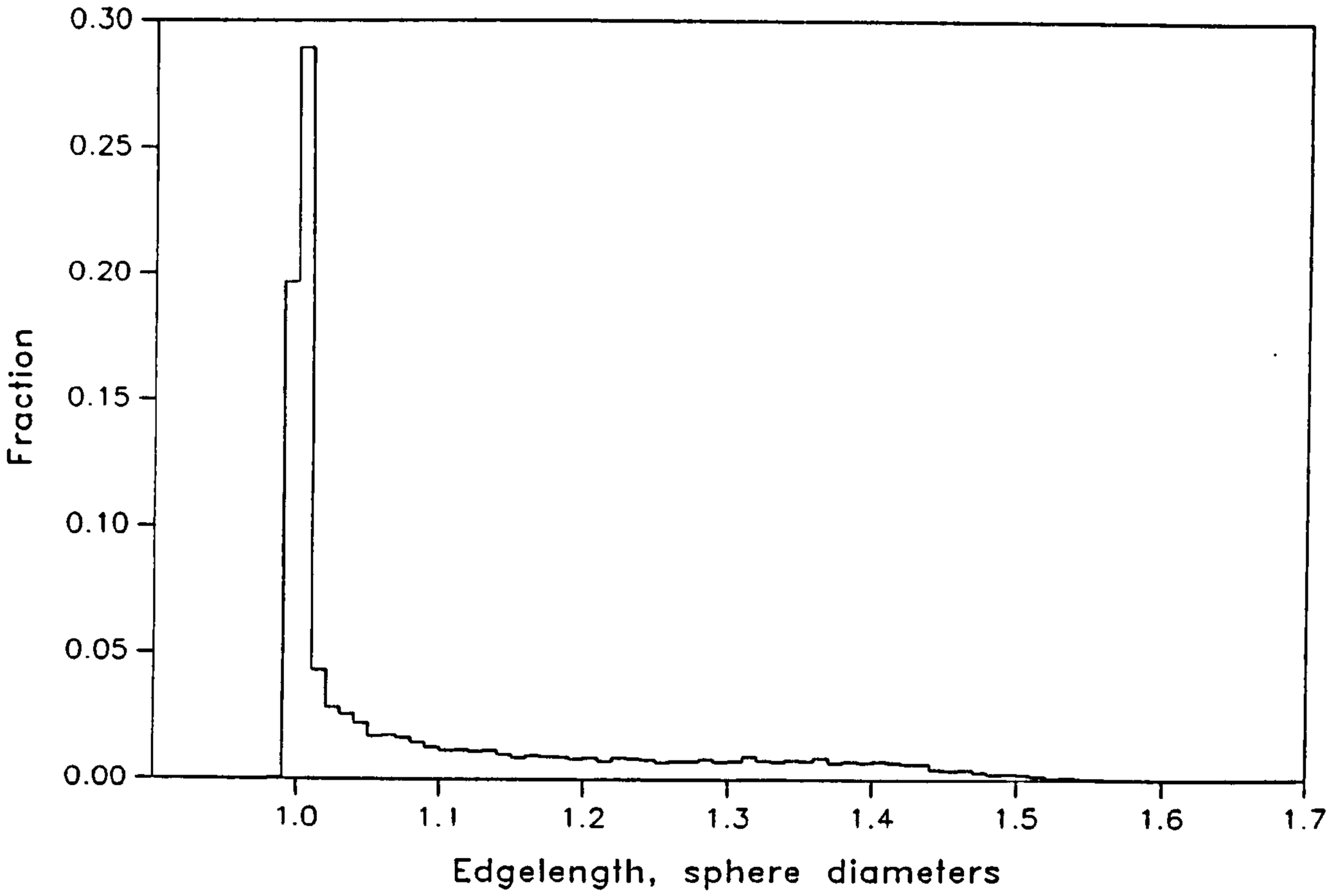

Figure 3.15 : Edgelength frequency distribution, Finney model

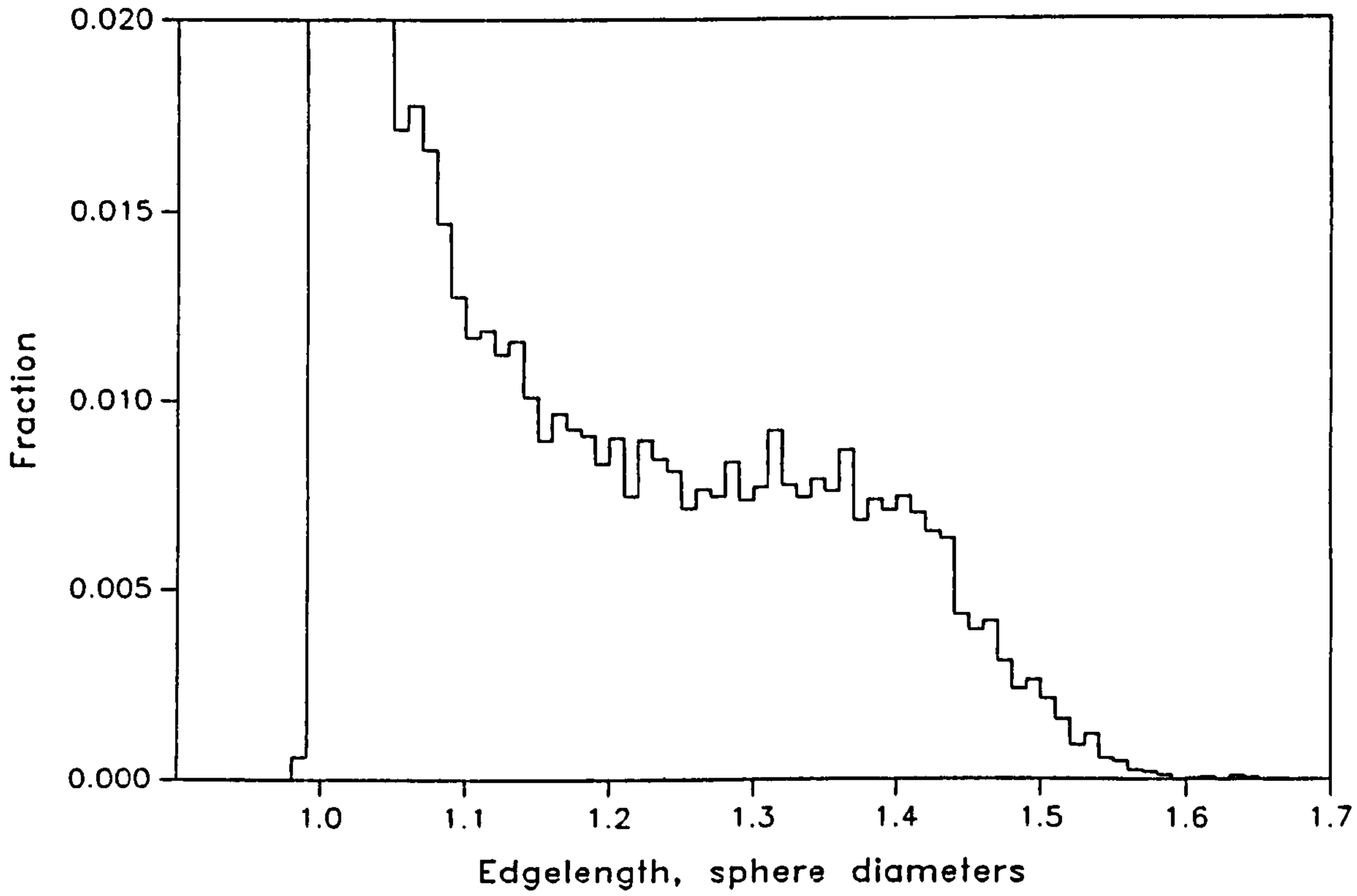

Figure 3.16 : Detail of figure 3.15

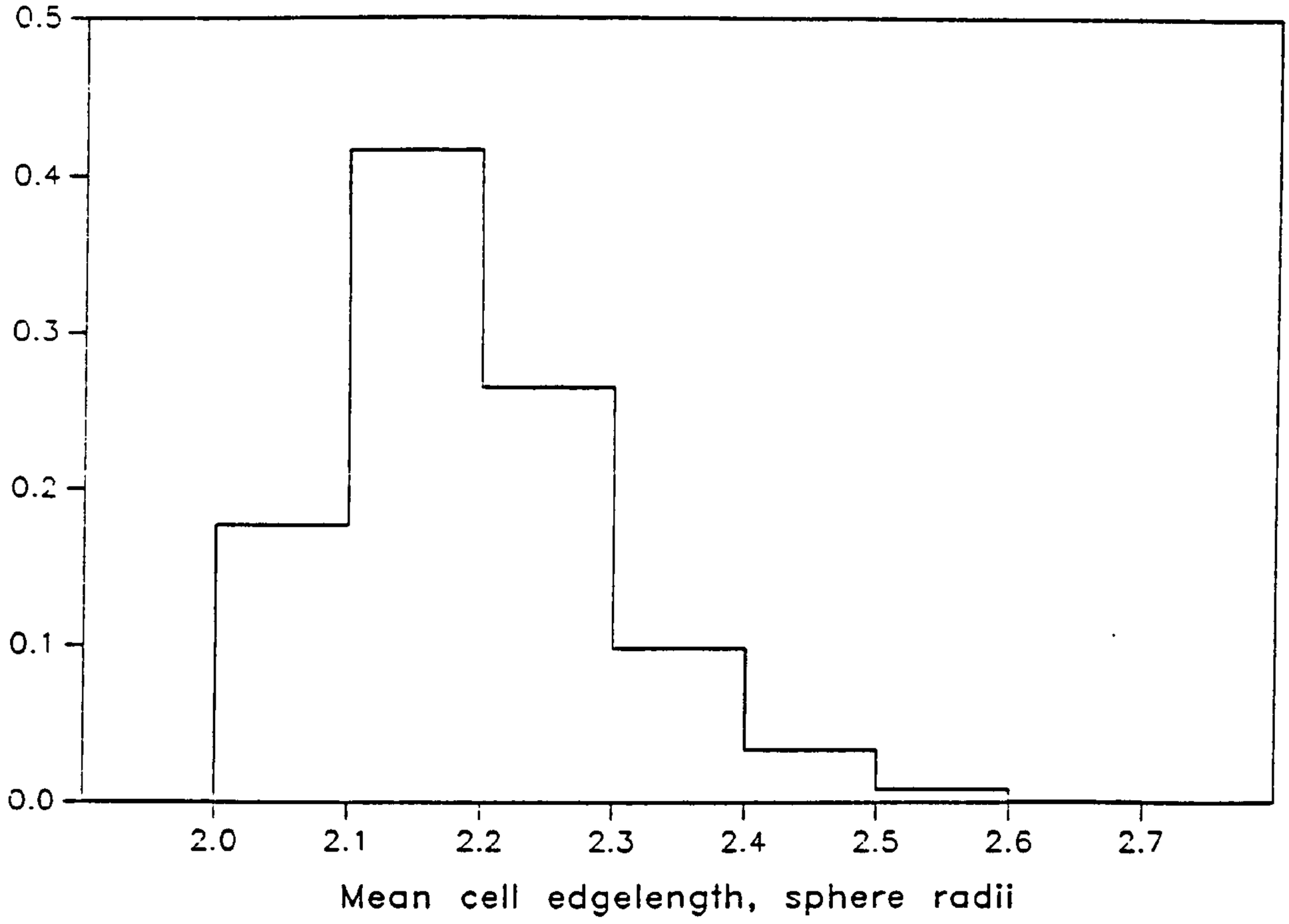

Figure 3.17 : Mean cell edgelength frequency distribution

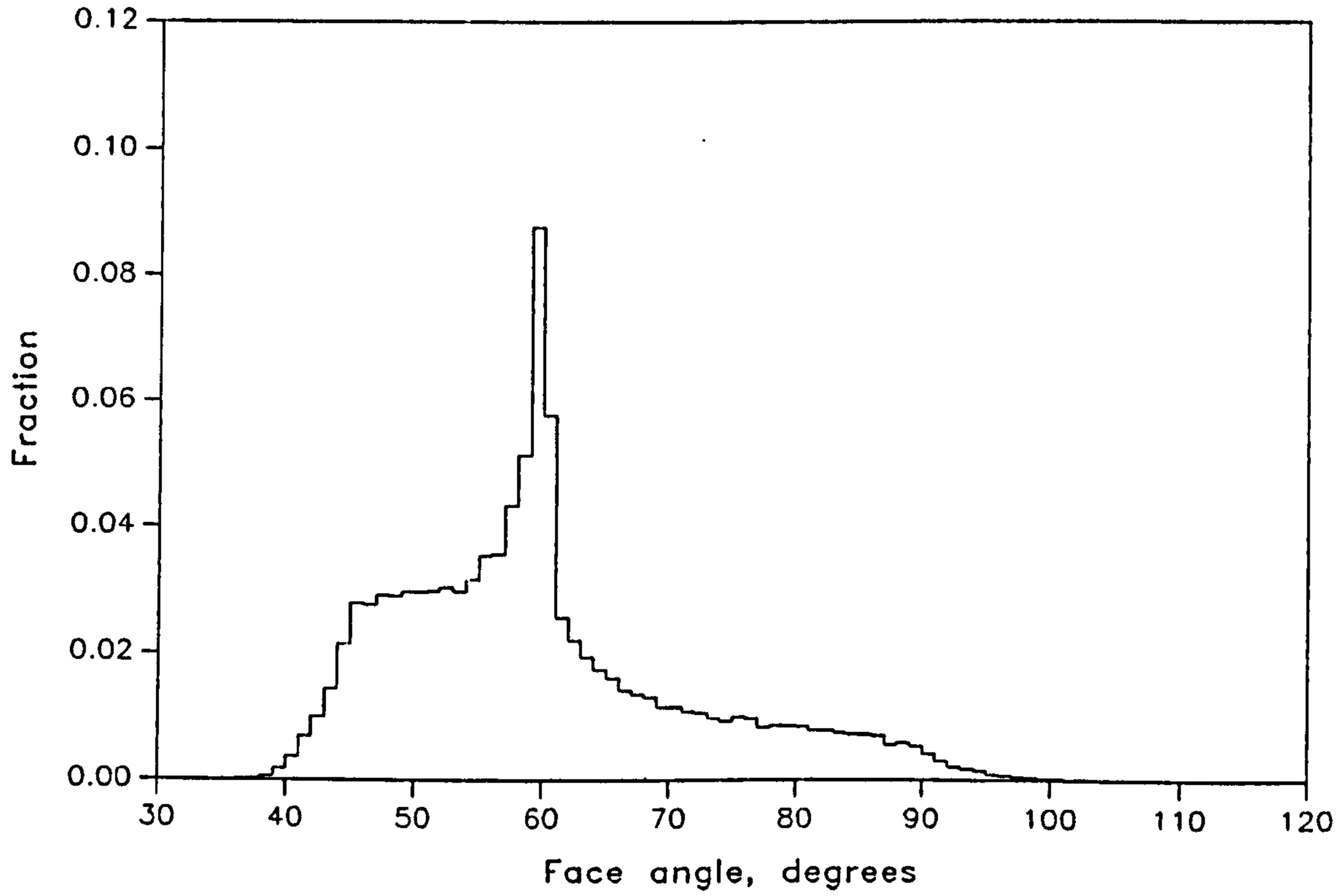

Figure 3.18 : Face angle frequency distribution, Finney model

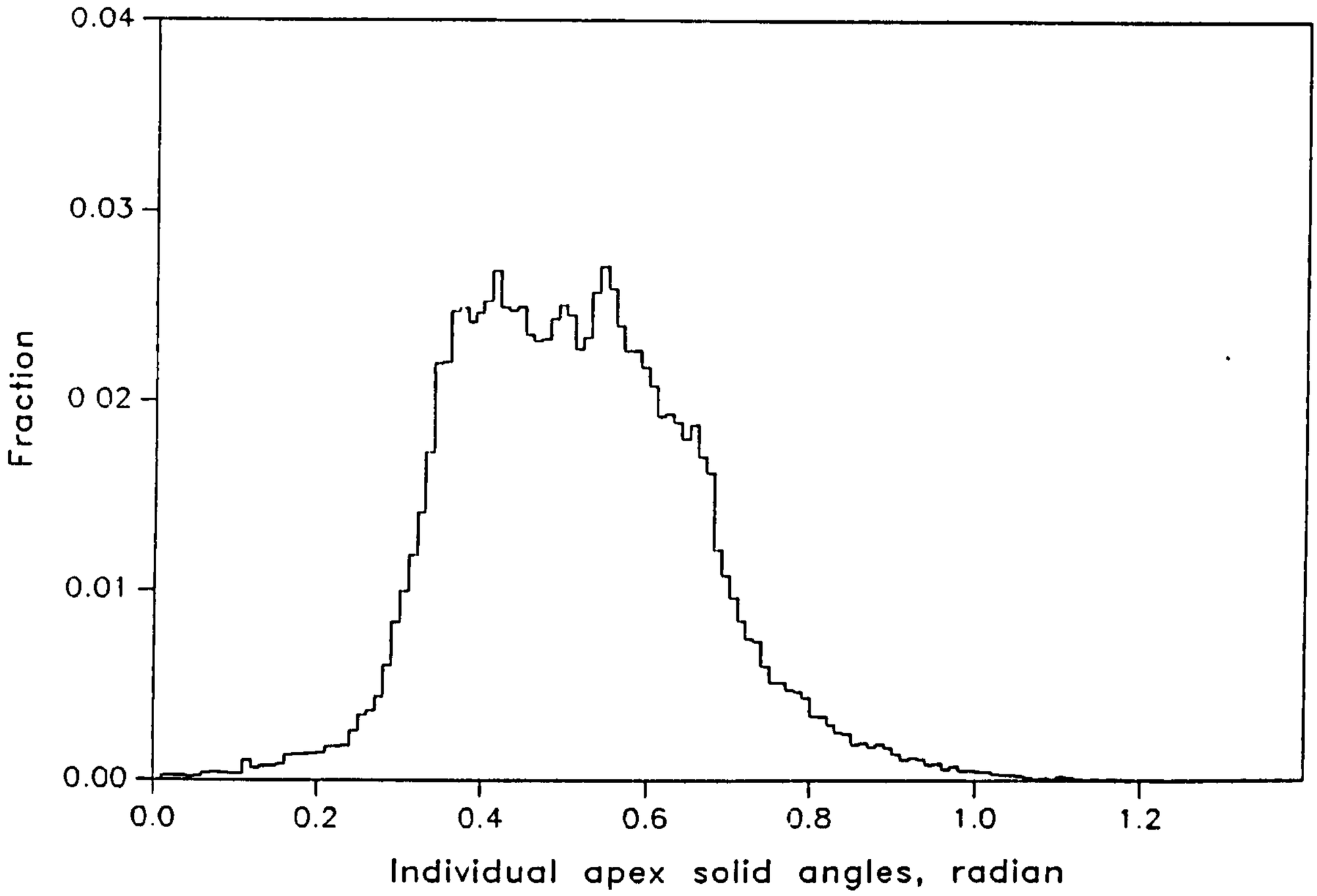

Figure 3.19 : Individual apex solid angle distribution

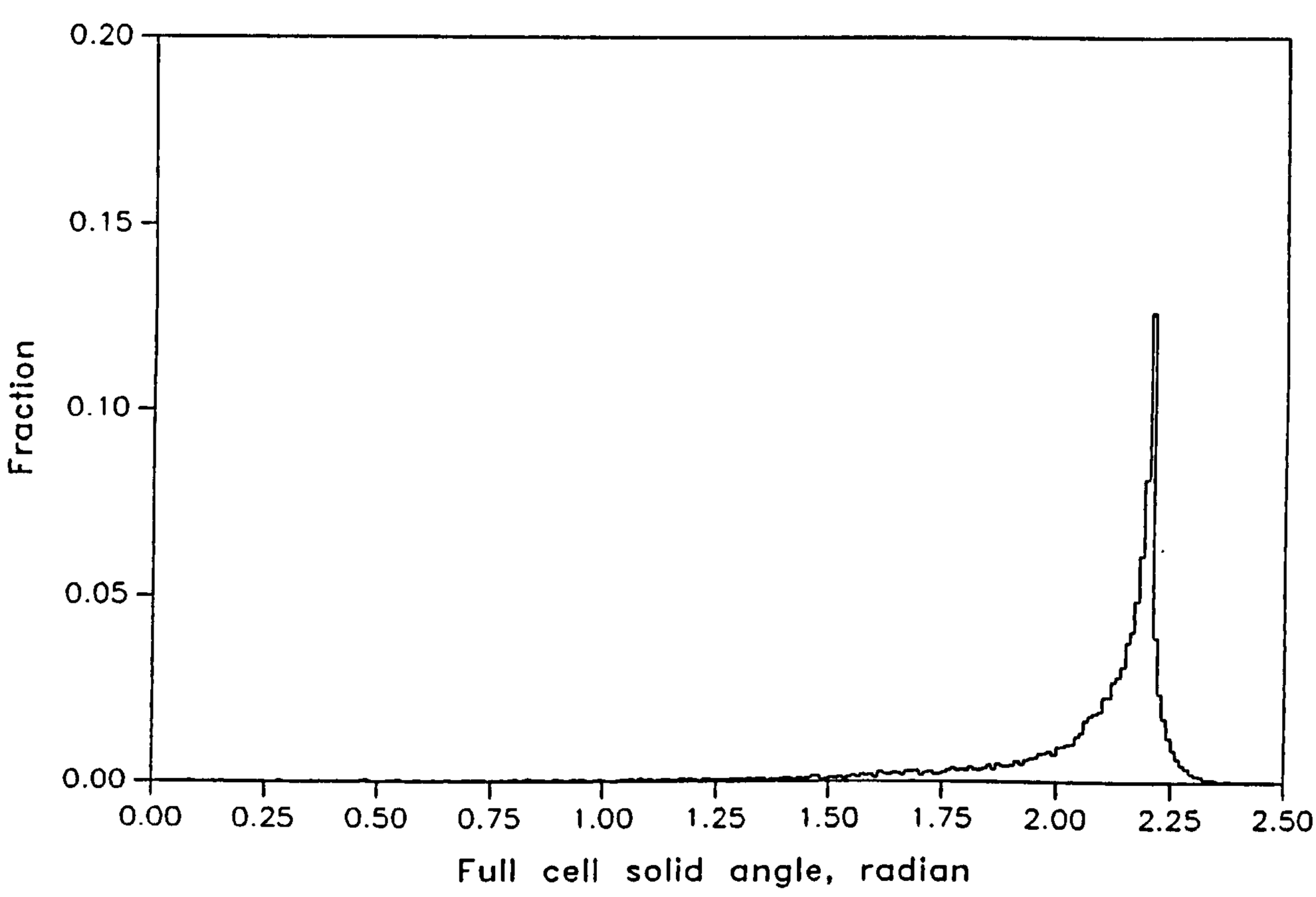

Figure 3.20 : Total cell solid angle distribution

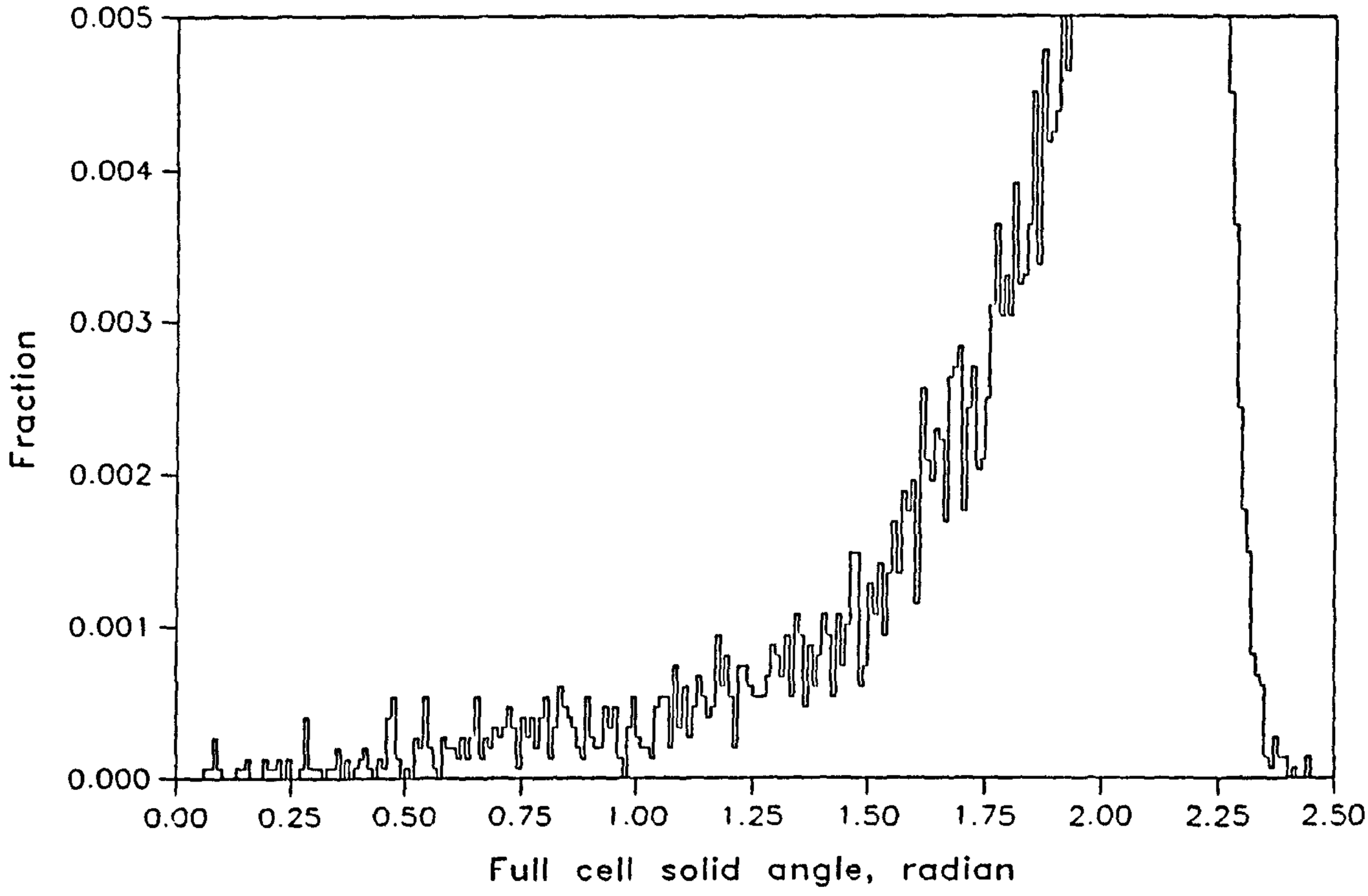

Figure 3.21 : Detail of figure 3.20

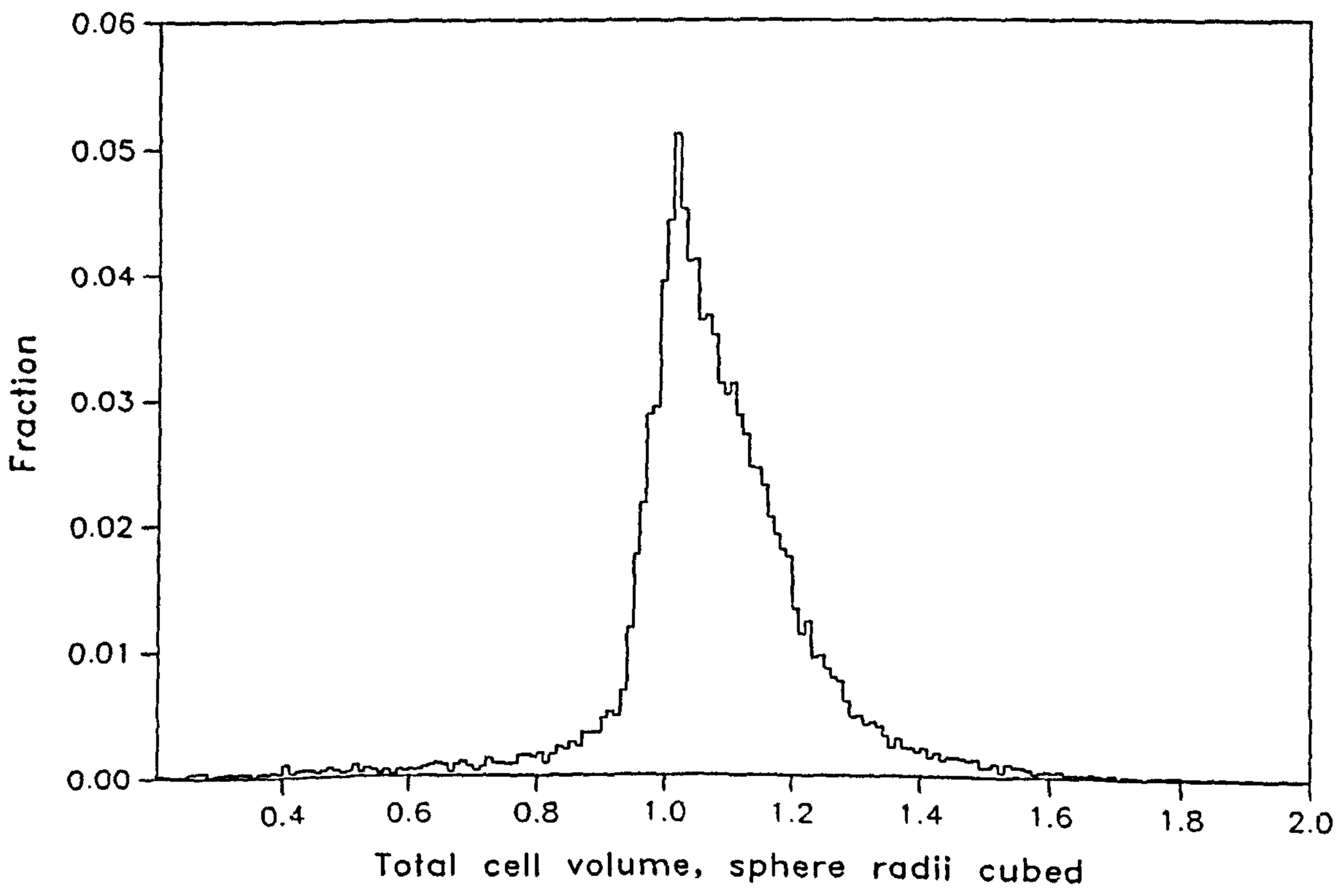

Figure 3.22 : Total cell volume frequency distribution

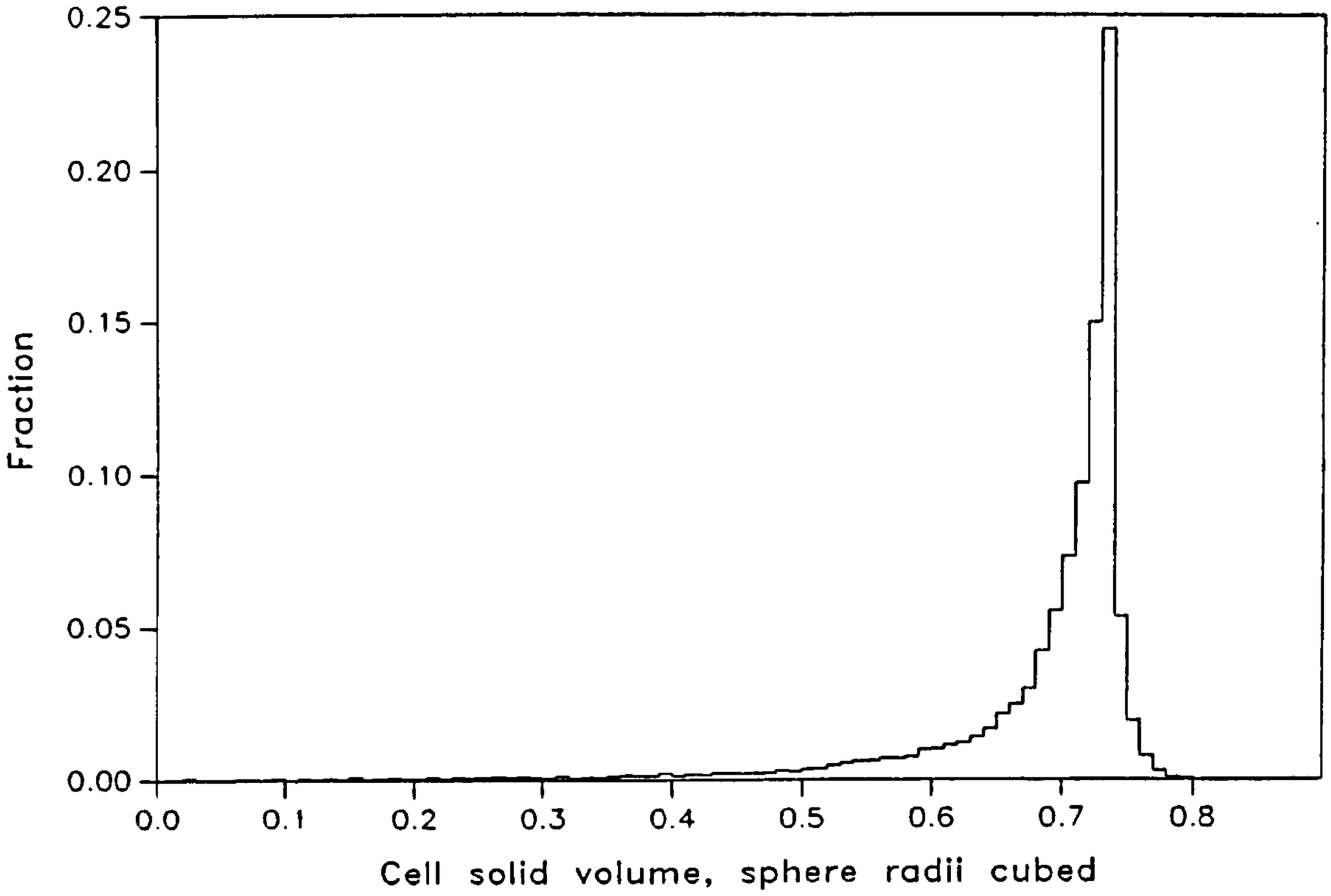

Figure 3.23 : Cell solid volume frequency distribution

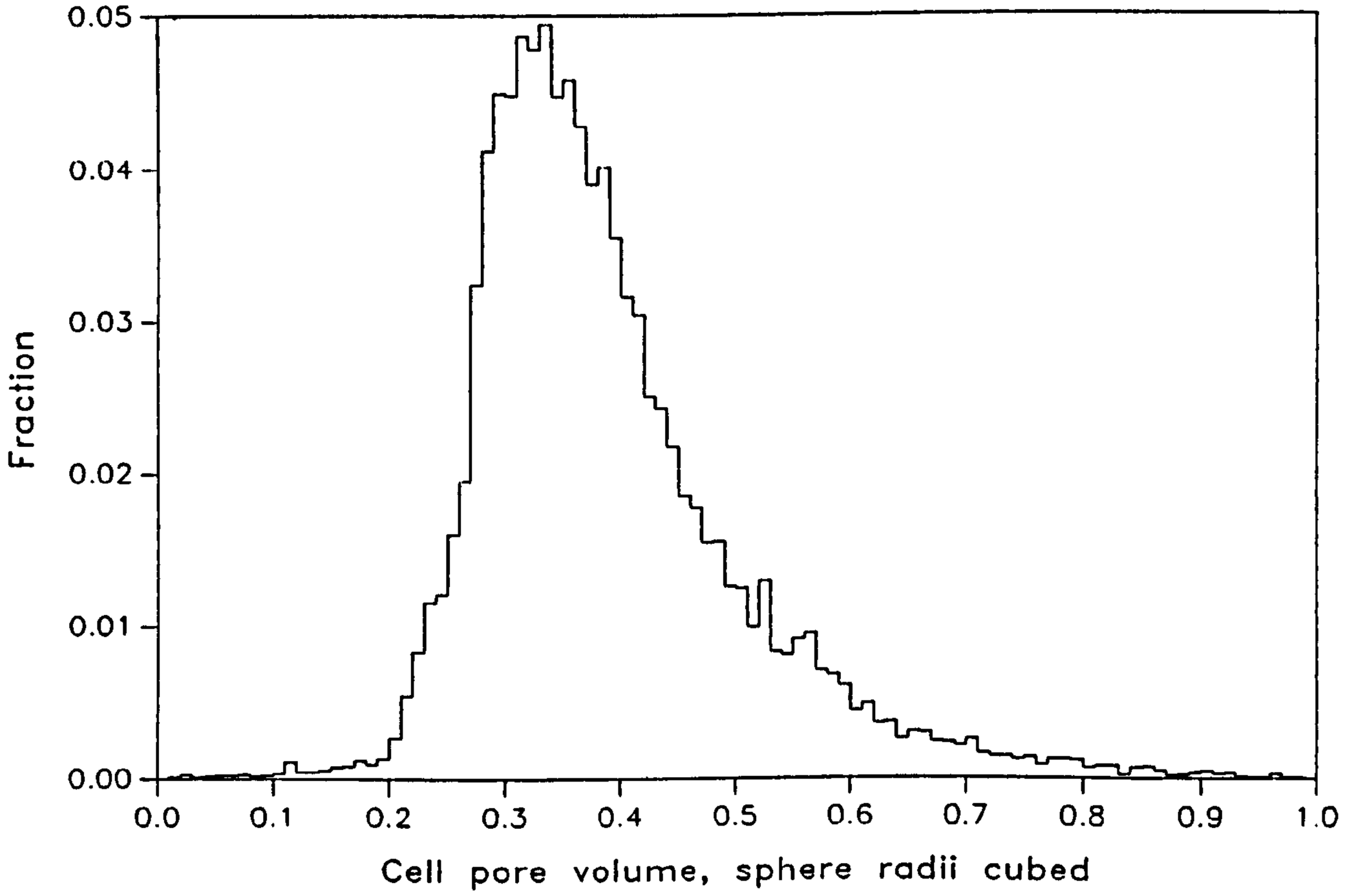

Figure 3.24 : Cell pore volume frequency distribution

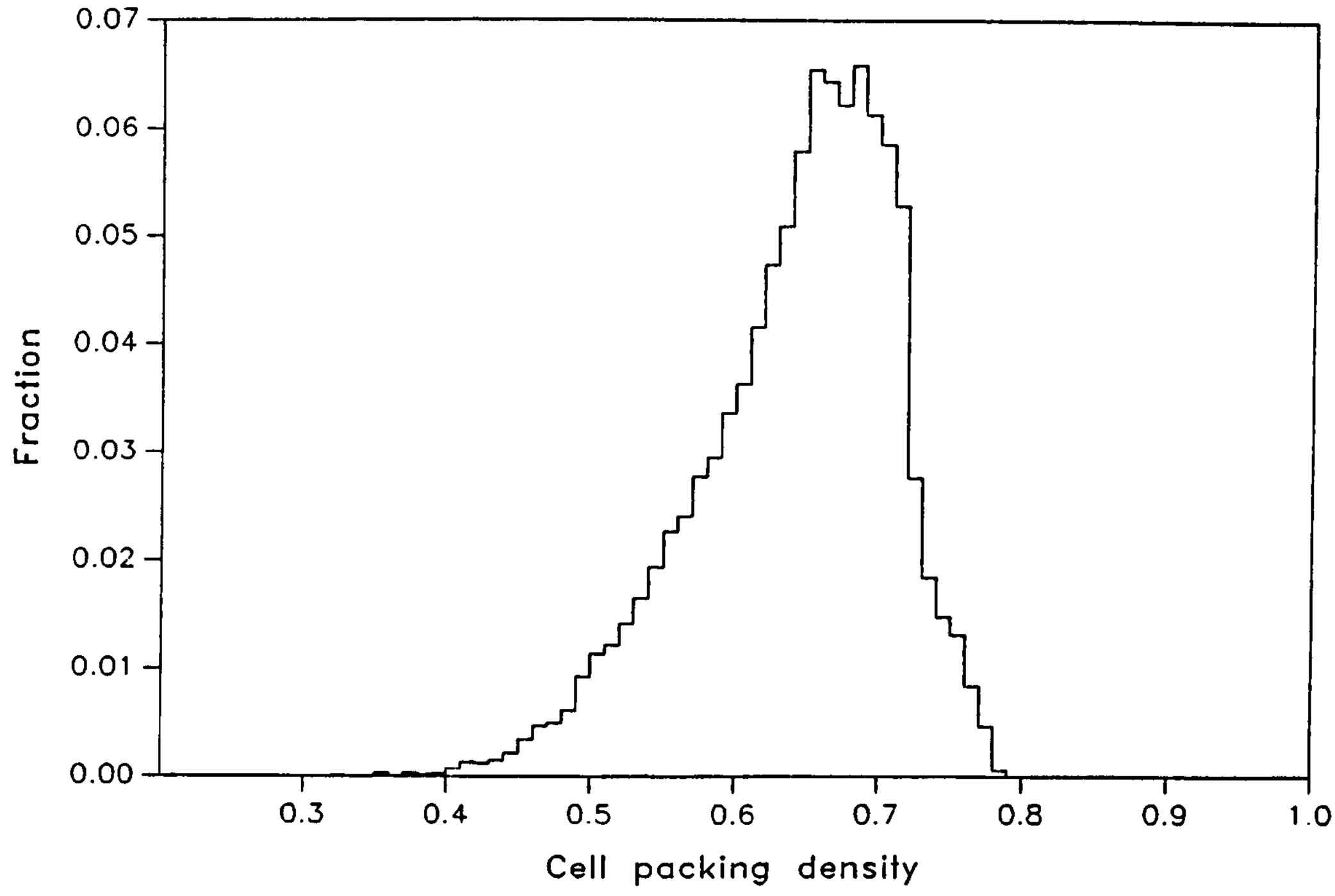

Figure 3.25 : Cell packing density frequency distribution

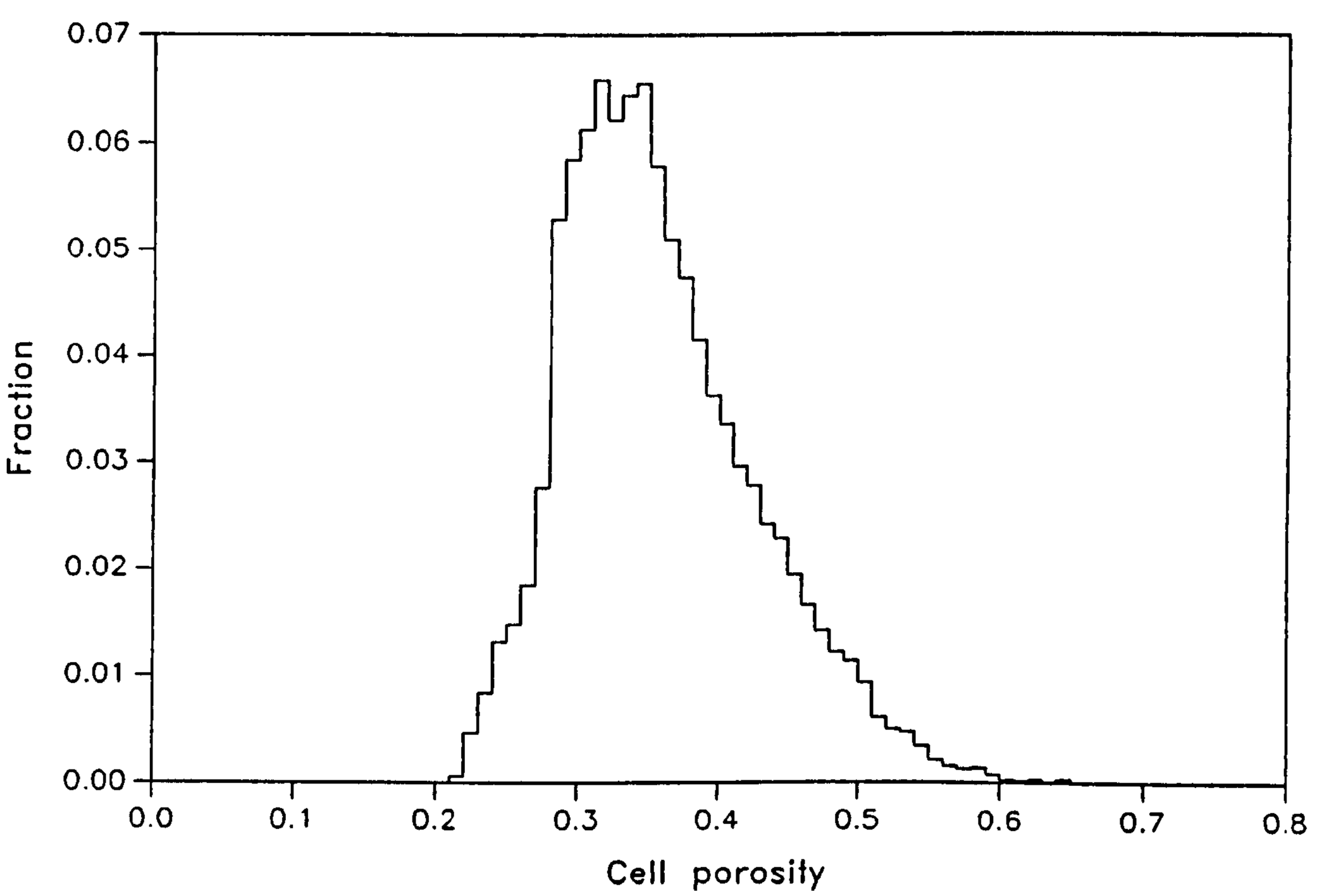

Figure 3.26 : Cell porosity frequency distribution

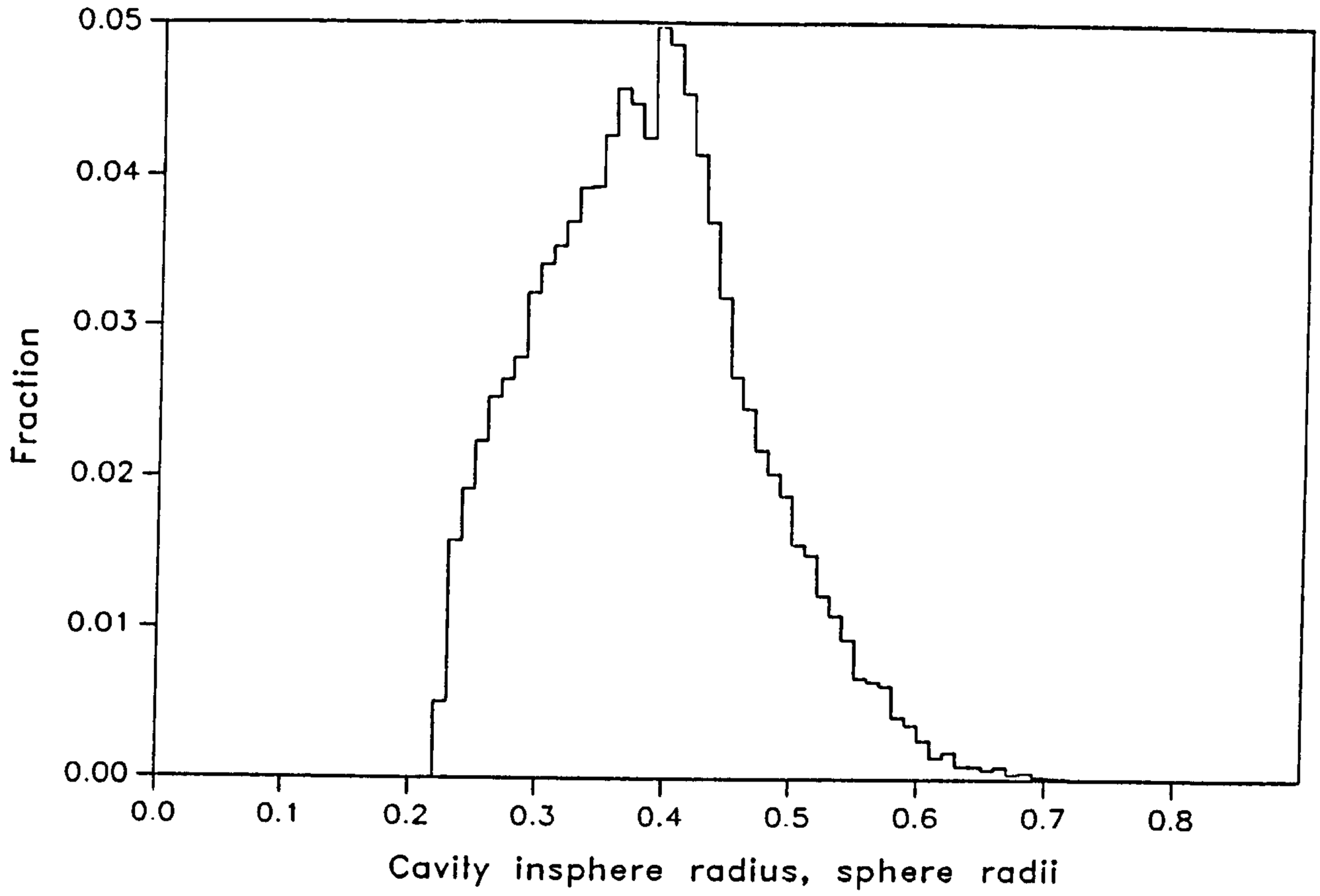

Figure 3.27 : Cavity insphere radius frequency distribution

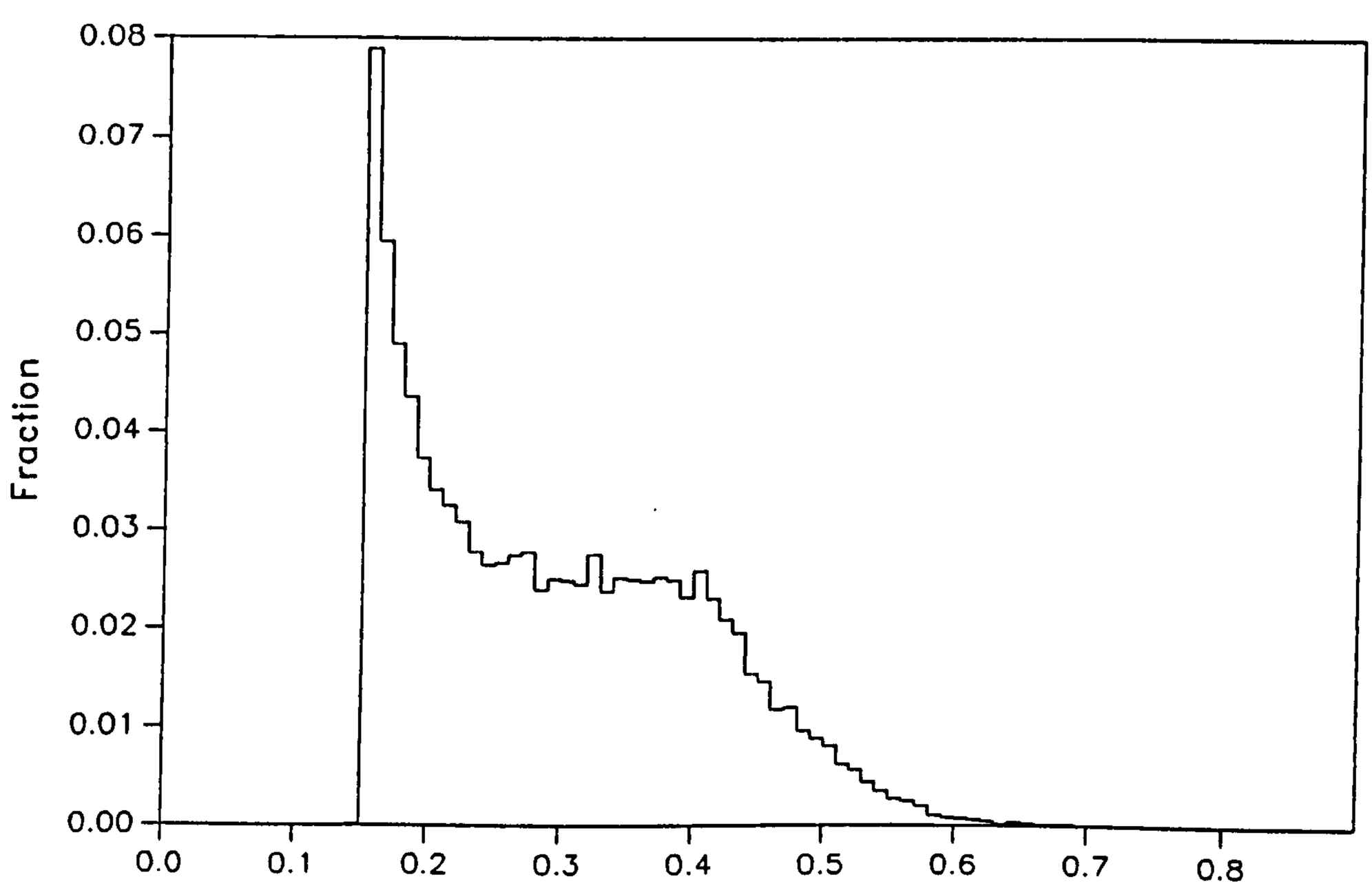

Figure 3.28 : Total face insphere radius distribution

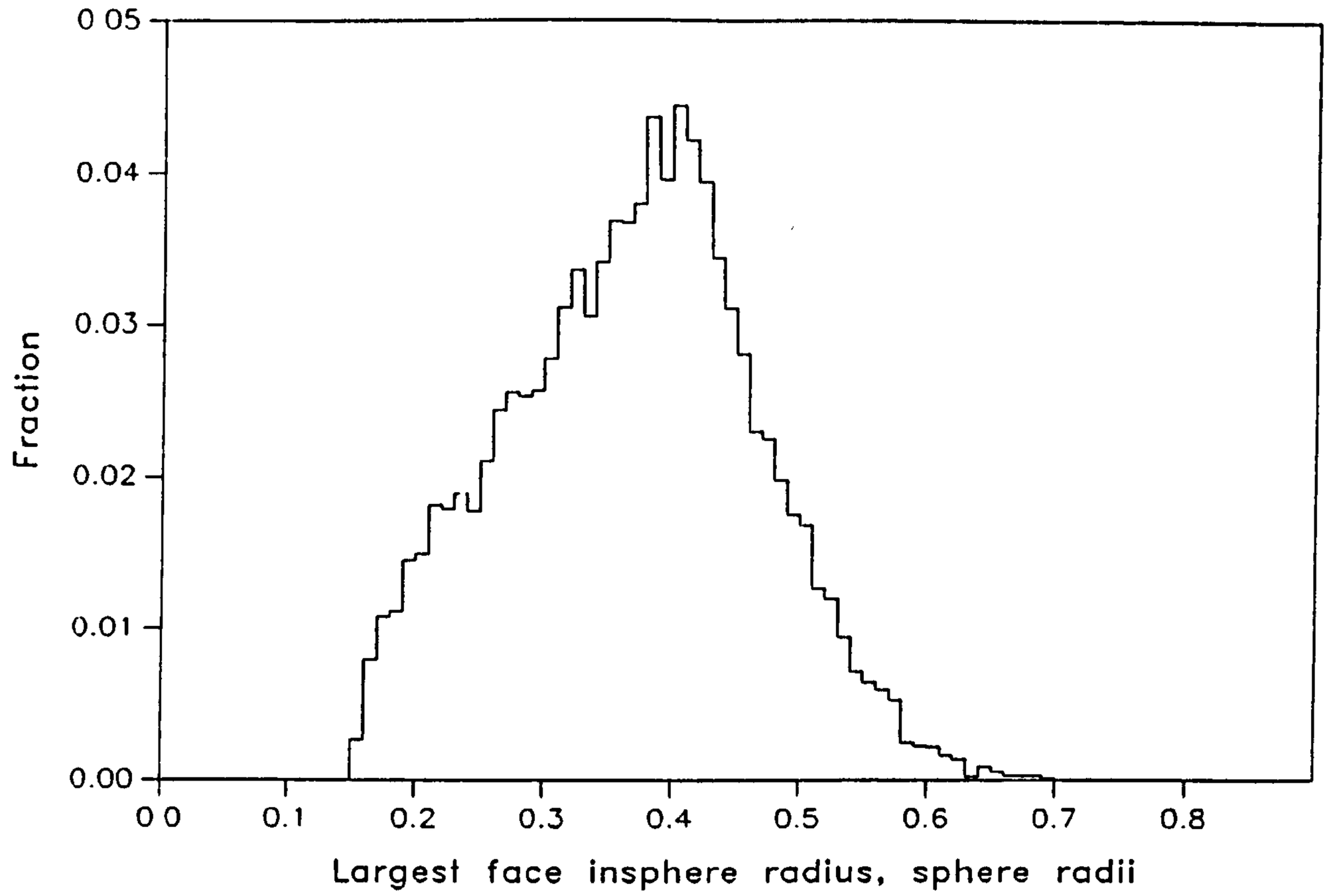

Figure 3.29 : Largest face insphere radius distribution

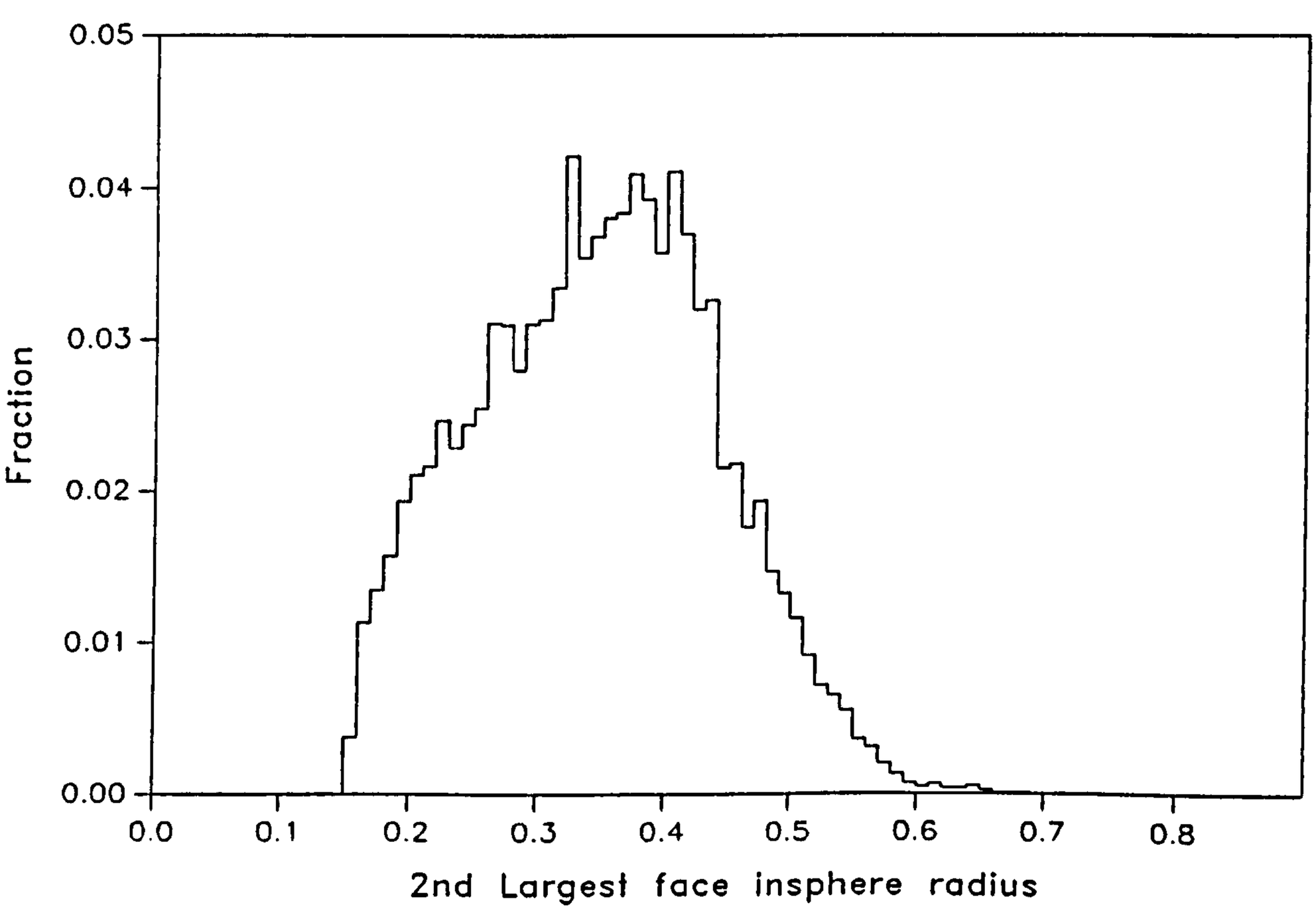

Figure 3.30 : 2nd largest face insphere radius distribution

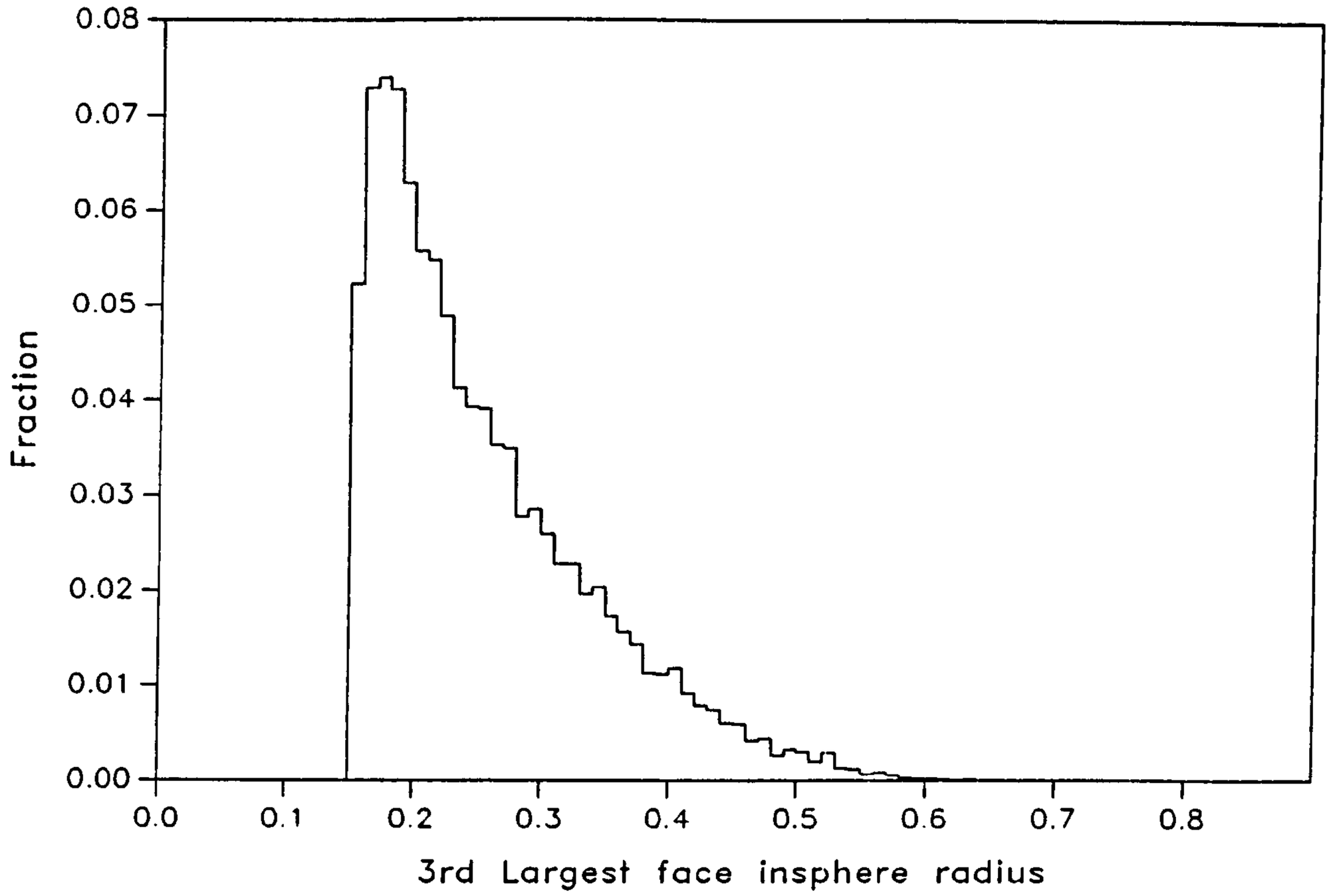

Figure 3.31 : 3rd largest face insphere radius distribution

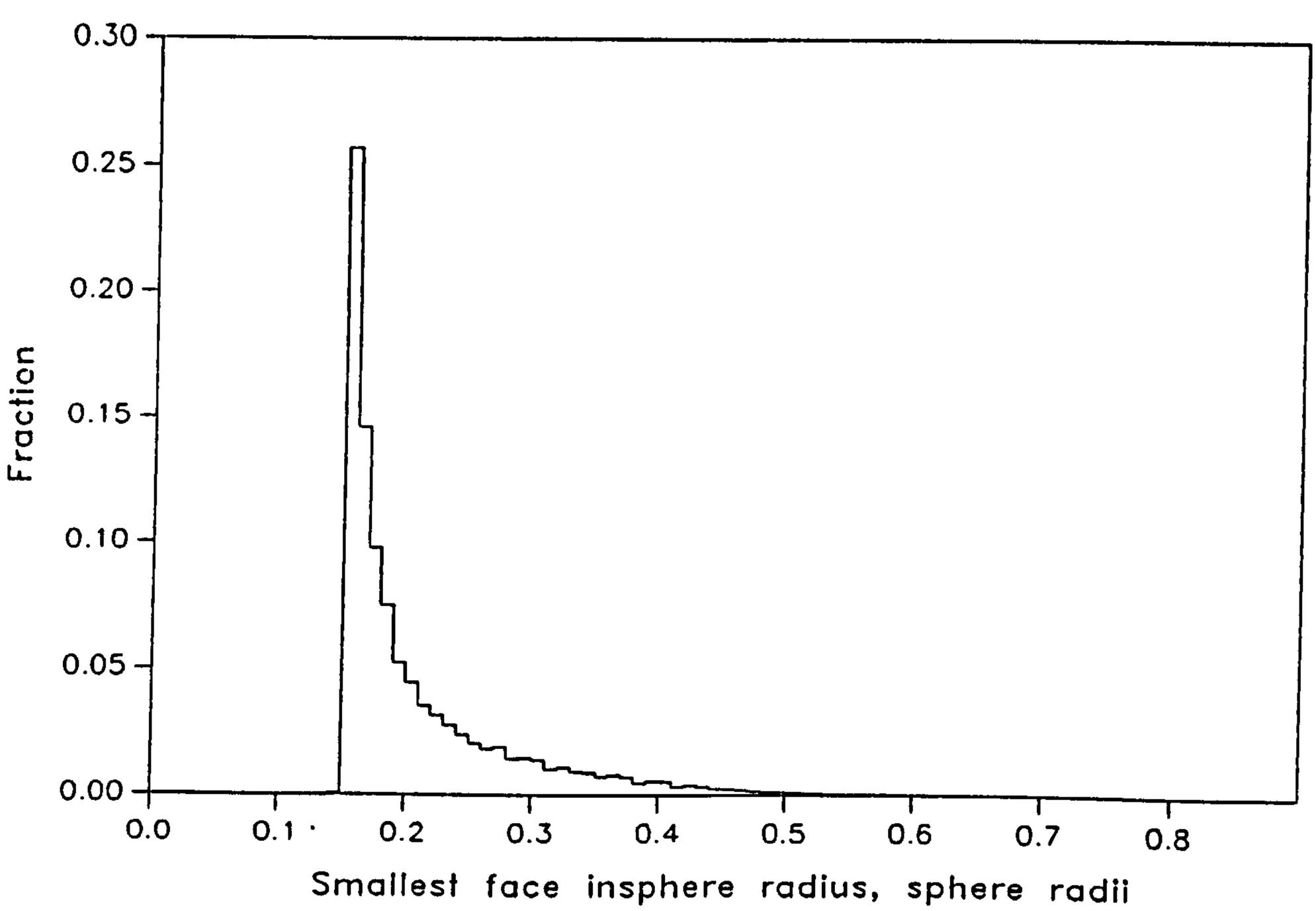

Figure 3.32 : Smallest face insphere radius distribution

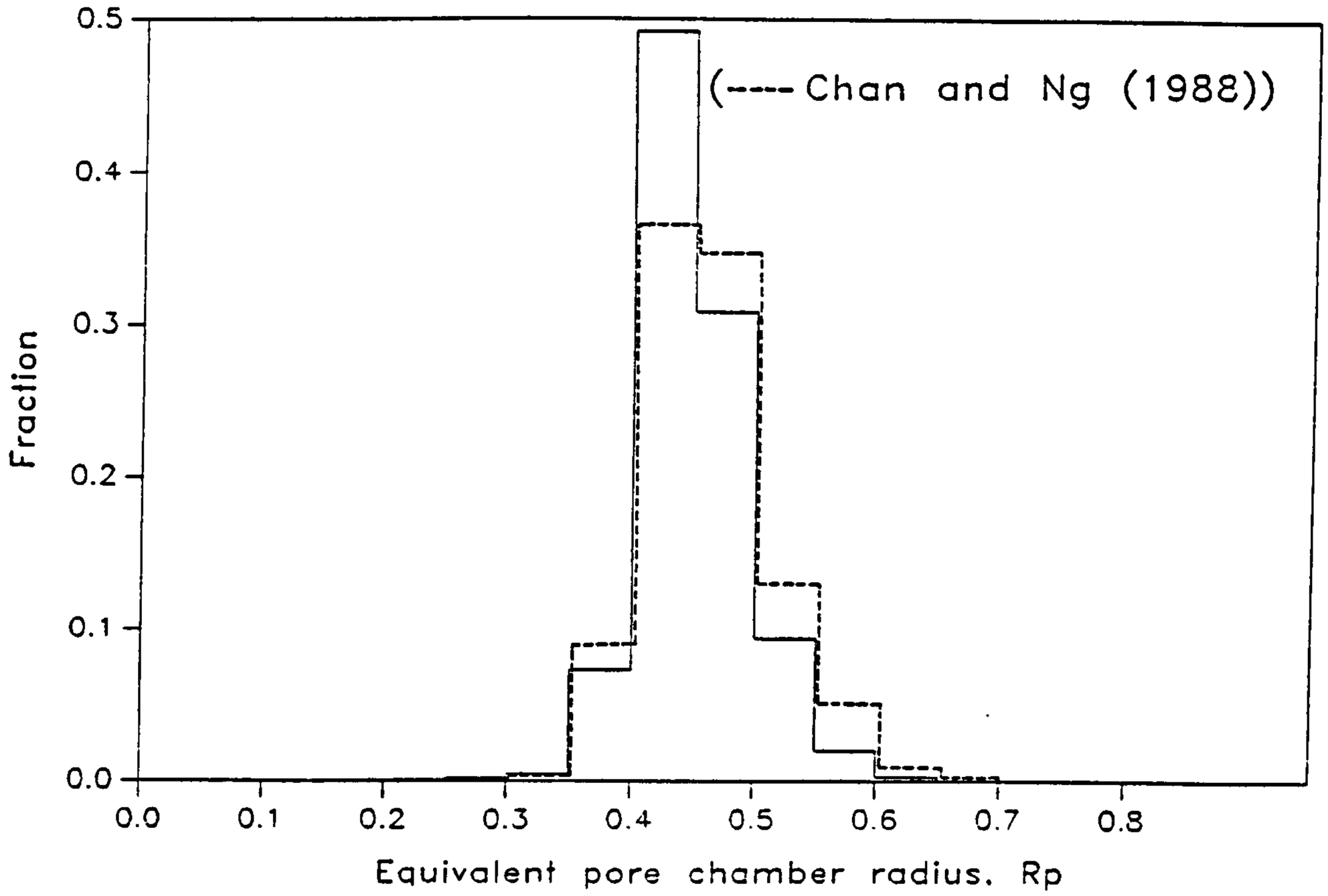

Figure 3.33 : Equivalent pore chamber radius distribution

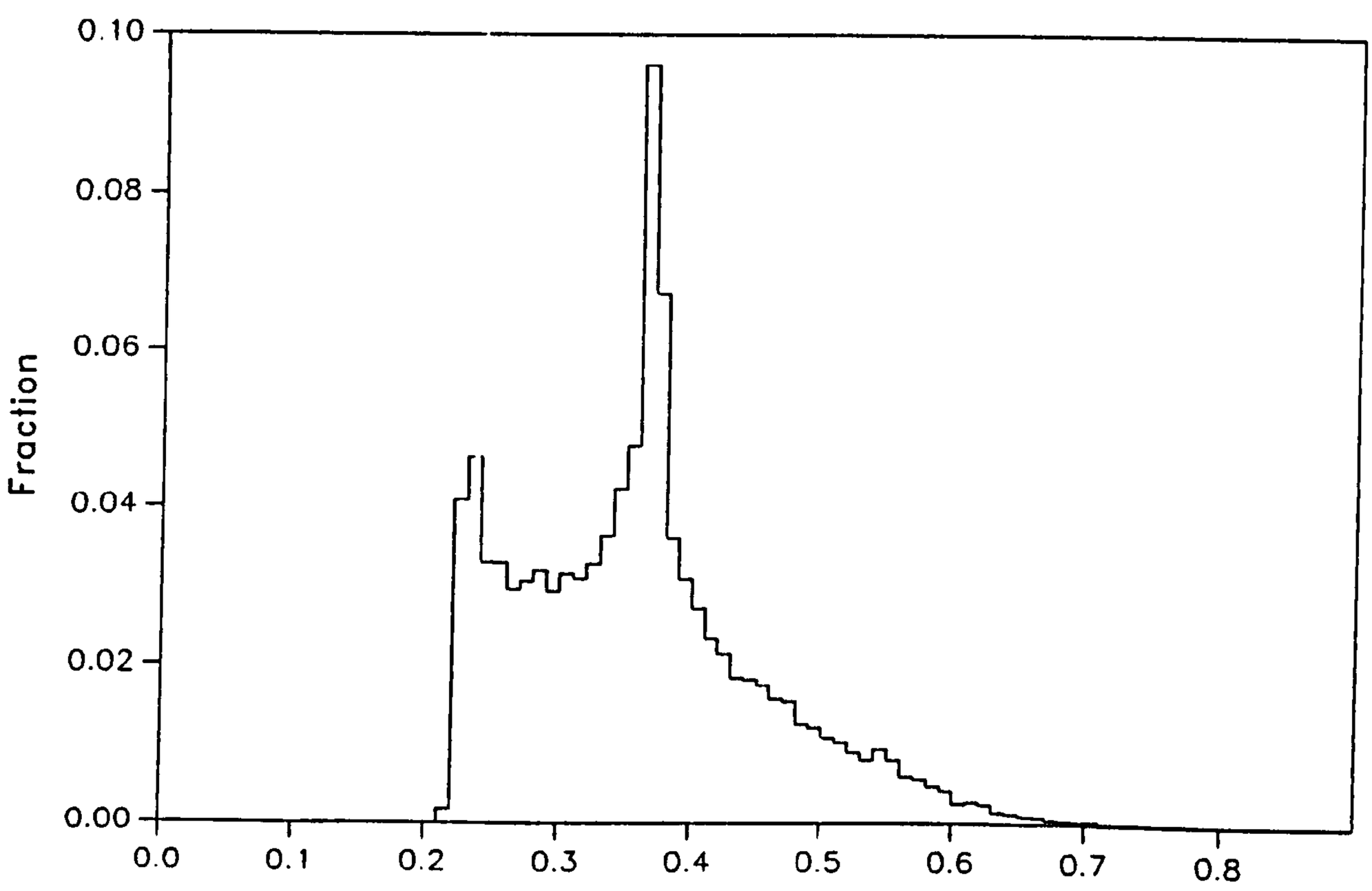

Figure 3.34 : Total equiv radii of constriction distribution

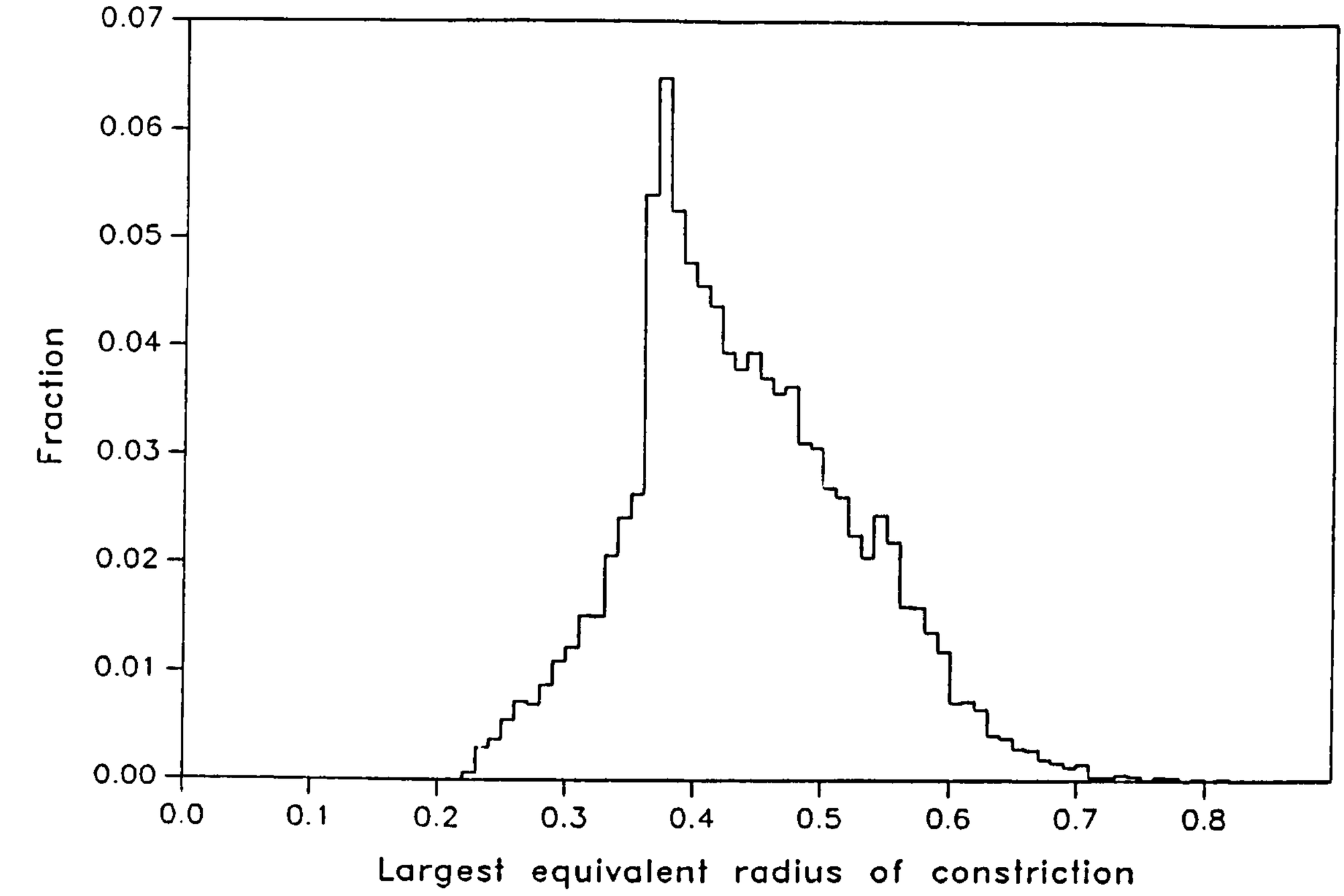

Figure 3.35 : Largest eq. radius of constriction distribution

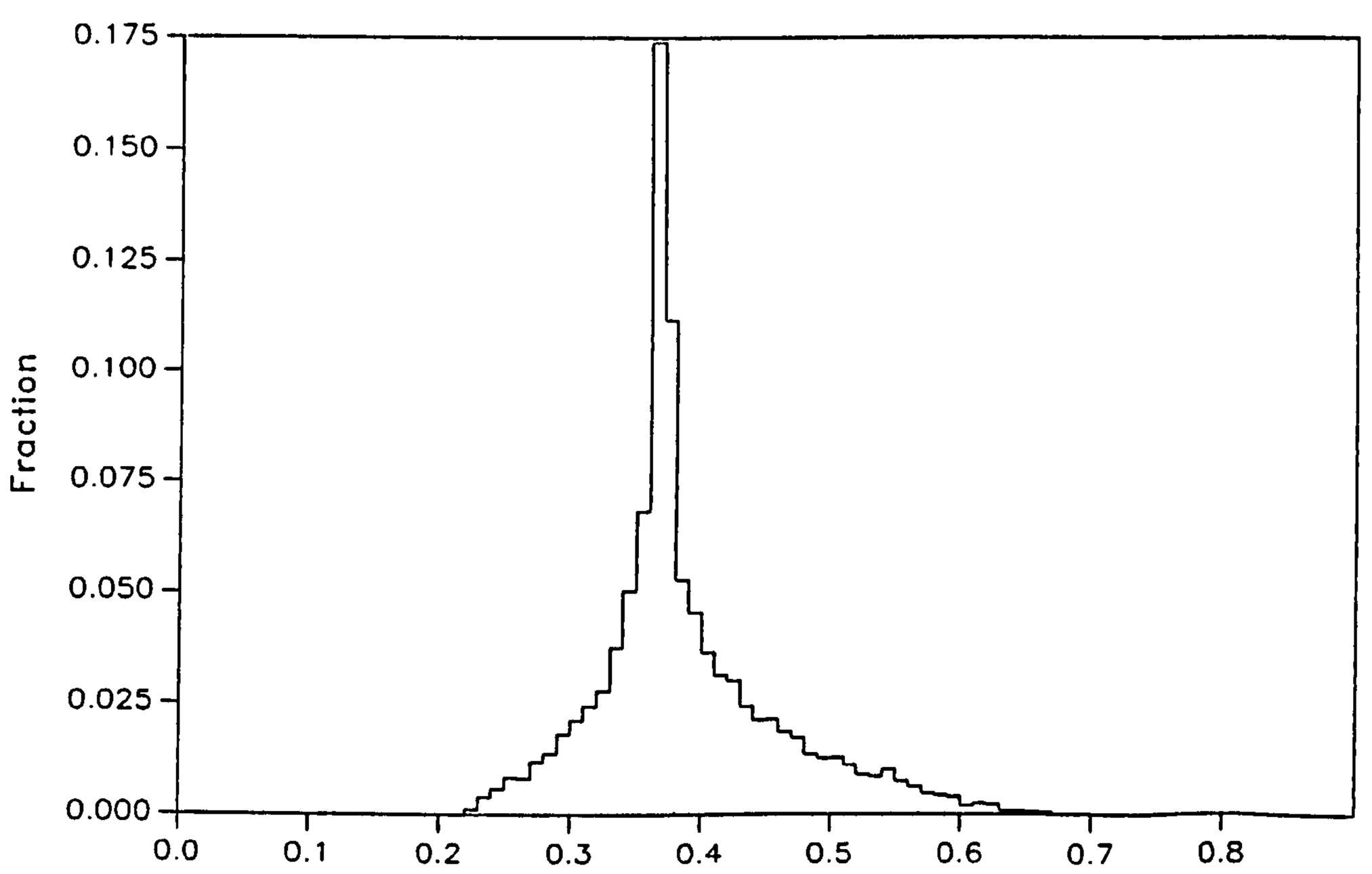

Fig 3.36 : 2nd largest eq radius of constriction distribution

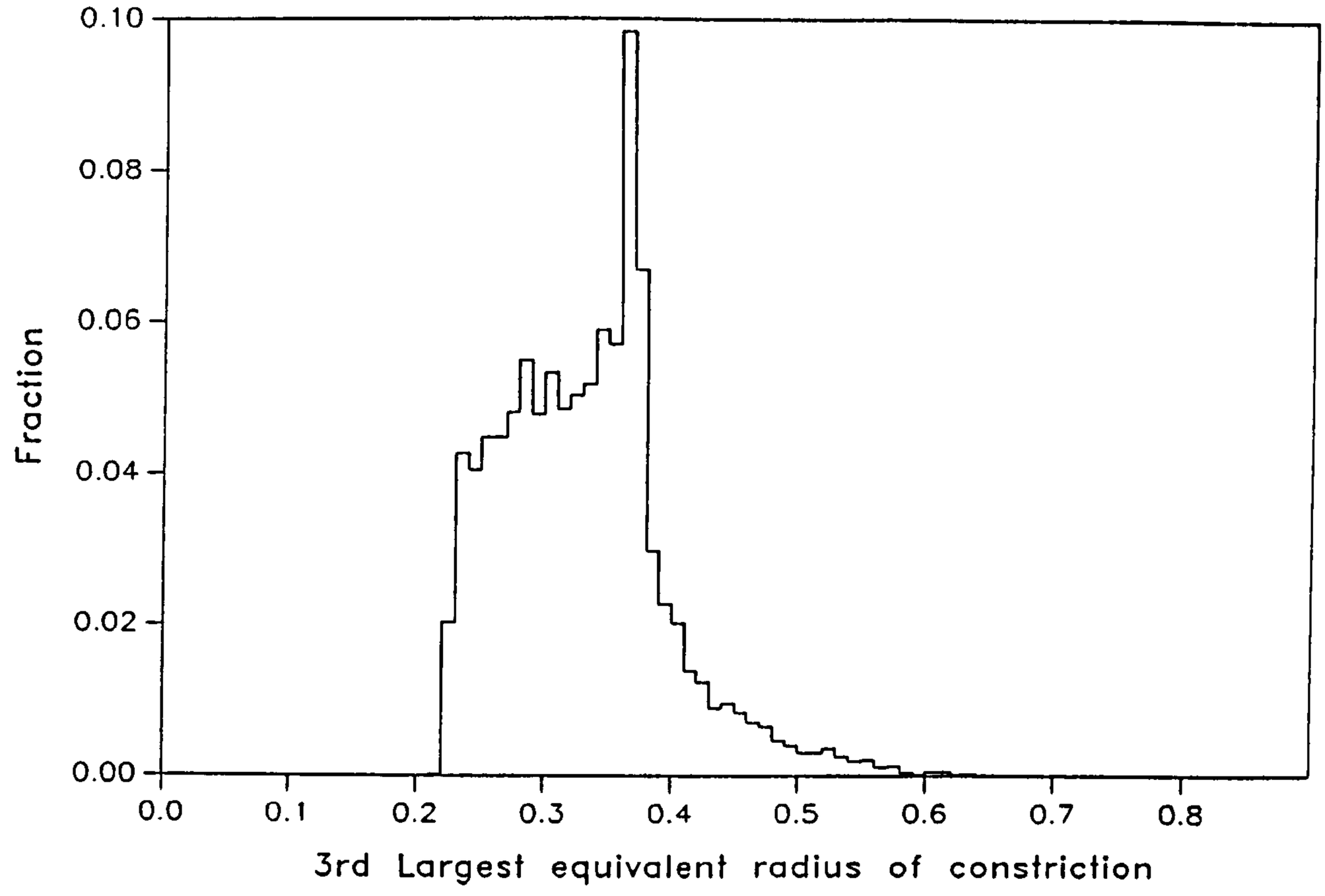

Fig 3.37 : 3rd largest eq radius of constriction distribution

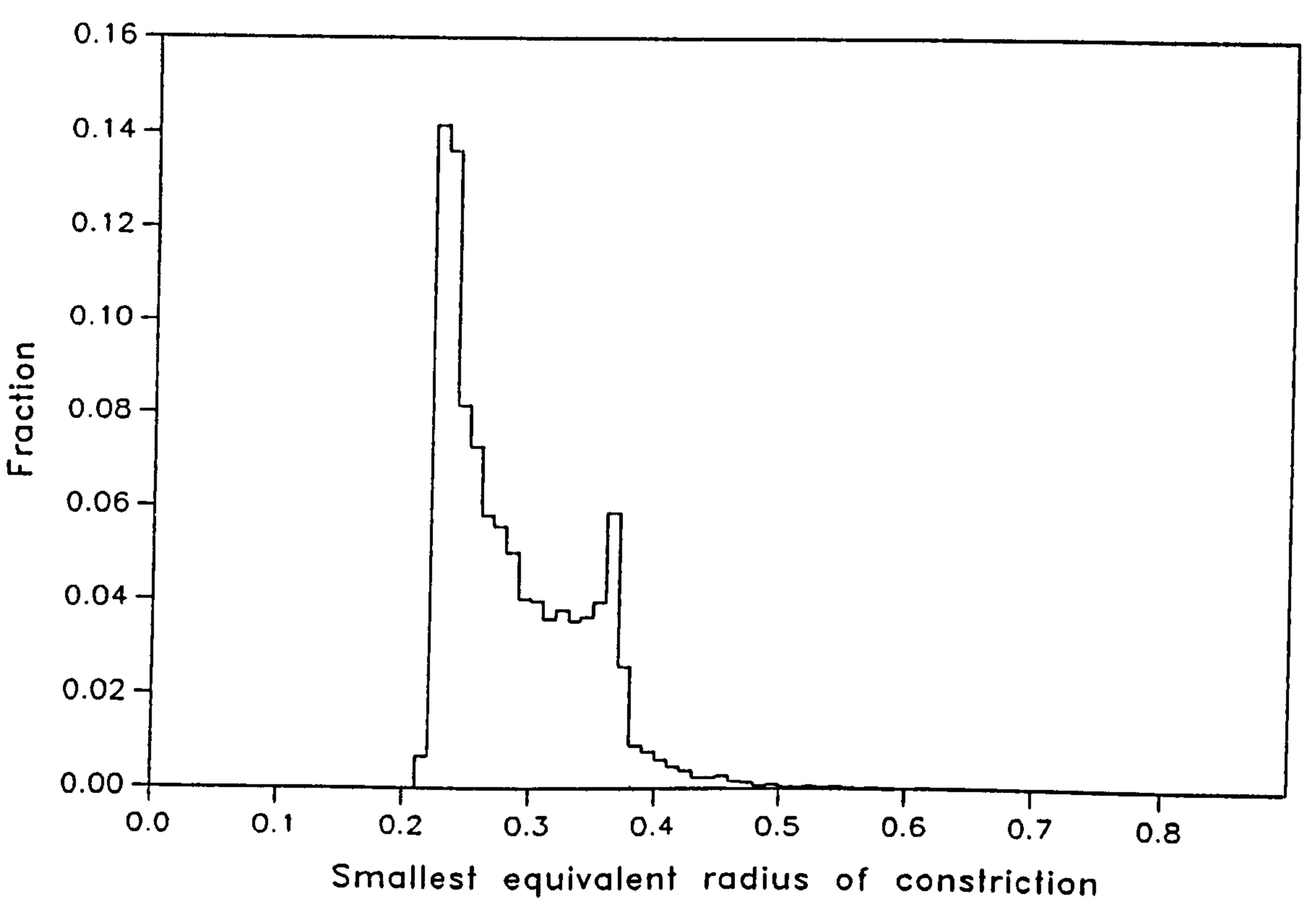

Fig 3.38 : Smallest eq radius of constriction distribution

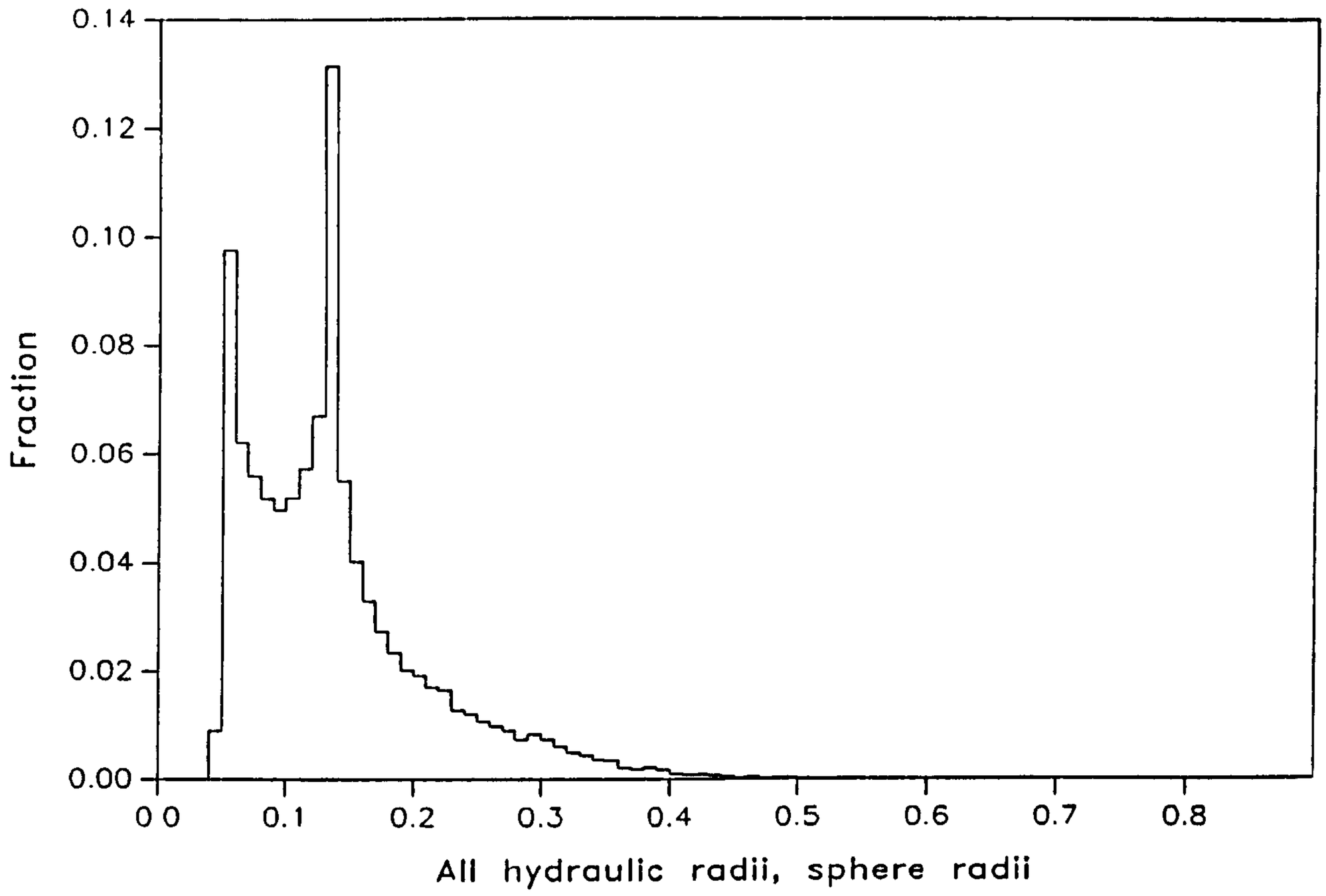

Fig 3.39 : Total hydraulic radius frequency distribution

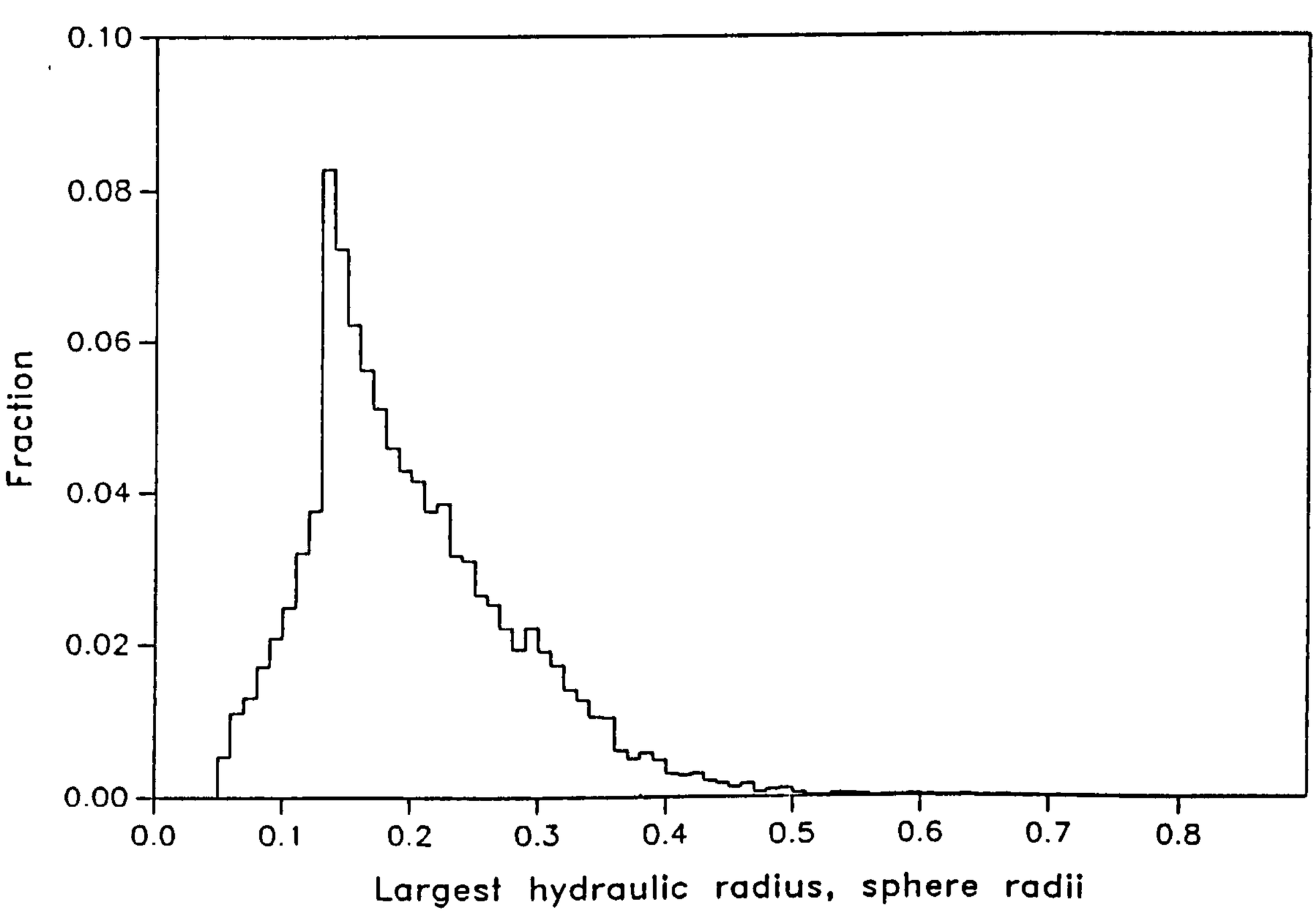

Fig 3.40 : Largest hydraulic radius frequency distribution

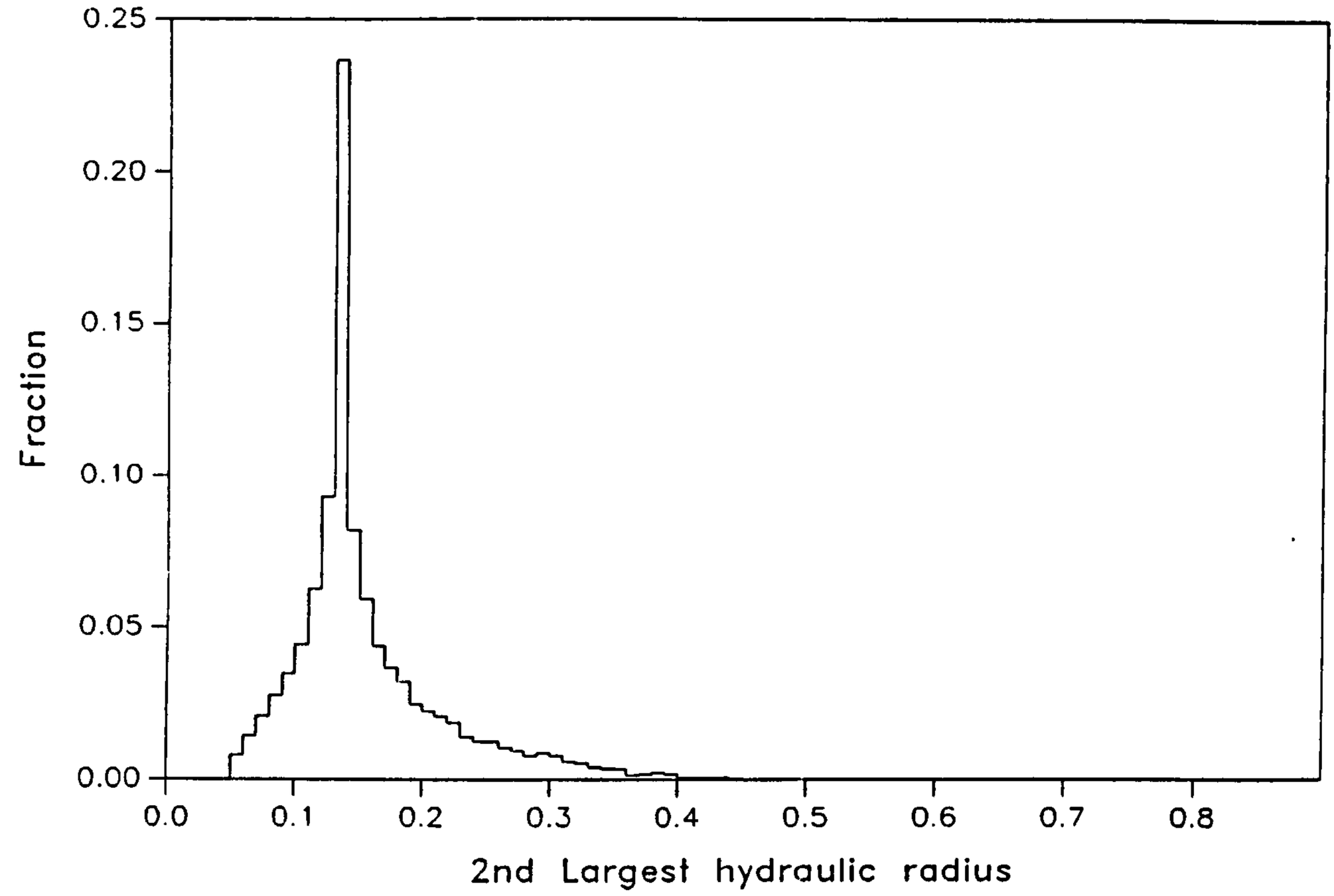

Fig 3.41 : 2nd largest hydraulic radius distribution

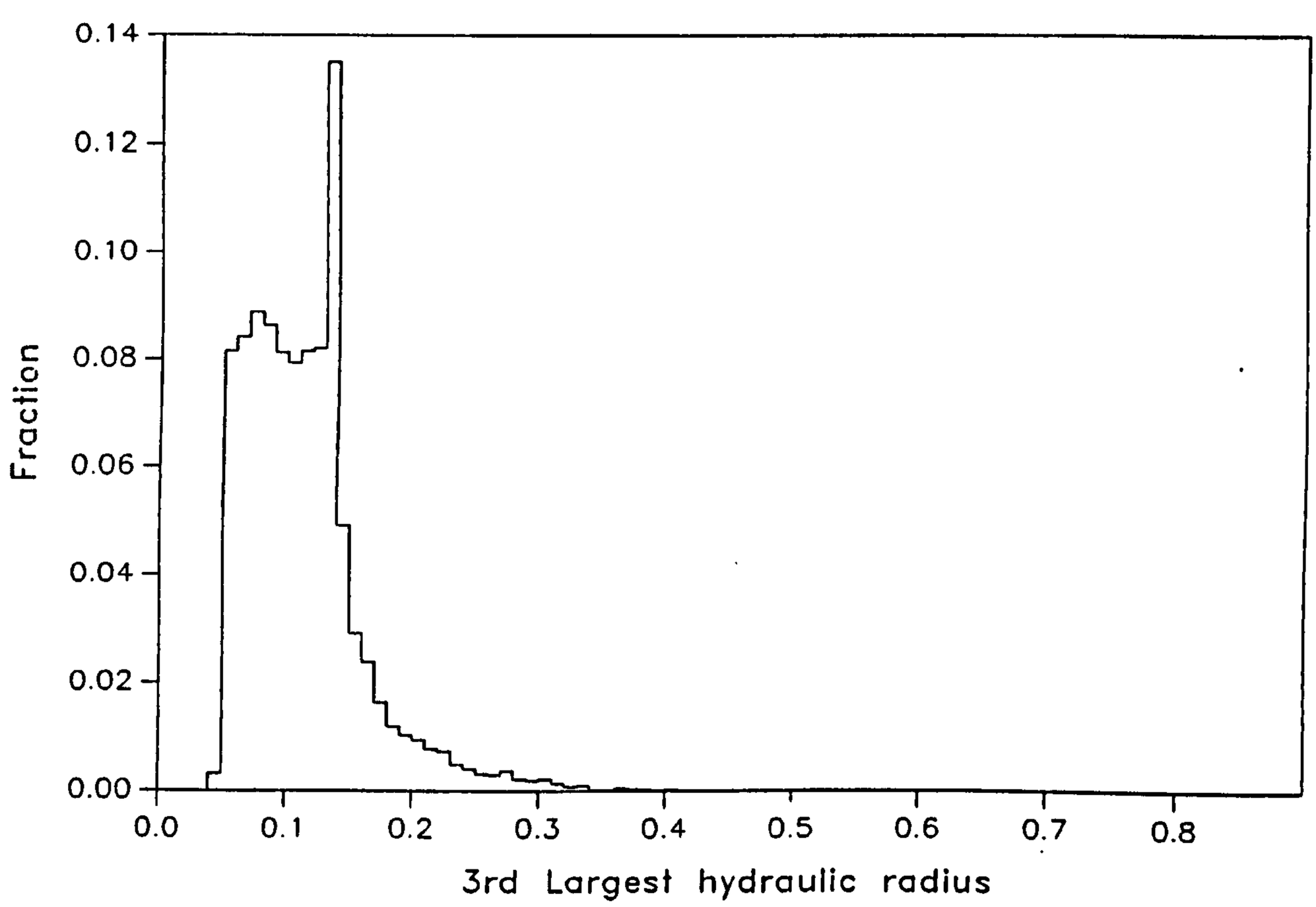

Fig 3.42 : 3rd largest hydraulic radius distribution

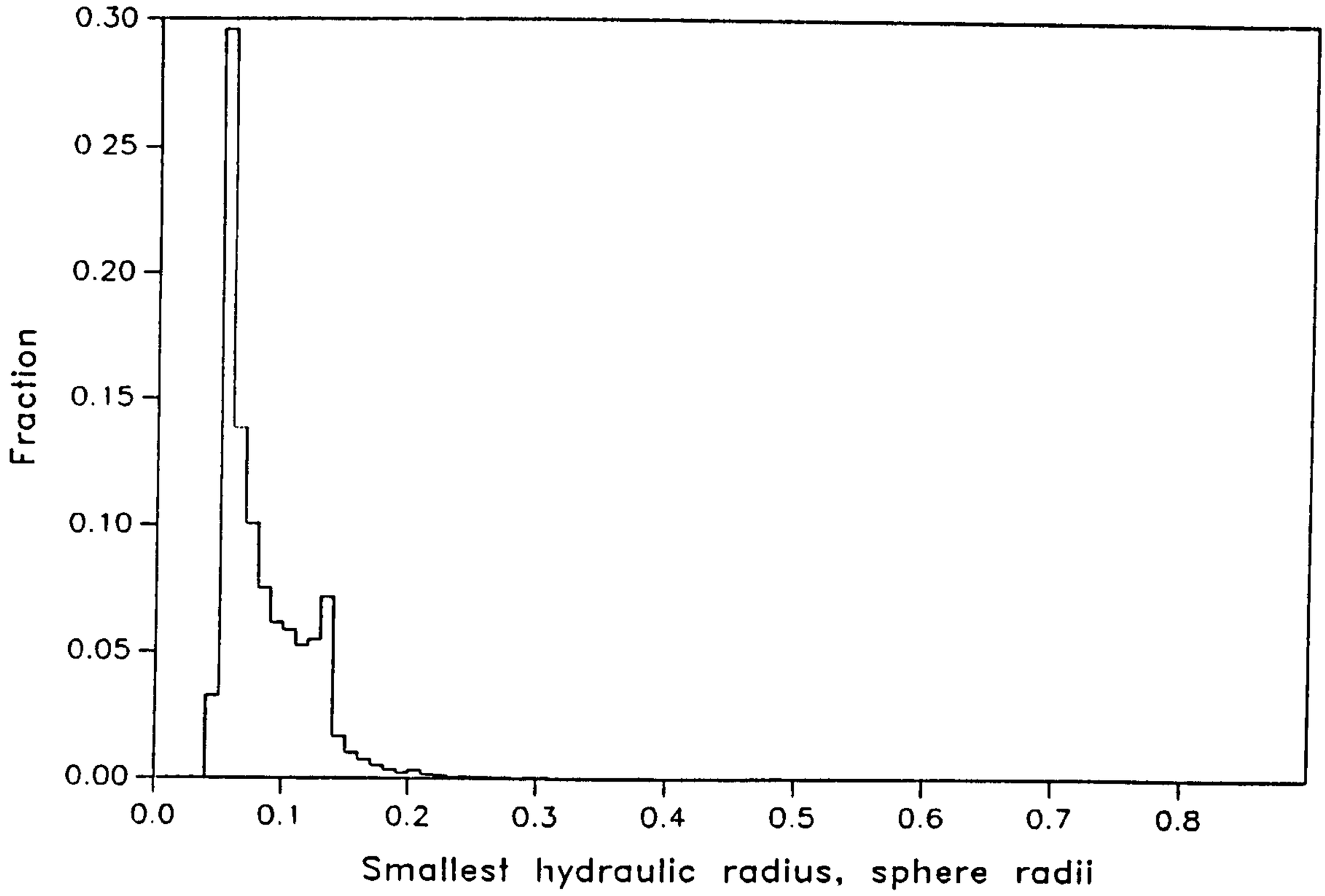

Fig 3.43 : Smallest hydraulic radius frequency distribution

3.5.19 Joint Frequency Distributions

Some of the individual frequency distributions presented in section 3.5 appear to be roughly similar in form, suggesting an approximate correlation may exist between some of the simplicial cell properties. It is possible to examine such apparent correlations using joint frequency distributions, and some of the most interesting and revealing of these are presented in figures 3.44 to 3.56.

The strong correlation between cavity insphere radius and the largest of the four face insphere radii is evident in figure 3.44. This is the most striking of all the joint frequency distributions considered in the present work, and is an important result. Making

the approximations that the imbibition meniscus curvature for an individual simplicial cell is identical to that of the cavity insphere, and that the four possible drainage meniscus curvatures for the cell are identical to those of the four face inspheres, figure 3.44 shows that an individual cell has a very high probability of having identical imbibition and drainage pressures. An individual simplicial cell, therefore, will not exhibit any significant capillary pressure hysteresis. Any such hysteresis exhibited by the packing as a whole can consequently be attributed to the phenomenon of connectivity as first postulated by Mason (1971). Thus if we consider a single simplicial cell, there is one face (insphere) which affords the same curvature as that of the cavity insphere. If we add further cells one at a time to the initial cell, each of the four additions represents a probability of 0.25 of occluding the largest face insphere of the original cell. A small cluster of five cells, therefore, would probably exhibit some significant degree of hysteresis, whilst the five individual cells would be less likely to exhibit any significant hysteresis.

There is a strong tendency for the second largest face insphere radius to be quite close in magnitude to that of the cavity insphere radius, as shown in figure 3.45. (This tendency is also evident from figure 3.50 which shows the joint frequency distribution for the largest and the second largest face insphere radii.). The physical significance of this relatively strong tendency is that not one, but two of the four face insphere radii per cell will be close in magnitude to that of the cell cavity insphere radius. An individual cell in isolation, therefore, will not only exhibit little or no capillary pressure hysteresis, but there is also quite a high probability that two of the four faces will drain and imbibe

at roughly similar meniscus curvatures.

Figure 3.46 and 3.47 show the joint frequency distributions for the third largest face insphere radius/cavity insphere radius and smallest face insphere radius/cavity insphere radius respectively. Below magnitudes of 0.4 neither of these two face inspheres can have magnitudes close to that of the cell cavity insphere radius. For face inspheres above 0.4, there exists only a low probability (of the order of 0.003) that either of the two smallest face inspheres can be close in magnitude to the cavity insphere radius.

It is of some interest to compare the equivalent pore chamber radius with the cavity insphere radius, since the former is a convenient measure of the cell pore volume available to conduct fluid flow through the cell (Chan and Ng, 1988), whilst the latter is an approximate measure of imbibition meniscus curvature (Mason, 1971). Figure 3.48, then, gives some indication of the relationship between these permeability-linked and capillary pressure-linked variables on an individual cell basis. As is to be expected, the majority of cells have an equivalent pore chamber radius considerably larger than the cavity insphere radius. This must be so, since the cavity insphere does not occupy all of the available pore space in order to contact the four hard spheres defining the cell. The equivalent pore chamber radius, by definition, accounts for all of the cell pore volume. It is interesting to note, therefore, that a significant fraction of cells have cavity insphere radii larger than the equivalent pore volume radius. The explanation for this observation is that the cavity insphere is not necessarily contained entirely by the cell, some of the cavity insphere protrudes through

one or more of the cell faces (this may be visualised by referring to figure 2.18). Indeed, there is no requirement for the centre of the cavity insphere to be inside the reference cell; odd shaped cells may well have the centre externally located in order to satisfy the condition that the surface of the cavity insphere is in contact with the four hard spheres of the cell. Figure 3.48 shows that equivalent pore chamber radius and cavity insphere radius are not functionally related in a significant manner, and are not conceptually interchangeable. This implies that for random sphere packings there exists no simple structural relationship between imbibition capillary processs and permeability processes on the scale of the individual pore. The implication is perhaps weak, as we have not yet considered the role of the cell face constrictions, but this aspect is considered shortly.

The cavity insphere radius will be a very poor estimator of cell pore volume. This is apparent from the discussion presented in the previous paragraph and is confirmed by figure 3.49 which shows the joint frequency distribution for cavity insphere radius and cell pore volume.

Figure 3.50 shows the joint frequency distribution for the largest face insphere radius and the second largest face insphere radius. This figure confirms the reasonably close correspondence in magnitude between these two parameters, as discussed earlier. Figures 3.51 and 3.52 confirm that there is no such close correspondence between either the third largest face insphere radius and the largest face insphere radius or the smallest face insphere radius and the largest face insphere radius.

To conclude this section of Chapter 3.5, the relationship between capillary properties and fluid flow properties are further examined. Figures 3.53 to 3.56 show the joint frequency distributions for the hydraulic radii and face insphere radii for the four cell faces ranked according to size. The hydraulic radius is in all cases less than the magnitude of the corresponding face insphere radius. Perhaps the most significant factor here is that none of the four joint frequency distributions shows any useful correlation between hydraulic radius and face insphere radius, other than that, for face inspheres below 0.3, there is an approximately linear correlation with hydraulic radius. However this correlation is only good for a third, or less, of all cells considered. The implication here is that, for random sphere packings, there exists no simple structural relationship between drainage capillary processes and permeability processes on the scale of the individual pore. This implication matches that considered earlier for imbibition processes and permeability. Together these two implications appear to preclude any possibility of being able to predict permeability of an individual cell given only information about the structural parameters which influence capillary properties of that individual cell. Conversely, it seems equally improbable that, given only information about the structural parameters which influence permeability of the cell, nothing useful could be deduced regarding the capillary properties of that individual cell.

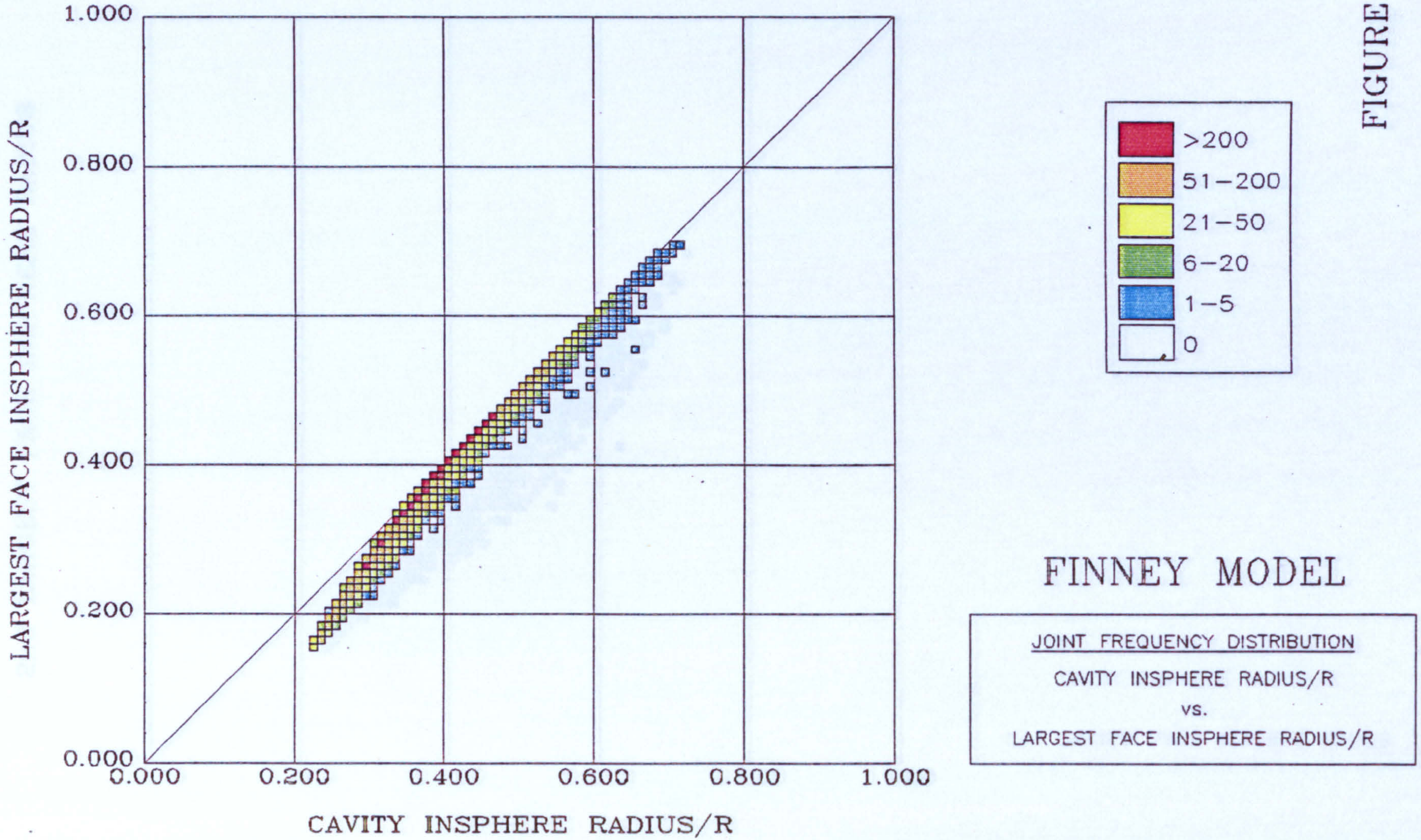
1.000
0.800
0.600
0.400
0.200
0.000
0.000
0.200
0.400
0.600
0.800
1.000
LARGEST FACE INSPHERE RADIUS/R
CAVITY INSPHERE RADIUS/R
>200
51–200
21–50
6–20
1–5
0
FINNEY MODEL
JOINT FREQUENCY DISTRIBUTION
CAVITY INSPHERE RADIUS/R
vs.
LARGEST FACE INSPHERE RADIUS/R

FIGURE 3.44

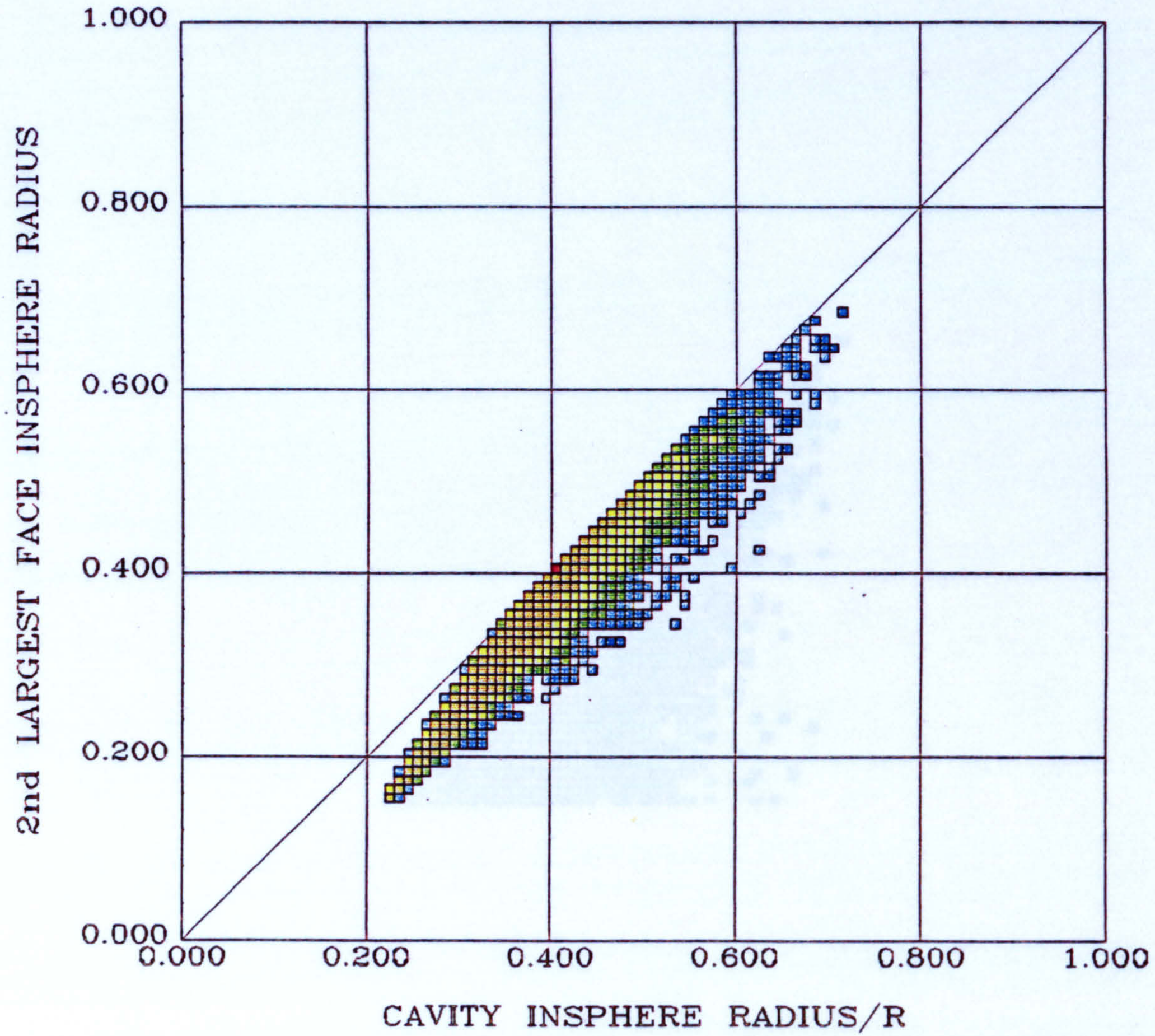

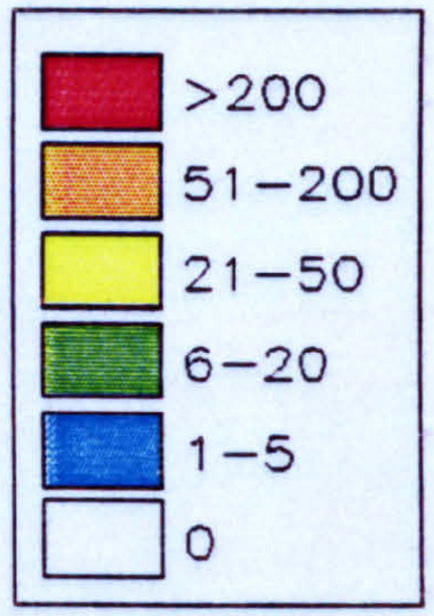

FIGURE 3·45

FINNEY MODEL

JOINT FREQUENCY DISTRIBUTION

CAVITY INSPHERE RADIUS/R

vs.

2nd LARGEST FACE INSPHERE RADIUS

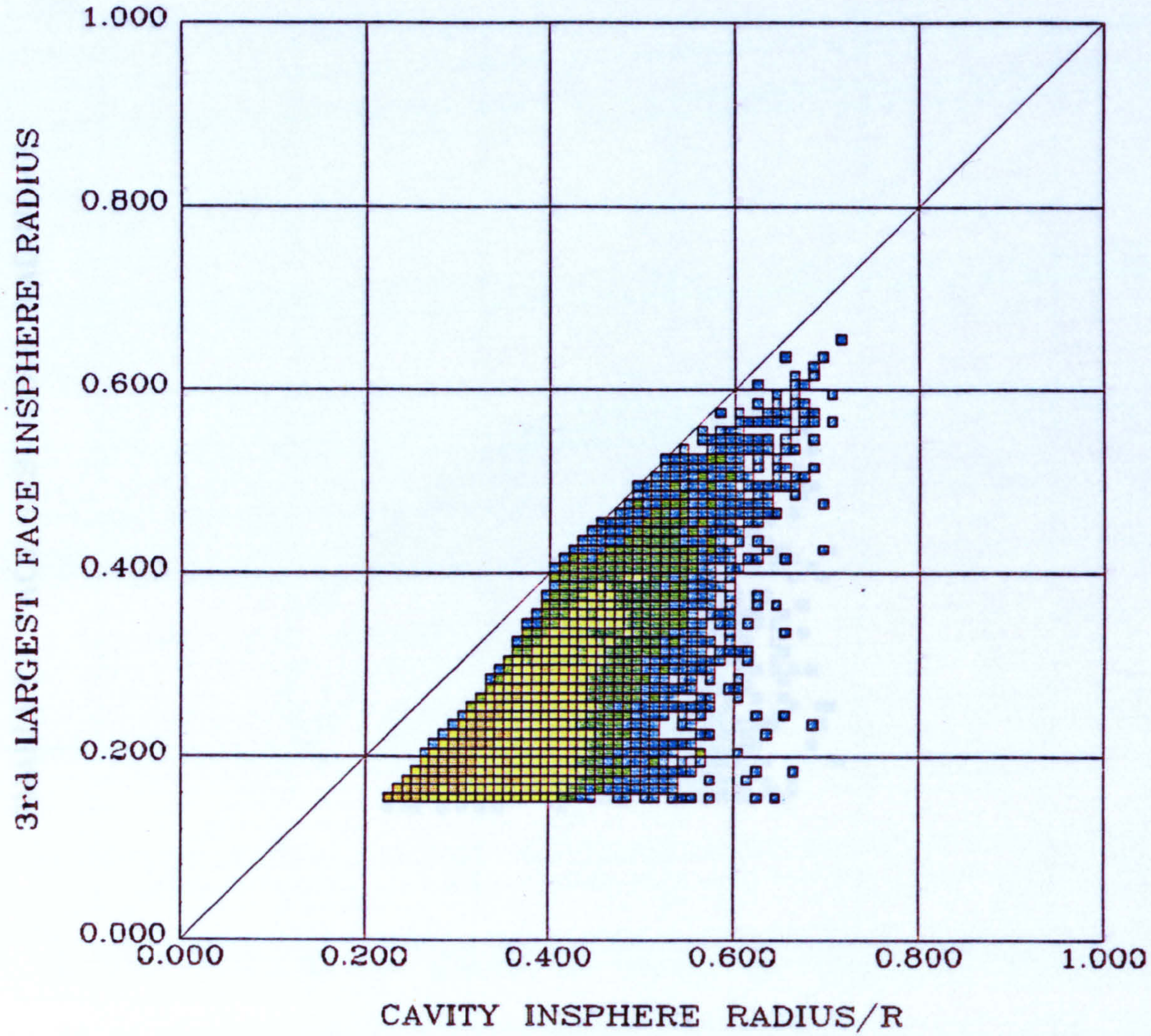

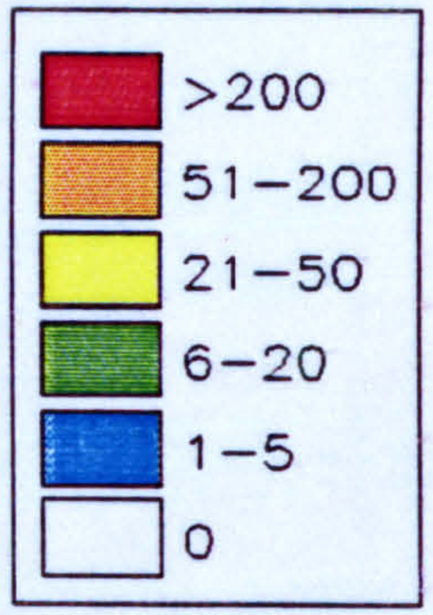

FIGURE 3.46

146.

FINNEY MODEL

JOINT FREQUENCY DISTRIBUTION

CAVITY INSPHERE RADIUS/R

vs.

3rd LARGEST FACE INSPHERE RADIUS

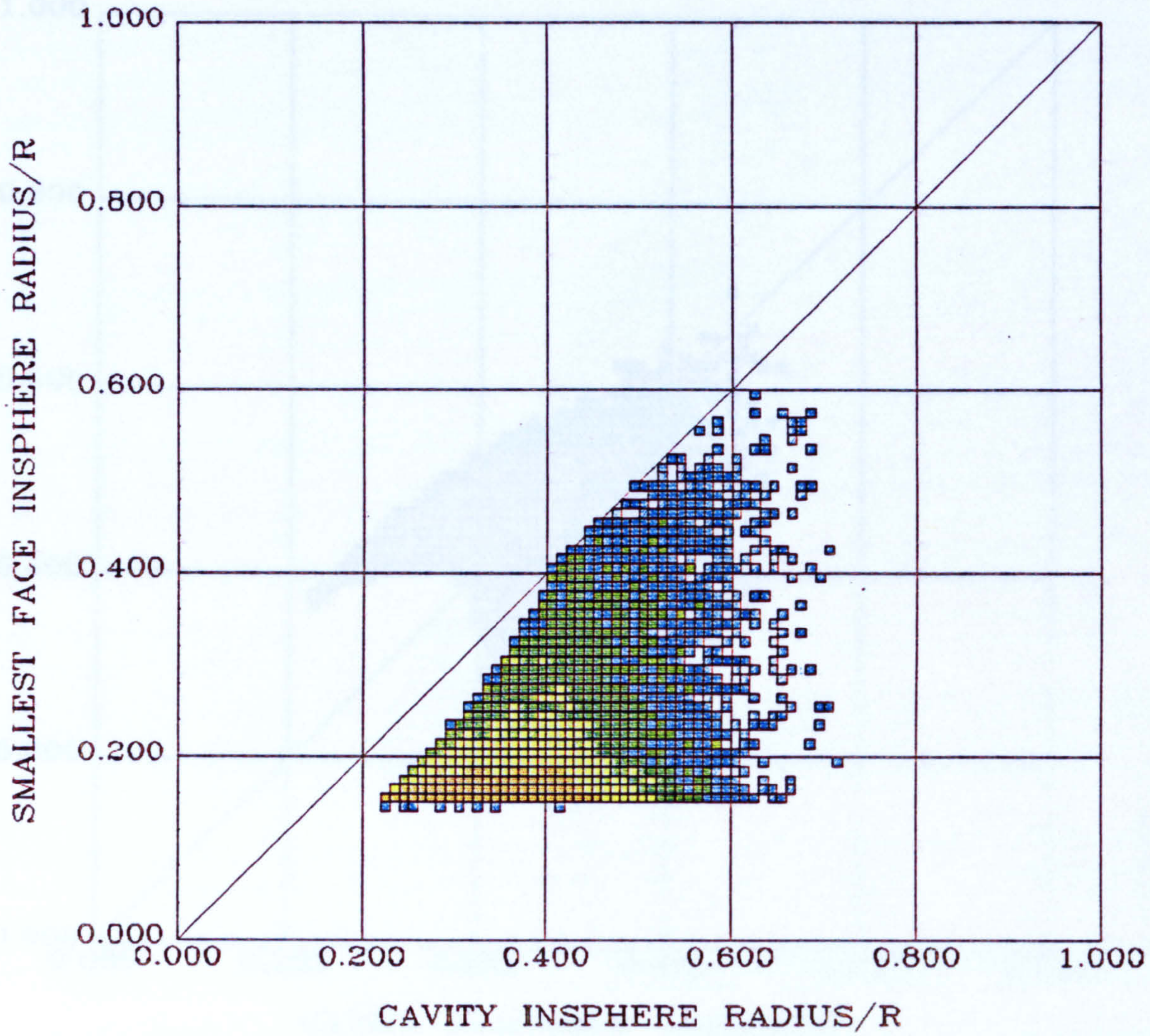

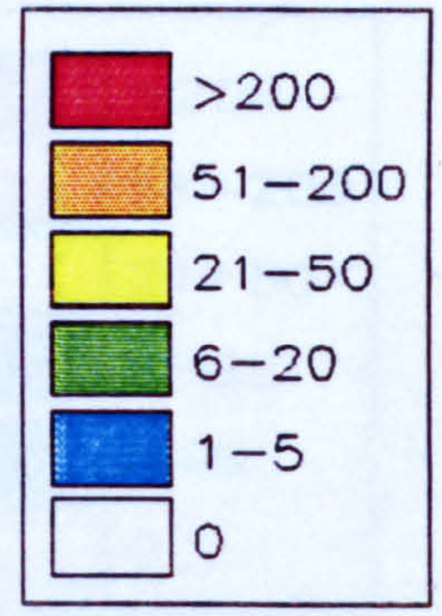

FIGURE 3·47

FINNEY MODEL

JOINT FREQUENCY DISTRIBUTION

CAVITY INSPHERE RADIUS/R

vs.

SMALLEST FACE INSPHERE RADIUS/R

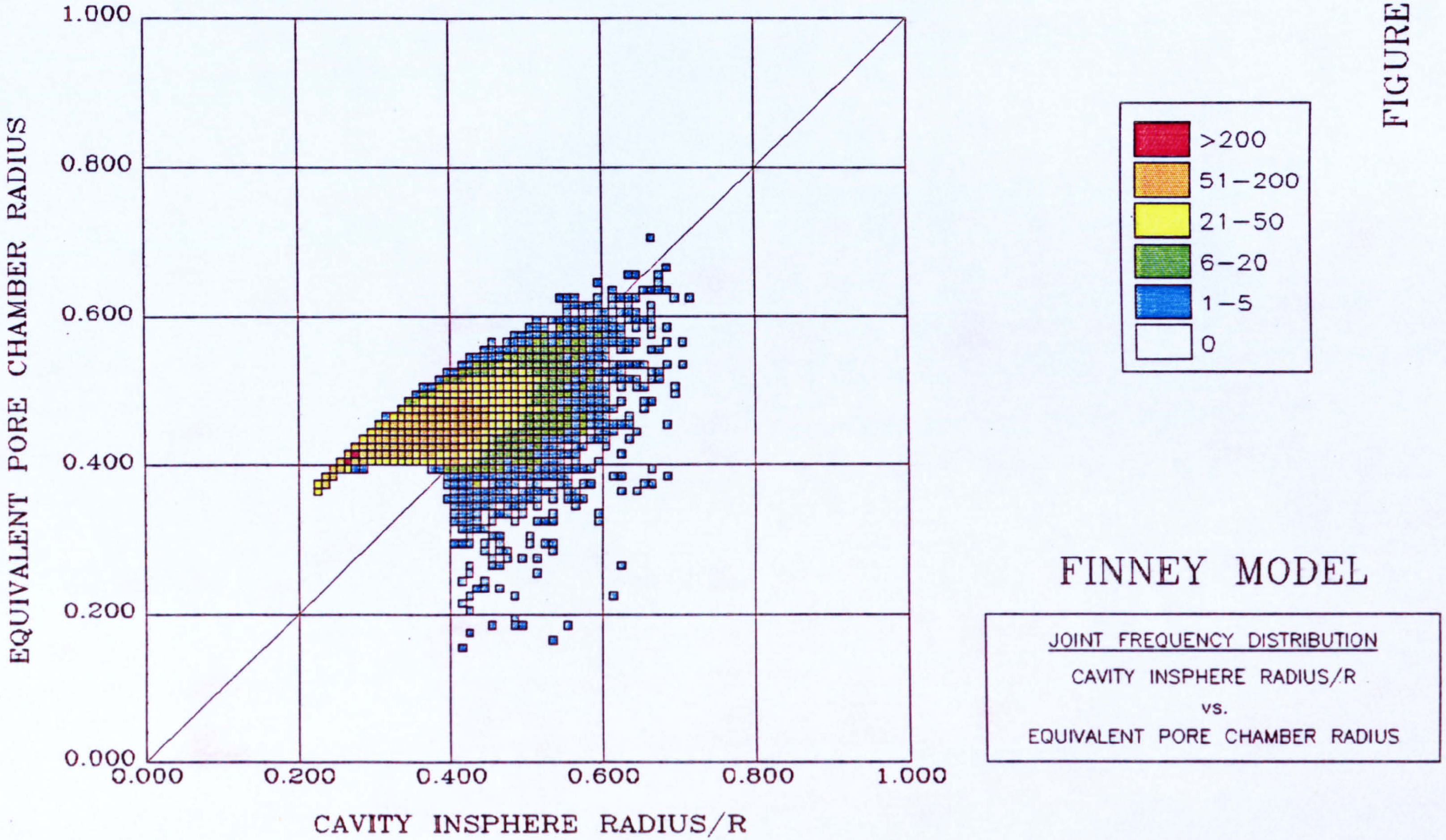
1.000
0.800
0.600
0.400
0.200
0.000
0.000
0.200
0.400
0.600
0.800
1.000
EQUIVALENT PORE CHAMBER RADIUS
CAVITY INSPHERE RADIUS/R
>200
51–200
21–50
6–20
1–5
0
FINNEY MODEL
JOINT FREQUENCY DISTRIBUTION
CAVITY INSPHERE RADIUS/R
vs.
EQUIVALENT PORE CHAMBER RADIUS

FIGURE 3-48

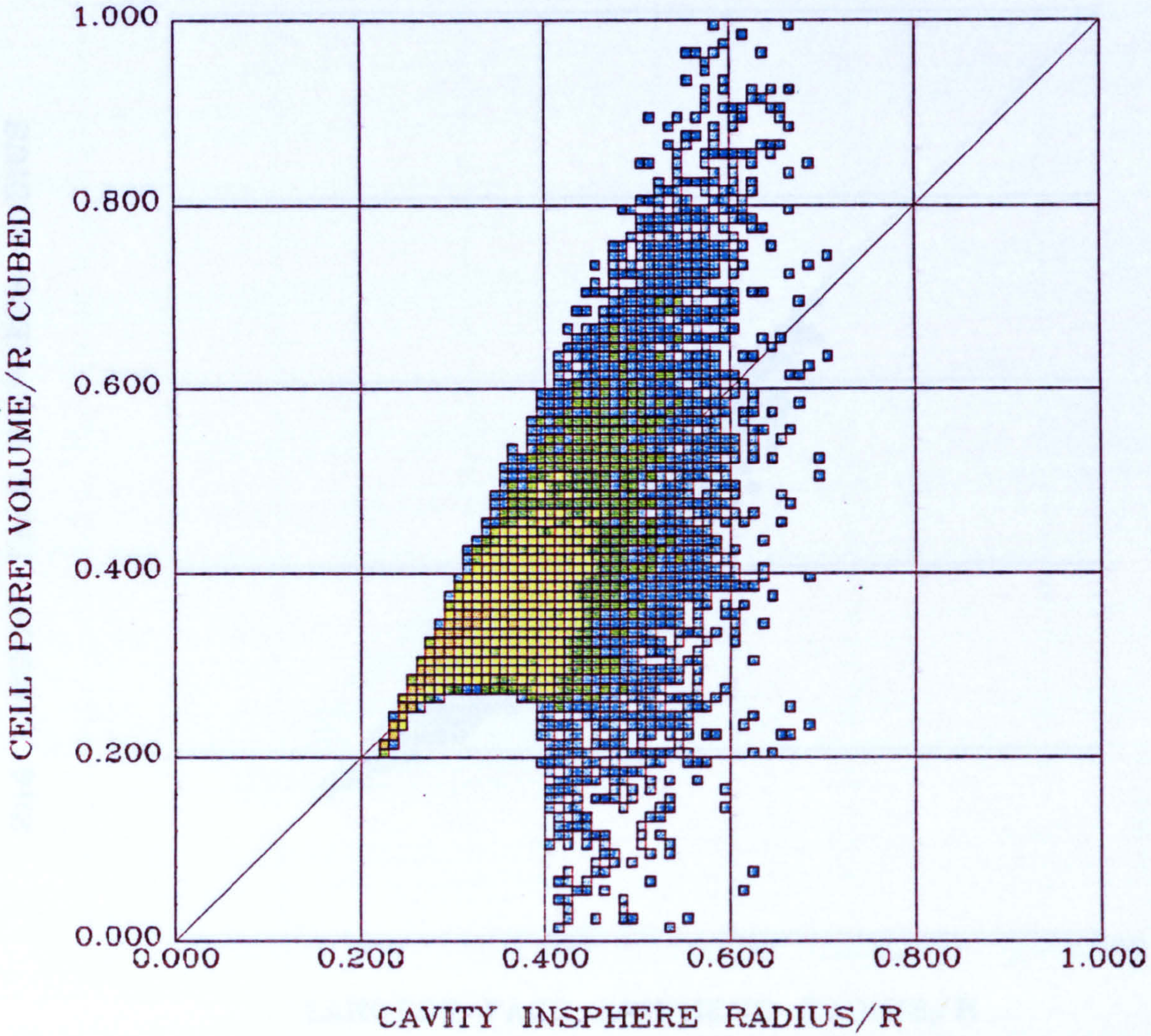

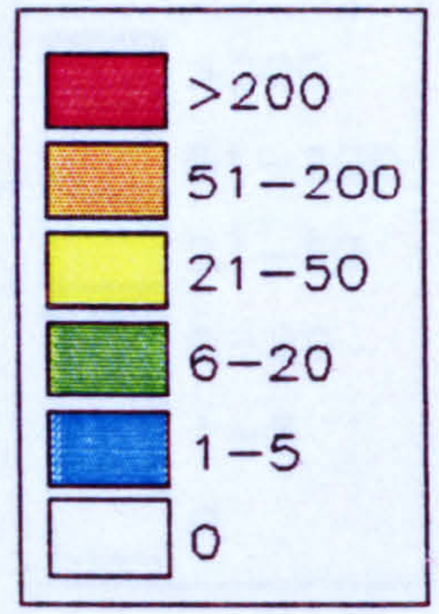

FIGURE 3·49

FINNEY MODEL

JOINT FREQUENCY DISTRIBUTION
CAVITY INSPHERE RADIUS/R
vs.
CELL PORE VOLUME/R CUBED

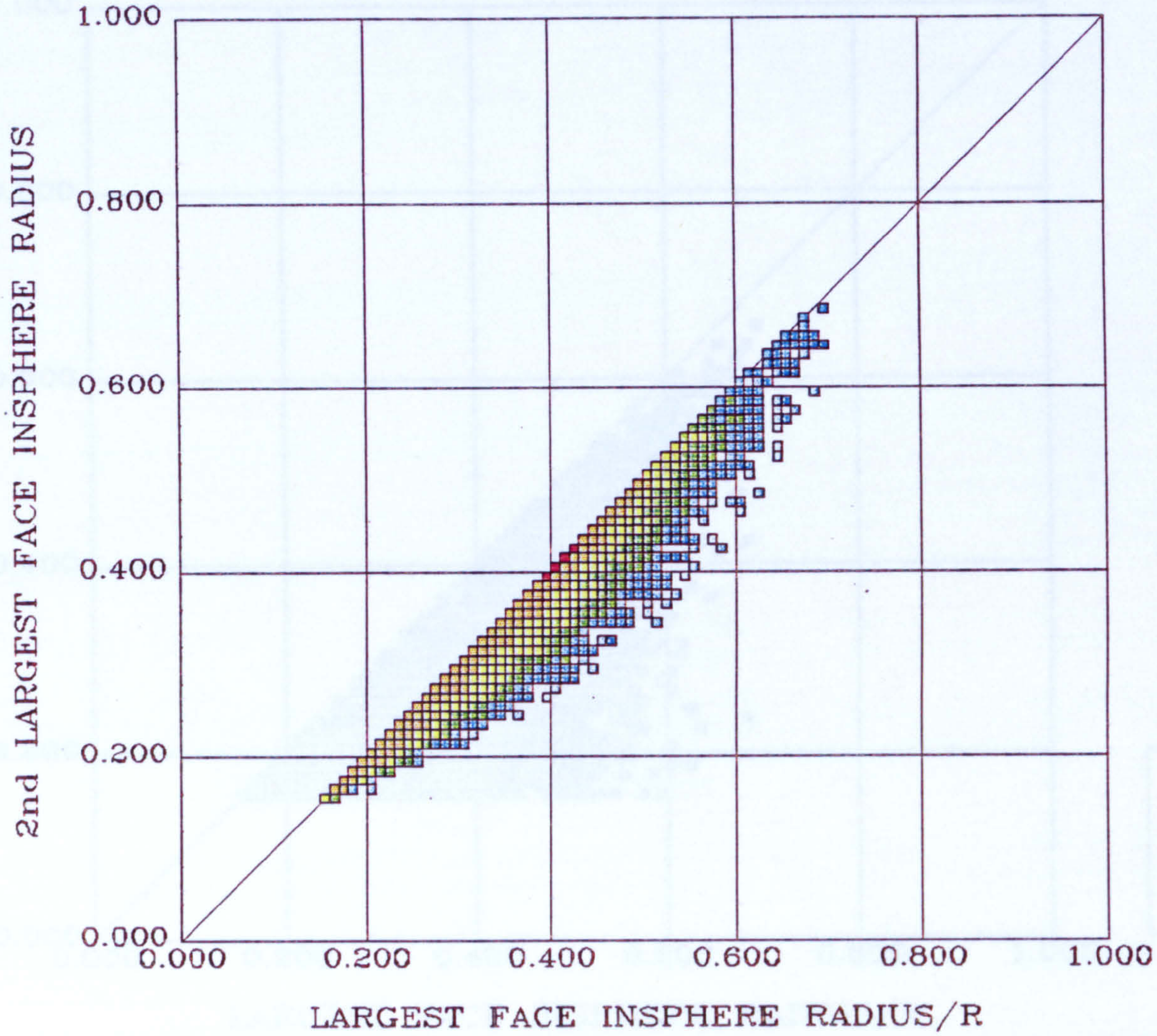

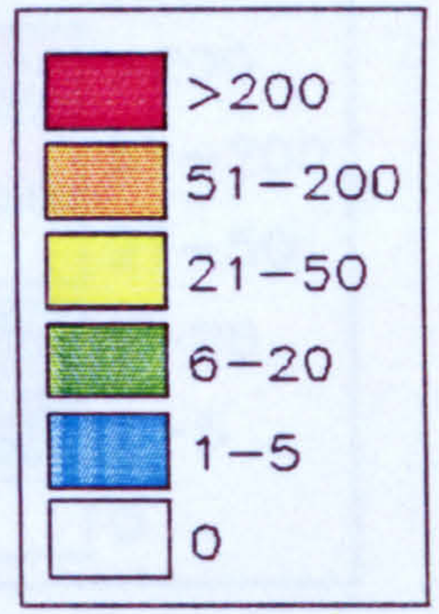

FIGURE 3·50

150.

FINNEY MODEL

JOINT FREQUENCY DISTRIBUTION

LARGEST FACE INSPHERE RADIUS/R

vs.

2nd LARGEST FACE INSPHERE RADIUS

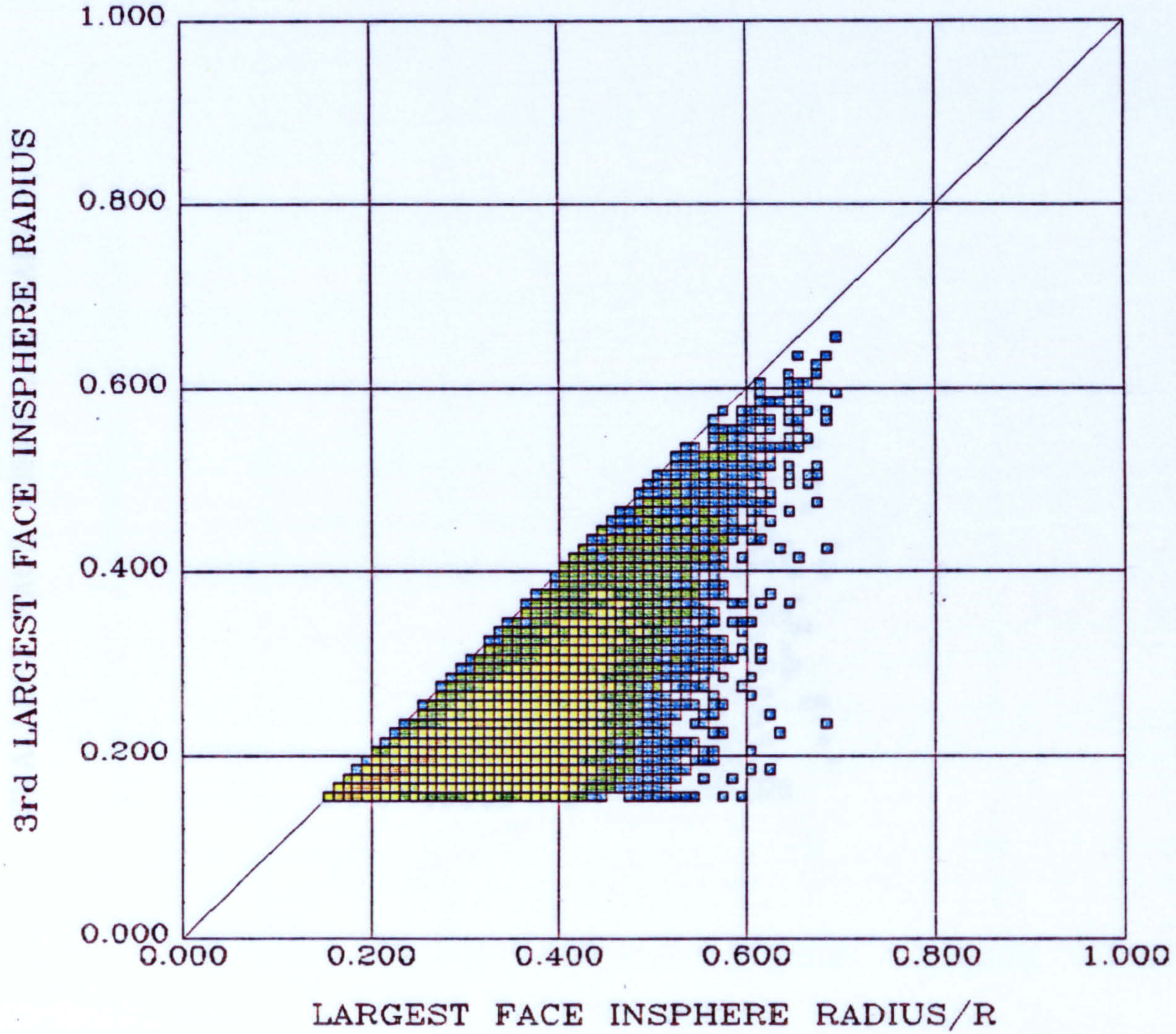

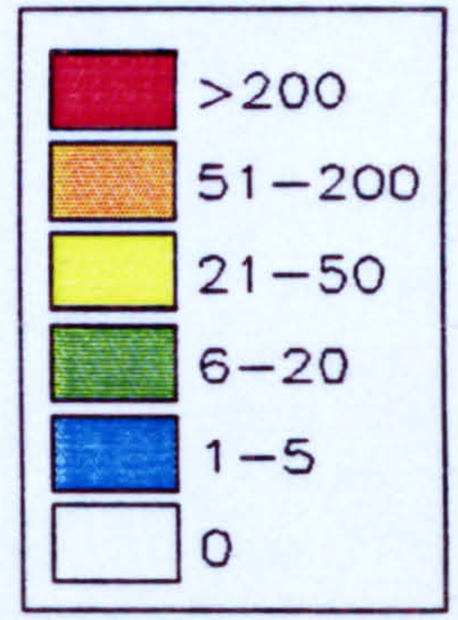

FIGURE **3-51**

FINNEY MODEL

JOINT FREQUENCY DISTRIBUTION

LARGEST FACE INSPHERE RADIUS/R

vs.

3rd LARGEST FACE INSPHERE RADIUS

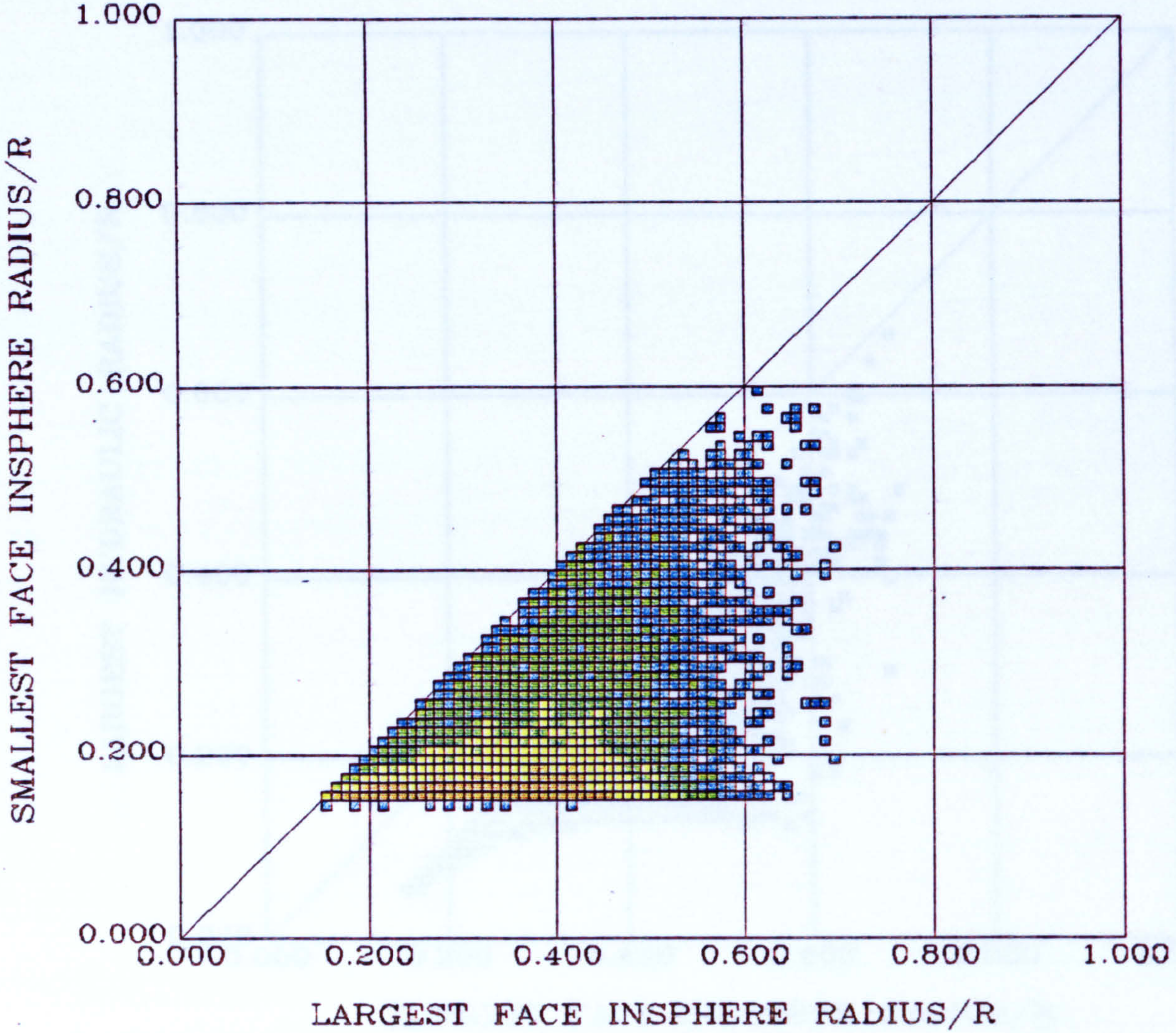

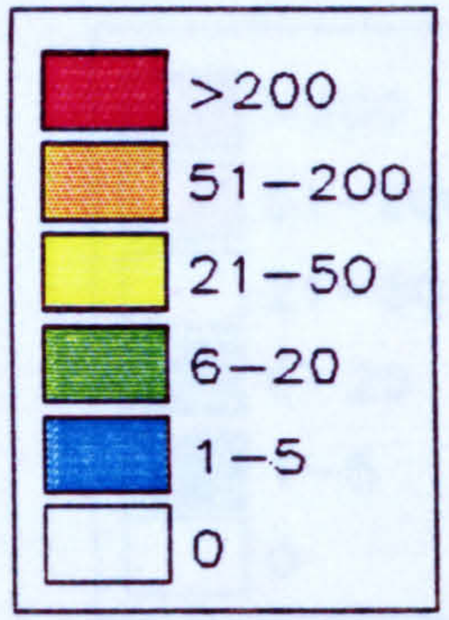

FIGURE 3·52

FINNEY MODEL

JOINT FREQUENCY DISTRIBUTION

LARGEST FACE INSPHERE RADIUS/R

vs.

SMALLEST FACE INSPHERE RADIUS/R

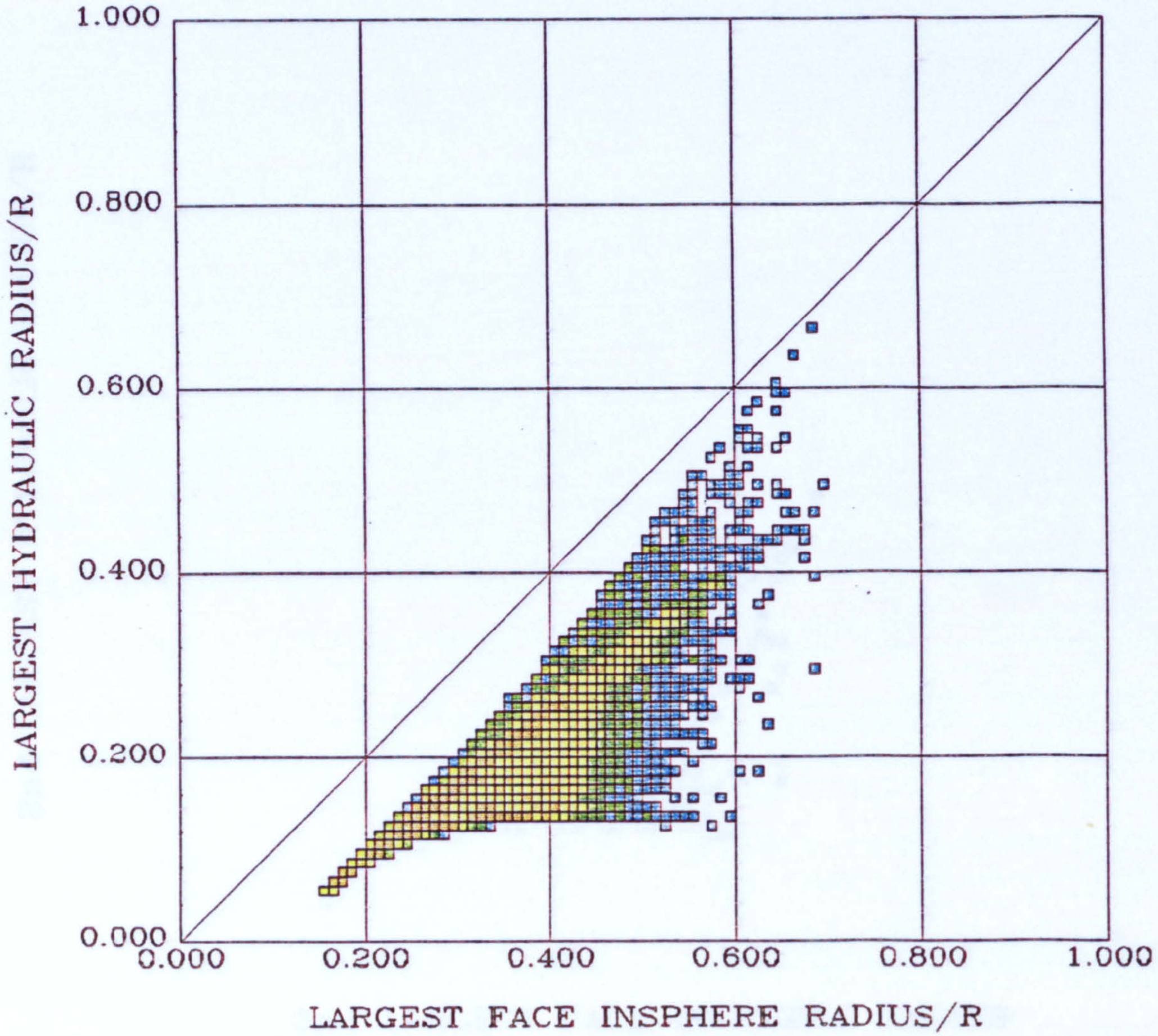

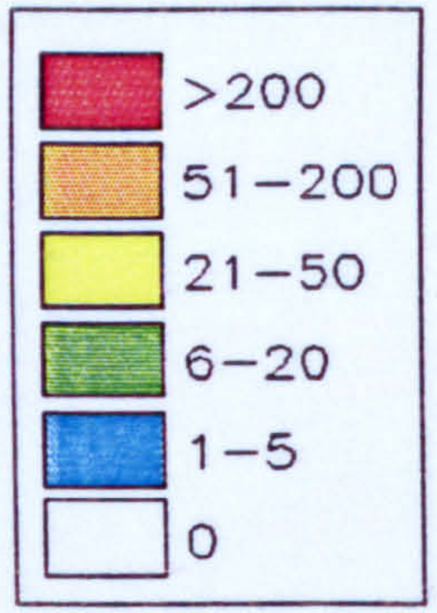

FIGURE 3-53

153.

FINNEY MODEL

JOINT FREQUENCY DISTRIBUTION

LARGEST FACE INSPHERE RADIUS/R

vs.

LARGEST HYDRAULIC RADIUS/R

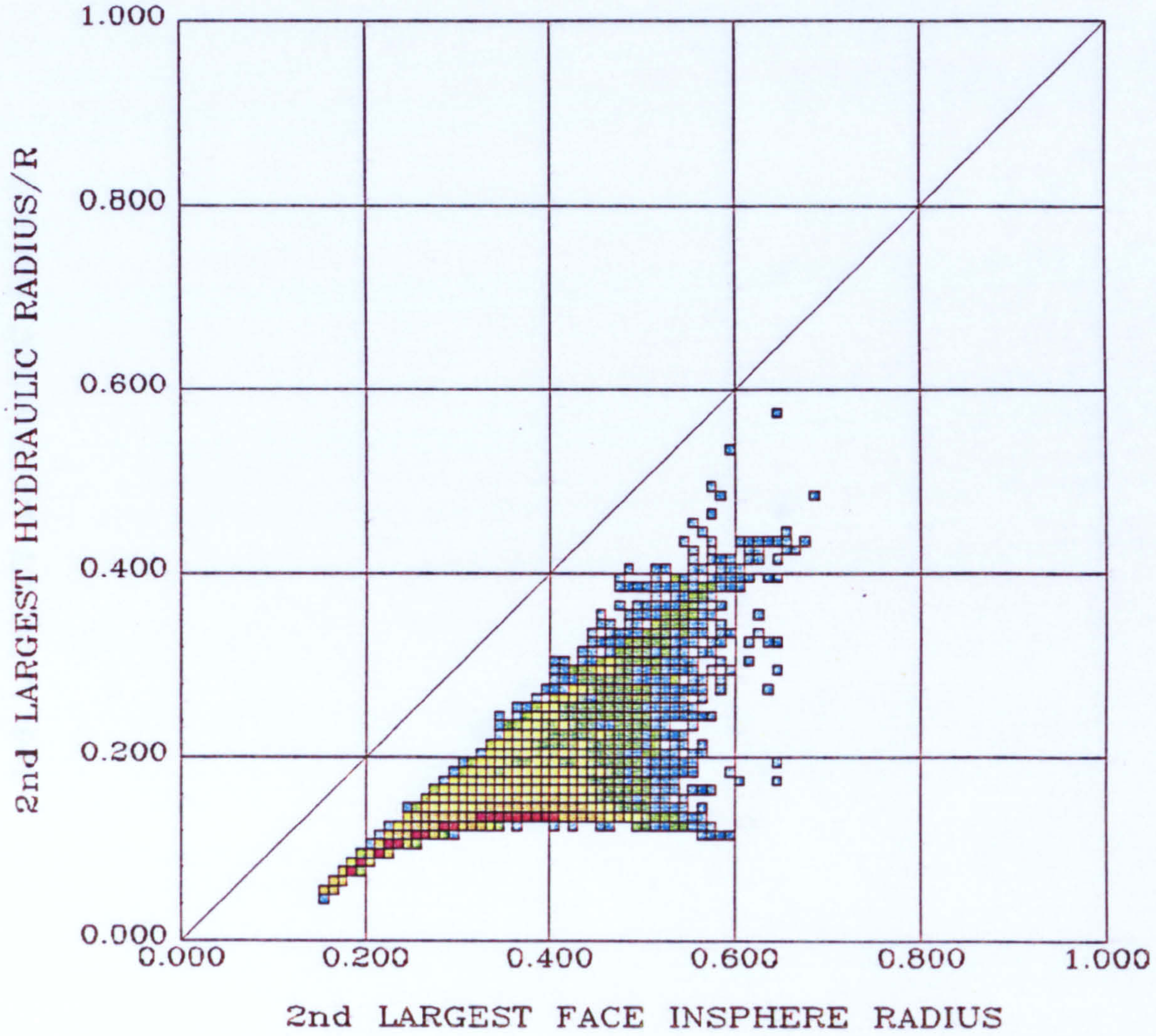

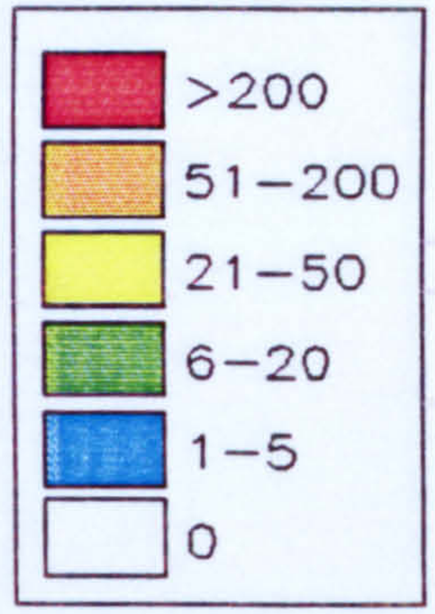

FIGURE 3·54

154.

FINNEY MODEL

JOINT FREQUENCY DISTRIBUTION

2nd LARGEST FACE INSPHERE RADIUS

vs.

2nd LARGEST HYDRAULIC RADIUS/R

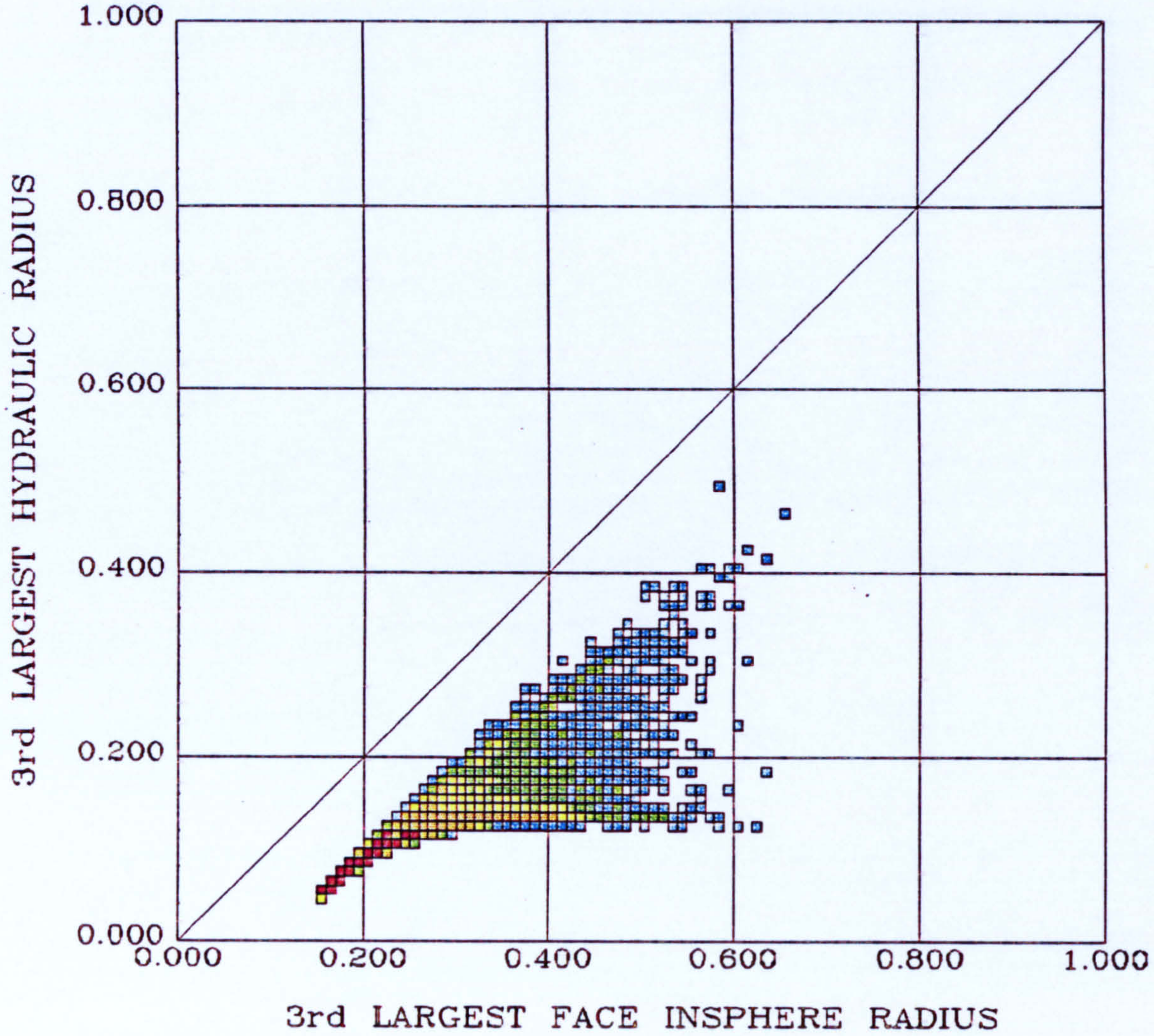

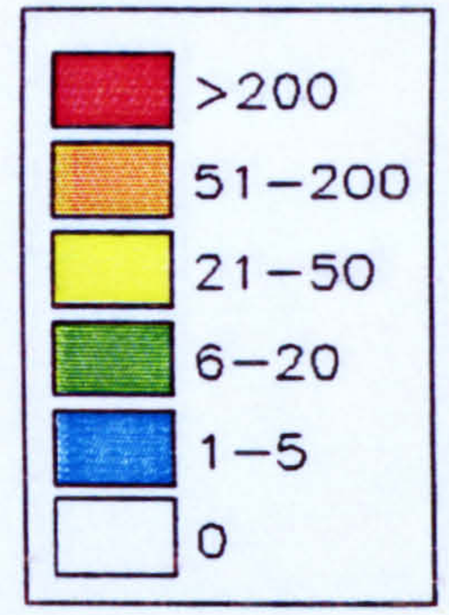

FIGURE 3·55

FINNEY MODEL

JOINT FREQUENCY DISTRIBUTION

3rd LARGEST FACE INSPHERE RADIUS

vs.

3rd LARGEST HYDRAULIC RADIUS

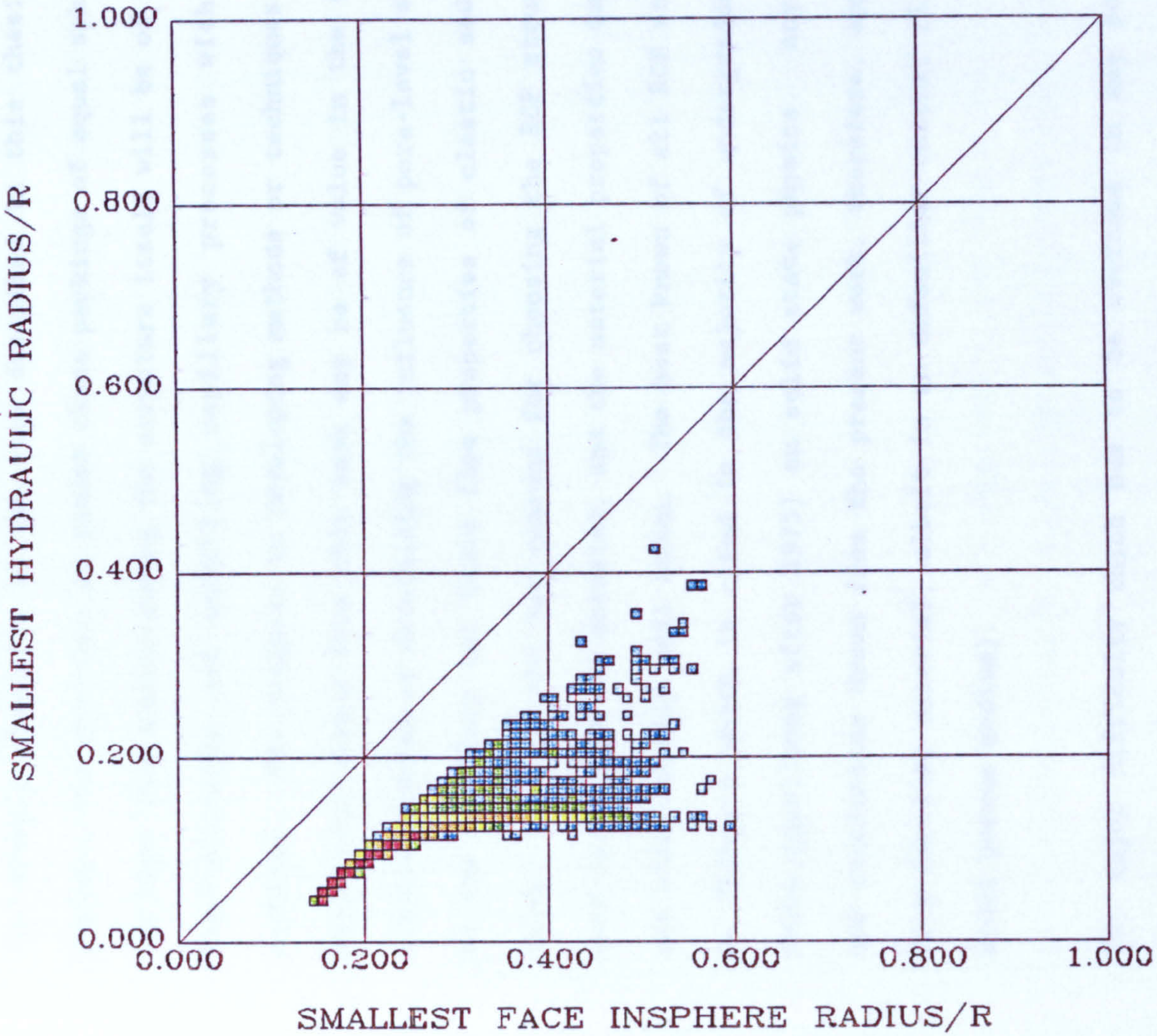

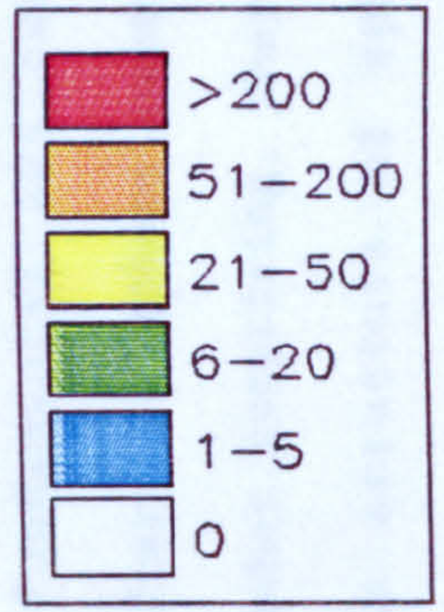

FIGURE 3·56

FINNEY MODEL

JOINT FREQUENCY DISTRIBUTION

SMALLEST FACE INSPHERE RADIUS/R

vs.

SMALLEST HYDRAULIC RADIUS/R

3.6 Summary and Discussion

The overall objective of the work described in this thesis is to evaluate the structure of random close packings of equal spheres, in the hope that understanding the structure itself will be of value in understanding and modelling capillary processes within such packings. Any progress in developing methods or techniques, or any major conclusions from this work may be of value in the far more complex problem of determining the influence of pore-level structure on the capillary and fluid flow properties of clastic sedimentary rocks. One of the key reasons for choosing the RCP structure to work on is that the material, and the material properties in general are exceptionally well known. The best known of all RCP structures is Finney's which is cited in the majority of undergraduate text books (published after 1975) on solid state physics. Any results and conclusions drawn from the present work, therefore, apply to a very familiar material, albeit in an unfamiliar context (i.e. as a model porous medium).

The major difficulty which has to be overcome in any pore-level structural analysis of a porous material is the definition of the pore itself. The simplicial cell embodies all of the essential requirements of a pore, as discussed in the preceding chapter, and is without doubt the most fundamental and cardinal spacial descriptor of RCP structure after the sphere centre co-ordinates themselves. It is perhaps somewhat surprising, therefore, that the extensive literature on the structure of sphere packings concentrates so heavily on the Voronoi discretisation of RCP space,

leaving the simplicial discretisation a largely unexplored area. This chapter of the present work, therefore, presents new results which have relevance both in the area of solid state physics (primarily an extension to the literature pertaining to the Finney model) and in the area of pore-level studies of porous media.

One of the most important stages in the work presented in this chapter is the verification of the simplicial cell discretisation, and the thorough estimation of errors. Although one discretisation error was detected, its overall effect on the subsequent analysis is negligible, representing one error in 14870. The experimental error in Finney's original work is evaluated within the context of a normally distributed error associated with a simplicial cell edgelength value. This error is found to be very small (± 0.002168 sphere diameters), and may be ignored for the most part in the subsequent simplicial cell analysis. The analytical results themselves are presented as a number of frequency distributions which show quite a wide variation in any given simplicial cell property. Individual cell edgelengths, for example, may be as low as 1.0 sphere diameters, or as high as 1.65 sphere diameters. Cell face angles may be slightly below 40 degrees through to just above 100 degrees. The variation in pore volume on an individual cell basis is large, ranging from just above 0.01 sphere radii cubed to almost 1.0 sphere radii cubed. The packing density varies from 0.35 to 0.78, and the cell porosity varies from 0.22 to 0.65, though there are long, thin tails to these distributions.

From the porous medium perspective, the most significant results are that the frequency distributions for cavity insphere radius, largest

and second largest face insphere radii are all quite similar. Investigating this correspondence further by using joint frequency distributions shows that, in general, there is a very high probability that an individual cell will have one or more face insphere radii either the same value as, or very close to, that of the cavity insphere radius for that cell. By using approximations for meniscus curvatures this suggests that drainage and imbibition pressures for individual cells considered in isolation are the same, or very nearly the same. An individual cell, therefore, is not likely to exhibit capillary pressure hysteresis. As far as sphere packings are concerned, this appears to rebut the (now rather old) independent domain theory whereby porous materials could be regarded as analogues of magnetic materials. Since magnetic hysteresis could successfully be ascribed to an individual and independent domain, it was thought that capillary pressure hysteresis also might be ultimately a property of the pore itself. This appears not to be the case for RCP structure, and the more thorough analysis presented in Chapter 6 confirms this view.

It is interesting to note that for the special case of a simplicial cell analysis of a monodisperse sphere packing, the hydraulic radius is simply the equivalent radius of constriction squared. For polydisperse systems, and for other analytical methods this simple relationship will not generally hold.

No straightforward or simple relationships between simplicial cell parameters thought to influence capillarity, and those thought to influence permeability could be found at the level of the individual pore. This may suggest that the way in which each individual cell

is "connected" to its neighbour is a dominant factor in understanding both bulk system capillarity and bulk system permeability. Because this chapter is specifically focussed on individual simplicial cell properties, it is not possible to infer very much about such connectivity issues, and these are dealt with in more detail in the subsequent chapters.

CHAPTER 4: RANDOMNESS AT THE SIMPLICIAL CELL LEVEL IN THE FINNEY MODEL

4.1 Introduction to Chapters 4 & 5

The term "random close packing" implies that randomness is an important feature of the packing itself. Randomness of what, however, is not altogether well defined in the literature, especially as there is no precise agreement or definition regarding the nature of random close packing itself (e.g. Gotoh and Finney 1974, Dodds 1980). What is meant conventionally by the term random when used to describe sphere packings is the disorder which makes it impossible to predict the spatial location of any sphere in the packing given only the co-ordinates of another sphere in the same packing. Interestingly, the amount, or nature, of disorder seems not to have been studied previously. One forms the impression from the literature that the question is naive, because the problem is intractable.

The subject of this thesis is the structure of random close packing. It therefore seems worthwhile to spend some effort examining randomness in the hope that some new insight or new information regarding RCP structure might emerge. More specifically, such a study of randomness has a direct bearing on two established problems:

(i) Mason (1971) developed a method for simulating individual simplicial cells which he used to represent the porespace of random close packing of equal spheres. The method assumes

that each of the six simplicial cell edgelengths occurs independently of the others in the cell - in other words the edgelengths may be selected randomly from an appropriate edgelength distribution function to form a cell. Although Mason's (1971) pore-level model of RCP has been used subsequently by several workers (e.g. Yadav and Mason, 1983; Smith, Gallegos and Stermer, 1987) the assumption of random edge length selection has not been rigorously tested prior to the present work.

(ii) The network which connects pores in a porous medium is important in theoretical studies of fluid transport within that network. Thus studies involving percolation theory and network modelling frequently involve the assumption that the distribution of size attributes of neighbouring pores is a random phenomenon. For example, in network modelling of porous media it is common to decorate randomly the chosen network with pore-size distribution parameters (see for instance Dullien, 1979; Lin and Slattery, 1981; Androutsopoulos and Mann, 1979; and reviews of the relevant literature in Ghabaee, 1986; Jerauld, 1985; and Heiba, 1985). This random decoration process means that the magnitude of a particular pore-size parameter for each cell is independent of the magnitude of the same pore-size parameter in immediately neighbouring cells. This assumption of random cell proximity has not been rigorously examined for any real porous medium prior to the present work.

In the present work the above two problems have been formalised as:

a. An analysis of randomness at the level of the <u>individual</u> simplicial cell. In this problem we are interested in attributes of randomness related to a dis-aggregated set of individual simplicial cells. These attributes yield information about the simplicial cells themselves, but tell us nothing directly about how they are connected together to fill space. This problem is addressed in this chapter.

b. An analysis of randomness at the level of the <u>network</u> which connects all simplicial cells together. Here we are interested not in the cells themselves, but the way in which they interact with each other as they fill space. This problem is dealt with in the next chapter.

<u>4.2 Some terminology and notation</u>

There is little or no literature pertaining to the definition and measurement of randomness in RCP structure specific to simplicial cells. Some terminology and notation is therefore proposed in order to develop the ideas presented in this thesis. The extent of this terminology and notation is intentionally kept to a minimum, and includes the following elements:

(i) Descriptive elements (which type of cells are we dealing with?)

(ii) Definition of randomness,

(iii) Predictive elements (how many cells of each type do we expect?)

4.2.1 Descriptive Elements

The three dimensional simplicial cell is always a tetrahedron, and always has precisely six edges. The length of an individual edge is used in the present work to form the basis of a notation, or classification system. Suppose the edgelength values for an individual cell are X_1, X_2, X_3 ....X_6. The individual values for all edges in the group of N individual cells are X_1, X_2, X_3....X_{6N}. A threshold value, X_T, is selected arbitrarily such that some edgelengths in the group are greater than X_T, whilst others in the group are less than X_T. The threshold value X_T, therefore defines two mutually exclusive groups, or states, to which an edgelength can belong. These states are conveniently identified as L (for Long) and S (for Short):

Condition for state 'S' is $X_i \leq X_T$

Condition for state 'L' is $X_i > X_T$.

For a group of N individual simplicial cells, the fraction of all edges occurring in state S is s, whilst the fraction of all edges occurring in state L is l.

$$\text{i.e. } (s + l) = 1.0 \qquad \text{-4.1-}$$

Total number of edges in group = 6N

Number of state 'S' edges = 6sN

Number of state 'L' edges = 6lN

Because we have identified two mutually exclusive states for all edgelengths in the group, each simplicial cell can exist as one of only seven possible combinations of states. For example, a simplicial cell might have all six edges corresponding to state 'L', with no edges corresponding to state 'S'. At the other extreme, another cell might have all six edges in state 'S', with no state 'L' edges. There are only five intermediate states, or cell classes, between these two extremes, as summarised in table 4.1.

Simplicial cell class description	Simplicial cell notation
0 long edges, 6 short edges	0LS6
1 long edge, 5 short edges	1LS5
2 long edges, 4 short edges	2LS4
3 long edges, 3 short edges	3LS3
4 long edges, 2 short edges	4LS2
5 long edges, 1 short edge	5LS1
6 long edges, 0 short edges	6LS0

Table 4.1 : Description of simplicial cell classes and notation adopted in the present work.

4.2.2 Definition of Randomness

Imagine a group of discrete three dimensional simplicial cells. Let there be a cell edgelength probability distribution function for this imaginary group. For each individual cell in the group there are six edgelengths, each of which has a discrete probability of occurrence. The definition of randomness adopted in the present

work is that these six discrete probabilities are independent of each other, and are determined only by the edgelength probability distribution function for the entire group.

In practical terms, a real sphere packing does not have a known simplicial cell edgelength probability distribution function. It is, however, possible to measure the simplicial cell edgelength frequency distribution function, as shown in figures 3.15 and 3.16 for the Finney RCP model. The theoretical definition of randomness based on an unknown probability distribution function may therefore be transformed into a practical definition based on an observed frequency distribution:-

"For an <u>individual</u> simplicial cell, the lengths of the six component edges are determined solely by the edgelength frequency distribution for the group of cells to which the individual cell belongs". This definition can be tested rigorously using a statistical approach, by comparing expected frequencies of cell classes with observed frequencies of cell classes for the Finney model. This comparison is analogous to a simple statistical test for a fair die (i.e. a random die) based on a large number of throws, in which the expected frequencies of ones, twos, threes etc, are compared with observed frequencies.

4.2.3 Predictive elements

Using the definition of randomness given above, it is straightforward to predict the frequencies with which each of he seven simplicial cell classes is expected. A cell requires six edges, so:

$$(1 + s)^6 = 1 \qquad \text{-4.2-}$$

- expanding this polynomial gives the seven terms:

$$E_0 + E_1 + E_2 + \ldots\ldots\ldots E_6 = 1 \qquad \text{-4.3-}$$

where E_i is the expected frequency of occurrence of a simplicial cell with (6-i) edges in state 'S' for a given value of s. The numerical values of these probabilities may be calculated as shown in table 4.2.

Class notation	Expected fractional frequency of occurrence in random group	Polynomial term (eqn. 4.3)
0LS6	s^6	E_0
1LS5	$6s^5 1$	E_1
2LS4	$15s^4 1^2$	E_2
3LS3	$20s^3 1^3$	E_3
4LS2	$15s^2 1^4$	E_4
5LS1	$6s1^5$	E_5
6LS0	1^6	E_6

s fraction of edgelengths $\leqslant$ threshold value x_T
1 1.0-s

Table 4.2 : Expected random fractional frequencies of occurrence of simplicial cell classes.

The expected frequencies are calculated for a real group of N simplicial cells by establishing s, which is the fraction of all edgelengths X_1, X_2, X_3.....X_{6N} in the group which satisfy the condition $X_1 \leq X_T$. The significance of X_T will be considered shortly.

4.2.4 Worked example

In Chapter 2 the tetrakaidecahedron was used to illustrate the relationship of the Voronoi cell to the body cubic centred (BCC) lattice. In the following worked example, the tetrakaidecahedron is used again, this time to demonstrate the method of establishing whether or not an assemblage of simplicial cells is random, when the only information available is the edgelength values for the simplicial cells and the observed distribution of simplicial cell classes. Of course in this worked example we know the outcome - the idealised BCC lattice is perfectly non-random. The test for randomness in this worked example must therefore be failed.

The body-centred atom of a cubic segment of the BCC lattice has, as its nearest neighbour atoms, eight "corner" atoms and six adjacent body centred atoms as shown in figure 4.1(a). Using the novel theorem given in Chapter 2, the number of component simplicial cells for the tetrakaidecahedron must be twenty four:

$2N-T = 4$ -2.7-

Where N = number of geometric neighbour atoms to the body centred atom (N = 14 for the BCC lattice), and T = the number of component tetrahedral simplicial cells.

Figure 4.1 : Simplicial cells of the body centred cubic lattice.

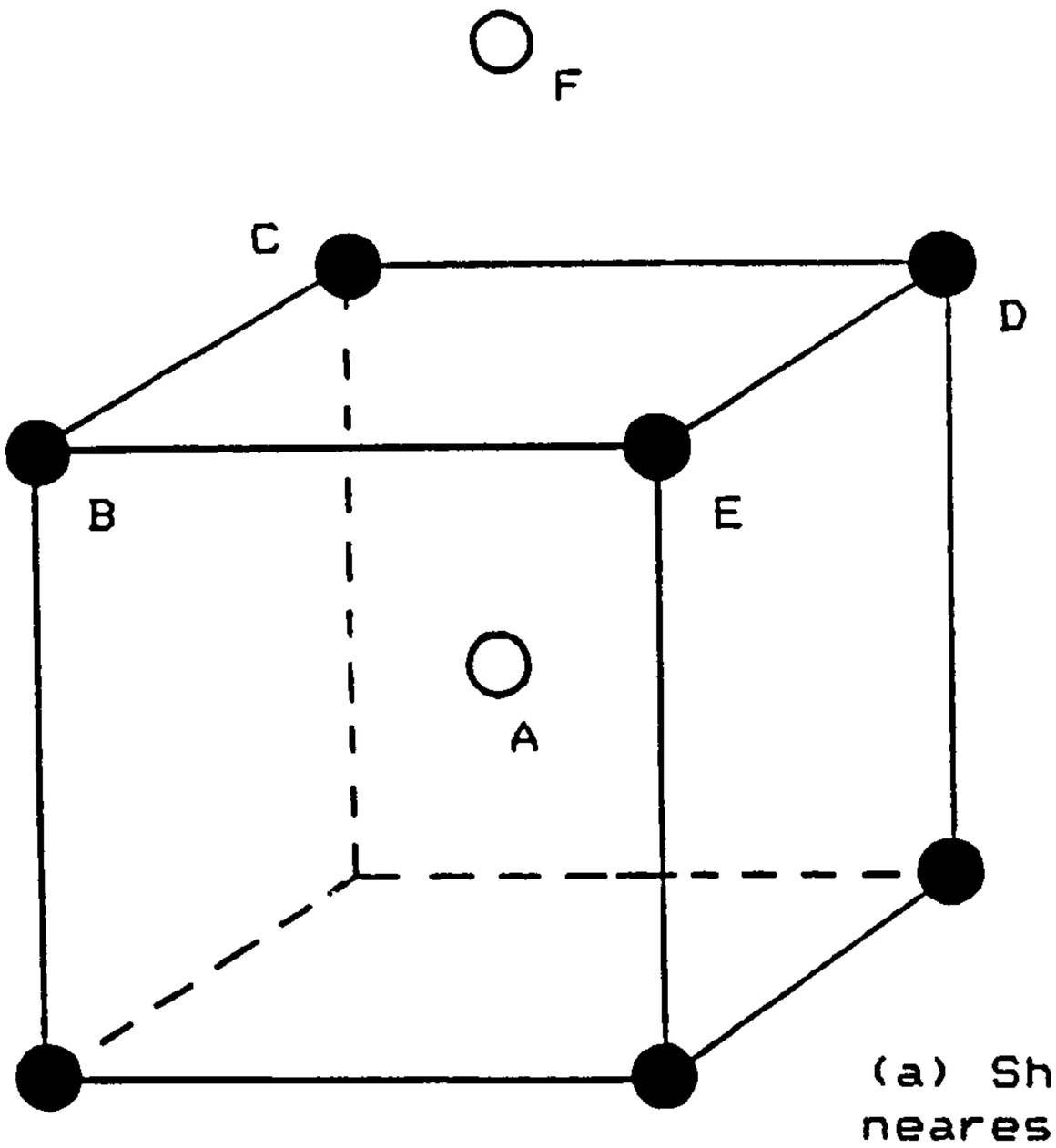

(a) Showing the 8 corner atom nearest neighbours to atom 'A' together with one of 6 adjacent body centred atoms, 'F'.

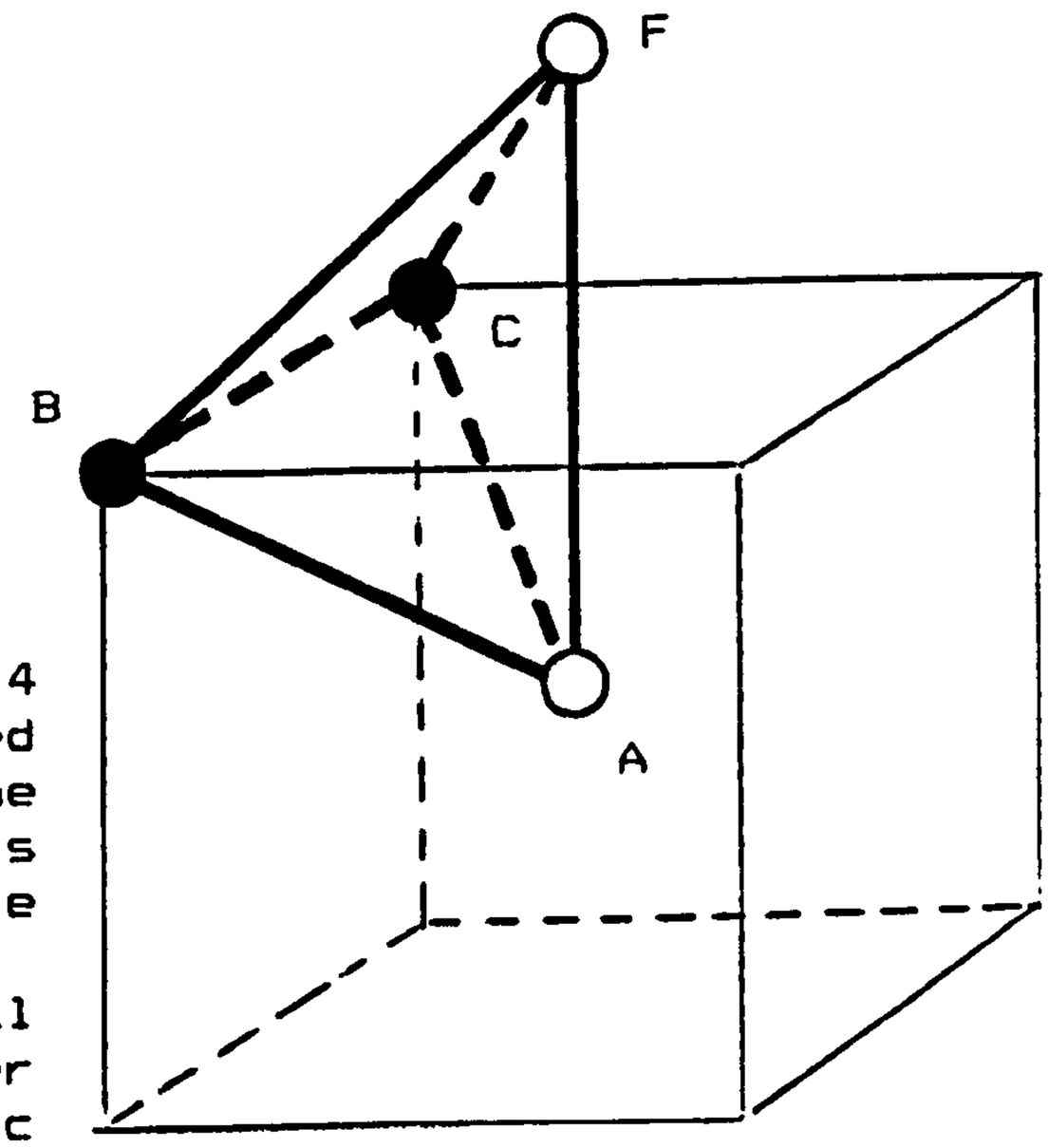

(b) Showing one of the 4 simplicial cells ABCF defined by the cube-face B-C-D-E. The remaining 3 simplicial cells defined by this face are A-C-D-F, A-D-E-F & A-B-E-F. Since there are 6 identical cube faces, the total number of simplicial cells specific to atom 'A' is 6 x 4 = 24.

Figure 4.1(b) shows one of these twenty four simplicial cells, and from inspection of this figure it is clear that all twenty four cells are identical geometrically. If we let the cube edge equal one arbitrary length unit, then the six edgelength values in the simplicial cell must be as shown in table 4.3:

Simplicial cell edge	Edgelength value
A-B	0.866
A-C	0.866
A-F	1.0
B-C	1.0
B-F	0.866
C-F	0.866

Table 4.3 : Edgelength values for the simplicial cell shown in figure 4.1(b). The cube edgelength is unity.

From table 4.3 it is evident that the discrete simplicial cell edgelength frequency distribution for an infinite, perfect BCC lattice comprises edgelengths of 0.866 at a frequency of 0.6667, and edgelengths of 1.0 at a frequency of 0.3333. Such a perfectly bimodal distribution of simplicial cell edgelength values strongly suggests that the BCC lattice is not random - however, of itself the edgelength distribution function alone is not proof that the BCC lattice is non-random. If we select an arbitrary threshold value, X_T, such that $0.866<X_T<1.0$, then we can compare the expected frequency (E_i) of occurrence of the seven simplicial cell types with the actual, or "observed" frequency (O_i) of simplicial cell types, as shown in table 4.4:

Simplicial cell class	Expected frequency in random group	Expected* frequency in 24 cells (E_i)	Actual frequency for BCC (O_i)
0LS6	S	2	0
1LS5	$6s^5 1$	6	0
2LS4	$15s^4 1^2$	8	24
3LS3	$20s^3 1^3$	5	0
4LS2	$15\ s^2 1^4$	2	0
5LS1	$6s1^5$	1	0
6LS0	1^6	0	0

$s=0.6667$ for $0.886<X_T<1.0$

* - rounded to nearest integer

Table 4.4 : Expected frequencies (E_i) of simplicial cells in a random group compared with actual frequencies (O_i) for the simplicial cells of the BCC lattice.

From table 4.4 it is clear that the observed frequencies of simplicial cell types for the BCC lattice are not those expected from a group of random simplicial cells with the BCC simplicial cell edgelength frequency distribution.

The chi-squared statistic may be used as a measure of how far observed (O_i) and expected (E_i) frequencies differ:

$$\text{i.e. } \chi^2 = \Sigma\left[\frac{(O_i - E_i)^2}{E_i}\right] \qquad \text{-4.4-}$$

For the example given in table 4.4, the value of chi-squared for the

24 simplicial cells of the tetrakaidecahedral Voronoi cell for the BCC lattice is 48.

There is only one restriction in calculating the expected frequencies, which is that they must have the same total as the observed frequencies. The number of degrees of freedom 'ν' is therefore six:-

ν = Number of classes minus number of restrictions

$\nu = 7 - 1 = 6$.

We are now in a position to address specific statistical questions. For example, at the 5% level of significance, do the results presented in table 4.4 indicate that the simplicial cells are random according to the definition presented in section 4.2.2? From published tables, the value of chi-squared corresponding to $\nu = 6$ at the 5% level is $\chi^2_{.05} = 12.59$. Since the calculated value of χ^2 in our worked example at 48 exceeds this, the result is significant and the hypothesis of random simplicial cells has to be rejected. For $\nu = 6$, a value of $\chi^2 = 48$ corresponds with a probability of $\ll 0.001$ that the results presented in table 4.4 could be obtained if the simplicial cells were random. Increasing the number of simplicial cells in the example from 24 results in a linear increase in chi-squared, as shown in figure 4.2, with a corresponding linear decrease from $\ll 0.001$ of the probability that the simplicial cells are random as defined in section 4.2.2. The test has worked - the simplicial cells of the BCC lattice are not random according to the definition given in section 4.2.2.

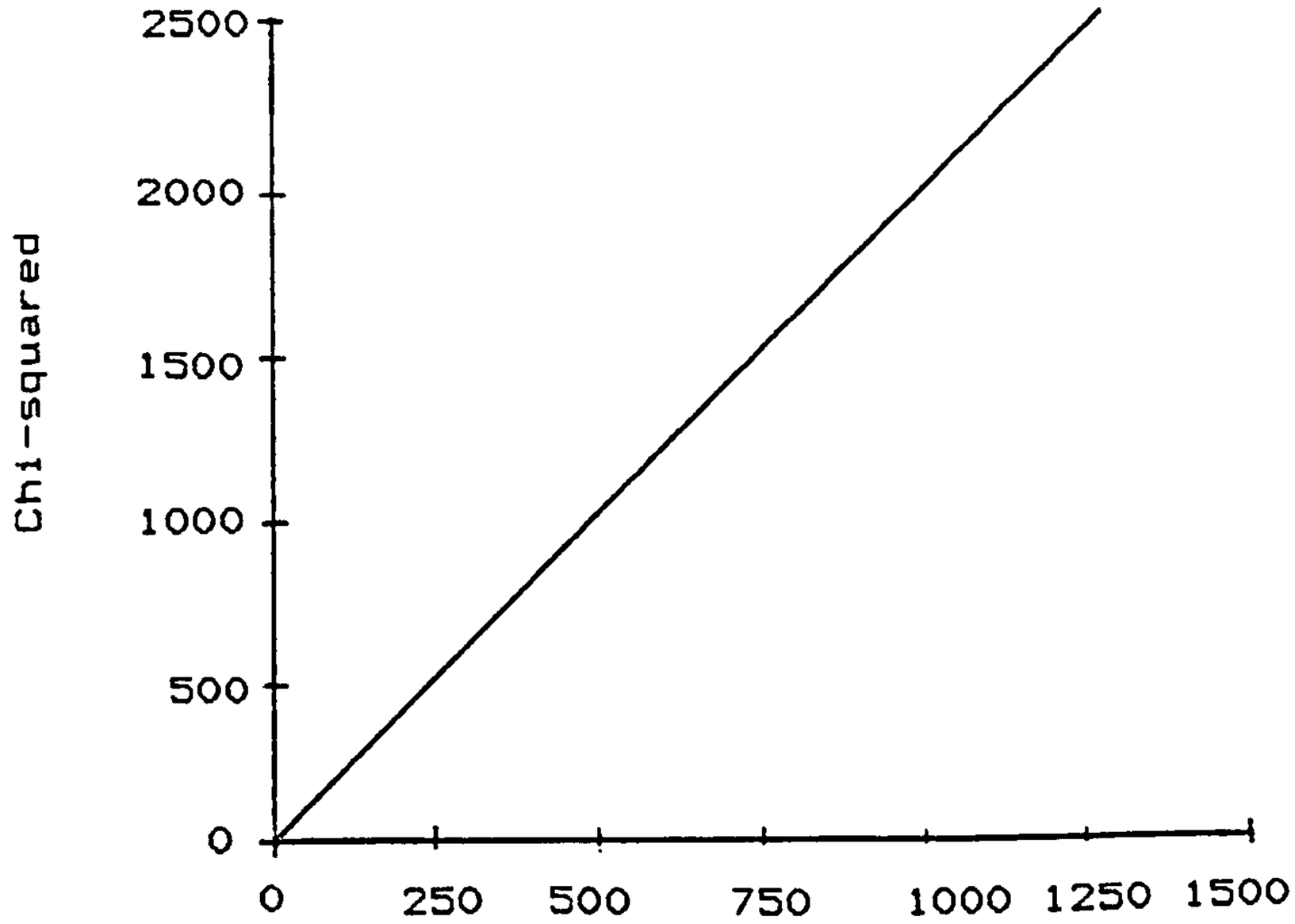

Figure 4.2 : Relationship between number of simplicial cells and chi-squared for simplicial cells of a perfect BCC lattice.

4.3 The Control Set

The concept of a control group, or set, is a well established experimental procedure in many scientific fields. The same concept may be used, with slight modification, in the present work. The control set, therefore, consists of a number of simplicial cells which have been simulated (as distinct from those observed by measurements of sphere centre co-ordinates) so that certain conditions have been fulfilled. These conditions are:

(i) The edgelength distribution function for the simplicial cell control set is identical, or virtually identical with the edgelength distribution function for the 14870 real simplicial cells of the Finney model.

(ii) All simplicial cells in the control set are generated from the real edgelength distribution function for the 14870 real simplicial cells of the Finney model using a randomising procedure. The definition of randomness given in section 4.2.2 is therefore adhered to.

Superficially, the procedure for generating an individual random simplicial cell of the control set appears to be trivial, and comprises the following four key sequences:

(i) All 89220 edgelength values of the 14870 simplicial cells of the Finney packing are read into an array, X().

(ii) A random number, Z, in the interval [1,89220] is generated.

(iii) The random number, Z, gives one edgelength value to the random simplicial cell, identical to X(Z).

(iv) Steps (ii) and (iii) are repeated a further 5 times to give a total of six edgelength values.

Leaving aside for one moment the issue of random number generation (this is dealt with in section 4.3.3), there is a fundamental problem with the above procedure which is not immediately obvious,

but which sheds considerable light on the nature of RCP simplicial cell randomness. This fundamental problem is that the procedural steps (i) to (iv) above will always give six random edgelength values, but there is no guarantee that these six edgelength values can form a three dimensional tetrahedron. This problem is referred to in the present work as the problem of existence, and is now considered in more detail.

4.3.1 Existence

Consider a perfectly regular unit edgelength tetrahedron in which one of the six edges is allowed to increase in length whilst the other five edges remain fixed in length. At some point the tetrahedron will be pushed flat into two dimensions, and cease to exist as a three dimensional structure. The point of collapse is easily calculated from simple trigonometry, and as shown in figure 4.3 this point is reached when the variable edgelength value reaches 1.73205 (or $\sqrt{3}$).

Since no edgelength value in the simplicial cell edgelength frequency distribution for the Finney model exceeds 1.7 sphere diameters, the exact point of collapse illustrated in figure 4.3 can never be reached by any simplicial cell in the control set. If, however, we now allow <u>two</u> of the six edges to increase in length whilst the other four remain constant, we reduce the edgelength threshold for collapse from 1.73205 (i.e. $\sqrt{3}$) to 1.4142 (or $\sqrt{2}$) as illustrated in figure 4.4.

There are 3977 edges above $\sqrt{2}$ in length in the 89220 edges of the 14870 simplicial cells of the Finney packing. It follows,

Figure 4.3 : The 'expanded' regular tetrahedron ABCD at the point of collapse as a 3-D structure when the following condition is met :

Length AB = AD = BC = BD = DC = 1.0
& Length AC is incremented >1.0

$$AX = \sqrt{AD^2 - XD^2}$$

$$AC = 2AX = \sqrt{3}$$

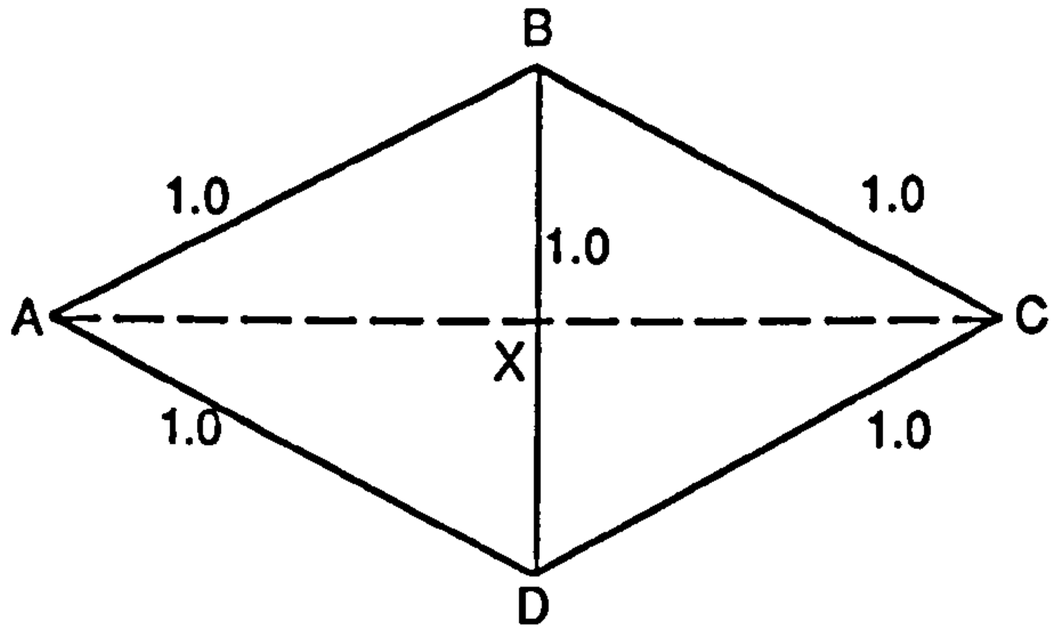

Figure 4.4 : The 'expanded' regular tetrahedron ABCD at the point of collapse as a 3-D structure when the following condition is met:

Length AB = AD = BC = DC = 1.0
& Lengths AC and BD are incremented >1.0
such that AC = BD

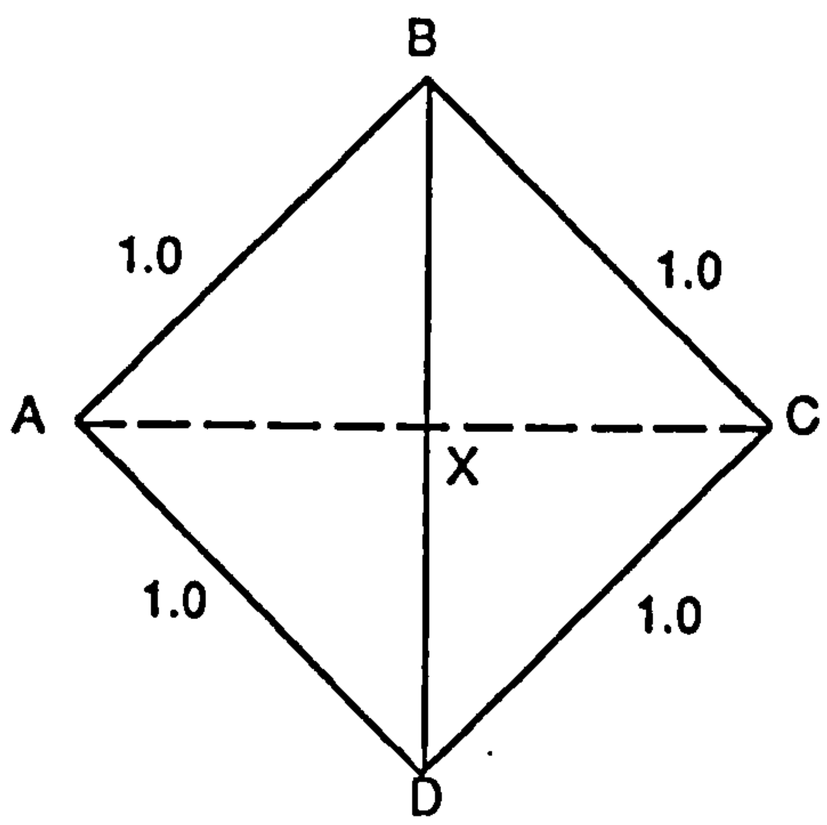

Since AC = BD,
max. value of AC is $\sqrt{2}$

ie. $\sqrt{AX^2 + BX^2} = 1$

$$\sqrt{2AX^2} = 1$$

$$\sqrt{2} \cdot AX = 1$$

$$AX = 1/\sqrt{2}$$

$$AC = BD = \sqrt{2}$$

therefore, that in generating the control set by following steps (i) to (iv) discussed earlier, there is a positive finite probability that "impossible" simplicial cells will be generated in the control set. In generating the control set, therefore a test for existence is required in order to prevent the cell generation procedure from producing cells which cannot physically exist in three dimensions.

Although the arguments developed here apply to the control set, we can begin to be a little suspicious of the real simplicial cells which go to make up the real Finney RCP model. Specifically, our suspicion is that, if we select a threshold value of $X_T = 1.0$, then we will observe a certain number of 2LS4 simplicial cells in the Finney packing. Since there are 3977 edges greater than $\sqrt{2}$ "available" to form the 'L' state edges, random chance demands that there is a finite positive probability that "impossible" simplicial cells ought to be formed - the RCP structure, however is forced to avoid forming these "impossible" cells, and so cannot, by definition, be considered to be perfectly random. This inferred departure from randomness is discused in further detail in section 4.3.4.

4.3.2 Test for existence

The purpose of the test for existence is simply to screen out those "impossible" simplicial cell structures generated by random chance in the process of creating the control set. Although each individual cell in the control set is created by random chance, the edgelengths retain the fixed positional sequence given by the standard tetrahedron geometry shown in figure 3.3. Even though the edgelength values themselves are generated at random, this fixed

positional sequence must be preserved in the test for existence. The test begins by selecting one of the six edgelengths as the initial test criterion. The remaining five edges form two triangles which share one edge in common. This hinged-pair of triangles is then considered to be laid flat, so that both triangles are in the same plane. The distance between the two triangle apices not associated with the common edge must be greater than the edgelength selected as the test criterion. If the tetrahedron fails this test, it is rejected as "impossible". If it passes the test, it is not yet accepted as "possible", since any of the five remaining edges may exceed this inter-apex distance. The test is therefore repeated a total of six times per tetrahedron in order to test all six inter-apex distances. Only when all six tests have given a positive result is a tetrahedron accepted as possible.

The subroutine which performs the test for existence is called EXIS. The listing for this routine is presented in Appendix 'B' of the present work. One of the functions of routine EXIS is to count the number of simplicial cells which were rejected on the basis of having no three dimensional validity. This rejection frequency is discussed in more detail in section 4.3.4.

4.3.3 Random Number Generator: AS 183

The VAX computer used for the present work supports a pseudo-random number generator. However, there is little in the way of documentation for the VAX generator, and no thorough tests of the code used in the generator have been reported in the literature. The possibility exists, therefore, that the VAX psuedo-random number generator is prone to some unknown statistical defect which may manifest itself in use. Furthermore, the same pseudo-random number

generator code may not be available to other researchers. Therefore, in order to avoid using a relatively unproven code, and to avoid using a code which may not be available to other research groups, the pseudo-random number generator known as AS 183 developed by the National Physical Laboratory was used. The algorithm for this code was written by Wichmann and Hill (1982 (i) and (ii)) and consists of three generators of the single multiplicative congruential type.

Initially, it was claimed (Wichmann and Hill, 1982 (i) and (ii)) that the cycle length of the generator is 2.78×10^{13}, so that continually calling the generator 1000 times per second results in no repeat sequences for over 880 years. However, subsequently this claim was revised downwards to a cycle length of 6.95×10^{12}, (Wichmmann and Hill, 1984). Nevertheless the cycle length is still impressive, though Wichmann and Hill did acknowledge that this reduced cycle length is due to the three sub-generators not operating completely independently of each other as was first thought. A further minor problem with Wichmann and Hill's function was highlighted by McLeod (1985) who showed that, depending on the machine used, some zero values may be produced owing to machine rounding error. In tests conducted by McLeod a sequence of 10^9 pseudorandom numbers was found to contain 364 values exactly equal to 0.0, whilst the remainder fell in the open interval (0, 1) as required. McLeod provides an additional algorithm which can be "bolted-on" to the Wichmann and Hills' generator to eliminate 0.0 numbers without otherwise altering the performance of the original generator. This McLeod modification has been included in the present work.

Perhaps somewhat of an aside, Zeisel (1986) was able to show that the Wichmann and Hill generator is little more than a method to implement a single multiplicative congruential generator with a cycle length greater than the maximal integer. Zeisel goes on the invoke the Chinese Remainder Theorem to prove that the same results can be achieved using only one multiplicative congruential generator. However, he does concede that Wichmann and Hill's original algorithm is still necessary to make a generator with such lengthy constants required by Zeisel's alternative.

In terms of using a random number generator to simulate "random" simplicial cells for the control set, the cells themselves are produced by calling random numbers in sequences of six. Each of the six random numbers is then used to select edgelength values from a list. The geometrical properties of the cell are dictated not only by the values of the edgelengths, but also by the sequence in which the edges are put together. For any practical algorithm this sequence must remain constant; therefore any significant non-randomness in the generation of sequential doubles, triples or quadruples by the generator might result in statistical "defects" in the cells generated. Wichmann and Hill's algorithm, AS 183, has been very exhaustively tested for precisely these conditions (e.g. Wichmann and Hill, 1982 (ii)). In the years following publication of AS 183, the literature contains no criticisms of, or references to statistical defects pertaining to either sequencing or to rectilinear distribution (excluding McLeod's remarks about the open interval 0,1 occurrences of 0) for AS 183. Accordingly, algorithm AS 183 is coded up in FORTRAN in program WANDOM. This program is documented and listed in Appendix 'B'.

4.3.4 Construction of the Control Set

The data file FINEDGE.DAT is, in effect, a list of 89220 sequenced edgelength values for 14870 simplicial cells of the Finney model. As such, it may be regarded as a sample (a frequency distribution) of a larger RCP model. In generating the control set we have to use this sample to fulfil the role of a population (a probability distribution). Therefore, in selecting edgelengths at random from the population it is important not to constrain the selection of edgelength values by using each edgelength value in the population only once. In practical computing terms this is an advantage, since it permits a very large control set to be created, whilst still preserving a control set edgelength frequency distribution which is virtually identical to that of the original Finney edgelength frequency distribution.

The procedure used to generate the control set is shown in figure 4.5 as a flow diagram, and is essentially that of steps (i) to (iv) outlined at the beginning of section 4.3. The procedure outlined in figure 4.5 is coded up into program CONTROL, which writes the control set as an output file called CONTROL.DAT. The listing for program CONTROL is presented in Appendix 'B' of this thesis. The size of the control set has been set at an arbitrary value of 10^5 cells (6 x 10^5 edges).

The control set, CONTROL.DAT, may be manipulated and interrogated by any of the analytical subroutines used to examine the real set of 14870 simplicial cells from the Finney model, FINEDGE.DAT. The edgelength frequency distribution for CONTROL.DAT is virtually

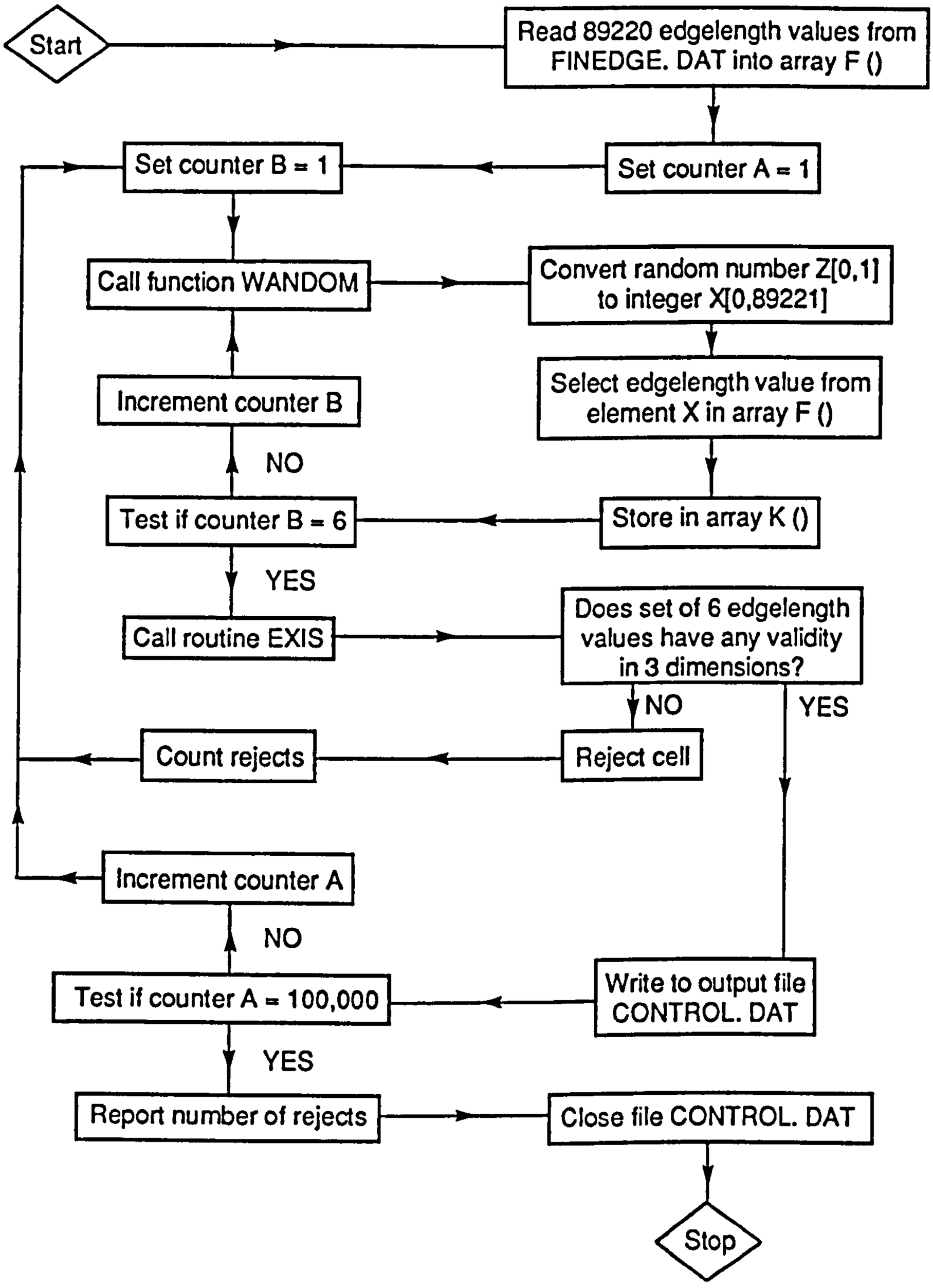

Figure 4.5 : FLOW DIAGRAM OF PROGRAM CONTROL

identical to that of FINEDGE.DAT, as is evident from comparisons of figure 4.6 with figure 3.15, and figure 4.7 with figure 3.16.

The number of simplicial cells rejected by routine EXIS as having no three dimensional existence, or validity, during the construction of CONTROL.DAT was 269, or 0.268% (i.e. 100 x 269/100269). If this proportion is applied to the 14870 simplicial cells of the Finney model, then we should expect that random chance alone would be responsible for the generation of some 39 or 40 simplicial cells which could not physically exist. In order to compensate for this, real RCP structure is forced to avoid certain simplicial cell configurations dictated by random chance - this is the first indirect evidence that RCP structure cannot possibly be perfectly random according to the definition presented in section 4.2.2. Further departures from ideal randomness are presented in section 4.4 following.

4.4 Tests of Randomness

4.4.1 The First Test

The first test of randomness considered in the present work is essentially that of the worked example presented in section 4.2.4. For the Finney model we have 14870 simplicial cells which can be analysed to yield the observation series O_0, $O_1 \ldots O_6$, and we are able to use the polynomial terms of equation 4.3 to calculate the (random) expected series E_0, $E_1 .. E_6$. Thus it is possible to calculate values of chi-squared and test a hypothesis. There are

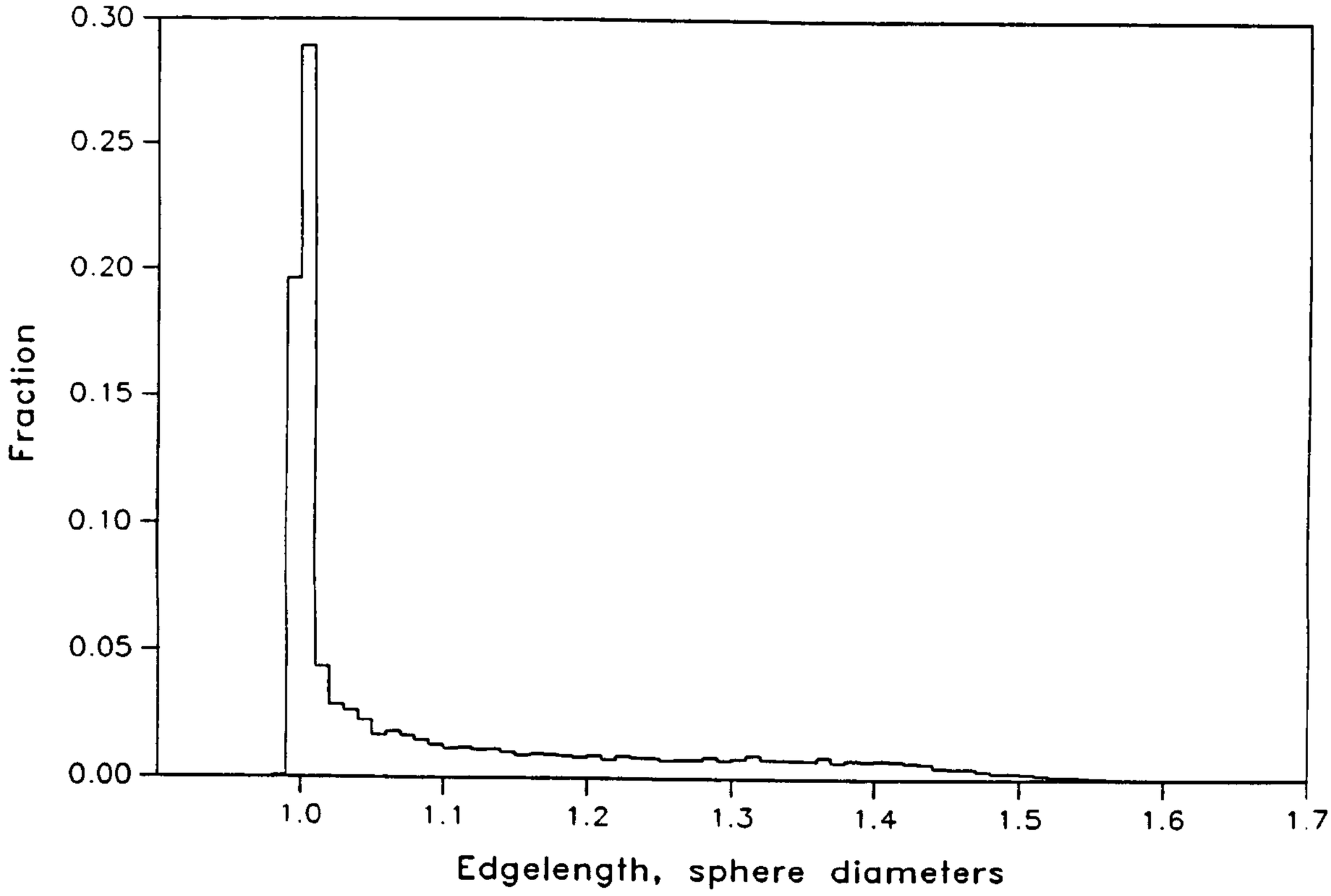

Figure 4.6 : Edgelength frequency distibution for the control set of simplicial cells

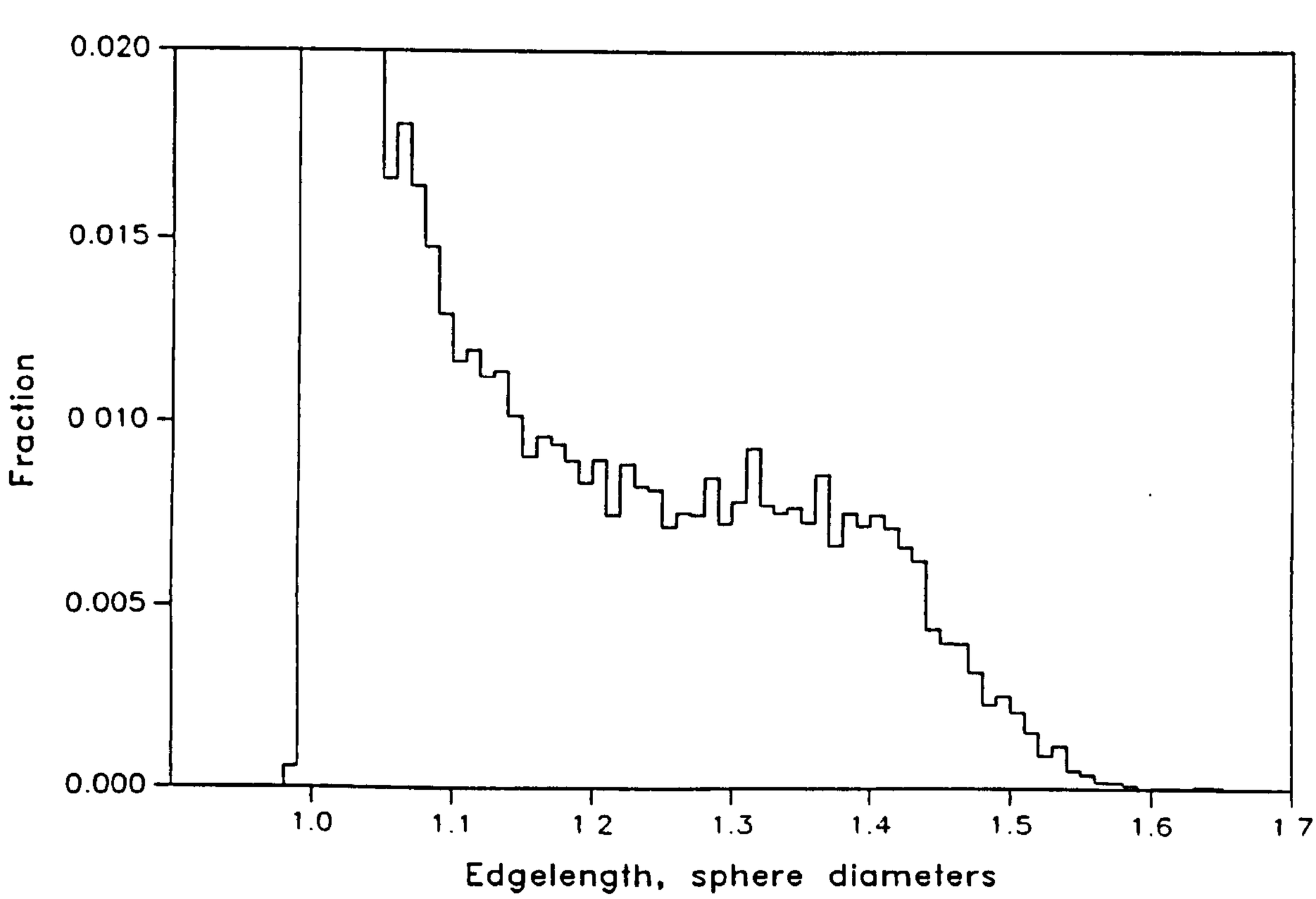

Figure 4.7 : Detail of figure 4.6

two essential questions to be answered before the test can be defined:

(i) What hypothesis is being tested?

and

(ii) Since the frequencies E_0, $E_1 \ldots E_6$ are functions of s (i.e. the fraction of edgelengths defined as short), what value of X_T will be used?

The answer to question (i) is that the hypothesis under test is the null hypothesis that there is no significant difference between the expected series E_0, $E_1 \ldots E_6$ and the observed series O_0, $O_1 \ldots O_6$. Rejection of the null hypothesis using a chi-squared test means that the definition of randomness given in section 4.2.2 is not correct.

The answer to question (ii) is a little more difficult, since a priori, we have no knowledge of how varying χ_T (and therefore s) may affect chi-squared. The solution is to find out, by finding chi-squared for a wide range of s values.

The first test of randomness, therefore, consists of the sequence of events summarised in flow diagram form in figure 4.8. In addition to analysing FINEDGE.DAT for the observed series O_0, $O_1 \ldots O_6$, the first 14870 cells of the control file CONTROL.DAT were also analysed to yield the control-observed series O'_0, $O'_1 \ldots O'_6$. The variation in chi-squared as a function of s is shown in figure 4.9. From this figure it is apparent that the value of chi-squared for the 14870 simplicial cells of the Finney model rises from a value of

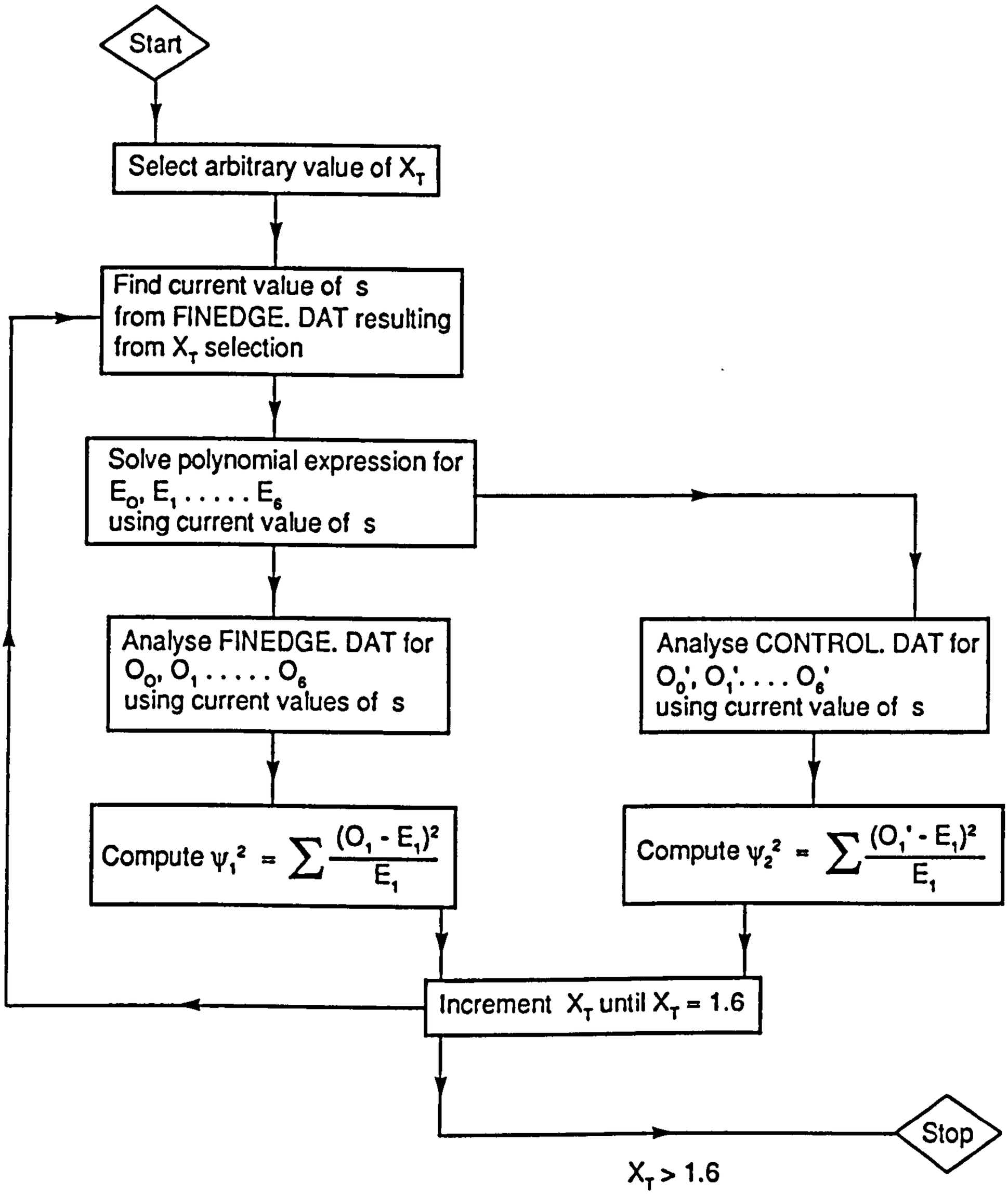

Figure 4.8 : FLOW DIAGRAM FOR FIRST TEST OF RANDOMNESS

about χ^2 = 10 at s = 0.2 to a maximum value of χ^2 = 1498 at s = 0.477 (χ_T = 1.0085), before falling back to a value of χ^2 = 47 at s = 0.9. The control set (identified as a "plus" symbol and the term "randomised model" on figure 4.9), however shows a value of χ^2 which varies between limits of 2.3 and 9.8.

There are six degrees of freedom (ν) for χ^2, as discussed in the worked example in section 4.2.4. From published tables, at the 5% level of significance the value of $\chi^2_{0.05}$ for ν = 6 is 12.59. Between the limits $0.2<s<0.9$, all values of χ^2 for the Finney simplicial cells exceed considerably 12.59. The null hypothesis is therefore rejected, and it is demonstrated that the simplicial cells of the Finney RCP model are distinctly non-random. The definition of randomness given in section 4.2.2 therefore does not apply to the Finney RCP model. As we might expect, however, the null hypothesis for the control set cannot be rejected, and we must conclude that the control set might be consistent with the definition of randomness given in section 4.2.2.

An interesting feature of the relationship between χ^2 and s for the real Finney cells shown in figure 4.9 is that the curve is not quite symmetrical about the peak value of χ^2. The reason for this is not understood, neither is it understood why the peak value of χ^2 occurs at a value of s = 0.477 and not 0.500.

4.4.2 Second test of Randomness

This is no more than a simple extension of the first test which showed that RCP simplicial cells from the Finney model exhibit

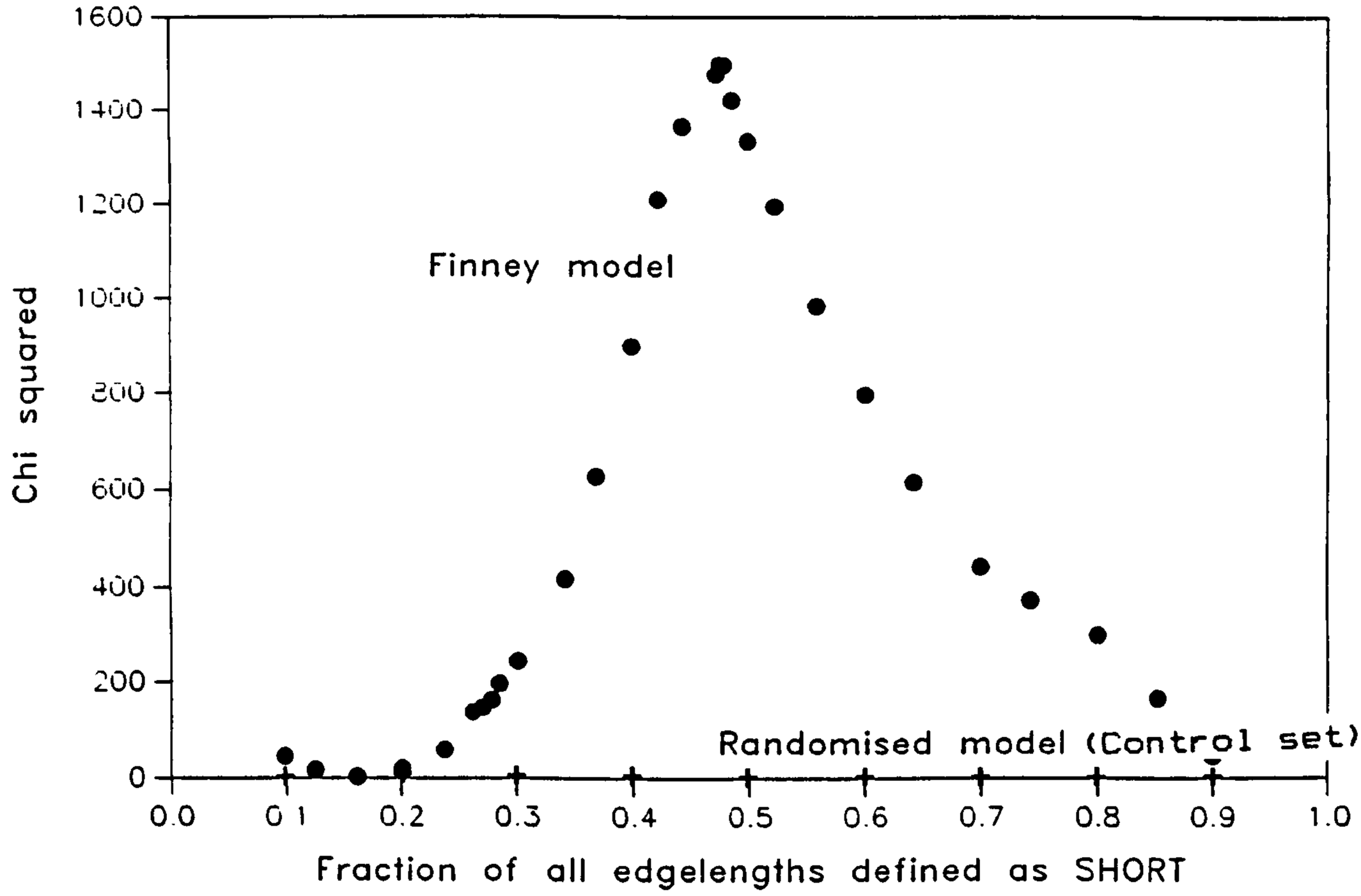

Figure 4.9 : Chi-square versus fraction of state '5' edges for the Finney model and the control set

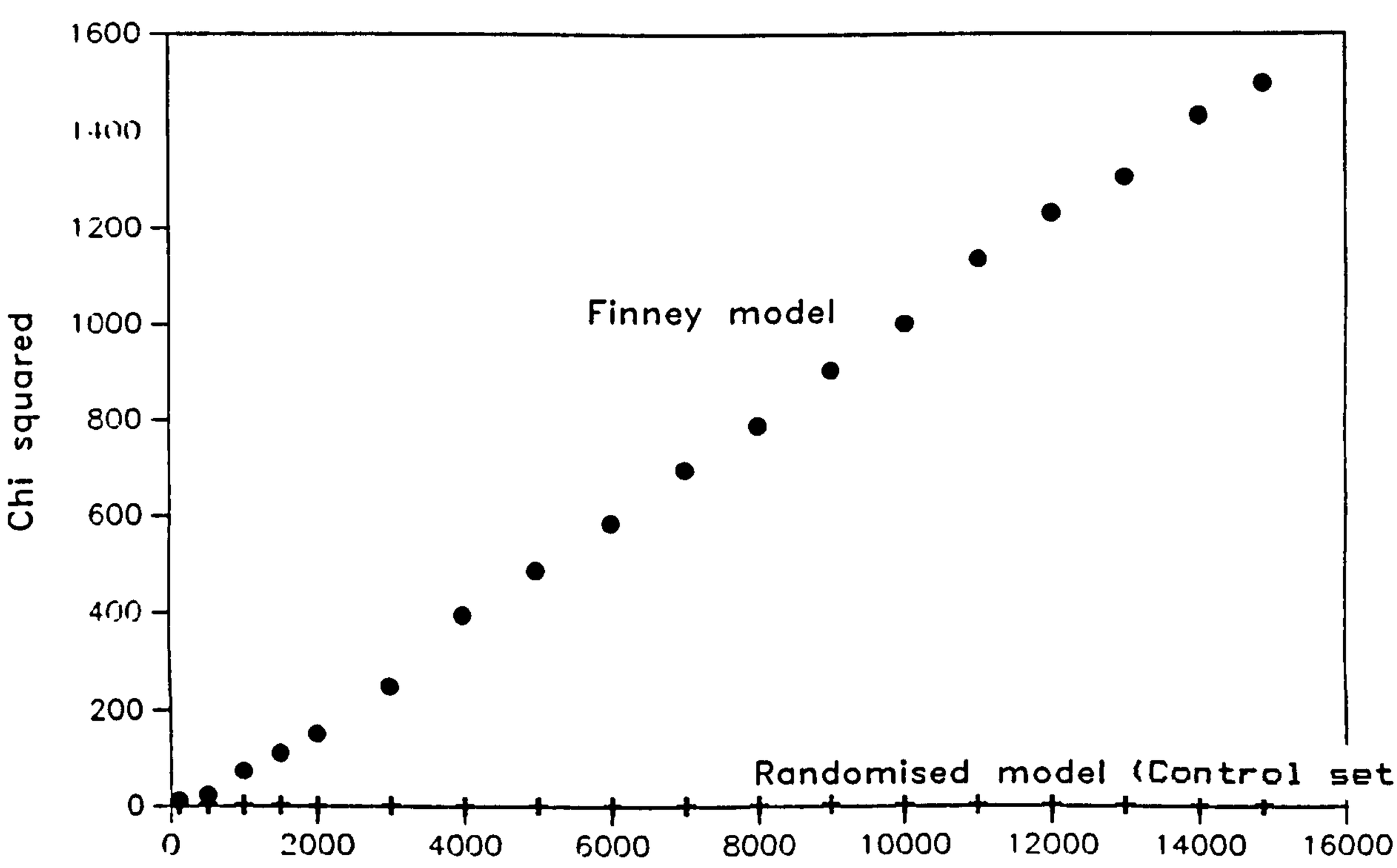

Figure 4.10 : Chi-square versus number of simplicial cells for the Finney model and the control set

maximum departure from randomness at x_T = 1.0085, equivalent to a value of s = 0.477. The second test of randomness uses a fixed value of s = 0.477, but a variable number of simplicial cells in the test, starting with the first 100 cells of FINEDGE.DAT, and increasing to 14870 cells. The relationship between number of simplicial cells and χ^2 is presented in figure 4.10 which shows that χ^2 is a smooth linear function of the number cells in the group. The value of χ^2 for the control set (identified in figure 4.10 as the "plus" symbol, and referred to as the randomised model) falls in the range 0.9 to 9.7 and is independent of the number of cells in the group. The tendency for χ^2 to increase indefinitely as the sample size is increased is a typical feature of a significant difference between the expected series and the observed series, confirming that the null hypothesis must be rejected for the Finney model.

The first and second tests of randomness have shown that the values of the six edgelengths of a real simplicial cell are not independent of each other, and that they do not occur with random chance. Knowledge of the simplicial cell edgelength frequency distribution function alone, therefore, does not provide enough information to generate a group of simplicial cells which are exactly like those found in a real RCP structure. This confirms the suspicion raised earlier in section 4.3.4 that random chance selection of edgelengths from the edgelength distribution function is not a viable mechanism for forming RCP simplicial cells. Avoiding selecting such "impossible" cells is consistent with a small departure from random behaviour. So far the tests of randomness have concentrated on a statistically valid rejection of the null hypothesis. The tests

themselves have not yet revealed the exact nature of this non-randomness. The following tests are designed to achieve this goal.

4.4.3 Third test of Randomness

The first test established that the Finney simplicial cells give the highest chi-squared value (i.e. appear to be maximally non-random) for a value of s close to 0.5. For the exact condition S = 0.5000, the expectation series E_0, $E_1 \ldots E_6$ becomes symmetrical about E_3:

i.e. $E_0 = E_6$

$E_1 = E_5$

$E_2 = E_4$

or $E_{(3-i)} = E_{(3+i)}$ for $s = \ell = 0.5$

The frequencies of the expectation series for 14870 simplicial cells for s = 0.5 are given in table 4.5:

Expectation series term	Frequency in 14870 cells	Cell types
$E_0=E_6$	232	0LS6,6LS0
$E_1=E_5$	1394	1LS5,5LS1
$E_2=E_4$	3485	2LS4,4LS2
E_3	4648	3LS3

Table 4.5 : Expected frequencies of random simplicial cells for s=l=0.5000

In order to attempt to visualise the nature of the non-randomness in the simplicial cells, we select a value of X_T such that s = 0.5, and compare the observed series O_0, $O_1 \ldots O_6$ for the Finney model with the expected series E_0, $E_1 \ldots E_6$. Additionally, we can compare the observed series $O'_0, O'_1 \ldots O'_6$ from the first 14870 cells of the control set with the real observed series.

In practice it is not possible to find a value of X_T for the 14870 simplicial cells of the Finney model such that s is exactly equal to 0.5. The nearest to s = 0.5 it is possible to achieve for the Finney set is s = 0.50012 for a value of X_T = 1.01229. Although very close to the ideal value of s = 0.5, the real value of 0.50012 does introduce a very small degree of non-symmetry in the expectation series E_0, $E_1 \ldots E_6$ since:

$$(0.50012)^6 \neq (1 - 0.50012)^6$$

- this very slight departure from symmetry in the terms of the expectation series is so small that it may be ignored for all practical purposes. The comparison between the expectation series and the observation series is given in table 4.6.

From table 4.6 two conclusions may be drawn regarding the simplicial cells of the Finney packing:

(i) The observed frequencies of the least probable cell forms (0LS6, 6LS0, 1LS5 and 5LS1) are much lower than expected from a group of random cells. Correspondingly, the observed frequency of the most probable cell type (3LS3) is much

higher than expected from a group of random cells.

(ii) The observed series O_0, $O_1 \ldots O_6$ is approximately symmetrical about O_3:

i.e. $O_0 \simeq O_6$

$O_1 \simeq O_5$

$O_2 \simeq O_4$

Simplicial cell class	Observed frequency in 14870 cells of CONTROL set $O'_0, O'_1 \ldots O'_6$	Expected frequency in 14870 cells of RANDOM set $E_0, E_1 \ldots E_6$	Observed frequency in 14870 cells of FINNEY set $O_0, O_1 \ldots O_6$
0LS6	246	233	56
1LS5	1383	1396	785
2LS4	3466	3487	3496
3LS3	4612	4647	6107
4LS2	3484	3483	3653
5LS1	1445	1393	719
6LS0	234	232	54

$X_T = 1.01229$, $s = 0.50012$

Table 4.6 : Comparison of expected and observed frquencies of simplicial cell classes in 14870 cells of the control set and the Finney model.

The consequences of this departure from random behaviour are that a straightforward random simulation of simplicial cells, such as that used to generate the control set, will not produce a good match with the real simplicial cells of the Finney model. In particular, all aspects concerning simplicial cell volume will be subject to significant statistical differences between the real simplicial cells of the Finney model and the simulated cells. These statistical differences are considered in some detail in the following section.

4.4.4 Consequences of Non-randomness

The main consequence of the non-random behaviour defined and isolated in this chapter concerns simulations of groups of tetrahedral simplicial cells. Mason (1971) for example used a pseudorandom number generator to select tetrahedron edgelength values from what is in effect an approximated simplicial cell edgelength frequency distribution. Gotoh and Finney (1974) used a statistical geometrical argument based on an estimate of the most likely form of tetrahedral cell to deduce the overall packing density of monodisperse random close packing. The present work has shown that any successful simulation must address the fact that the real simplicial cells of the Finney model have reduced frequencies of very small cells (0LS6 and 1LS5 forms), reduced frequencies of very large cells (6LS0 and 5LS1 forms), and increased frequencies of "average" cell forms (i.e. 3LS3) over those predicted from random chance.

An unsuccessful simulation method relying entirely on random selection of edgelength from some edgelength distribution function

will overestimate the frequencies of small and large cell classes and will underestimate the frequencies of more "average" cell classes such as the 3LS3. This is readily illustrated by regarding the control set as an unsuccessful simulation, and comparing a few frequency distributions from the control set with those of the Finney simplicial cells presented in Chapter 3 of this thesis.

Figure 4.11 shows the cavity insphere radius frequency distribution for 10^5 cells of the control set. If this distribution is compared with the dashed line for the Finney model (taken from figure 3.27), it is very clear that the control set overestimates the frequencies of very small cavity inspheres (up to 0.28 sphere radii) and very large cavity inspheres (greater than 0.45 sphere radii). Correspondingly, the control set underestimates the frequencies of

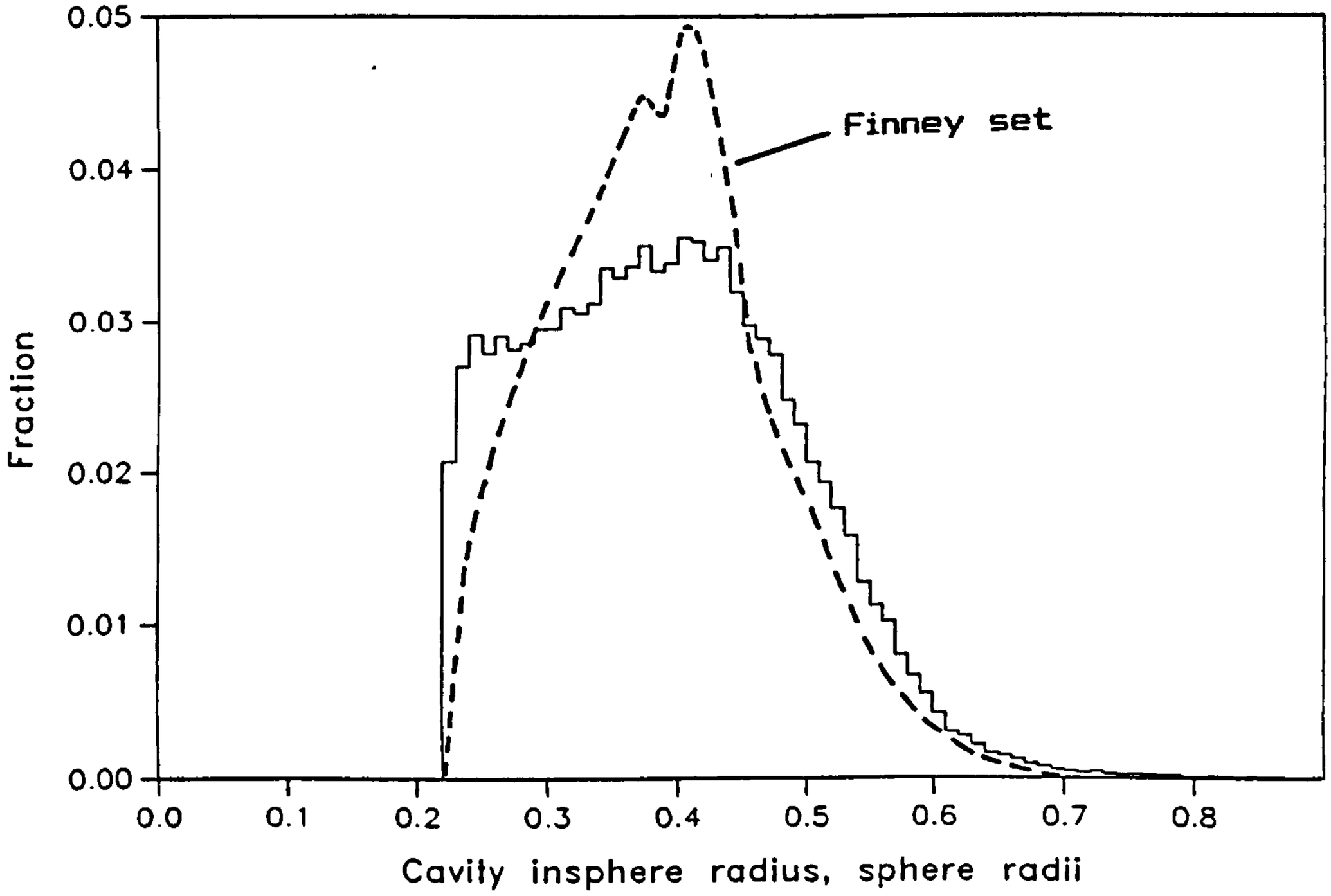

Figure 4.11 : Cavity insphere radius frequency distribution function for the control set

the "average" cavity inspheres in the range 0.29 to 0.44 sphere radii. The smallest cavity insphere which can exist is that of the unit regular tetrahedron, which has a cavity insphere radius of 0.224745 sphere radii (see table 3.5). The frequency of occurrence of this tetrahedron, which would be identified as a OLS6 cell for $X_T \leq 1.01229$, is clearly overestimated by the control set.

Figure 4.12 shows the frequency distribution of individual apex solid angles for the control set. When compared with the dashed line for the Finney model (taken from figure 3.19), it is clear that the control set is substantially overestimating apex solid angles in the range 0.55 to 0.56 radians. Table 3.5 shows the apex solid angle for the regular unit tetrahedron to be 0.5513 radian, again confirming that the control set overestimates the frequency of the unit regular tetrahedron.

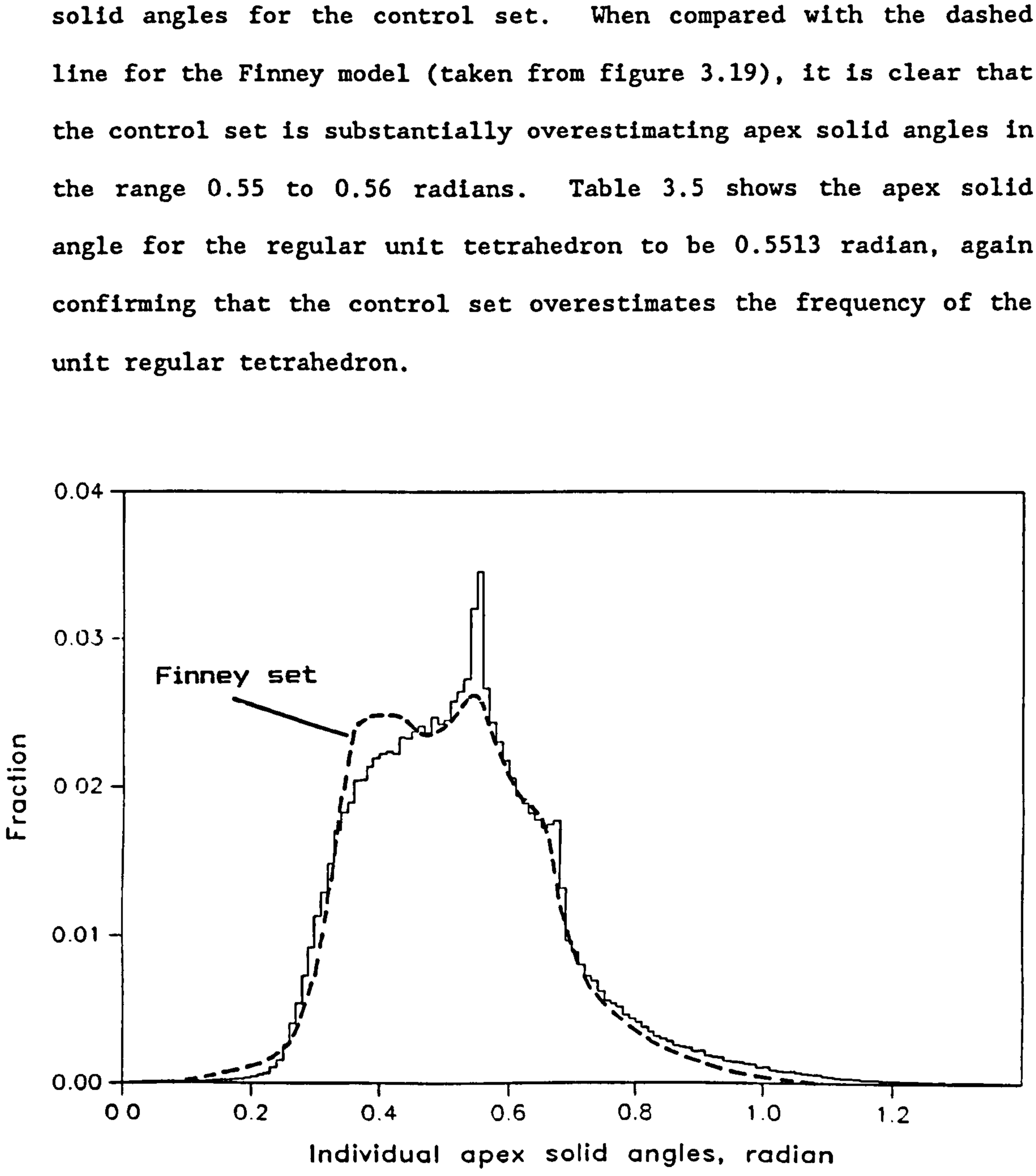

Figure 4.12 : Individual apex solid angle frequency distribution for the control set

Figures 4.13 and 4.14 shows the full cell solid angle frequency distribution for the 10^5 cells of the control set. By comparison with the dashed line for the Finney model (taken from figure 3.21), it is apparent that the control set cells have an increased frequency of total solid angle in the range 2.20 to 2.21 radians. From table 3.5, the unit regular tetrahedron has a total solid angle of 2.205 radians. The real simplicial cells of the Finney packing have a continuously higher frequency than the control cells of all total solid angles below 1.9 radians. This is evident from figure 4.14, which shows a detail of the full cell solid angle frequency distribution for the control set.

4.4.5 Advantages conferred by non-randomness

It seems reasonable to suppose that there is a reason, or a set of reasons, why the simplicial cells of the Finney monodisperse RCP model are distinctly non-random. This section of chapter 4 takes an anthropomorphic view of the issue of non-randomness, and assumes that some "advantage" is conferred on the packing by non-random simplicial cell formation. In this anthropomorphic approach for example, we can imagine that the whole packing is trying to achieve the maximum packing density possible - perhaps non-randomness assists in achieving this goal. We can test this hypothesis fairly easily, by calculating the average packing densities for the 14870 cells of the Finney model, and comparing those results with those for the first 14870 cells of the control set. This comparison is shown in table 4.7, from which it is evident that the average packing densities of cells from both the Finney model and the control set are virtually identical. Whatever advantage non-

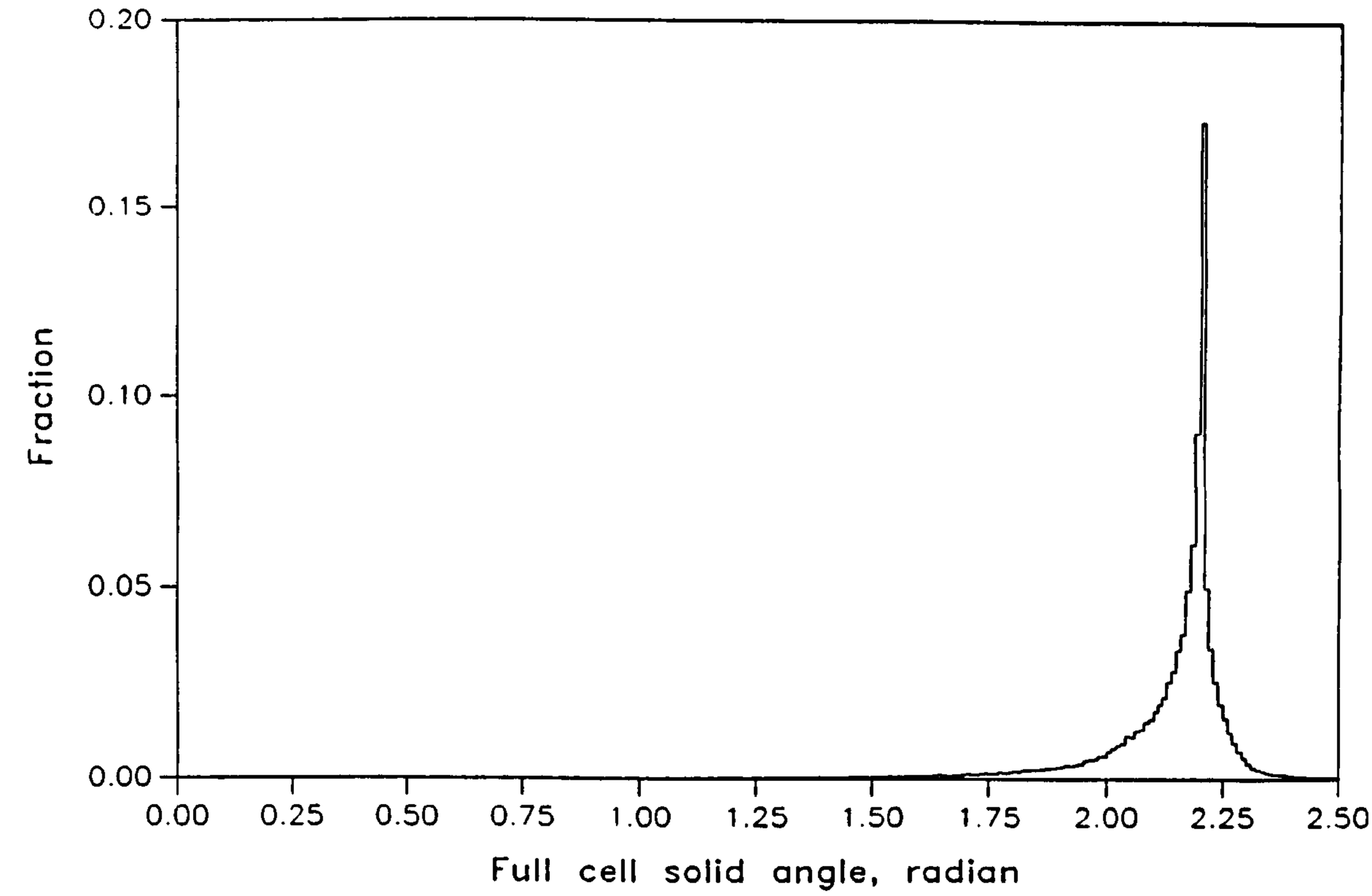

Figure 4.13 : Full cell solid angle frequency distribution for the control set

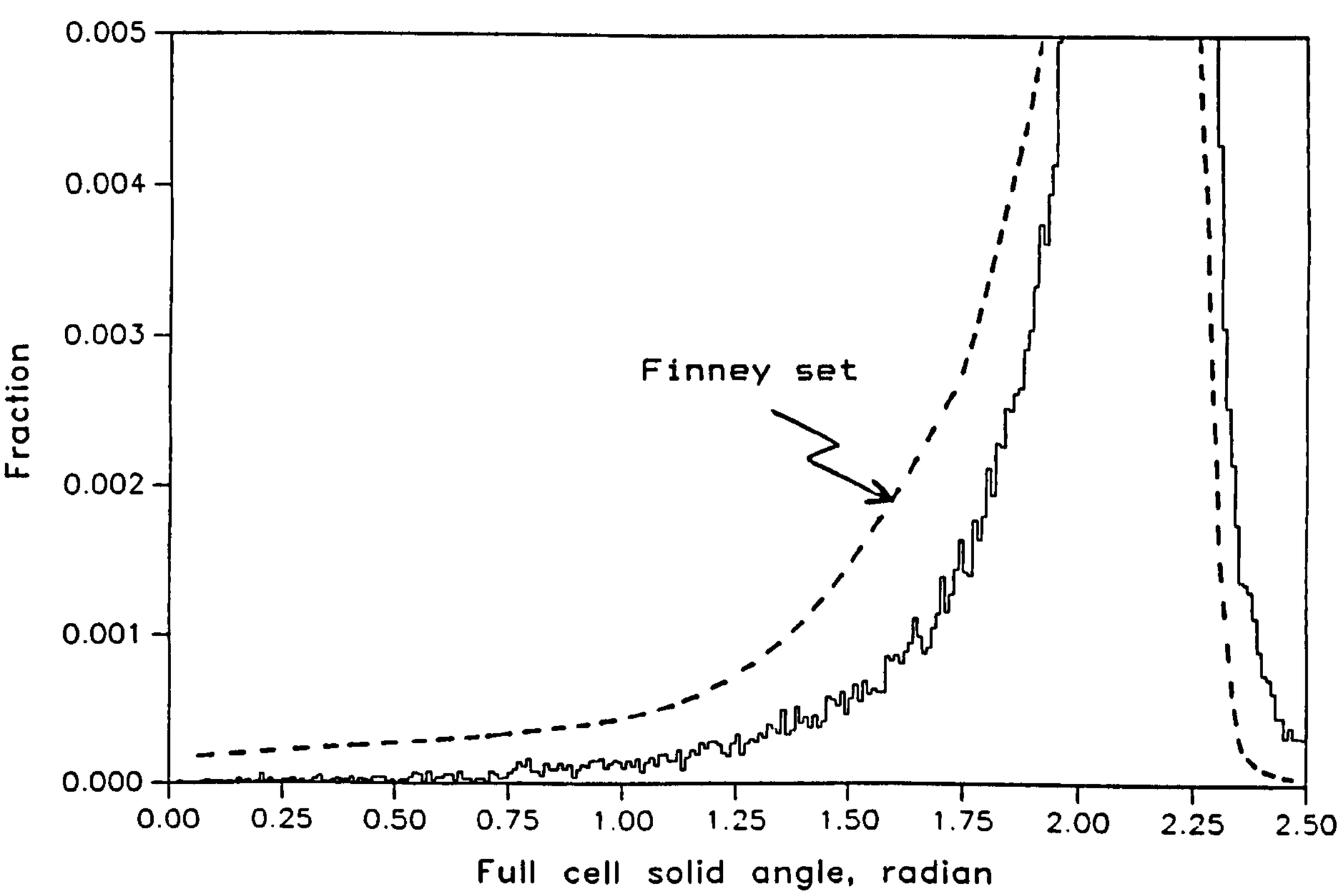

Figure 4.14 : Detail of figure 4.13

CELL CLASS	FINNEY MODEL		CONTROL SET	
	Frequency	Average packing density	Frequency	Average packing density
0LS6	56	0.7761	243	0.7769
1LS5	785	0.7332	1378	0.7389
2LS4	3496	0.6897	3465	0.6949
3LS3	6107	0.6432	4614	0.6459
4LS2	3653	0.5910	3484	0.5952
5LS1	719	0.5402	1450	0.5411
6LS0	54	0.4847	236	0.4821
	*OVERALL MEAN 0.6380		*OVERALL MEAN 0.6375	

$X_T = 1.01229$, $s = 0.50012$

*Note: OVERALL MEAN is calculated within the program as TOTAL VOID VOLUME/TOTAL CELL VOLUME

Table 4.7 : Packing densities of the Finney model and control set (first 14870 cells).

randomness (at the simplicial cell level) confers on the packing then, is not simply one of efficiency in packing density. Looked at another way, measurement of packing density alone offers no clue as to the reasons for non-randomness at the simplicial cell level.

Perhaps the advantage we are looking for is simply that the real simplicial cells fit perfectly together to fill three dimensional

space - the control set are not required to undertake this exacting task. If we calculate the total volume of all 14870 cells in the Finney model, we find a value of 15,936 sphere-radii cubed. Remarkably, this is significantly less than the total volume (16,545 sphere radii cubed) of the first 14870 cells of the control set. Not only do the real simplicial cells of the Finney model fit together, they occupy less volume in space than the same number of random cells of the control set. This is an important result, though at first sight paradoxical, as we have already established that the average packing densities of the control set and the Finney model cells are virtually identical. The Finney cells achieve this paradoxical result by putting significantly less solid-sphere volume into the simplicial cells than the control set cells do. Thus table 4.8 shows the total cell volumes (i.e. volume of sphere-segment plus void space) and solids-only volumes (i.e. volume of sphere segments only) for both the Finney model and the control set cells.

This minimisation of space occupied by real simplicial cells has already been touched upon indirectly in section 4.4.4. Specifically, figure 4.14 shows that the full simplicial cell solid angle distribution is systematically shifted towards lower values for the set of Finney cells compared with the set of control cells. For the moment, this is the nearest we can get to isolating the "advantage" conferred upon the packing by adopting a non-random simplicial cell "strategy". The real non-random simplicial cells occupy less space than purely randomly generated cells are able to. In chapter 5 we will see that the constraints of space filling introduce another interesting facet of non-randomness - that of isomerism.

CELL CLASS	FINNEY MODEL			CONTROL SET		
	Frequency	Total cell volume (r^3)	solids only volume (r^3)	Frequency	Total cell volume (r^3)	solids only volume (r^3)
0LS6	56	53.0	41.2	243	229.9	178.6
1LS5	785	767.1	562.4	1378	1340.1	990.2
2LS4	3496	3500.4	2414.2	3465	3537.6	2458.4
3LS3	6107	6465.4	4158.7	4614	5044.4	3258.3
4LS2	3653	4184.2	2472.9	3484	4134.5	2461.0
5LS1	719	892.6	482.2	1450	1908.1	1032.5
6LS0	54	73.4	35.6	236	350.7	169.1
	TOTALS	15936.1	10167.0	TOTALS	16545.4	10548.2

$X_T = 1.01229,\ s = 0.50012$

Finney average packing density =10167.0/15936.1=0.6380
Control average packing density =10548.2/16545.4=0.6375

Table 4.8 : Total cell volumes and solids-only cell volumes for the Finney model and Control set simplicial cells.

4.5 Mason's Method

Mason (1971) developed a method for simulating tetrahedral pores of a sphere packing, based on the concept that the tetrahedron edgelength values may be selected at random from an appropriate edgelength distribution function. The present chapter therefore would not be complete without commenting in some detail on Mason's method, since it remains the only practical published technique for simulating the pores of a random sphere packing.

First, Mason's tetrahedral pores are not rigorously defined as simplicial cells; they are not intended to be related precisely to either the Voronoi graph or the simplicial graph of a real packing, but rather they should be viewed as <u>approximate</u> simplicial cells. Second, Mason restricts the maximum cell edgelength to 1.4 sphere diameters. This expedient eliminates all possibilities of generating the "impossible" tetrahedra referred to in section 4.3.1. Third, he uses a linear approximation for the edgelength frequency distribution:

$$N = 7.5 + 15.62\ (x - 1) \qquad \text{-4.5-}$$

where N is the mumber of sphere centres within a distance x (in sphere diameters) of the reference sphere centre. Truncation of the edgelength frequency distribution at $1 < x < 1.4$ therefore demands 7.5 contacts per sphere and a total of 13.748 neighbours per sphere. It

is this truncated linear approximation which produces the most significant defect in the Mason model. Mason's earlier work (Mason, 1968) for example, showed that the cumulative near neighbour distribution function (i.e. that which is approximated by equation 4.5) can fall to around 5 or less for the Scott model - this is clearly shown in figure 1.16. The nature of the significant defect in the Mason model, then, is that it overestimates the number of sphere-sphere contacts. This in turn will produce far more state 'S' cell edgelengths than can exist in a real set of simplicial cells.

In order to evaluate the similarities between random tetrahedral cells produced by Mason's (1971) method, and the real simplicial cells of the Finney packing, a simulation using the Mason method was undertaken. This simulation has previously been reported by Mellor (1987), and entailed the generation of 10^6 tetrahedral pores. The simulation routine is summarised in figure 4.15 and the analysis routines are those used in chapter 3 and presented in Appendix 'B' to this thesis.

Some of the results of the simulation using Mason's method are shown in figures 4.16 to 4.25. These figures include the various face insphere radius frequency distributions specific to the Mason model, and may be compared directly with their real, observed counterparts for the Finney model presented in Chapter 3. The most striking feature of such a comparison is that Mason's simulation results in a prominent "spike" in the frequency distributions associated with the unit-regular tetrahedron. This "spike" for example, is prominent in figure 4.17 which shows the cavity insphere radius frequency

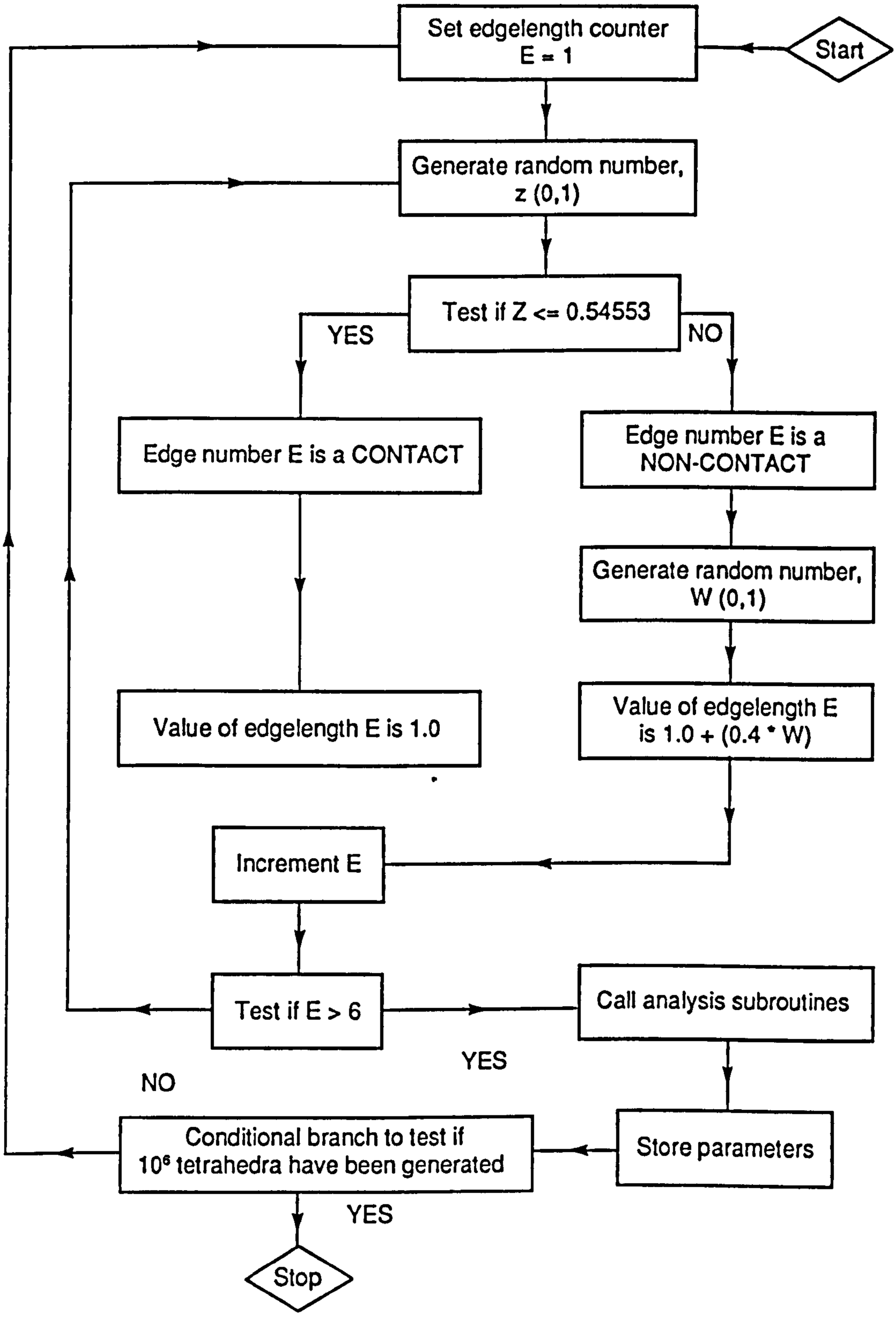

Figure 4.15 : FLOW DIAGRAM FOR MASON'S METHOD

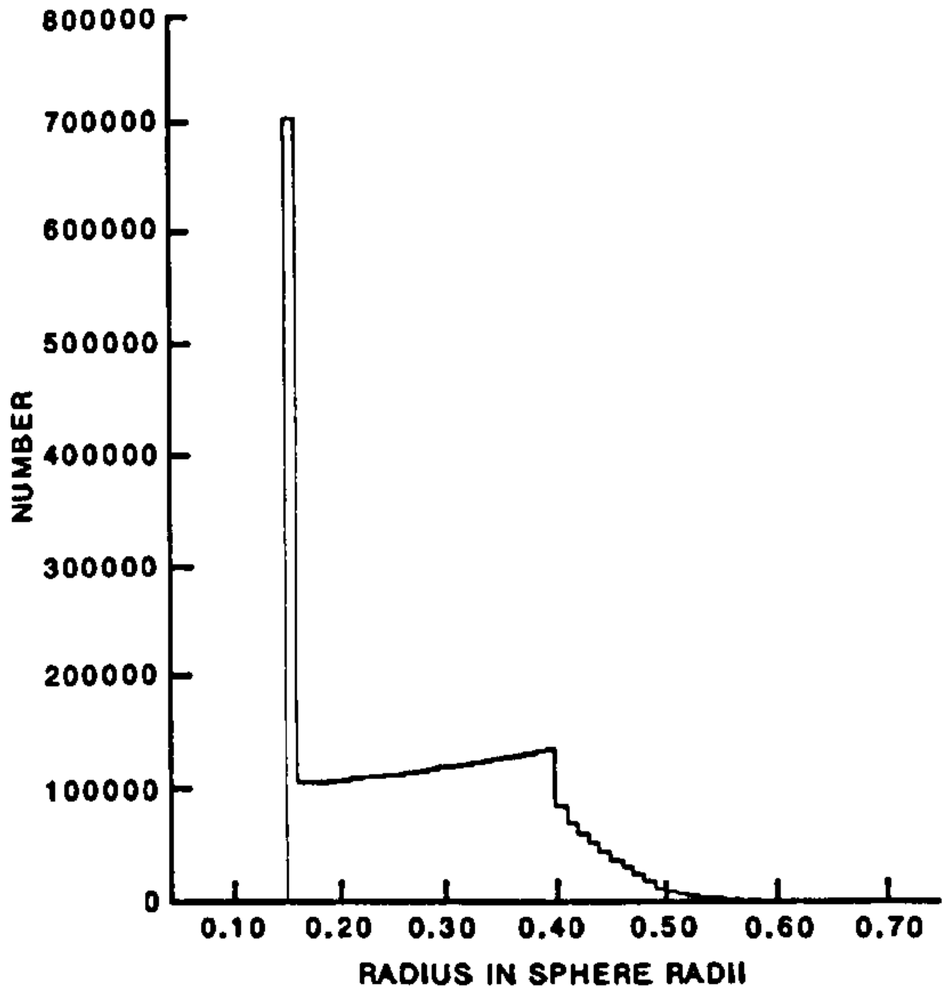

Figure 4.16 : Mason's method
Total face insphere radius
distribution for 10^6 cells

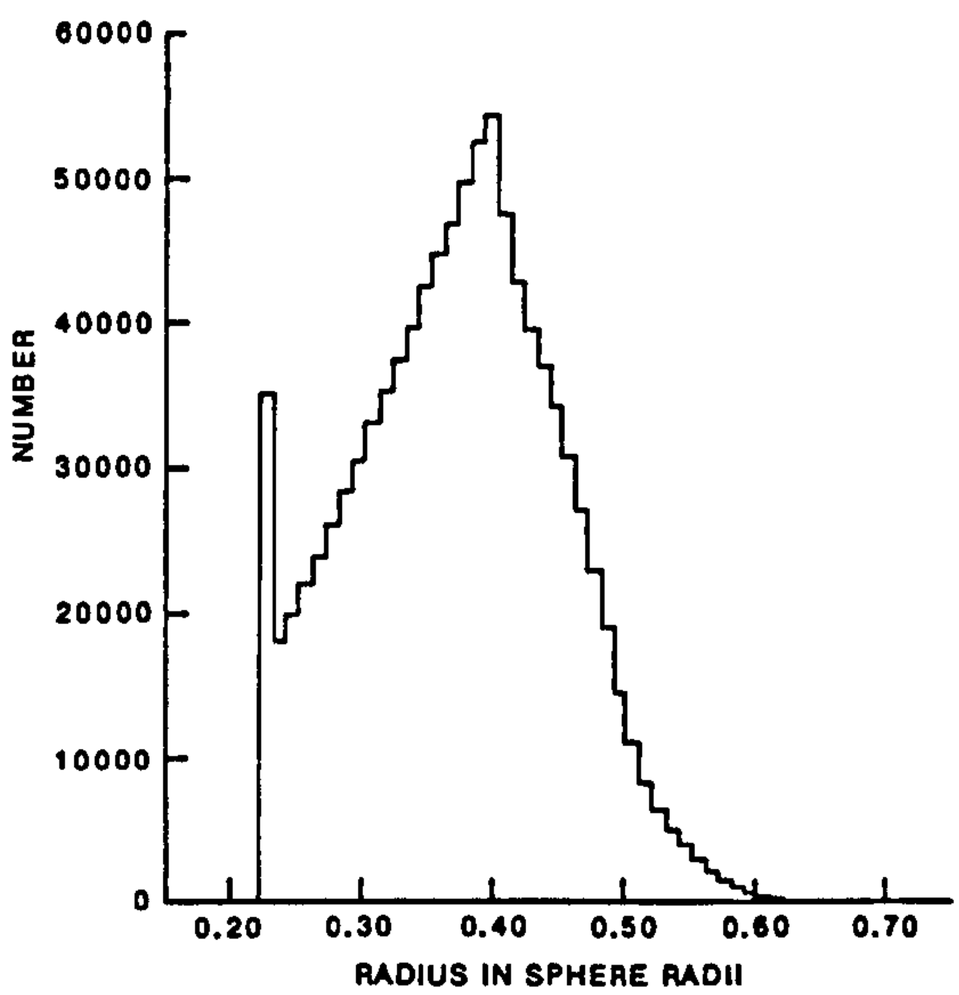

Figure 4.17 : Mason's method
Cavity insphere radius
distribution for 10^6 cells

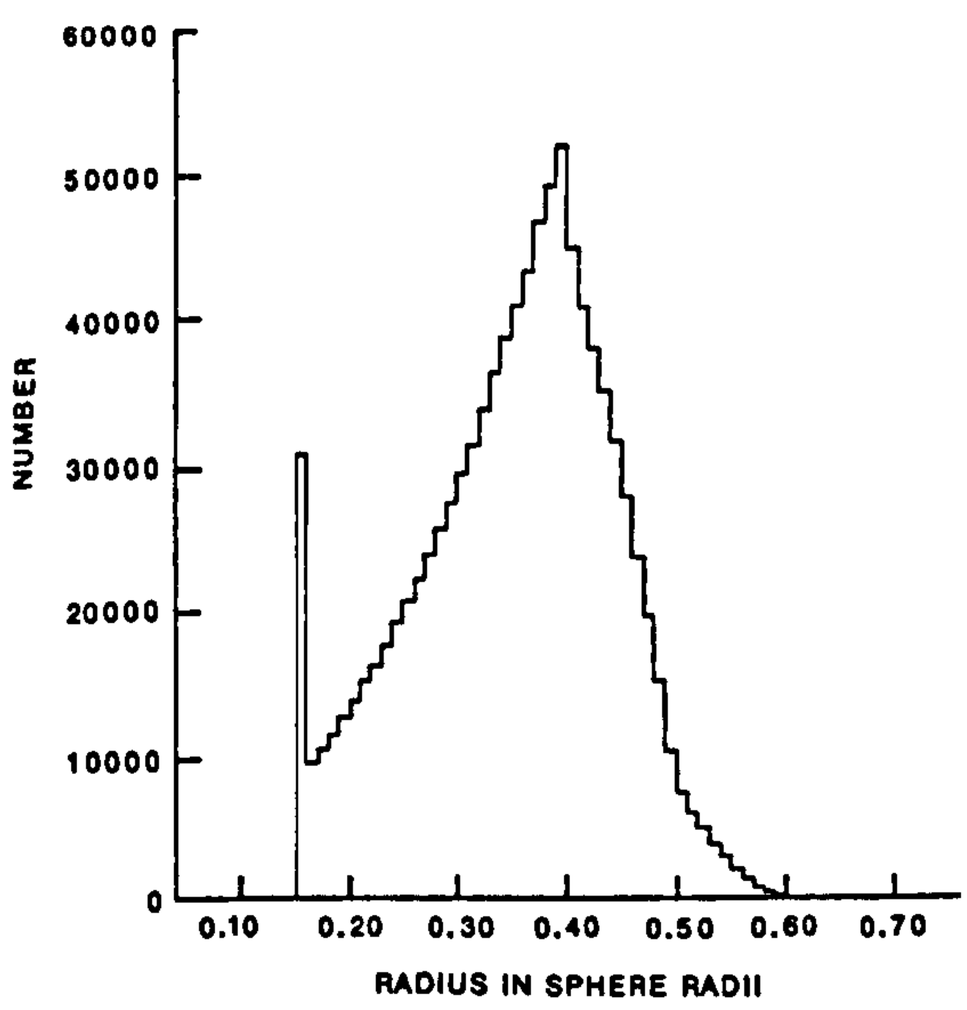

Figure 4.18 : Mason's method
Largest face insphere radius
distribution for 10^6 cells

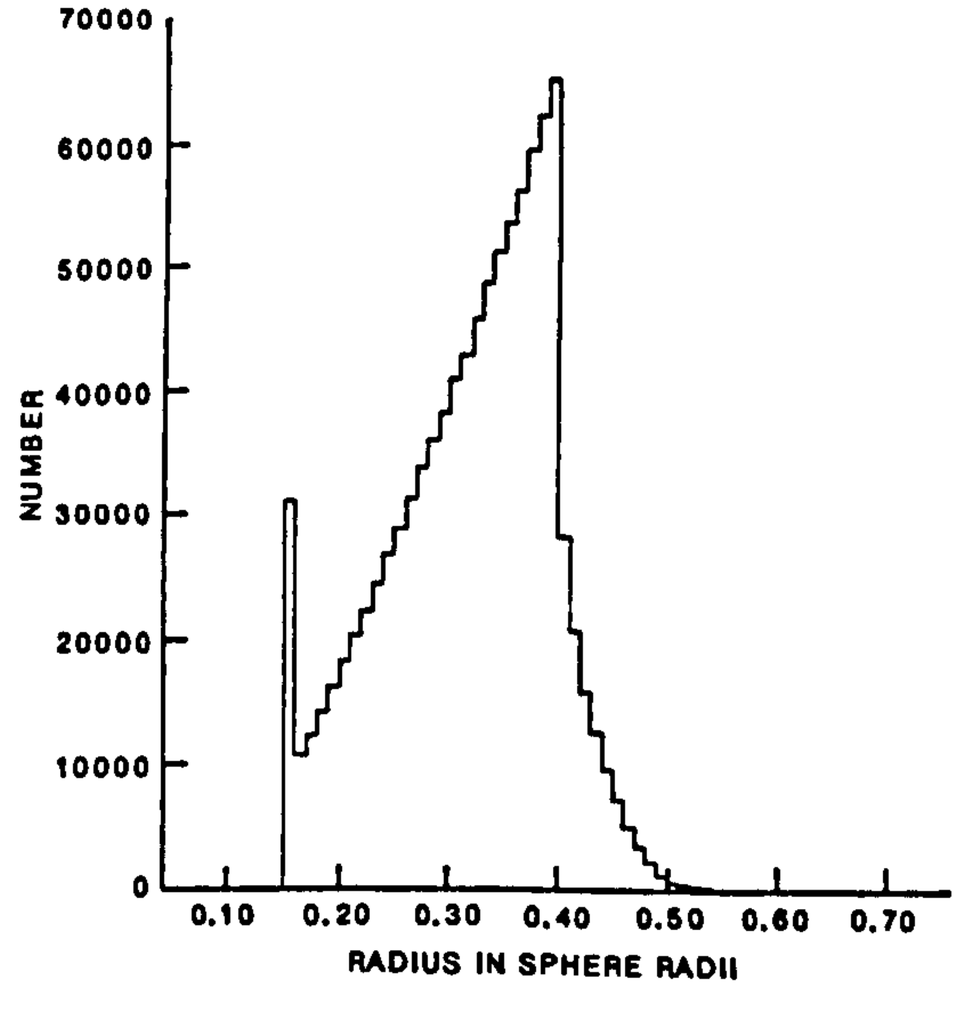

Figure 4.19 : Mason's method
2nd largest face insphere radi
distribution for 10^6 cells

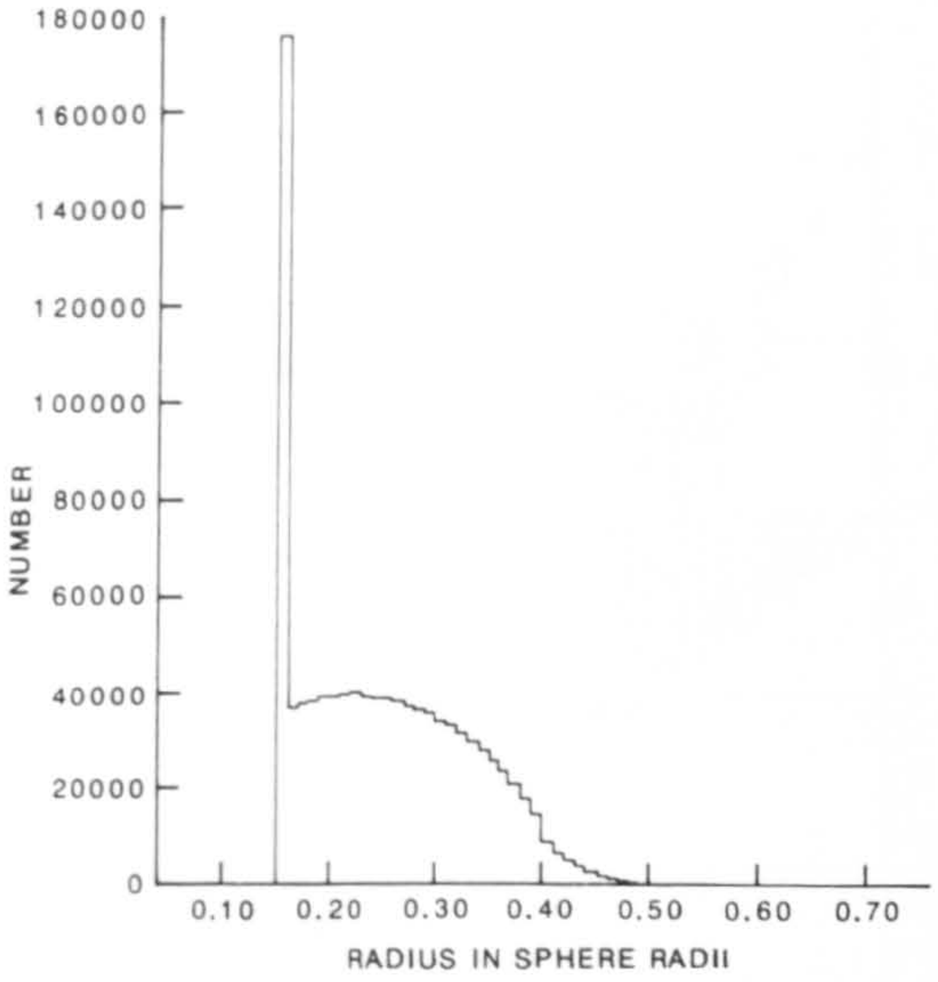

Figure 4.20 : Mason's method
3rd Largest face insphere radius
distribution for 10^6 cells

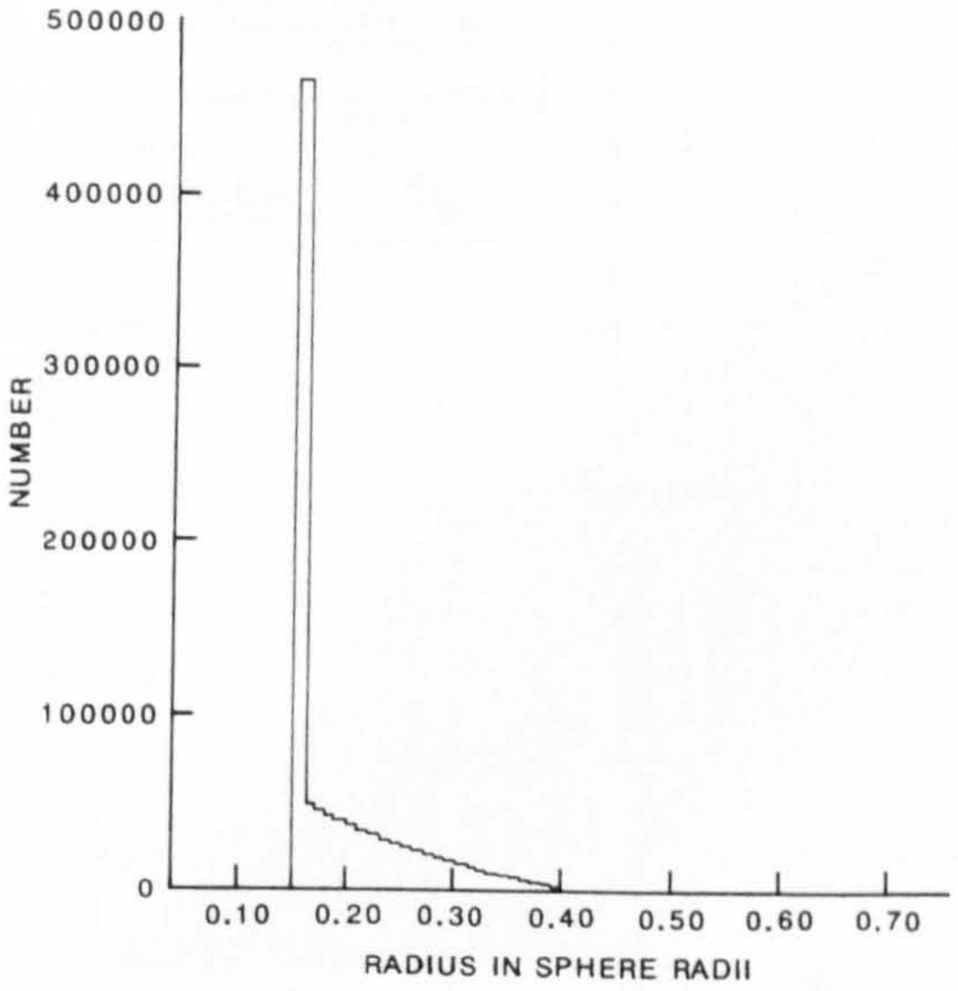

Figure 4.21 : Mason's method
smallest face insphere radius
distribution for 10^6 cells

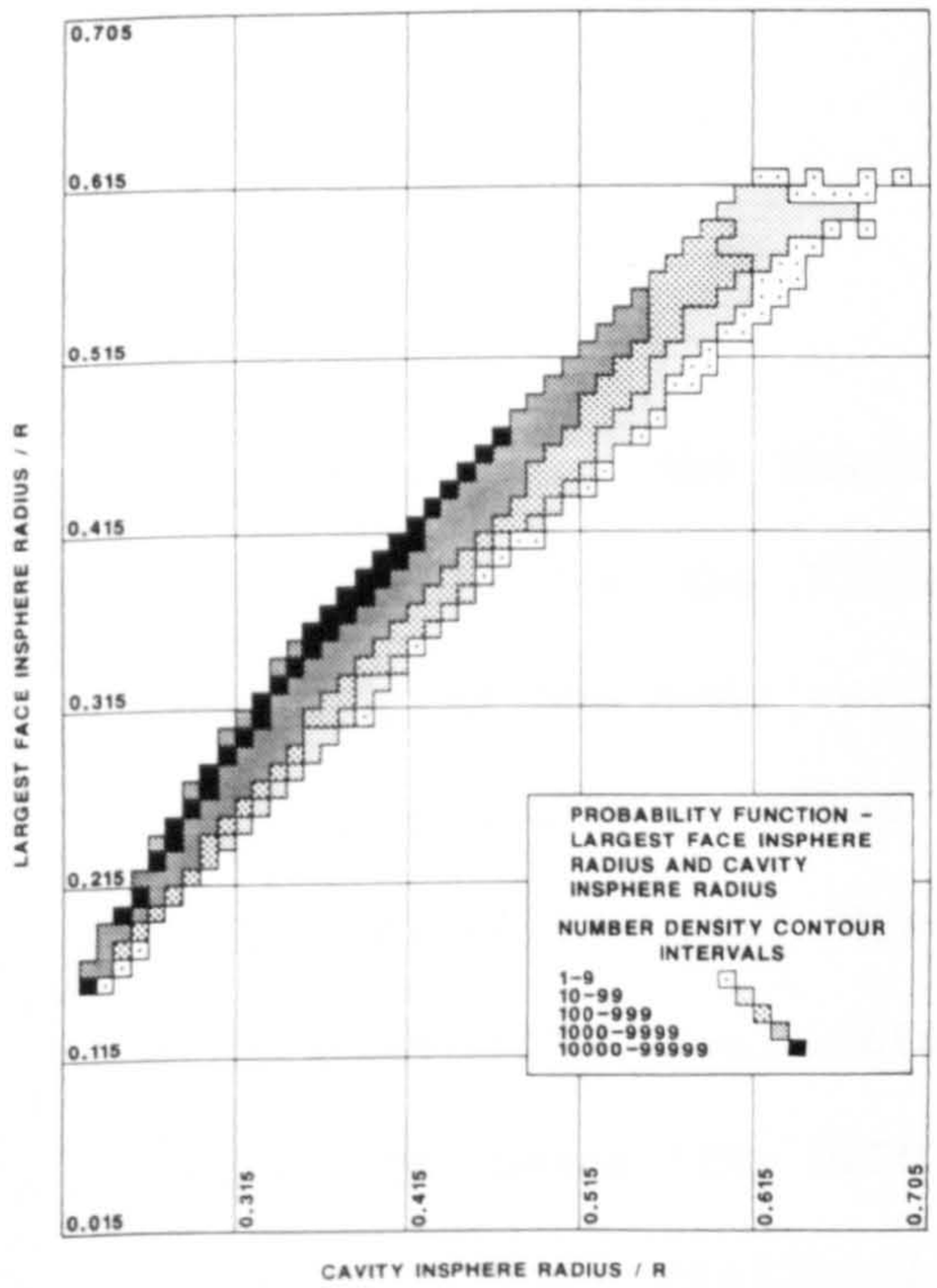

Figure 4.22 : Mason's method
Joint frequency distribution
Cavity insphere/largest face
for 10^6 cells

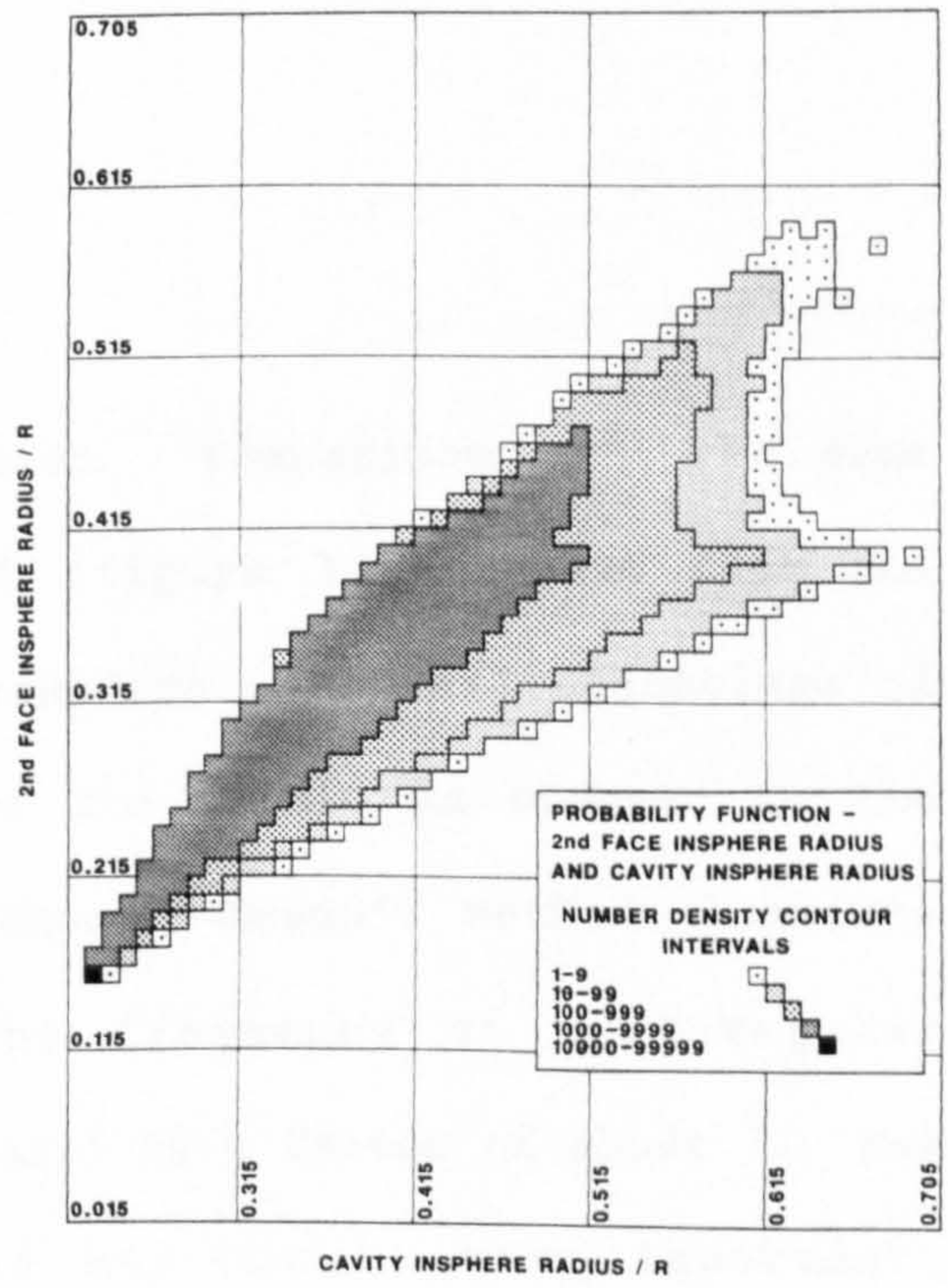

Figure 4.23 : Mason's method
Joint frequency distribution
Cavity insphere/2nd largest face
for 10^6 cells

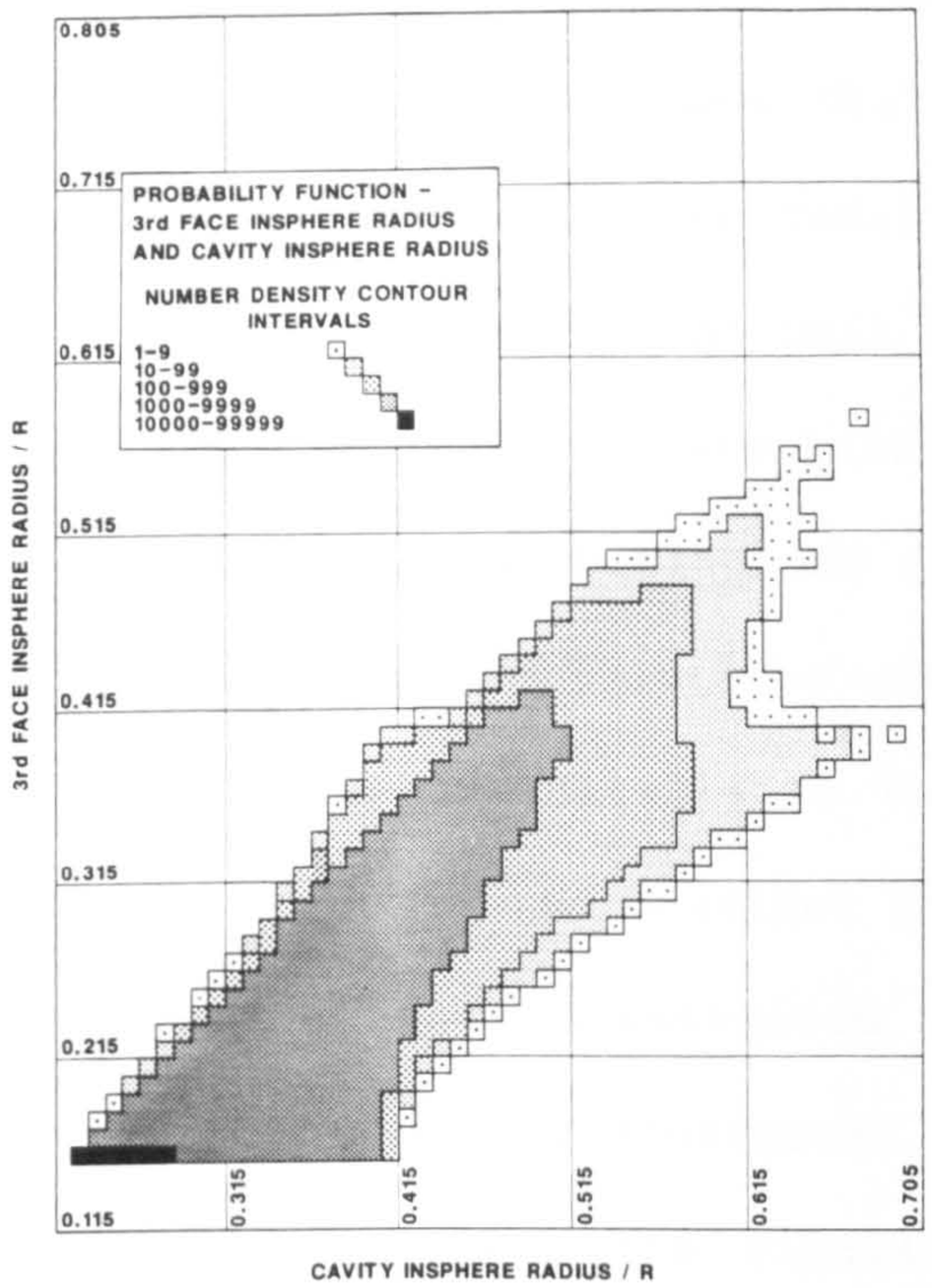

Figure 4.24 : Mason's method
Joint frequency distribution
Cavity insphere/3rd largest face
for 10^6 cells

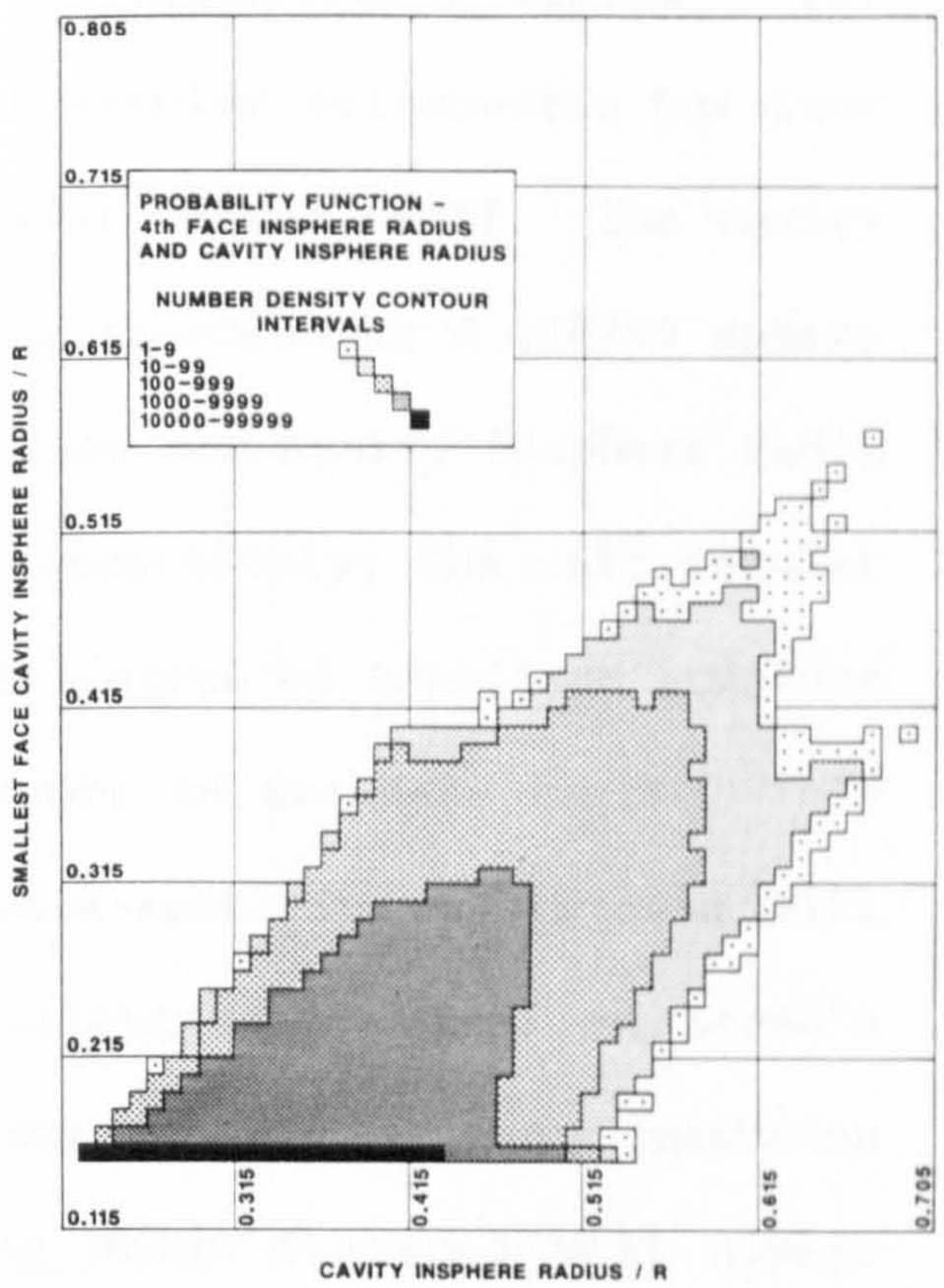

Figure 4.25 : Mason's method
Joint frequency distribution
Cavity insphere/smallest face
for 10^6 cells

distribution for the Mason simulation. Comparison with the same distribution for the Finney model (figure 3.27) shows that the frequency of the unit regular tetrahedron in a real assemblage of simplicial cells is about 0.005 of the total, as opposed to the 0.035 predicted using Mason's method. Mason's method therefore systematically overestimates the frequency of unit-regular tetrahedral pores (the OLS6 cell class) by a factor of about 7. For many practical applications this may not be very important. However, for applications in which capillary properties of sphere

packings are being considered, overestimating the frequency of unit-regular tetrahedral pores may lead to significant errors. For example, table 3.5 shows that the unit regular tetrahedron has four identical face insphere radii of 0.154701 sphere radii. The cavity insphere radius for the unit regular tetrahedron is 0.224745 sphere radii. Making the approximation that face and cavity insphere radii control cell imbibition and drainage respectively, the unit regular tetrahedron will therefore exhibit some degree of capillary pressure hysteresis attributable to the difference in insphere radii. This cell-specific, as distinct from network-specific, hysteresis will therefore be overestimated in any calculations based on Mason's (1971) method. Furthermore, estimations of, say, mercury intrusion into a set of cells simulated using Mason's method will always overestimate the frequency of the unit regular tetrahedral face. This latter point may be a problem for workers attempting to reconcile experimental mercury injection of real sphere packings with theoretical models (e.g. Smith and Stermer, 1986).

Having identified the key weaknesses of the Mason simulation, it must be said that the accuracy of the predicted cavity insphere radius frequency distribution is quite remarkable. Mason's (1971) method gives a reasonable estimation of many of the properties of interest in packed beds, and has the advantage of rapid and easy calculation. The joint frequency distributions derived from Mason's method, presented in figures 4.22 to 4.25, compare favourably with those observed for the Finney model presented in figures 3.44 to 3.47. The main conclusions regarding capillary pressure hysteresis for the Finney model arrived at in chapter 3 can also be arrived at using Mason's method which also shows that, in the main, tetrahedral pores drain and fill at approximately the same capillary pressure (Mellor, 1987).

4.6 Discussion and Conclusions

In this chapter the structure of random close packing has been examined from the point of view of a dis-aggregated assembly of simplicial cells. This has enabled progress to be made in measuring the extent to which simplicial cells may be regarded as random. The major conclusion to emerge from the work presented in this chapter is that the simplicial cells of the Finney model are not random, and that they have formed according to some systematic departure from expected random behaviour. This departure is consistent with reducing the frequencies of what might be termed "extreme" simplicial cell forms such as 6LSO and OLS6 in favour of more "average" 3LS3 cells, compared with our expectations. This result in itself is quite remarkable, yet it in turn leads to an even more remarkable result. This is that the often encountered view that random close packing merely converges on the maximum packing density is wrong. A random set of cells (i.e. the control set) also converges on the observed maximum packing density, and yet such a random set fails to achieve two critically important results - they cannot be packed to fill space, and they occupy too large a total volume of space compared with a real set of cells (i.e. the Finney set). An important spin-off result from this work, therefore, is that using packing density as a check on structural validity for a simulation of RCP is not as useful or reliable as the existing literature suggests. Any check involving packing density must therefore be used with caution - a simulation which fails to achieve its target packing density is probably wrong. A simulation which succeeds in achieving its target packing density is not necessarily correct.

The observed frequency distribution of simplicial cell classes presented and discussed in this chapter could form the basis of a new method for validating computer realisations of RCP structure. Since the Finney model has been shown to be non-random at the level of the simplicial cell, this raises the question of the extent to which individual simplicial cells of computer realised models are also non-random. This question is beyond the scope of the present work, but may be of passing interest to some computer simulation specialists in sphere packing.

The work presented in this chapter shows that the individual simplicial cells of the Finney model are non-random. This is a very important result for any research group attempting to model or simulate the pore structure of sphere packings. However, there is a critically important aspect of the structure of the Finney packing which is not considered in the present chapter. This aspect concerns the way in which the simplicial cells of the Finney packing are distributed within the packing itself, and forms the subject of the next Chapter.

CHAPTER 5: RANDOMNESS AT THE NETWORK LEVEL IN THE FINNEY MODEL

5.1 Introduction

Chapter four showed that the individual simplicial cells of the Finney packing depart significantly from random behaviour. This individual non-random aspect of the Finney simplicial cells is wholly irrelevant to the present chapter, in which it is only necessary to distinguish between one cell type and another (e.g. between 4LS2 and 3LS3). The present chapter examines whether the Finney simplicial cells are homogeneously, randomly distributed throughout the packing, or whether certain cell types cluster together in some non-random manner. In order to address this question, use is made of the concept of the network which connects together all the cells of the packing. The problem then reduces to that of forming an expectation of how the cells "ought" to be distributed on the network, and comparing this expected distribution with the observed distribution for the Finney packing. The present chapter, therefore, deals specifically with the simplicial cell network of the Finney model, and the extent to which the distribution of cell types on that network can be said to be random.

There are two fundamental reasons for addressing the issue of network randomness characteristic of the Finney RCP model. The first is to do with percolation theory, and the second is to do with a classical solid state physics problem. Percolation theory was

devised by Broadbent and Hammersley in 1957 as a mathematical tool, aimed at quantifying the flow of fluids in disordered porous media. Within a few years of the original work, the mathematics and physical applications of this theory had expanded considerably (see for example review articles by Frisch and Hammersley, 1963; Shante and Kirkpatrick, 1971; Kirkpatrick, 1973) and are discussed in more detail in the next chapter. The basic concepts of percolation theory in relation to porous materials were reviewed briefly and succinctly in a paper by Mason (1988), in which one of the underlying assumptions of the theory was highlighted. This assumption is that the distribution of pores on the network is <u>random</u>. The assumption is <u>absolutely central</u> to any application of the theory, and yet owing to the complexity of the task no detailed analysis of the network of a real, disordered porous medium had been undertaken until the present work.

The issue of network randomness in RCP structure represents one feature of an old problem in solid state physics, known variously as the crystallite hypothesis (Bartenev, 1970), the significant structure theory (Walter and Eyring, 1941 ; Eyring and Jhon, 1969) and the paracrystalline model (Hosemann and Bagchi, 1962). This problem is well reviewed in Ziman (1982), and is summarised briefly here.

The various theories of the paracrystalline state differ in detail, but all require the existence of pseudo- or semi- crystalline regions of RCP space comprising localised clusters of <u>ordered</u> material (spheres). In terms of simplicial cell classes defined in chapter four such clusters must show up as localised groups of cells

of the same type. For example, suppose the clustering material were the perfect, regular unit-edgelength tetrahedron. This would be identified as a OLS6 cell, and clustering would be evident as higher than expected occurrences of OLS6 cells sharing faces in common with other OLS6 cells. Because chapter 4 has shown that both expected frequencies and observed frequencies of cell classes are symmetrical when S = 0.5 (i.e. $E_0 = E_6$, $O_0 = O_6$ etc), a clustering of OLS6 cells would also produce a requirement for 6LSO complementary cells to either cluster together, or to be in any event distinctly <u>non-randomly allocated to the network</u>.

In its day, the paracrystalline theories of the solid state were considered to be powerful arguments for a particular view of amorphous solids. Today, however, the paracrystalline model of amorphous solids is not accepted as a valid model of disordered solids in general (Ziman, 1982). Until the present work, no rigorous attempt to establish whether the Finney RCP model consists of clusters (paracrystals) or homogeneously, randomly distributed cells had been undertaken.

In order to begin to analyse the network of 14870 simplicial cells of the Finney model, some additional concepts are required.

5.2 Fundamental Concepts

The overall aim of this chapter is to examine the extent to which the simplicial cells (pores) of the Finney model are randomly distributed on the network which connects them. In order to do this it is essential to have a clear understanding of what the network

is. It is also essential to be able to make simple "measurements" of cell distribution on the network, and to compare the results of these "measurements" with predictions made from a theory. The theory, of course, should encapsulate the essence of the kind of randomness we believe to be important to consider, as well as being logical and defensible. In chapter four we saw that, because there is no established terminology or method for measuring randomness in RCP structure, some terminology had to be invented in order to progress. This terminology is developed further in sections 5.2.1 to 5.2.7.

5.2.1 The network

The concept of representing a porous medium as a network has become extremely well established in the literature since the pioneering work of Fatt (1956). All networks have two fundamental components, namely structure and decoration. The structure of a network is its overall geometrical and topological configuration. For example the two dimensional network models used by Shante and Kirkpatrick (1971) consist of squares, triangles and other simple geometrical structures as shown in figure 5.1. The decoration of a network is the process of distributing dimensions of pores to the network structure. This decoration process is totally independent of the network structure itself, and is a two stage process. The network structure may be regarded as consisting of bonds and sites. A bond is no more than an individual straight line segment from figure 5.1, whilst a site is a point of intersection of bonds. Thus the sites in figure 5.1 (b) consist of intersections of 6 bonds, sites in

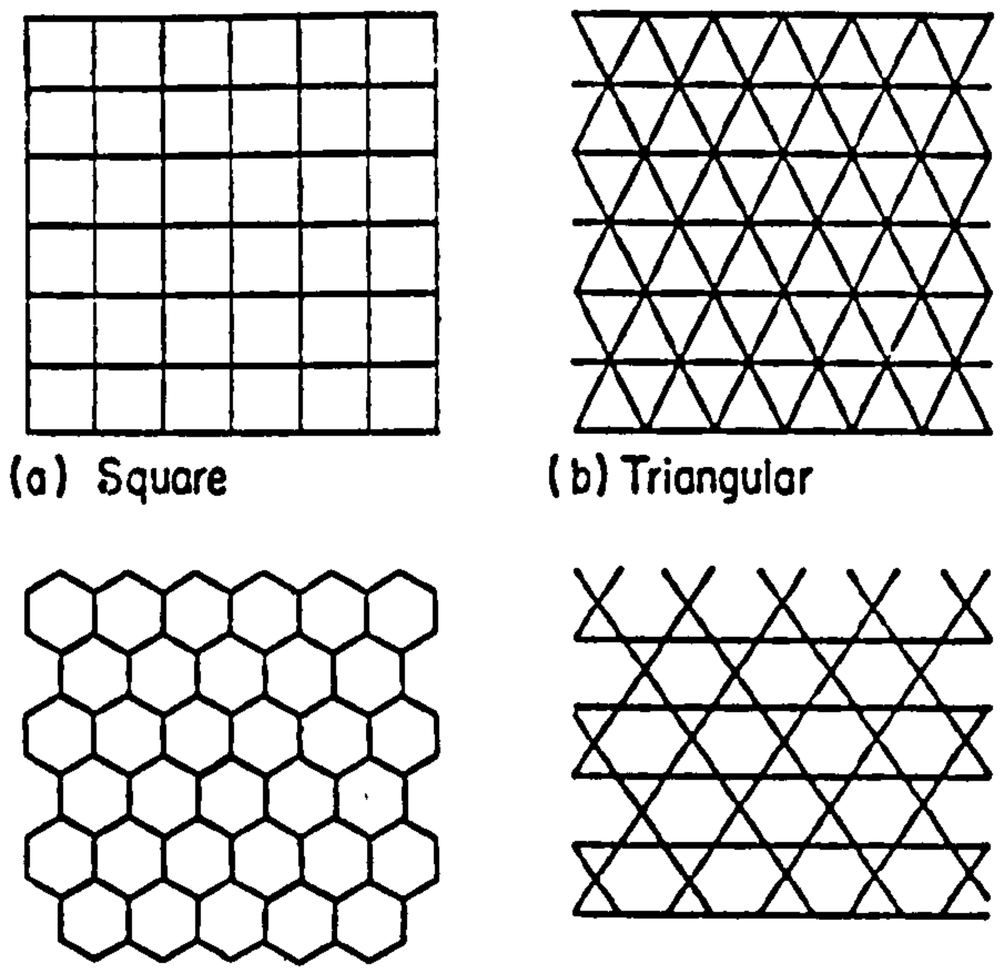

Figure 5.1 : Two dimensional network models.

(after Shante and Kirkpatrick, 1971).

figure 5.1 (a) consist of intersections of 4 bonds and sites in figure 5.1 (c) consist of intersections of 3 bonds. The two stages of decoration, therefore are firstly to decide upon the physical meaning of the bonds and sites, and secondly to distribute dimensions to the bonds and sites. For example, it may be decided that sites represent pore bodies, whilst bonds represent the connecting links (throats) between these bodies. Distribution of dimensions might then proceed according to some particular preference or theory.

For many (almost certainly the majority of) networks in the literature relevant to the study of porous media both the structure and the decoration are arbitrary processes. However the <u>structure</u> of the network of the Finney model considered in the present work is not arbitrary - it is an absolute and immutable property of the Finney RCP model. The Finney simplicial cell network is defined

absolutely by two factors. The first of these is the set of spatial co-ordinates of the sphere centres, and the second factor is the decision to analyse the packing in terms of its component simplicial cells. Once the packing has been divided up into its component simplicial cells, therefore, the network is automatically defined and available. In order to describe the structure of the entire network, a relatively large data file is required. The organisation and validation of this data file is described in detail in section 5.4.1, but in general terms it is no more than a long list of cell identities. This list identifes which simplicial cells any given (reference) simplicial cell communicates directly with. Since all simplicial cells in the network are tetrahedra with four faces, each cell has four neighbours. A cell and one of its four neighbours occupy adjacent regions of space, and share one face in common as shown in figure 5.2. The faces of the cells, therefore, may be thought of as important features of the network itself. It will become apparent later on in this chapter just how critical the cell faces are to understanding the network structure of the Finney RCP model.

5.2.2 Finite size limitations - surface cells

The network we are dealing with in the present work connects together 14870 simplicial cells. The majority of these cells are likely to be entirely within the packing, and each of these cells will have four immediate neighbour cells. The external surface of the packing, however, will contain a number of cells which connect only with three neighbouring cells - the fourth face being "exposed" in the outer surface of the packing itself. The convention

(i)

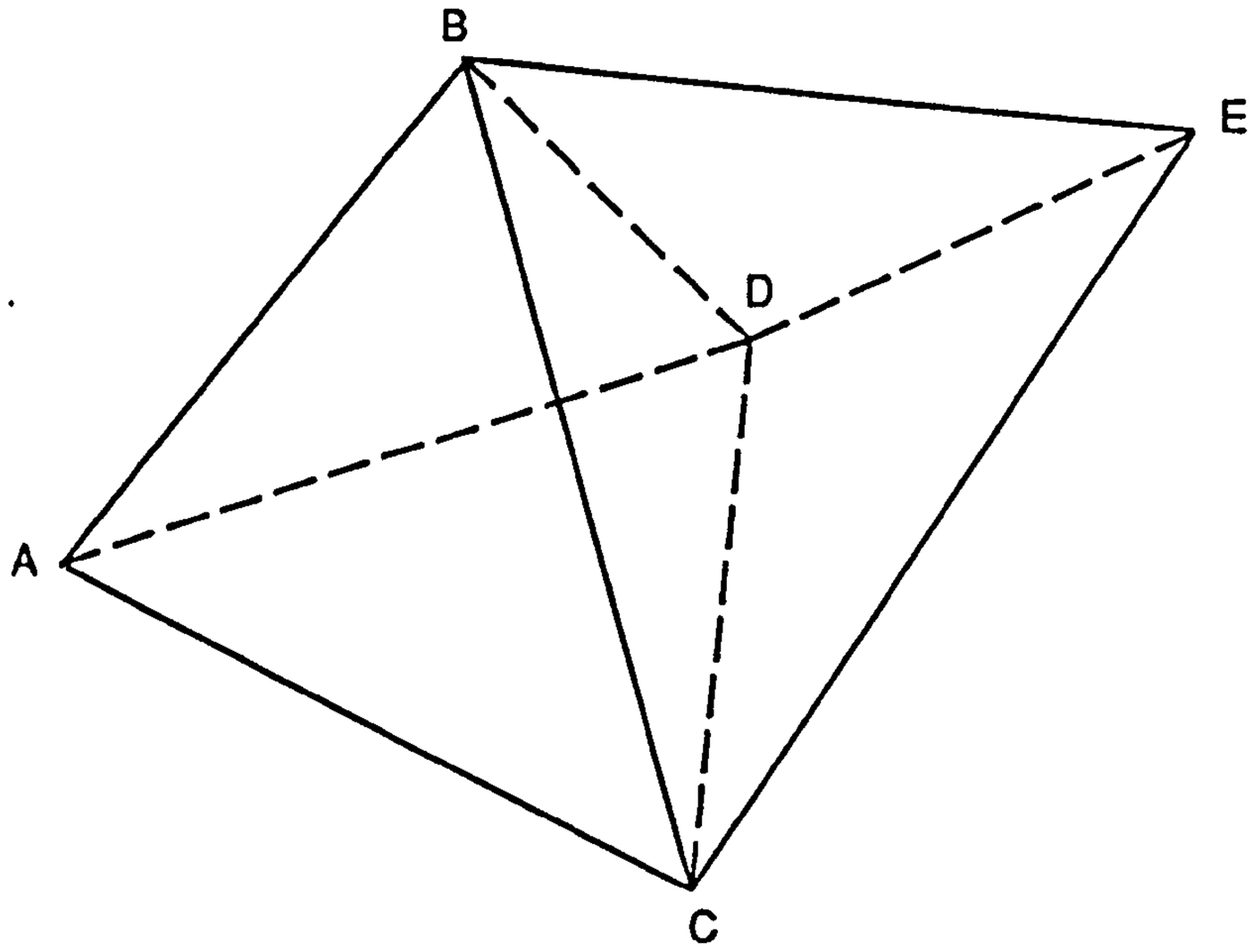

(ii)

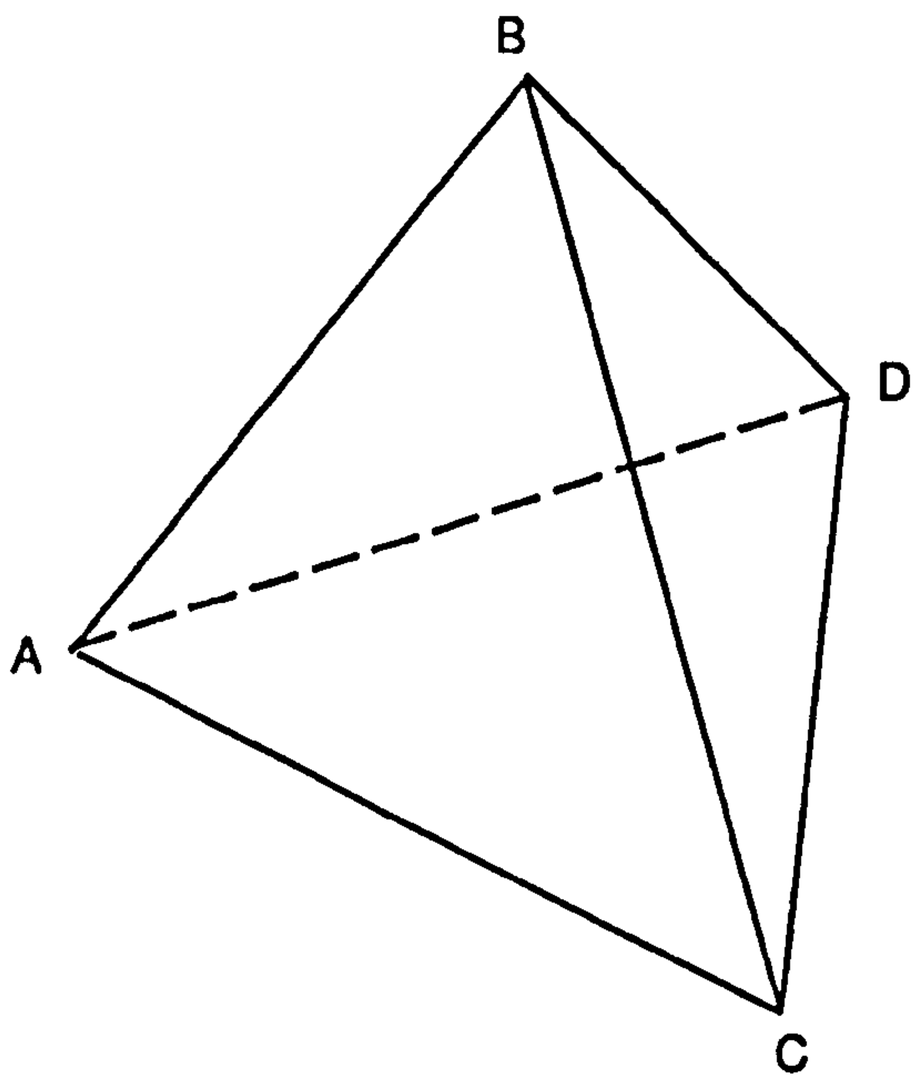

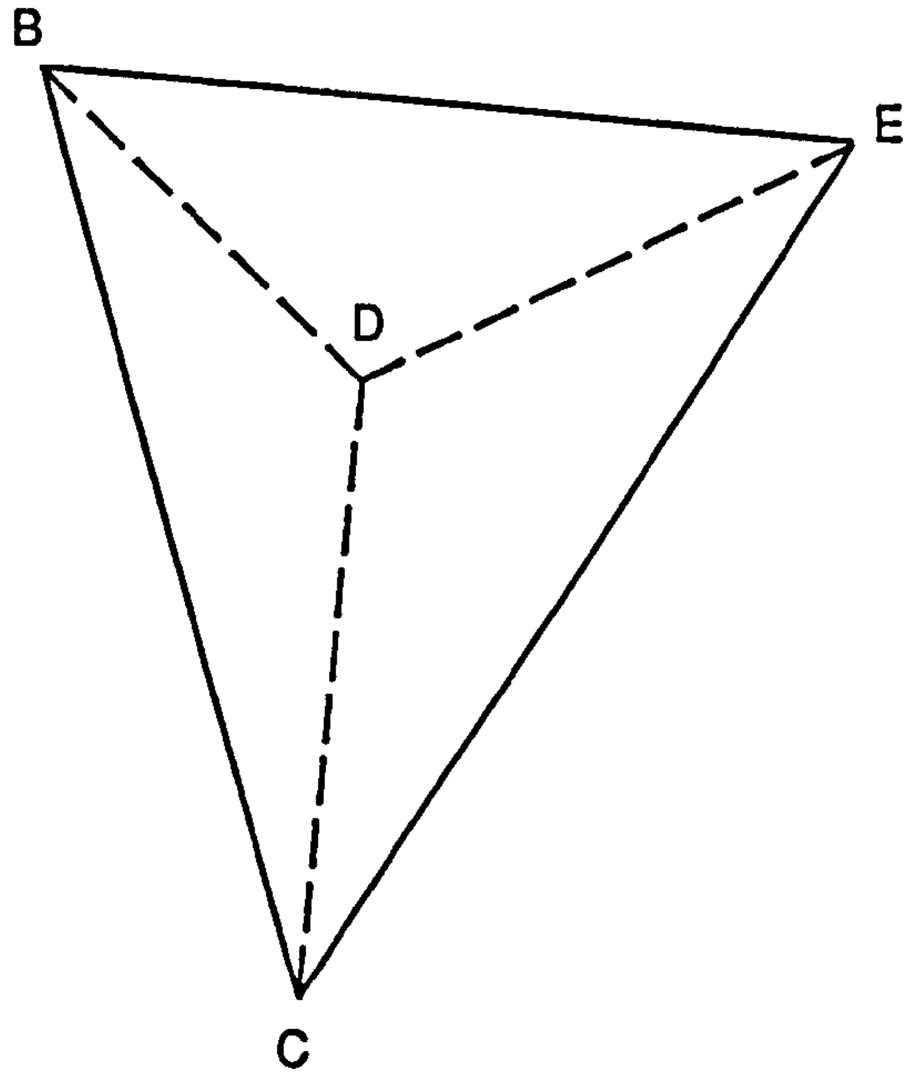

Figure 5.2 : TWO NEIGHBOURING SIMPLICIAL CELLS ABCD AND BCDE SHOWING :
(i) SHARING THE COMMON FACE BCD and
(ii) SEPARATED TO SHOW THE INDIVIDUAL CELLS

adopted in the present work is that each simplicial cell is identified by an integer number in the range (1,14870). Cell identity zero is therefore not allocated to any real individual simplicial cell. This identity is instead reserved for what might be termed "undifferentiated space" which is deemed to surround the 14870 cells we are concerned with. Any cell number with cell zero as a neighbour is therefore by convention on the outer surface of the packing and has only three (real) simplicial cell neighbours. There is a tangible benefit arising from this convention. Cell zero can be considered to be "filled" with a fluid which then effectively surrounds the entire packing and communicates immediately with all the surface cells. This concept facilitates fluid displacement calculations and is developed more fully in chapter 6. The frequency of surface occurring cells becomes important in the prediction of cell-cell distributions. This importance is discussed more fully in section 5.4.1.

5.2.3 Face Forms

Each simplicial cell in the network shares either three or four faces with other simplicial cells in the network. Given that the aim of this work is to establish whether or not the network structure is random, it is important to be able to differentiate between different types, or forms of face. The approach adopted here is compatible with that developed to describe the seven classes of simplicial cells (i.e. 0LS6 to 6LS0). Since each face is a triangle, and each edge of the triangle can be in either state 'L' or 'S', there are four mutually exclusive face forms. These are 0LS3, 1LS2, 2LS1 and 3LS0. Note that there is no confusion with

simplicial cell classes, since the total number of edges in a face form adds up to three, whilst the total number of edges for a cell is six.

5.2.4 Cell-Face Distribution [P]

The common terminology adopted for both cells and faces makes it immediately apparent that there are some combinations of cells and faces which cannot exist. A 6LS0 cell, for example, can only exist with 3LS0 faces. The full range of permitted and prohibited combinations for faces and cells is shown in table 5.1.

SIMPLICIAL CELL CLASS \ FACE FORM	0LS3	1LS2	2LS1	3LS0
0LS6	✓	✗	✗	✗
1LS5	✓	✓	✗	✗
2LS4	✓	✓	✓	✗
3LS3	✓	✓	✓	✓
4LS2	✗	✓	✓	✓
5LS1	✗	✗	✓	✓
6LS0	✗	✗	✗	✓

✓ = Permitted
✗ = Prohibited

Table 5.1 : Relationship between simplicial cell class and face form.

Out of the total of 28 possible cell-face combinations, 12 are prohibited. Interestingly, the least frequently observed cells (i.e. OLS6 and 6LSO) are the most restricted in network structure scope; each have only one permitted face form for sharing. In contrast the most frequently observed cell class, the 3LS3, can have any of the four possible face forms. This observation of permitted and prohibited combinations of cell class and face form suggests that the actual frequency with which a particular cell class occurs with a particular cell face may be useful in understanding the structure of the network. This distribution of frequencies is called the cell-face joint frequency distribution, [P], and is a 7 x 4 element matrix.

It is important to remember that [P] is an intrinsic property of a dis-assembled group of simplicial cells. The joint frequency distribution [P] therefore carries no information whatsoever regarding any actual or real organisation of network structure. Our hope is that we may be able to use [P] as the basis of a definition and prediction of what a random network structure might be like. This in turn should permit a comparison to be made between our prediction based on [P] and an observation of the real Finney model network structure. To prove the point that [P] does not "contain" information about network structure, consider the simulation of 10^6 simplicial cells by Mason's method described in chapter 4. Each of those cells could easily be analysed to provide its cell class, and its four face forms. This procedure would undoubtedly lead to a perfectly valid cell-face joint frequency distribution, [P], for the Mason model. However, the group of 10^6 cells has no network, and the individual cells cannot be "fitted together" to fill space.

Numbering the elements of the matrix [P] from 0,0 instead of from 1,1 affords a particular convenience in notation. The matrix element number then becomes identical to the number of state 'L' edges in the face or cell. For example, the numerical value of $P_{2,0}$ is the frequency with which 2LS4 simplicial cells are observed to have 0LS3 faces. The form of the matrix [P] is illustrated in table 5.2, note that the matrix is not symmetrical, values for j (face) and i (cell) are not interchangeable.

		FACE FORM			
		j = 0 0LS3	j = 1 1LS2	j = 2 2LS1	j = 3 3LS0
SIMPLICIAL CELL CLASS	i = 0 0LS6	0,0	(0,1)	(0,2)	(0,3)
	i = 1 1LS5	1,0	1,1	(1,2)	(1,3)
	i = 2 2LS4	2,0	2,1	2,2	(2,3)
	i = 3 3LS3	3,0	3,1	3,2	3,3
	i = 4 4LS2	(4,0)	4,1	4,2	4,3
	i = 5 5LS1	(5,0)	(5,1)	5,2	5,3
	i = 6 6LS0	(6,0)	(6,1)	(6,2)	6,3

Note : () indicates zero value elements of prohibited combinations.

Table 5.2 : The cell-face distribution matrix [P] showing the relationship between element number and number of 'L' state edges.

5.2.5 Cell-Cell Distribution, [N]

The cell-cell distribution is the joint frequency distribution for which a particular cell class occurs as an immediate neighbour to another particular cell class. This distribution might also be called the cell neighbour distribution. This distribution is an intrinsic property of the network structure, and as such it represents a complete summary of the distribution of cells relative to each other within the network, and is a direct measure of any tendency towards cell clustering. Since there are seven classes of simplicial cell, [N] is a 7 x 7 matrix.

As with the cell-face distribution, there is an advantage of convenience in numbering the elements of the matrix [N] from 0,0 instead of from 1,1. The matrix element numbers then become identical to the numbers of state 'L' edges in the reference cell and neighbouring cell. For example, the numerical value of $N_{5,6}$ is the observed frequency with which 5LS1 simplicial cells are observed to have 6LS0 simplicial cells as neighbours. The matrix [N] is illustrated in table 5.3. Clearly, [N] must be symmetrical about its diagonal elements,

$$\text{i.e. } N_{3,5} = N_{5,3} \text{ etc.}$$

Prohibited combinations (e.g. $N_{1,6}$) occur in [N] as zero values.

5.2.6 Isomerism

Before beginning a detailed examination of the methods used to detect the presence or absence of cell clustering, one further concept is required - that of isomerism. The term isomer is used in

		SIMPLICIAL CELL CLASS						
		j = 0	j = 1	j = 2	j = 3	j = 4	j = 5	j = 6
		0LS6	1LS5	2LS4	3LS3	4LS2	5LS1	6LS0
SIMPLICIAL CELL CLASS	i=0 0LS6	0,0	0,1	0,2	0,3	(0,4)	(0,5)	(0,6)
	i=1 1LS5	1,0	1,1	1,2	1,3	1,4	(1,5)	(1,6)
	i=2 2LS4	2,0	2,1	2,2	2,3	2,4	2,5	(2,6)
	i=3 3LS3	3,0	3,1	3,2	3,3	3,4	3,5	3,6
	i=4 4LS2	(4,0)	4,1	4,2	4,3	4,4	4,5	4,6
	i=5 5LS1	(5,0)	(5,1)	5,2	5,3	5,4	5,5	5,6
	i=6 6LS0	(6,0)	(6,1)	(6,2)	6,3	6,4	6,5	6,6

Note : () indicates zero value elements of prohibited combinations.

Table 5.3 : The cell-cell distribution matrix [N] showing the relationship between element number and number of 'L' state edges.

the present work to indicate a specific variant of simplicial cell form. An isomer of a simplicial cell is analagous to an isomer of a chemical species, in that there may be more than one way of putting together the same component parts (i.e. cell edgelengths). For example, if we are given six state 'S' edgelengths, we can make a 0LS6 simplicial cell - however, any individual form we make is the same as any other. Now, supposing we are given four state 'S' edgelengths and two state 'L' edgelengths in order to make a 2LS4 cell. This time, it is possible to construct two structurally discrete forms, or isomers, of the 2LS4 cell. One of these isomers is arranged such that the two long edges join at an apex, forming one of the twelve face angles of the cell as shown in figure 5.3(a).

The other isomer is arranged such that the two long edges never join together at an apex, and never occur in the same face as shown in figure 5.3(b). The significance of this is that the four faces of each of the two isomeric forms are quite different. If the first isomer is identified as alpha (being, as we shall see, the most probable of the two), and the second as beta, the resulting face forms are as shown in table 5.4.

The significance of isomeric forms in terms of the simplicial cell network is profound. For example, a 2LS4 alpha cell can have cell neighbours sharing on 2LS1, 1LS2 and OLS3 faces. These faces make it possible to share with 5LS1, 4LS2, 3LS3, 2LS4, 1LS5 and OLS6 simplicial cells - in other words with 6 of the 7 possible simplicial cells. In contrast to this, however, a 2LS4 beta form can only have simplicial cell neighbours sharing on 1LS2 faces as shown in table 5.4. These neighbours can include 4LS2, 3LS3, 2LS4 and 1LS5 simplicial cells only - 4 out of 7 possible simplicial cells. Thus the 5LS1 and OLS6 simplicial cells are permitted neighbours to the 2LS4 alpha isomer, but not to the 2LS4 beta isomer.

The face forms for each isomer are constant and invariant. All 2LS4 alpha isomers therefore always have precisely 1 2LS1 face, 2 1LS2 faces and 1 OLS3 face per simplicial cell. All 2LS4 beta isomers have exactly 4 1LS2 faces. The full range of isomers, together with their invariant face frequencies is given in figure 5.4.

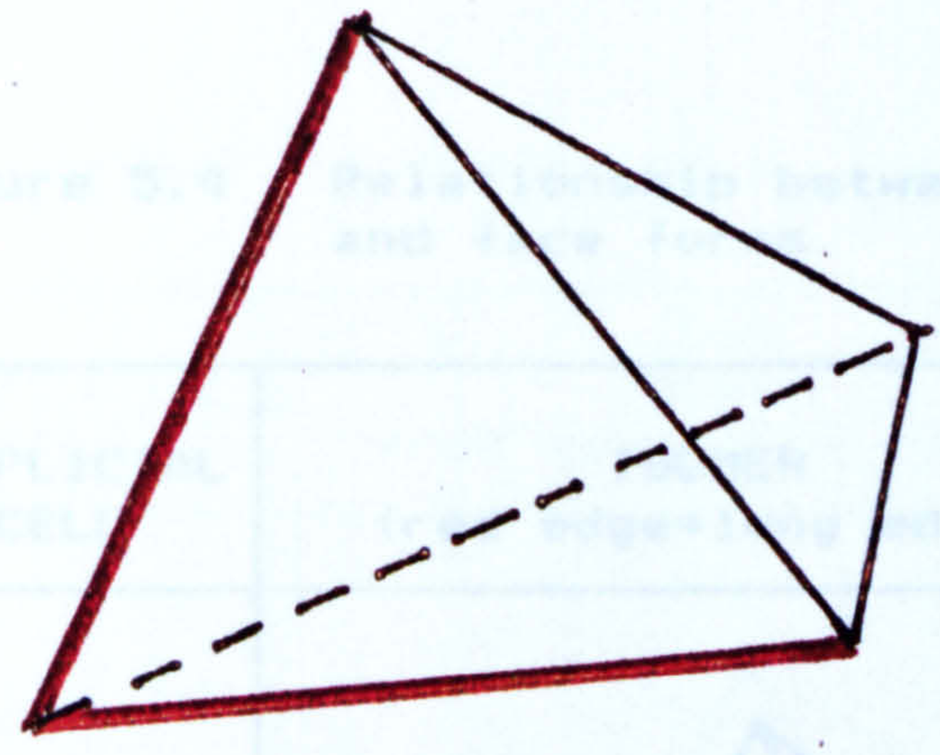

(a)

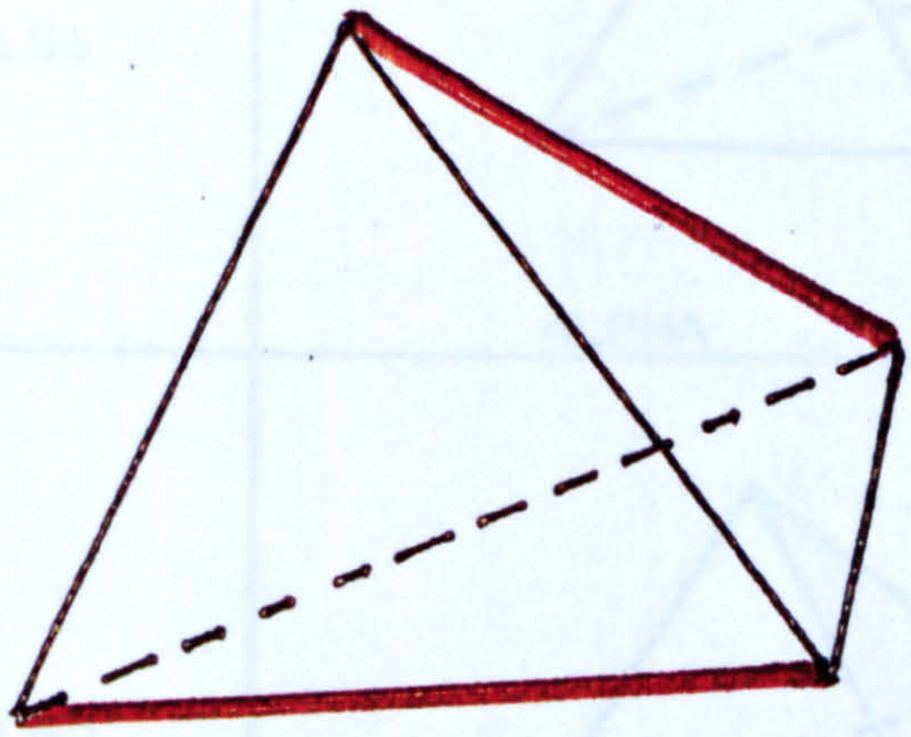

(b)

(Red edge = Long edge)

Figure 5.3 : The 2LS4 simplicial cell showing,
(a) the alpha isomer, (b) the beta isomer

ISOMER	FACE FORM FREQUENCY			
	3LS0	2LS1	1LS2	0LS3
2LS4 α	0	1	2	1
2LS4 β	0	0	4	0

Table 5.4 : Isomeric forms of the 2LS4 simplicial cell.

Figure 5.4 : Relationship between simplicial cell isomers and face forms.

SIMPLICIAL CELL	ISOMER (red edge=long edge)	FIXED FACE FREQUENCY
0LS6	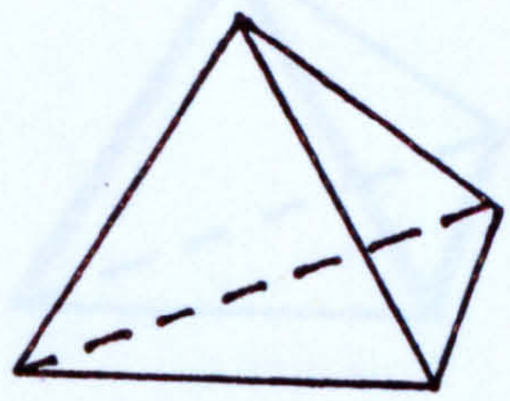 ALPHA	0LS3 1.0
1LS5	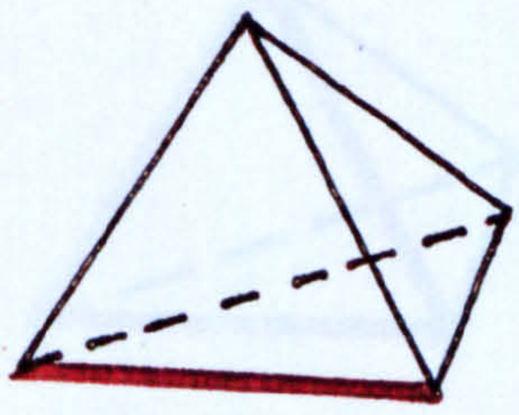 ALPHA	1LS2 0.5 0LS3 0.5
2LS4	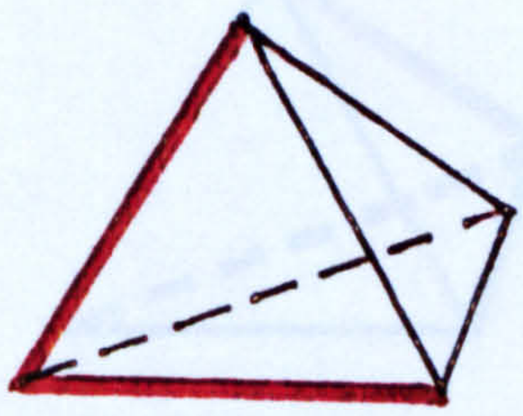 ALPHA	2LS1 0.25 1LS2 0.5 0LS3 0.25
	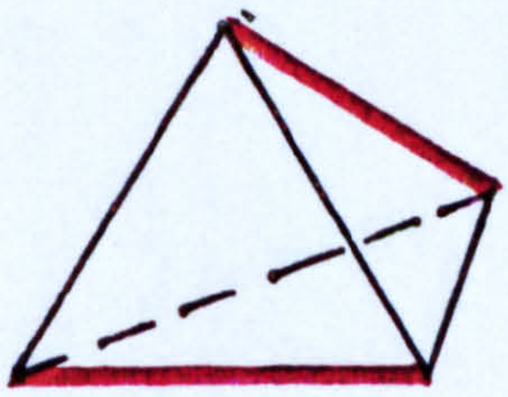 BETA	1LS2 1.0

Figure 5.4 : (continued)

SIMPLICIAL CELL	ISOMER (red edge=long edge)	FIXED FACE FREQUENCY
3LS3	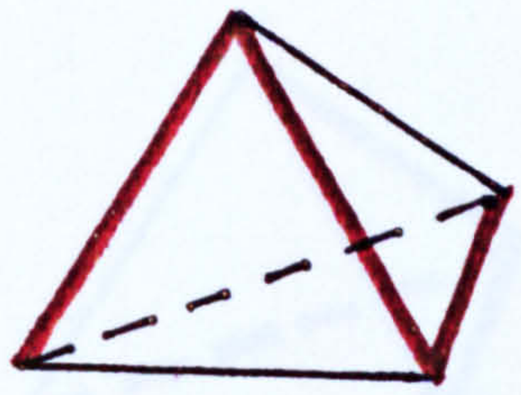 ALPHA	2LS1 0.5 1LS2 0.5
	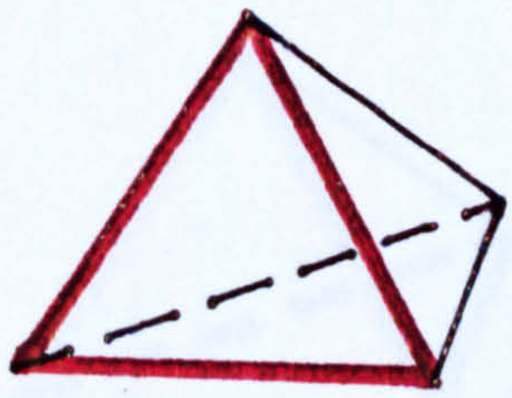 BETA	3LS0 0.25 2LS1 0 1LS2 0.75
	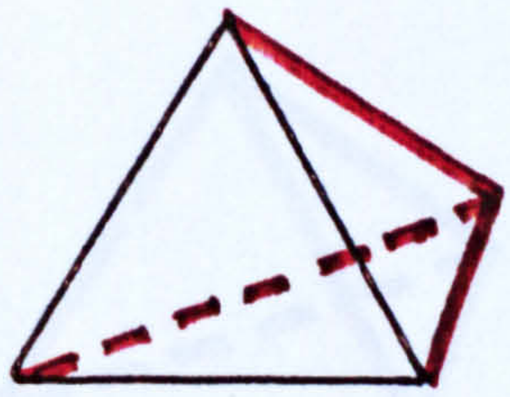 GAMMA	2LS1 0.75 1LS2 0 0LS3 0.25

Figure 5.4 : (continued)

SIMPLICIAL CELL	ISOMER (red edge=long edge)	FIXED FACE FREQUENCY
4LS2	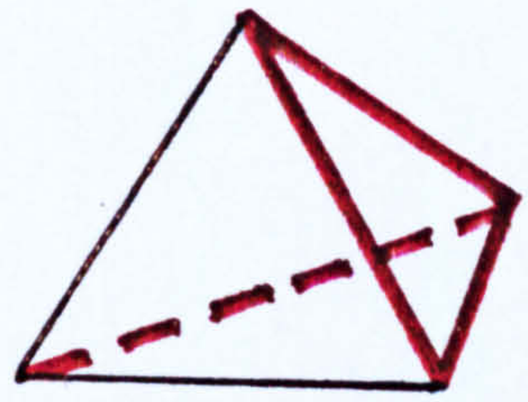 ALPHA	3LS0 0.25 2LS1 0.5 1LS2 0.25
	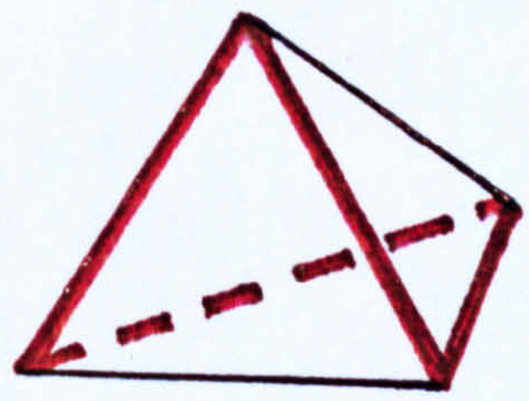 BETA	2LS1 1.0
5LS1	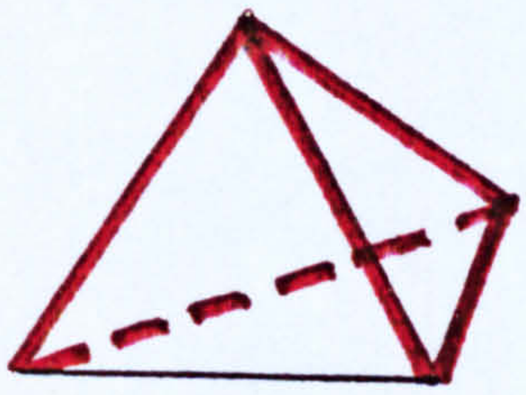 ALPHA	3LS0 0.5 2LS1 0.5
6LS0	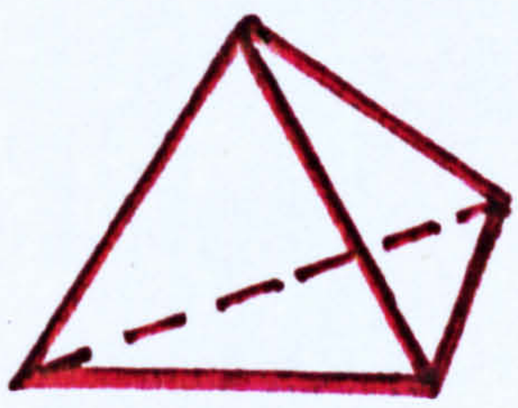 ALPHA	3LS0 1.0

5.3 Network Data File

This section describes the data file which contains, or represents, the network which connects the 14870 simplicial cells of the Finney RCP model.

5.3.1 Construction and Format

The most convenient form for the network is that of a simple look-up table. Each of the 14870 simplicial cells is uniquely defined in the present work by an integer number in the interval (1,14870). The network can therefore be represented as a list of cell numbers which can be accessed directly from each individual cell. For example, cell number one happens to be quite close to the centre of the packing, and its four immediate neighbouring cells are numbers, 2, 5, 8 and 25. Similarly, the immediate neighbours of cell number two are cell numbers 1, 7, 10 and 26. The look-up table could therefore be organised to look like the following list:

Reference Cell	Neighbouring Cells
1	2, 5, 8, 25
2	1, 7, 10, 26
3	4, 6, 11, 29
4	3, 5, 12, 27
5	1, 4, 14, 27
6	3, 7, 15, 33

This approach pre-supposes that each cell has four neighbouring cells. As discussed in section 5.2.2, some cells will occur on the outer surface of the packing. Such cells will have only three, and not four neighbouring cells. The format adopted in the present work, therefore, is to construct a network look-up table with the following format:

Reference Cell	Number of Neighbouring cells	Identity of Neighbouring cells
1	4	2, 5, 8, 25
2	4	1, 7, 10, 26
3	4	4, 6, 11, 29
4	4	3, 5, 12, 27
5	4	1, 4, 14, 27
6	4	3, 7, 15, 33

- where the number of neighbouring cells is found to be three, the undifferentiated space outside the packing is identified as cell zero, as discussed in section 5.2.2.

Programe NET1 was written to output the network in the above look-up table format. The program uses the simplicial cell identity file, NEWFILE3.DAT, as primary input. This input file contains the identities of the four component spheres which define individual simplicial cells. The first five lines of NEWFILE3.DAT are:

1, 2, 3, 5

1, 2, 3, 9

1, 2, 4, 6

1, 2, 4, 8

1, 2, 5, 8

Thus simplicial cell number one is defined by sphere numbers, 1, 2, 3 and 5, simplicial cell number two is defined by sphere numbers, 1, 2, 3 and 9 and so on. Program NET1 determines the network look-up table by testing all possible neighbouring cells (i.e. the 14869 other cells) for the presence of any one of the four faces of the reference cell. For example, simplicial cell number one has its four faces defined as follows:

sphere numbers 1, 2 and 3 define one face,

sphere numbers 1, 2 and 5 define another face,

sphere numbers 1, 3 and 5 define a third face,

whilst

sphere numbers 2, 3 and 5 define the last face.

By inspection of the first five lines of NEWFILE3.DAT above, it is clear that simplicial cell number two is a neighbour of cell number one since spheres 1, 2 and 3 are common to both simplicial cells one and two. It is also clear that simplicial cells three and four are not neighbours to simplicial cell one, since neither cells three nor four have three defining spheres in common with cell one. Simplicial cell number five, however, is a neighbour to cell number

one because spheres 1, 2 and 5 are common to both simplicial cells one and five. This logical procedure is employed until either four neighbouring cells have been identified, or until all 14869 possible neighbouring cells have been examined. Although this procedure is relatively simple, and is reduced to a few lines of code in program NET1, it is very heavy in computing time. Thus program NET1 took 13.6 cpu hours of run time to execute. No attempt was made to optimise the code for computing efficiency, as this was not an objective of the work. The code was run only once, and was written so that all output data is preserved in the event of a fatal run-time error (crash).

5.3.2 Error checking and validation

Because the network is an absolute topological property of the packing, it is essential to ensure that there are no errors in the network produced by program NET1. From the subdivision verification work reported in section 3.3.2 of this thesis it is clear that there is an error in the original subdivision performed by Wright (1987). In section 3.3.2 this error was isolated as a malfunction in the subdivision of space surrouding sphere number 2000. It seems reasonable to suppose, that program NET1 may crash (i.e. suffer a fatal error leading to termination of run-time) when dealing with certain simplicial cells in which sphere number 2000 occurs. This crash indeed happened when NET1 attempted to identify neighbours to simplicial cell number 14865 which has sphere number 2000 as one of its four apices. In order to complete the network look-up table output by NET1, the neighbours to the last six simplicial cells in the list (i.e. 14865 to 14870) were determined manually by inspection of datafile NEWFILE3.DAT. The manually completed network

look-up data file output by program NET1 is called NET1.DAT.

In order to be validated, NET1.DAT must pass certain fundamental tests. The first of these is that each simplicial cell can only have either 3 or 4 neighbouring simplicial cells. Thus any cell in NET1.DAT which claims to have 0, 1, 2, 5, 6 or other numbers of neighbours represents a significant error in the network. No such errors were detected. The second, and final test of the network is that each of the neighbouring cells for any given reference cell must in turn cite that reference cell as one of its own neighbouring cells. In other words, each individual cell must point to its neighbours, and its neighbours must point back to that individual cell. When this test was executed on NET1.DAT, three cells were identified as violators of this rule. These cells were 4240, 4241 and 4779. Each of these three cells has four neighbouring cells, and program NET1 had correctly identified the first three of the four neighbours for each of them. Each of three cells however, showed "impossible" references back from the fourth declared neighbour. The repairs to the network were performed manually by inspection and editing of the datafile NET1.DAT, and were relatively straightforward to complete successfully. The repaired network was called WRINED.DAT in order to differentiate it from NET1.DAT (WRINED derived from WRIght Network EDitted).

The data file WRINED.DAT is the network which connects all 14870 simplicial cells of the Finney model and contains the identity of neighbouring simplicial cells in simple look-up table form. This data file is fully validated and error-checked, and contains no

logical errors. It is interesting to note that had the frequency of errors in the network been significantly greater, say more than twenty cells affected, then manual repairs to the network would have been very time consuming and difficult to complete. This suggests that the initial subdivision of RCP space calculations should be performed at the highest level of machine precision available, and in any event not less than double-precision, in order to reduce the frequency of subdivision errors.

5.4 Network Analysis

5.4.1 Surface occurring cells

Because the packing of 14870 simplicial cells is finite, a number of cells occur on the outer surface of the packing. These surface occurring cells have only 3, and not 4, neighbouring cells as discussed in section 5.2.2. By counting the number of cells with cell zero as a neighbour, the frequency of surface occurring cells shown in table 5.5 was observed for the Finney packing.

The total number of triangular faces of simplicial cells available for sharing within the packing is 57,522:

$$\text{Total Faces shared} = [(14870 - 1958) \times 4] + (1958 \times 3)$$

$$= 57,522.$$

It is interesting to note from table 5.5 that the average fraction

of cells with a face exposed on the surface of the packing is 13.2%. All seven simplicial cell classes appear to be roughly homogeneously distributed within the surface of the packing. This result tends to suggest that there is no strong tendency for clustering, and that the network is homogeneously random. However, this should be regarded only as circumstantial evidence in favour of a homogeneously random network. More conclusive evidence is presented in section 5.5.

SIMPLICIAL CELL TYPE	TOTAL NUMBER OF CELLS OBSERVED	NUMBER OF CELLS OCCURRING AT PACK SURFACE	FRACTION OF SURFACE CELLS
0LS6	56	8	0.143
1LS5	785	106	0.135
2LS4	3496	464	0.133
3LS3	6107	794	0.130
4LS2	3653	485	0.133
5LS1	719	96	0.134
6LS0	54	5	0.093
TOTALS	14870	1958	0.132

Table 5.5 : Observed frequencies of surface occurring simplicial cells in the Finney model. (X_T = 1.01229, s = 0.50012)

5.4.2 Cell-Face Distribution [P]

In order to measure the real cell-face joint frequency distribution, [P], a threshold edgelength criterion (X_T) must first be established as discussed in Chapter 4. The value of X_T used was $X_T = 1.01229$, consistent with the work presented in chapter 4. The procedure used to measure [P] is fairly straightforward, and is summarised in flow diagram form in figure 5.5. The logic summarised in figure 5.5 is encoded in program P, presented in Appendix 'B' to this thesis. This program interrogates four data files:

WRINED.DAT - the network data file.

NEWFILE3.DAT - the file which contains the identities of the four spheres defining each of the 14870 simplicial cells.

NEWFILE5.DAT - the file which contains the sphere-centre co-ordinates of the individual spheres, and

TYPE.DAT - a file which lists each simplicial cell by number and cell class for the threshold conditions $X_T = 1.01229$.

All four data files are described in Appendix 'B' to this thesis. The resulting joint frequency distribution [P] is shown in table 5.6. As already recorded, the observed matrix [P] sums to 57,522. In section 5.6 we shall see how we can use [P] to estimate [N] and determine how random is the distribution of cell types on the network of the Finney model.

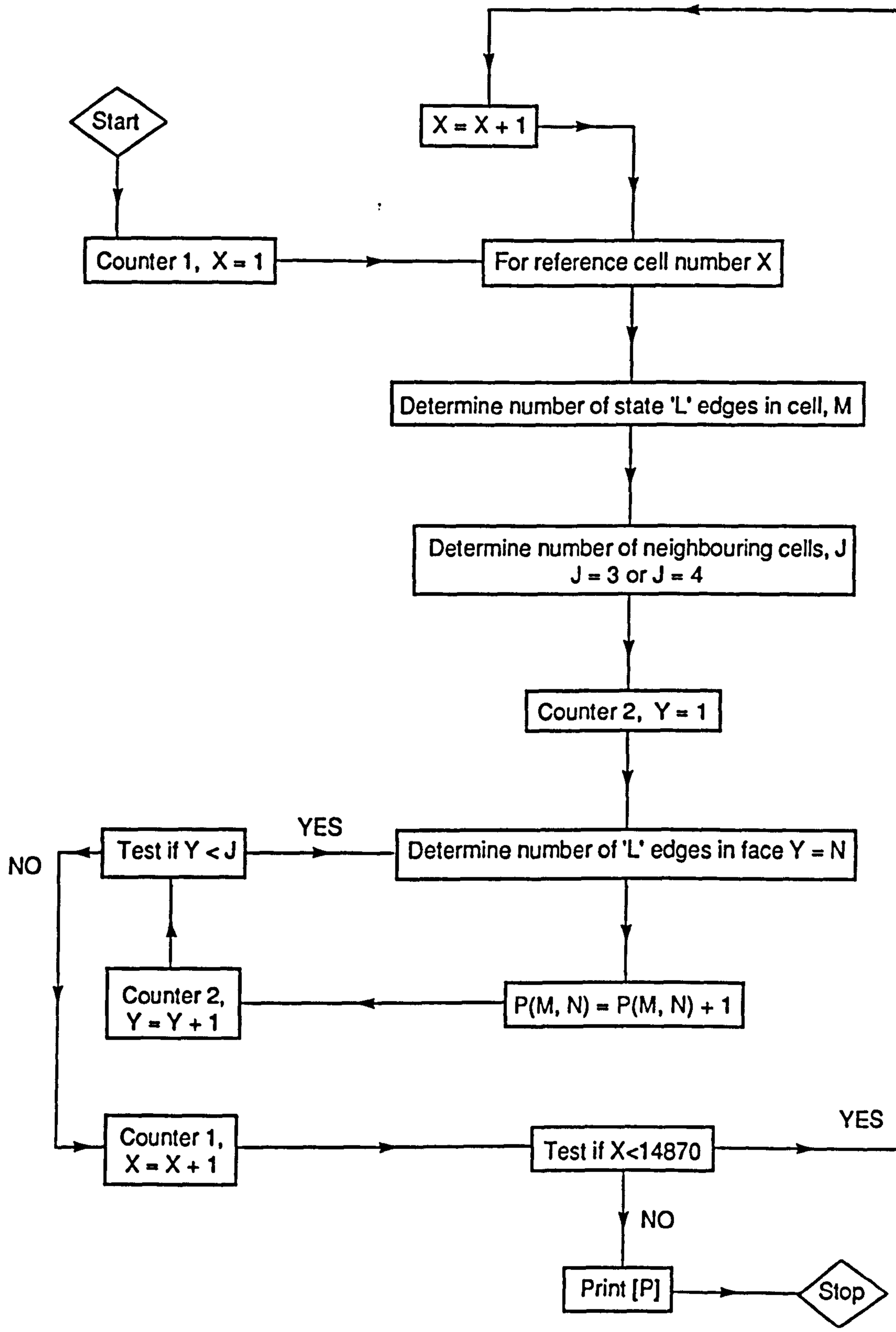

Figure 5.5 : FLOW DIAGRAM FOR MEASUREMENT OF [P]

	j = 0	j = 1	j = 2	j = 3
	0LS3	1LS2	2LS1	3LS0
i = 0 0LS6	216	0	0	0
i = 1 1LS5	1511	1523	0	0
i = 2 2LS4	2252	8982	2286	0
i = 3 3LS3	627	11356	10736	915
i = 4 4LS2	0	2379	9330	2418
i = 5 5LS1	0	0	1378	1402
i = 6 6LS0	0	0	0	211

Table 5.6 : Fully observed cell-face joint frequency distribution [P] for the Finney packing obtained using program P_o.

(Note : $\sum_{i=0}^{6}\sum_{j=0}^{3} P_{ij} = 57522$)

(X_T = 1.01229, s = 0.50012)

5.4.3 Cell-Cell Distribution [N]

The joint frequency distribution [N] for the Finney packing is readily obtained by interrogating the network data file WRINED.DAT and the cell class file TYPE.DAT. The distribution [N] was obtained using the seven programs NEIGH-0 to NEIGH-6 presented in Appendix 'B' to this thesis. The results are presented in table 5.7 which constitutes a complete summary of the network structure which connects all 14870 simplicial cells of the Finney packing.

If there is evidence for clustering of any particular cell class, or if one cell class consistently neighbours preferentially with another specific cell class, then this information is entirely contained in matrix [N] in table 5.7. What we need to be able to do in order to extract this information is to make a statistically valid prediction of what [N] should look like if the network structure is perfectly and homogeneously random. A comparison of our predicted distribution, [N'], with the observed distribution, [N], will then reveal the degree to which the network structure of the Finney model may be regarded as random. This prediction and comparison procedure is discussed in the next section.

	j = 0 0LS6	j = 1 1LS5	j = 2 2LS4	j = 3 3LS3	j = 4 4LS2	j = 5 5LS1	j = 6 6LS0
i=0 0LS6	12	69	107	28	-	-	-
i=1 1LS5	69	612	1320	892	141	-	-
i=2 2LS4	107	1320	4730	5396	1822	145	-
i=3 3LS3	28	892	5396	10501	5804	944	68
i=4 4LS2	-	141	1822	5804	5059	1206	96
i=5 5LS1	-	-	145	944	1206	446	39
i=6 6LS0	-	-	-	68	96	39	8

Table 5.7 : The fully observed cell-cell joint frequency distribution [N] for the Finney packing.

(X_T = 1.01229, s = 0.50012)

5.5 Tests for Randomness of Network Structure

5.5.1 Predicting [N] from [P]

We have now arrived at the point where we have two basic joint frequency distributions which characterise completely different aspects of the Finney packing. These are:

(i) [P] which is a fully observed measure of the frequency with which each particular cell class is observed to be associated with each particular face class. This is an intrinsic property of the dis-aggregated set of cells.

and

(ii) [N] - which is a complete summary of the frequency with which each cell class is observed to be an immediate neighbour of each particular cell class. This is an intrinsic property of the network structure. Any evidence for or against clustering of cell types is contained in [N].

The basis of any test for randomness in [N] lies in the hypothesis that [N] is some homogeneous function of [P]. The simplest definition of randomness possible, therefore is:

$$N'_{qi} = \sum_{i=o}^{6} \sum_{j=o}^{3} ((P_{ij}/S_j).P_{qj} \qquad -5.1-$$

where $$S_j = \sum_{i=o}^{6} P_{ij} \qquad -5.2-$$

If [N'] is statistically similar to [N], then [N] is shown to be homogeneously random. The meaning and derivation of these two equations is best understood by means of a worked example:

Worked Example: [N'] as a function of [P]

In this example we will predict the random chance distribution of neighbouring cells to the OLS6 cell (i.e. i = 0). To begin with, the observed frequency of all OLS6 neighbouring cells is,

$$\sum_{j=0}^{3} P_{0,j} = P_{0,0} \text{ (Since } P_{0,1} = P_{0,2} = P_{0,3} = 0)$$

From table 5.6, $P_{0,0} = 216$

So, the task is to distribute, or "allocate", 216 suitable neighbours to the OLS6 reference cell. This allocation is performed according to an assumed, perfectly homogeneous and unbiased random distribution. The first stage of the task is to identify the permitted classes of neighbouring cells, and eliminate the prohibited classes (in the algorithm represented by equation 5.1 all prohibited neighbours are automatically eliminated by multiplication with zero values in the matrix [P], and permitted neighbours are "identified", or counted, by multiplication with non-zero values in the matrix [P]).

Clearly from table 5.3, the permitted neighbours are OLS6, 1LS5, 2LS4 and 3LS3 cells. The second step, then, is to count the total number of all permitted neighbours to the OLS6 reference cell. In this instance, this quantity, S, is:

$$S = P_{0,0} + P_{1,0} + P_{2,0} + P_{3,0}$$

(noting that $P_{4,0} = P_{5,0} = P_{6,0} = 0$)

The general definition of S is:

$$S_j = \sum_{i=0}^{6} P_{i,j}$$

in this example, $S_0 = 216 + 1511 + 2252 + 627$

$= 4606.$

The final stage in the task is to allocate 216 neighbours to the 216 OLS6 cells in direct proportion to the frequency of potential neighbours:

i.e. number of OLS6 neighbours to OLS6 ($N'_{0,0}$) = 216 x 216/4606

= 10.129

to nearest integer, $N'_{0,0}$ = 10

number of 1LS5 neighbours to OLS6 ($N'_{1,0}$) = 216 x 1511/4606

= 70.859

to nearest integer, $N'_{1,0}$ = 71

number of 2LS4 neighbours to OLS6 ($N'_{2,0}$) = 216 x 2252/4606

= 105.608

to nearest integer, $N'_{2,0}$ = 106

number of 3LS3 neighbours to OLS6 ($N'_{3,0}$) = 216 x 627/4606

= 29.403

to nearest integer, $N'_{3,0}$ = 29

and

$$N'_{4,0} = N'_{5,0} = N'_{6,0} = 0$$

- Equation 5.1 and 5.2 are formalised representations of this worked example, suitable for implementation as a simple algorithm to test the hypothesis that it is possible to predict [N] given [P]. Implicit in these equations is the concept that the predicted matrix of [N'] is homogeneously random.

5.5.2 Fundamental Test

Equations 5.1 and 5.2 are extremely readily implemented as algorithms within a program, together with the observed cell-face matrix [P] shown in table 5.6. This program PMATRIX, presented in Appendix 'B' to this thesis, uses these equations and data in order to estimate a random network expectation of the cell-cell joint frequency distribution, [N']. The values thus obtained for [N'] are presented in table 5.8.

	j = 0 0LS6	j = 1 1LS5	j = 2 2LS4	j = 3 3LS3	j = 4 4LS2	j = 5 5LS1	j = 6 6LS0
i=0 0LS6	10	71	106	29	0	0	0
i=1 1LS5	71	591	1303	919	149	0	0
i=2 2LS4	106	1303	4650	5549	1780	133	0
i=3 3LS3	29	919	5549	10432	5783	883	39
i=4 4LS2	0	149	1780	5783	5084	1227	103
i=5 5LS1	0	0	133	883	1227	477	60
i=6 6LS0	0	0	0	39	103	60	9

Table 5.8 : Prediction of [N'] using [P] with equation 5.1.

Comparison of the predicted cell-cell matrix [N'] in table 5.8 with the observed cell-cell matrix [N] in table 5.7 shows that the two matrices are extremely similar. For example, selecting the OLS6 cell which was used in the worked example in section 5.5.1, we find the following:

Neighbour Class	Predicted Neighbour Frequency [N']	Observed Neighbour Frequency [N]
OL56	10	12
ILS5	71	69
2LS4	106	107
3LS3	29	28
4LS2	0	0
5LS1	0	0
6LS0	0	0

It is evident, therefore, that the simplicial cells of the Finney packing are randomly distributed (by class) on the network. This assertion is consistent with the view that there is no clustering of cell types within the Finney model, and supports the case that the paracrystalline model does not adequately describe the Finney packing. From the percolation theory perspective, the founding assumption of a random distribution of pores on the network is supported by the assertion.

Given the importance of this assertion to both percolation theory (supported) and paracrystalline theories (condemned) for the Finney model, it is instructive to examine the assertion in some detail.

The statistical significance of the assertion is assessed using the chi-square statistic:

$$\chi^2 = \sum_{i=0}^{6} \sum_{j=0}^{6} (N'_{ij} - N_{ij})^2/N'_{ij} \qquad \text{-5.3-}$$

Use of equation 5.3 is not quite straightforward, since matrices [N] and [N'] are both perfectly symmetrical about the diagonal elements. In order to obtain the correct number of degrees of freedom for chi-square, therefore, it is essential to count only <u>one set</u> of off-diagonal elements, together with the diagonal elements themselves. In other words, equation 5.3 is only meaningful when constrained such that:

$$\chi^2 = \sum_{i=0}^{6} \sum_{j=0}^{6} (N'_{ij} - N_{ij})^2/N'_{ij} \qquad \text{-5.3-}$$

for $i = j$ and $ij \neq ji$.

This constraint gives 7 diagonal elements and 21 off-diagonal elements. The appropriate number of degrees of freedom in chi-square is therefore 27 (i.e. 28 classes minus 1 restriction).

Evaluating equation 5.3 using data for [N] and [N'] presented in tables 5.7 and 5.8 respectively gives a value for chi-square of 47.1. Using standard chi-square significance tables, the probability of $\chi^2 = 47.1$ occurring by chance is only about 1%. This is extremely surprising, since this result implies that [N] is <u>not</u> statistically similar to [N'] after all. However, an examination of individual values of $(N'_{ij} - N_{ij})^2/N'_{ij}$ reveals the following:

$$(N'_{3,6} - N_{3,6})^2/N'_{3,6} = 21.6$$

This is an astonishing result since it proves that the reason [N] is not statistically similar to [N'] is that there is some slight degree of clustering between 3LS3 and 6LS0 cells. Although not strictly a statistically valid approach, if $(N'_{3,6} - N_{3,6})^2/N'_{3,6}$ is eliminated altogether from equation 5.3, a value of $\chi^2 = 25.5$ is obtained. From standard tables, the probability of $\chi^2 = 25.5$ occurring by chance is roughly 60%. This approach is very important, since it demonstrates that the "commonsense" approach of comparing [N] and [N'] by glancing at tables 5.7 and 5.8 gives the overall impression that [N] and [N'] are very similar; a more rigorous, statistical approach confirms that [N] and [N'] are not quite so similar. To put this view into perspective it is helpful to remember that, out of 57522 neighbour pairs represented by [N], there are only 136 observed occurrences (i.e. about 0.2% of all neighbour pairs) of 3LS3 cells neighbouring with 6LS0 cells. Clearly, the chi-square test represented by equation 5.3 is extremely sensitive to slight clustering tendencies between cells.

For the moment it is evident that there is no clear reason why 3LS3 cells and 6LS0 cells do not form neighbours with the frequency expected of a perfect, homogeneously random distribution of simplicial cell types given by equation 5.1. In fact a detailed explanation for this behaviour must wait until the discussion of isomers is presented in the next chapter. To complete the discussion on slight clustering tendencies, it is worth noting that:

$$(N'_{5,6} - N_{5,6})^2/N'_{5,6} = 7.4$$

The significance of this is that if $(N'_{5,6} - N_{5,6})^2/N'_{5,6}$ is also eliminated from equation 5.3, the value of χ^2 falls to 18.1. From statistical tables, the probability of $\chi^2 = 18.1$ (for 27 degrees of freedom) occurring by chance is about 90%, in line with our expectation of a random distribution. The very slight non-random characteristics of 5LS1 - 6LS0 and 3LS3 - 6LS0 neighbour-pairs are related, as we shall see in the next section. For the moment, it is worth summarising what has been learned so far before proceeding to that section.

5.5.3 Summary

A novel theorem has been developed, in which the cell-face distribution [P] is used to predict an expectation, [N'], of the cell-cell distribution for the Finney packing. Comparison of [N'] with the observed cell-cell distribution, [N], shows that the component simplicial cells of the Finney model are essentially homogeneously randomly distributed throughout the packing. This important result confirms that paracrystalline theories do not adequately describe the structure of the Finney packing, as strong evidence of cell clustering has not been found. The result also confirms that the founding assumption of percolation theory, that the pores (simplicial cell types) are randomly distributed on the network, is apparently valid for sphere packings. (This last statement, however, must not be taken out of context as proof that percolation theory can be directly applied to sphere packings. Work presented in chapter 6 casts considerable doubt on the application of percolation theory to sphere packings).

Application of a simple statistical test to the novel theorem shows that whilst the distribution of component cells is <u>essentially</u> random, there is a very slight tendency for certain groups of cells to depart from random behaviour. In particular, 3LS3 cells form neighbours with 6LS0 cells <u>slightly more often</u> than expected, whilst 5LS1 cells form neighbours with 6LS0 cells <u>slightly less often</u> than expected. The magnitude of these departures from homogeneously random behaviour is extremely small - more than 99.5% of all the cells in the packing conform to random distribution within the overall structure.

<u>The present work has arrived at an extremely important view of the simplicial cell structure of the Finney packing which, when taken into account with chapter 4, poses a severe paradox;</u>

- the simplicial cells are <u>non-random</u> on an individual basis. Hence the relative frequencies of "extreme" cell types such as 6LS0 and 0LS6 are less than predicted by random chance. The relative frequencies of the more "ordinary" cell types such as 3LS3 are far higher than expected by random chance.

- the spatial distribution of all cell types within the packing is almost perfectly homogeneously random.

- the nature of the paradox is that there is a reduced requirement to connect "extreme" cells within the structure. Overall, therefore, the simplicial cells of the Finney packing must generate a small number of "extreme" faces (i.e. 3LS0 and 0LS3) in order to accommodate a small number of "extreme" cells. The paradox is

resolved by isomerism which permits different face forms to exist for identical simplicial cell types.

5.6 Isomer Distribution of the Finney model

The essential link between the concept of simplicial cells which are individually non-random, and the concept of simplicial cells which are spatially randomly distributed is that of isomerism. This essential link is now discussed in some detail in the following sections.

5.6.1 Theoretical Distribution

If, for a moment, we relax all constraints on simplicial cells fitting together and filling space, it is possible to predict the distribution of isomers based solely on random chance. For example, in the case of the 2LS4 simplicial cell illustrated in figure 5.3, suppose that we are set the task of making, say, a wire-frame model of the cell. We are given two long edges (wires) and four short ones. We begin by selecting an edgelength position for one of the long edges. This fixes one of the six edgelength positions, and in order to place the second long edge we have to choose one of the five available positions. Inspection of figure 5.3 shows that 4 out of these 5 positions will result in the formation of the alpha isomer (refer to figure 5.4). The random chance probability that a 2LS4 cell will be an alpha isomer is therefore 4/5 or 0.8. The random chance probability that a 2LS4 cell will be a beta isomer is 0.2.

The random chance probabilities for all the other isomers are readily calculated, and are presented in table 5.9. The random chance probabilities of isomer distribution shown in table 5.9 are, of course, not necessarily representative or characteristic of the relative frequencies of real isomers in the Finney model. In fact the assertion made in the introduction to this section is that the network structure can only remain homogeneously random itself for an observed non-random distribution of simplicial cell classes if the isomer distribution is distorted significantly from that presented in table 5.9. We shall now examine this assertion.

SIMPLICIAL CELL	ISOMER	RANDOM CHANCE RELATIVE PROBABILITY
0LS6	N/A	1.0
1LS5	N/A	1.0
2LS4	ALPHA	0.8
2LS4	BETA	0.2
3LS3	ALPHA	0.6
3LS3	BETA	0.2
3LS3	GAMMA	0.2
4LS2	ALPHA	0.8
4LS2	BETA	0.2
5LS1	N/A	1.0
6LS0	N/A	1.0

Table 5.9 : Theoretical random chance relative probabilities of occurrence of isomers of simplicial cells.

5.6.2 Observed Distribution

The isomer frequency distribution for a real set of simplicial cells, such as those of the Finney packing, can only be determined for a fixed value of the edgelength threshold, X_T. The value of X_T used in the analysis reported here is $X_T = 1.01229$, which gives a value of $S = 0.50012$ and follows from the analysis presented in Chapter 4. The first step in determining the isomer distribution is to produce a list (data file) describing which simplicial cell class each of the 14870 simplicial cells belongs to. This data file is called TYPE.DAT, and reference has already been made to its construction and format in section 5.4.2. Additional information on TYPE.DAT is given in Appendix 'B' to this thesis. The second step in determining the isomer distribution consists of examining each simplicial cell, together with its class description, in order to decide the isomer. This function was performed by program ISOMER, which is presented in Appendix 'B' to this thesis, and which writes an output datafile called ISOMER.DAT. Finally, the observed isomer frequency distribution for the Finney model was obtained using program ISOCOUNT, also presented in Appendix 'B'. The distribution of observed isomer frequencies is presented in table 5.10.

The observed frequencies presented in table 5.10 can be converted into relative frequencies for the purposes of direct comparison with the theoretical relative probabilities presented in table 5.9. This comparison is shown in table 5.11, from which two key facts emerge:

(i) As asserted earlier, the observed frequency distribution does not match the theoretical prediction based on random chance,

(ii) There is a systematic pattern to the "distortion" of the real distribution relative to the theoretically predicted distribution.

This latter point is now discussed in more detail.

	α	β	γ	CELL TOTAL
0LS6	56	0	0	56
1LS5	785	0	0	785
2LS4	2354	1142	0	3496
3LS3	4521	927	659	6107
4LS2	2479	1174	0	3653
5LS1	719	0	0	719
6LS0	54	0	0	54
			TOTAL	14870

Table 5.10 : Observed distribution of isomer forms within the Finney packing.

SIMPLICIAL CELL	ISOMER	RANDOM CHANCE PROBABILITY	OBSERVED RELATIVE FREQUENCY
0LS6	N/A	1.0	1.0
1LS5	N/A	1.0	1.0
2LS4	ALPHA	0.8	0.673
2LS4	BETA	0.2	0.327
3LS3	ALPHA	0.6	0.740
3LS3	BETA	0.2	0.152
3LS3	GAMMA	0.2	0.108
4LS2	ALPHA	0.8	0.679
4LS2	BETA	0.2	0.321
5LS1	N/A	1.0	1.0
6LS0	N/A	1.0	1.0

Table 5.11 : Comparison of predicted and observed isomer frequencies for 14870 simplicial cells of the Finney model.

5.6.3 Significance of the observed distribution

Inspection of table 5.11 shows that the alpha isomers of both the 2LS4 and the 4LS2 classes are less frequent than predicted, whilst the alpha isomer of the 3LS3 class is more frequent than predicted on the basis of random chance. These differences constitute a single trend, which is, simply to reduce the frequencies of the OLS3 and 3LS0 face forms below that predicted on the basis of random chance. This is easily confirmed by reference to figure 5.4 which shows that the 2LS4 α isomer has a OLS3 face, whilst the 2LS4 β isomer does not. Similarly, the 4LS2 α isomer has a 3LS0 face, whilst the 4LS2 β isomer does not. Finally, the 3LS3 β and γ isomers have a 3LS0 and a OLS3 face respectively, whilst the 3LS3 α isomer has neither 3LS0 nor OLS3 faces.

The reason that the 3LS0 and OLS3 faces are restricted by this distortion in the isomer distribution is simple - there are less OLS6 and 6LS0 simplicial cells found in the Finney packing than expected on the basis of random probabilities. Therefore, there is a reduced requirement to connect these cells within the network. Because the network is (practically) homogeneously random, isomeric "distortion" of individual simplicial cells is essential in order to match the reduced number of "extreme" cells to the correct face forms of the "average" cells.

Close inspection of tables 5.10 and 5.11 reveals a curious feature of the 3LS3 isomers. Theoretically, the 3LS3 β and 3LS3 γ isomers occur with the same frequency (0.2). In the Finney model, these two isomers occur with different frequencies (3LS3 β @ 0.152 and 3LS3 γ

@ 0.108). The question arises as to whether or not this is a significant finding. In order to assess the question, it is useful to ask a different, more anthropomorphic question - is there any material advantage to be gained in selecting 3LS3 β isomers rather than 3LS3 γ isomers? The answer to this question turns out to be a resounding yes.

Imagine constructing a 3LS3 cell given 3 edges of 1.0 sphere diameters in length and 3 edges of 1.4 sphere diameters in length, and making first a 3LS3 β, and then a 3LS3 γ isomer. It is possible, in our imaginary example, to measure the total volume of each cell, as well as the volume of sphere solid and packing density of each cell. These calculations for the imaginary example are easily executed using the subroutines developed for chapter 3 (and presented in Appendix 'B').

The results are:

	TOTAL CELL VOLUME (r^3)	SOLID VOLUME (r^3)	PACKING DENSITY
3LS3 β	1.33254	0.852088	0.639444
3LS3 γ	1.47271	0.767092	0.520869

- Clearly the β isomer is much more space efficient than the γ isomer, since the β isomer takes up less total space and consumes more solid (sphere) space, resulting in a higher packing density than the γ isomer.

So it is possible to see a plausible reason why RCP structure might produce significantly more 3LS3 β isomers than 3LS3 γ isomers. However, the fact that the relative frequencies of 3LS3 β and 3LS3 γ isomers are different raises another problem altogether - what is the effect on the network structure (i.e. [N])? The answer to this question is that enhancing the frequency of 3LS3 β isomers relative to 3LS3 γ isomers means that more 6LS0 cells must occur as neighbours to the 3LS3 β isomer than OLS6 cells to the 3LS3 γ isomer. This constitutes a small departure from the concept of homogeneously random network structure, and the departure must show up predominantly in the value of $N_{6,3}$ and $N_{3,6}$ in [N]. This is precisely the same region of [N] isolated as non-random in section 5.5.2. In our imaginary example, we used edgelengths of 1.0 and 1.4 sphere diameters. In the rest of the work presented in this thesis, however, the edgelength threshold condition used is $X_T = 1.01229$. This means that the contrast in total cell volume and packing density between 3LS3 β and 3LS3 γ in the Finney packing will be less than that of the example. This in turn means that the non-random network aspect of $N_{6,3}$ in [N] will be small.

5.7 Discussion: Gotoh and Finney's "Most Probable Tetrahedron"

It was shown in chapter 4 that, for a value of $X_T = 1.01229$ (i.e. $S \simeq 0.5$), by far the most frequent class of simplicial cell in the Finney packing is the 3LS3. In many ways, the 3LS3 cell can be thought of as the "backbone" or fundamental building block of the RCP network. In addition to its high frequency of occurrence, only

the 3LS3 cell can form faces such that any of the seven cell classes can be neighbouring cells to 3LS3. The fact that the 3LS3 simplicial cell is one of the most characteristic features of RCP structure had been previously identified by Gotoh and Finney (1974), though they did not use either the concept of the simplicial subdivision or the notation developed in the present work. Instead, Gotoh and Finney (1974) postulated that, for any given sphere in a packing to be stable against displacement in a given direction, it must be supported by three spheres in that direction. Thus the given sphere, and its three supporting spheres comprise a group of four spheres forming a tetrahedron. This same stability to displacement criterion must also apply for displacement in the opposite direction. The given sphere, therefore, may be regarded as having a co-ordination number of exactly six.

The tetrahedron so formed by the group of four spheres is called by Gotoh and Finney the most probable tetrahedron, and it looks like that shown in figure 5.6. In terms of simplicial cell classes, the stability against displacement criterion is consistent with three point contacts, equivalent to state 'S' edgelengths. From figure 5.6 it is clear that the remaining three edgelengths are definitely appreciably longer than point contacts, and are equivalent to state 'L' edgelengths (i.e. >1.01229 sphere diameters). Clearly then, the Gotoh and Finney most probable tetrahedron is identical to a 3LS3 simplicial cell. To this extent the work of Gotoh and Finney (1974) and the present work are entirely in accord.

If we consider the isomeric form represented by the most probable tetrahedron of Gotoh and Finney, we discover that the three state

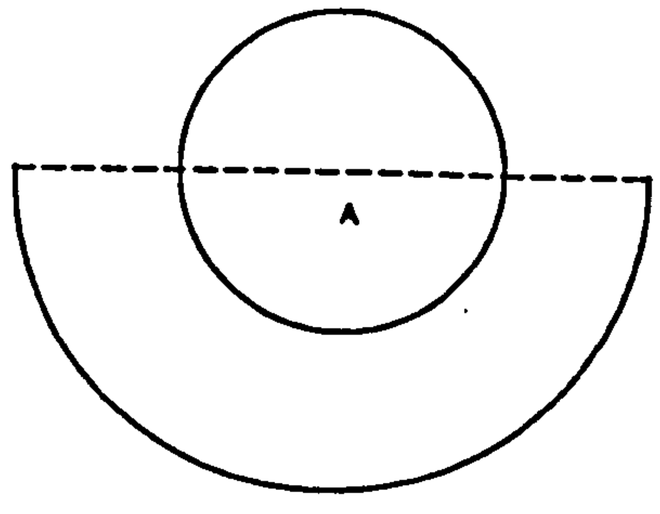

Hemispherical envelope of R = 1.0
diameters forms locus of centres
of supporting spheres (B,C and D)

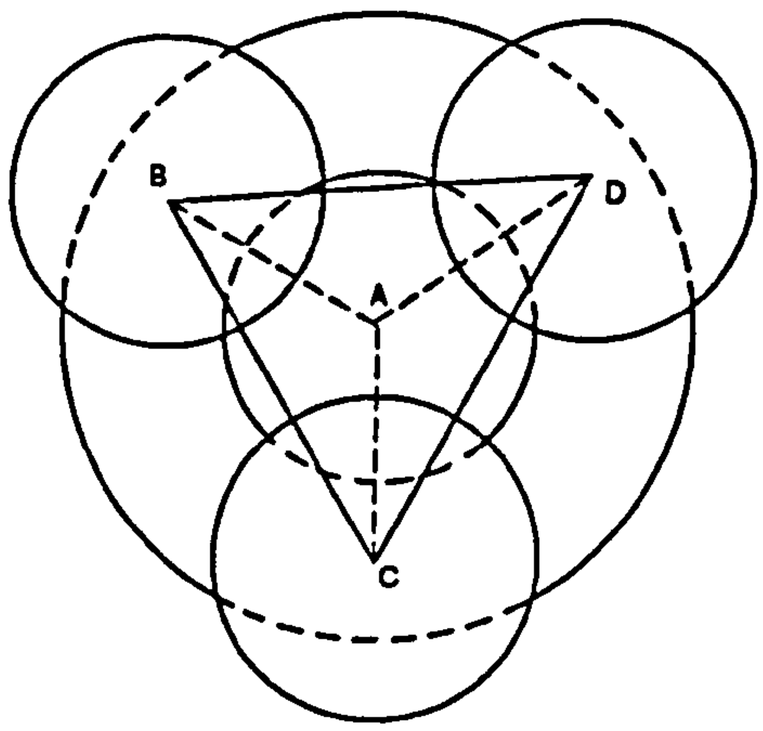

Figure 5.6 : THE MOST PROBABLE TETRAHEDRON OF GOTOH AND FINNEY (1974)

'S' (i.e. point contact) edges all form a single common apex. This isomer is therefore identified in the present work as a 3LS3 beta, as shown in figure 5.4. At this point the present work, and the work of Gotoh and Finney (1974) begin to diverge. The reason they diverge is that the 3LS3 alpha, and not the 3LS3 beta is the most frequently observed isomer in the Finney packing, as shown in table 5.12. The "most probable tetrahedron" described by Gotoh and Finney (1974) is therefore not, in fact, the most probable tetrahedron after all. The 3LS3 alpha isomer constitutes 30.4% of all cells in the Finney packing. The 3LS3 beta, in contrast, represents only 6.2% of the packing.

Using the approach developed by Gotoh and Finney (1974), figure 5.7 shows a 3LS3 alpha isomer formed at a given sphere (A). This figure implies a co-ordination for the given sphere (A) of 4, and not 6 as required by the Gotoh and Finney (1974) reasoning. This is an interesting point, particularly as Gotoh and Finney (1974) refer to Mason's (1968) work which clearly shows some evidence for co-ordinations of between 4 and 5 at point contact (as shown in figure 1.16). So, whilst their "most probable tetrahedron" may have been useful to Gotoh and Finney in their theoretical calculations, it should have been somewhat of an embarrassment to them because it demands a <u>minimum</u> co-ordination of 6, which appears not to be a characteristic property of RCP structure. It is suggested here that the theoretical calculations of packing density defined by Gotoh and Finney be treated with some degree of caution in view of the fact that they incorrectly isolated the most common tetrahedral sub-unit of the Finney packing.

5.8 DISCUSSION AND CONCLUSIONS OF CHAPTERS 4 AND 5

Chapters 4 and 5 of this thesis represent an attempt to define and measure the most elusive feature of random close packing - that of randomness itself. Prior to the present work it has not been possible to address the question of measuring the amount of randomness present in random close packing.

The issue of randomness has been divided into two separate aspects in the present work. The first of these aspects concerns the

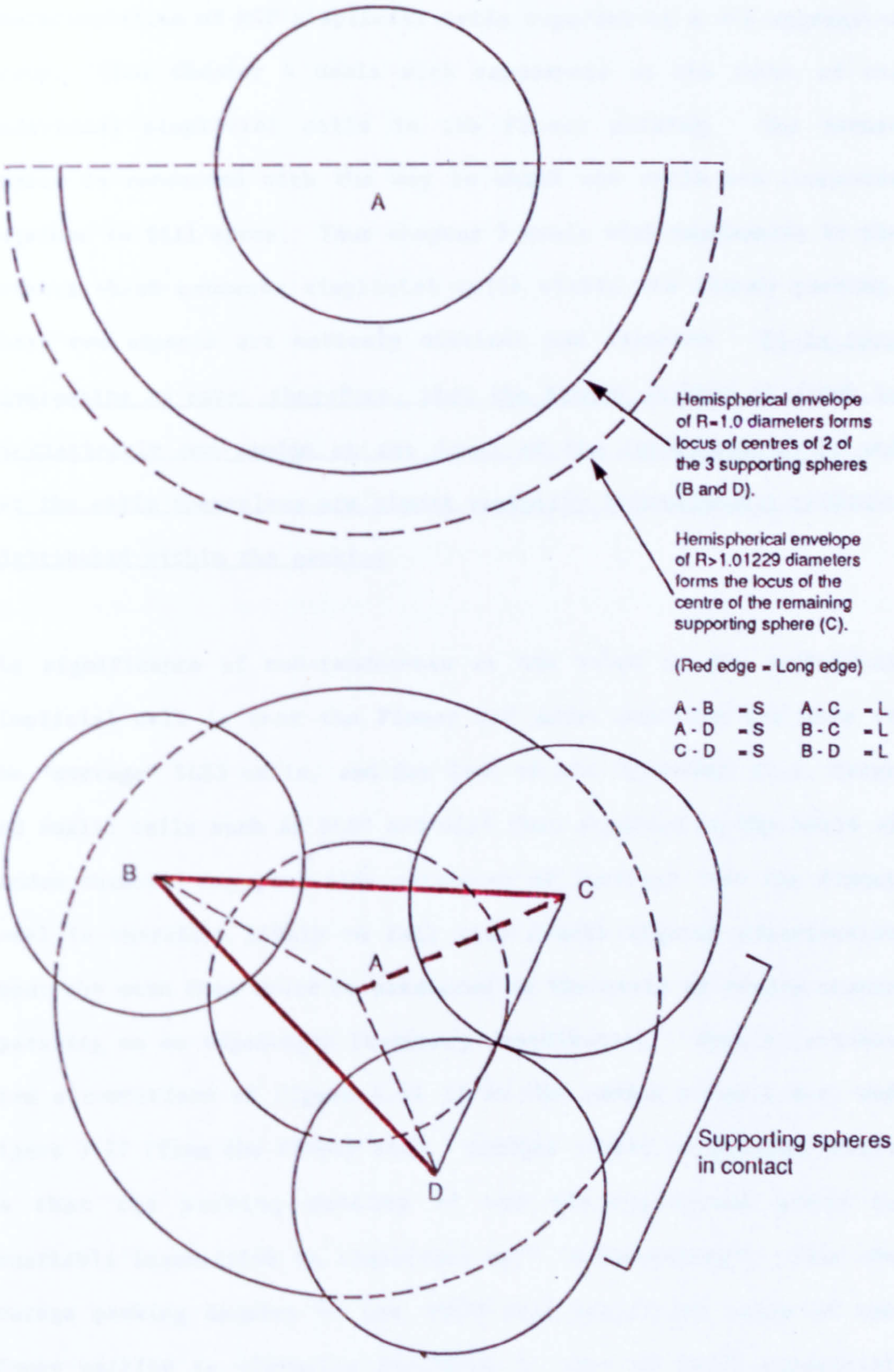

Figure 5.7 : THE MOST FREQUENTLY OBSERVED TETRAHEDRON IN FINNEY PACKING - THE 3LS3 ALPHA

characteristics of RCP simplicial cells regarded as a dis-aggregated group. Thus Chapter 4 deals with randomness at the level of the individual simplicial cells in the Finney packing. The second aspect is concerned with the way in which the cells are connected together to fill space. Thus chapter 5 deals with randomness in the network which connects simplicial cells within the Finney packing. These two aspects are entirely distinct and separate. It is very interesting to note, therefore, that the Finney packing is shown to be distinctly non-random at the level of the individual cell, and yet the cells themselves are almost perfectly homogeneously randomly distributed within the packing.

The significance of non-randomness at the level of the individual simplicial cell is that the Finney RCP model produces far more of the "average" 3LS3 cells, and far less of the "extreme" (i.e. large and small) cells such as 6LS0 and 0LS6 than expected on the basis of random chance. Any pore-size parameter of interest from the Finney model is therefore likely to fall into a much tighter distribution about the mean than could be predicted on the basis of random chance operating on an edgelength frequency distribution. This is evident from a comparison of figure 4.11 (from the random control set) and figure 3.27 (from the Finney set). Another rather surprising result is that the packing density of the dis-aggregated group is remarkably insensitive to simplicial cell "authenticity". Thus the average packing density of the 14870 real simplicial cells of the Finney packing is virtually identical to that of 14870 simplicial cells artificially created by random selection from the real edgelength distribution. This finding casts considerable doubt upon the practice of validating computer simulations of monodisperse

sphere packings by comparing the overall packing density with that of the Finney model. The best that can be said of this practice is that if the simulation does not achieve the density of the Finney model it is not correct. Simulations achieving the density of the Finney model are not necessarily correct. It is suggested that computer simulations of sphere packings are best described for the purpose of comparison with other sphere packings in terms of their simplicial cell attributes such as packing density frequency distribution, total cell volume frequency distribution and solid angle frequency distribution. Additionally the frequency distribution of simplicial cell classes (i.e. OLS6 to 6LSO) may also be utilised as a descriptor for the purpose of comparison between sphere packings.

In Chapter 5 the issue of randomness of the network which connects the simplicial cells of the Finney packing was addressed by defining two joint frequency distributions. The first of these is the simplicial cell-face joint frequency distribution, [P], which is an intrinsic property of the dis-aggregated group of cells. This distribution was used to predict an estimate of the simplicial cell-cell joint frequency distribution, [N'], which is in effect a summary of the entire network. This predicted distribution is very similar indeed to the observed simplicial cell-cell joint frequency distribution, [N], confirming that the spatial distribution of cell types within the network is essentially random. This is a significant and useful result in terms of percolation theory, which can only model flow in porous media on the assumption that pore parameters (cell types) are randomly distributed throughout a network. The present work represents the first analysis of a real,

disordered porous medium for which this founding assumption has been tested, and indicates that the assumption is reasonable. Work presented in Chapter 6, however, casts considerable doubt about the application of percolation theory to sphere packings.

The concept of isomers of simplicial cells was introduced in Chapter 5. This concept is particularly useful in understanding how the network can be random, whilst the distribution of simplicial cell classes is distinctly non-random. Thus in order to reduce cell connectivity to the "extreme" simplicial cells (0LS6, 6LS0) from that expected on the basis of random chance, the isomer distribution is distorted such that far less of the "extreme" face forms (0LS3, 3LS0) are produced than expected on the basis of random chance. Correspondingly more of the "average" face forms (0LS2, 2LS1) are produced in order to provide connections between the most frequent 3LS3 simplicial cells. The concept of isomers was also used to demonstrate that the "most probable tetrahedron" of the Finney packing described by Gotoh and Finney (1974) is in fact <u>not</u> the most frequently observed tetrahedral sub-unit of the packing. Gotoh and Finney's sub-unit is equivalent to the 3LS3 beta isomer of the present work, which only represents 6.2% of the Finney packing. The present work identifies the 3LS3 alpha isomer as the most frequent discrete tetrahedral sub-unit of the Finney model, accounting for 30.4% of all the cells in the packing. This is a particularly important distinction to make, because the Gotoh and Finney sub-unit is arguably the best and most detailed attempt to interpret the fundamental structure of the Finney model prior to the present work. The Gotoh and Finney sub-unit, unfortunately, demands a minimum sphere co-ordination of six, despite the fact that earlier

experimental evidence supports a co-ordination of around 4 to 5. The 3LS3 alpha isomer requires a minimum sphere (contact) co-ordination of 4.

In terms of the old solid state physics issue of paracrystalline regions of RCP-like materials, the present work shows that such regions do not exist in the Finney model. A homogeneously random distribution of cell types on the network precludes the possibility of such regions. Although this result is not surprising, it has not previously been demonstrated for the Finney packing.

In conclusion, Chapters 4 and 5 constitute a novel and original attempt to quantify one of the most important structural features of the Finney packing. The attempt is worthwhile just for the sake of increasing knowledge about RCP structure. Indeed, it demonstrates that one of the most *detailed structural* analysis published to data (Gotoh and Finney, 1974) is incorrect. In terms of *understanding* the capillary properties of the Finney model, however, the attempt may be regarded as crucial.